2013

Titanium dioxide nanoparticle uptake across the isolated perfused intestine of rainbow trout: physiological mechanisms and a comparison with Caco-2 cells

Al-Jubory, Aliaa Rasheed

Copyright Statement

TITANIUM DIOXIDE NANOPARTICLE UPTAKE ACROSS THE ISOLATED PERFUSED INTESTINE OF RAINBOW TROUT: PHYSIOLOGICAL MECHANISMS AND A COMPARISON WITH CACO-2 CELLS

By

ALIAA RASHEED AL-JUBORY

A thesis submitted to the Plymouth University in

partial fulfilment for the degree of

DOCTOR OF PHILOSOPHY

School of Biomedical and Biological Sciences

Faculty of Science and Technology

July 2013

Titanium dioxide nanoparticle uptake across the isolated perfused intestine of rainbow trout: physiological mechanisms and a comparison with Caco-2 cells

Aliaa R. Al-Jubory

Abstract

The wide use of nanoscale materials in food and health care products raises the concern of their possible uptake across the gastrointestinal tract, but very limited data are available on their uptake kinetics, and the potential hazards for humans. In this study, the uptake mechanism of titanium dioxide (TiO_2) across the isolated perfused fish intestine and human intestinal Caco-2 cells were evaluated. The *in vitro* preparation of the whole gut sac and the isolated perfused intestine of rainbow trout were performed using both bulk and nano TiO_2 in a concentration of 1 mg l^{-1} for up to 4 h. The results showed that the Ti from both bulk and TiO_2 NPs were mainly accumulated in the mid and hind intestine, with 80% or more of the accumulation in the mucosa rather than the underlying muscularis. Perfused intestines showed a saturable, time-dependent accumulation of the Ti from TiO_2 and the uptake of Ti from exposure to NPs was faster than that of the bulk form. The uptake of Ti from exposure to TiO_2 NPs increases 10 fold when the CO_2 in the gas mixture was lowered to 0.5%. Subsequently, further investigation on the mechanisms of uptake of TiO_2 was applied using different kinds of inhibitors. Adding 10 mmol l^{-1} cyanide did not stop Ti uptake from TiO_2 exposures, and 100 µmol l^{-1} vanadate (ATPase inhibitor) caused a 2.8 fold reduction in the net uptake rate of Ti for the TiO_2 NP exposure. Luminal additions of 120 IU ml^{-1} nystatin (endocytosis inhibitor) blocked the uptake of Ti from both bulk and TiO_2 NPs treatments. The results indicate that Ti accumulation from TiO_2 exposures was sensitive

to both nystatin and vanadate; the former suggesting that there is an endocytosis involvement in the uptake of TiO_2 across the intestinal epithelium. Human intestinal Caco-2 cell showed a steady, saturable and time-dependent accumulation of Ti over 24 h exposures to 1 mg l^{-1} TiO_2 (for all forms of TiO_2). A scanning electron microscope study indicated the appearance of the particles underneath the cells, increasing the evidence of the Ti uptake from different forms of TiO_2 by Caco-2 cells. Both nystatin and vanadate increase the accumulation of TiO_2 which suggests interference of these drugs with endocytic pathways. All the data in the thesis demonstrates Ti uptake across the intestinal epithelium from TiO_2 exposures involving CO_2-dependent and nystatin-sensitive mechanisms. The results in this thesis have contributed to some understanding on the behaviour, uptake and effects of the TiO_2 NPs across the intestine; and highlight the possible dietary hazard of the NPs to human health.

Table of Contents

Content **Page Number**

Content **Page Number**

List of Figures

List of Tables

Abbreviations

Abbreviation	Glossary
%	Percent
ºC	Degree Centigrade
µg	Micrograms
µl	Microliter
µm	Micrometer
µmol	Micromole
A431	Human epidermal cell line
A549	Human lung adenocarcinoma epithelial cells
Ag	Silver
ANOVA	Analysis of variance
ARPE-19	Human retinal pigment epithelial cells
ATP	Adenosine triphoshate
BAL	Bronchoalveolar lavage
BCA	Bicinchoninic acid
BEAS-2B	Human bronchial epithelial cells
BSI	Backscatter image
C_{60}	Buckminsterfullerene
Ca	Calcium
$CaCl_2 \cdot 2H_2O$	Calcium chloride dihydrate
Caco-2	Human colon adenocarcinoma cell line
CARS	Coherent anti-Stokes Raman scattering
CB	Carbon black
Cd	Cadmium
CH_3Hg	Methylmercury
Cl	Chloride
cm	Centimetre
cm^2	Square centimetre

CNT	Carbon nanotubes
CO_2	Carbon dioxide
CO_3	Carbon trioxide
Cu	Copper
DEPs	Diesel exhaust nanoparticles
DIDS	4,4'-diisothiocyano stilbene-2,2'-disulfonic acid
DLVO	Derjaguin, Landau, Verwey and Overbeek
DMEM	Dulbecco's modified eagle medium
DNA	Deoxyribonucleic acid
D.O.M	Dissolved Organic Matter
DPBS	Dulbecco's phosphate buffered saline
E171	Titanium dioxide
EDTA	Ethylene diamine tetraacetic acid
EDS	Energy dispersive spectrophotometry
EGTA	Ethylene glycol tetraacetic acid
FBS	Fetal bovine serum
Fe^{3+}	Ferric iron
Fig	Figure
g	Gram
GIT	Gastrointestinal tract
GSH	Glutathione
GTP	Guanosine triphosphate
H^+	Hydrogen ion
h	Hour
HaCaT	Human keratinocyte cell line
HBDH	Alpha-hydroxybutyrate dehydrogenase
HCl	Hydrochloric acid
HCO_3	Bicarbonate
H & E	Haematoxylin and eosin stain
HEPES	4-(2-hydroxyethyl)-1-piperazineethanesulfonic acid

Hg	Inorganic mercury
His	Histidine
ICP-OES	Inductivity coupled plasma-optical emission spectrome
IU	International unit
K	Potassium
KCl	Potassium chloride
KCN	Potassium cyanide
Kg	Kilogram
kGy	Kilogray
kHz	Kilohertz
l	Litre
LC_{50}	Median lethal concentration
LD_{50}	Median lethal dose
LDH	Lactate dehydrogenase
M	Molar
M cells	Microfold cells
MD	Minimal Davis medium
MDCK	Madin darby canine kidney cells
Mg	Magnesium
mg	Milligram
$MgCO_3$	Magnesium carbonate
$MgSO_4$	Magnesium sulphate
Milli-Q	Ultra-pure ion free water
min	Minute
ml	Millilitre
mM	Millimolar
mm	Millimetre
mmol	Millimole
Mn	Manganese
MnO_2	Manganese dioxide

mol	Mole
mosm	Milliosmole
mW	milliwatt
MWCNTS	Multi-walled carbon nanotubes
n	Number of observations
Na	Sodium
NaCl	Sodium chloride
NADH	Nicotine amide adenine dinucleotide
$NaHCO_3$	Sodium bicarbonate
$NaH_2PO_4 \cdot 2H_2O$	Sodium dihydrogen phosphate dehydrate
Na_3Vo_4	Sodium orthovanadate
ng	Nanogram
nm	Nanometer
NMs	Nanomaterials
nmol	Nanomole
NPs	Nanoparticles
NRR	Neutral red retention
NTA	Nanoparticle tracking analysis
O_2	Oxygen
OsO4	Osmium tetroxide
P	Statistical probability
P25	Titanium dioxide nanoparticles
PC-3M	Human prostate carcinoma cells
pCO_2	Partial pressure of carbon dioxide
PM	Particulate matter
pH	Potential hydrogen ion
PHFK	Primary human foreskin keratinocytes
PLGA	Poly (lactic-co-glycolic acid)
PTRF	Polymerase l and transcript release factor
QDs	Quantum dots

r	Round
RBC	Red blood cell
REACH	Registration, Evaluation, Authorisation of Chemicals
ROS	Reactive oxygen species
sCT	Salmon calcitonin
sec	Second
SEI	Secondary electron image
S.E.M	Standard error of mean
SEM	Scanning electron microscopy
SiO_2	Silicon dioxide
SSA	Specific surface area
SWCNTS	Single-walled carbon nanotubes
TBARS	Thiobarbituric acid reactive substance
TEM	Transmission electron microscopy
Ti	Titanium
TiO_2	Titanium dioxide
$Ti(OH)_4$	Titanium hydroxide
$TiO(OH)_2$	Metatitanic acid
USL	Unstirred layer
UV	Ultraviolet
UVA	Ultraviolet A
vit	Vitamins
WBC	White blood cell
Zn	Zinc
ZnO	Zinc oxide

Publications (Please refer to Appendix I):

Handy RD, Al-Bairuty G, **Al-Jubory A**, Ramsden CS, Boyle D, Shaw BS and Henry TB 2011. Effects of manufactured nanomaterials on fishes: a target organ and body systems physiology approach. *Journal of Fish Biology,*79, 821-853.

Al-Jubory AR and Handy RD 2012. Uptake of titanium from TiO_2 nanoparticles exposure in the isolated perfused intestine of rainbow trout: nystatin, vanadate, and novel CO_2-sensitive components. *Nanotoxicology,* DOI: 10.3109/17435390. 2012.735268.

Platform presentations:

Al-Jubory AR, Handy RD and Henry T 2009. The physiological effects of nanoparticles. University of Plymouth, 3rd April 2009, Plymouth, UK.

Al-Jubory AR, Handy RD and Henry T 2012. Mechanisms uptake of TiO_2 nanoparticles across the isolated perfused intestine of rainbow trout (*Oncorhynchus mykiss*). UoP Nano Group Meeting, University of Plymouth, 3rd Annual Meeting, 10th May 2012, Plymouth, UK.

Al-Jubory AR, Handy RD and Henry T 2012. Uptake of TiO_2 nanoparticles across the isolated perfused intestine of rainbow trout: nystatin, vanadate, and novel CO_2-sensitive componenets. Ecotoxicology Research and Innovation Centre (ERIC), University of Plymouth, 2nd Annual Conference, 13th July 2012, Plymouth, UK.

Poster presentations and conferences abstracts (Please refer to Appendix II):

Handy RD, Jha AN and **Al-Jubory A** 2009. *In vitro* techniques and their application to nanoparticles. Society for Experimental Biology annual meeting, 28th June-1st July 2009, Glasgow, UK. Abstract No. A4.12 In: Comparative Biochemistry and Physiology, 153A, S87.

Al-Jubory A and Handy RD 2010. Uptake of TiO_2 nanoparticles across the isolated perfused intestine of rainbow trout (*Oncorhynchus mykiss*). Nanotoxicology 2010, Edinburgh, UK, 2nd-4th June 2010, abstract book, pp. 70, No. p 95.

Al-Jubory A and Handy RD 2010. Uptake of TiO_2 nanoparticles across the isolated perfused intestine of rainbow trout (*Oncorhynchus mykiss*). Society of Environmental Toxicology and Chemistry UK branch annual meeting, London, 13-14th September 2010. Abstract book, SETAC.29, p 25.

Al-Jubory A and Handy RD 2011. Uptake of TiO_2 nanoparticles across the isolated perfused intestine of rainbow trout (*Oncorhynchus mykiss*). 3rd NanoImpactNet Conference, "Building a Bridge from NanoImpactNet to Nanomedical Research", 14-17th February 2011, Lausanne, Switzerland, abstract book, 4.2.6, p 70.

Al-Jubory AR and Handy RD, 2011. Mechanisms uptake of TiO_2 nanoparticles across the isolated perfused intestine of rainbow trout (*Oncorhynchus mykiss*). Society of Environmental Toxicology and Chemistry UK Branch Annual Meeting, "Polluted Planet: Sustaining Ecosystems and Biodiversity", London, 12-13th September 2011. Abstract book, SETAC.113.

Al-Jubory AR and Handy RD, 2012. Uptake of TiO_2 nanoparticles across the isolated perfused intestine of rainbow trout: nystatin, vanadate, and novel CO_2-sensitive componenets. The Postgraduate Society Annual Conference, Plymouth University, 26th June 2012, Plymouth, UK.

Gitrowski C, **Al-Jubory AR** and Handy RD 2012. Uptake and retention of TiO_2 nanoparticles in Caco-2 cells implications for human health. Centre for Research in Translational Biomedicine (CRTB) Research Day, University of Plymouth, 2nd Annual Conference, Plymouth, 4th July 2012.

Gitrowski C, **Al-Jubory AR**, Handy RD 2013. The gastrointestinal uptake of TiO_2 nanoparticles and associated toxicity. Society of Environmental Toxicology and Chemistry, SETAC Europe 23rd annual meeting, "Building a better future: Responsible innovation and environmental protection", 12-16th May 2013, Glasgow, UK. Abstract book, No. TU058, p229-230.

Acknowledgments

I would like to express my sincere gratitude to my first supervisor Professor Richard Handy for his help, advices, encouragement and immense knowledge along the way from the beginning up to the completion of this study. I would like to extend my sincere thanks to my second supervisor Dr. Ted Henry for his support and encouragement throughout my study.

I would like also to thanks the technical colleagues, especially William Vevers, Andy Atfield and Benjamin Eynon for their technical support where needed. Special thanks go out to Dr. Andrew Fisher for his help with ICP-OES analysis and a big thanks to Peter Bond for his help in TEM and SEM work. Christopher Ramsden is thanked for metal analysis advices and answering my questions, Genan Al-Bairuty for histology advices and help. I would like to acknowledge Constantinos Gitrowski who worked with me as a team. We worked together in the Caco-2 cell experiment. I would like also to express my sincere appreciation to all my colleagues and friends in the School of Biomedical and Biological Sciences who answered my request for help, especially Helena Reinardy, Sahar Karieb and Sahar Al Kutby. Professor Waleed Al-Murrani is thanked for his support and encouragement. I would like to express my gratitude to all those people, though their names are not listed, who supported me in one way or another.

Many thanks to the Ministry of Higher Education and Scientific Research-Republic of Iraq for providing the financial support and Iraqi cultural attaché in London for their kind support. Finally, I would like to express my heartfelt thanks to all my family especially my beloved parents for their blessing and supports, sisters and brothers for their encouragement. Lastly, my special heartfelt thanks go to my husband Mudhafar who supported me along the time of my study, my children Noor and Mohammed for their patient and encouragement.

Author's declaration

At no time during the registration for the degree of Doctor of Philosophy has the author been registered for any other University award without prior agreement of the Graduate Committee. This study was fully funded by the Ministry of Higher Education and Scientific Research of Republic of Iraq.

Word count of main body of thesis: 49,286 (56,947 including references)

Signed ----------

Date----------

Dedication

This work is dedicated to my beloved husband, Mudhafar Al-Zandee and my two children, Noor and Mohammed

Chapter 1

General Introduction

1.1 Introduction to nanoparticles and nanotechnology

Nanotechnology and the use of nano-scale materials is a relatively new area of science and technology which has become a significant worldwide industry, and is growing rapidly (www.nano.org.uk). Nanoparticles (NPs) are defined as particles with at least one dimension less than 100 nm (Masciangioli and Zhang, 2003; Roco, 2003) and the range size of these NPs should be between a lower limit of 1 nm and upper limit of 100 nm (Lövestam et al., 2010). This definition is not absolute, according to toxicological studies which have included work on aggregates of particles with dimensions of a few hundred nanometers (Handy and Shaw, 2007; Handy et al., 2008a). Clearly for NPs, the primary size should be considered (e.g., the diameter of a single particle). In addition, the sizes of aggregates of NPs, which can be several hundred nanometers or more, and the distribution of particle sizes present in the material also need to be considered. In mammalian toxicology particles sizes (PM, particulate matter) have been defined as coarse particles (diameter between 10 μm and 2.5 μm, PM 10-2.5), fine particles (2.5 μm or less, PM 2.5), or ultrafine particles (< 0.1 μm, PM 0.1), so NPs could be regarded as ultrafine particles or smaller (Handy et al., 2008a).

There are a wide variety of nanomaterials (NMs) and particles at the nanoscale range, because these NMs are purposefully designed for a particular application it may be difficult to classify these materials into chemical groups, and the use of the product (risk according to how products are used) may be more important for the exposure aspects of risk assessment of these materials (Hansen et al., 2008). Considerable effort has therefore focused on the classification of NMs according to the industrial aspect they are used in, for example: domestic appliances, electronics and computers, food and food packaging, health and fitness which includes (personal care products, cosmetics, sunscreen and sporting goods), home and garden, water treatment technology and

environmental remediation (Masciangioli and Zhang, 2003; Roco, 2003; Aitken et al., 2006; Hansen et al., 2008).

There is also another classification of NMs proposed by Hansen et al. (2007) which broadly classifies NMs, not in terms of products, but according to how the material is incorporated into the product, including three main categories: whether NMs are the bulk of the material in the product, whether they exist on the surface (surface coated products), or forming part of the structure (NPs matrix within the product). These main categories could be also divided into subcategories; the bulk of the material may consist of just one type of NMs or more than two different types (Hansen et al., 2007). For the surface coated products, the surface coated with NMs consist of the same structure material like the bulk, surface covers with un-patterned film of NMs thickness different from the substrate material, or the surface is consist of pattern film on a substrate (the nanoscale material is either the film or the pattern). The NPs in the third category may be present in four subcategories depending on the environment; the NPs may be bound to another solid structure surface, suspended in liquid, dispersed into a solid, or the NPs can be suspended in air (airborne NPs) (Hansen et al., 2007).

Risk assessment of new materials is traditionally based on a chemicals approach, and so there has also been debate about how to chemically classify NPs and NMs. The many different chemical structures may justify the classification of these materials into some broad chemical categories initially (Jortner and Rao, 2002; Rao, 2004; Handy et al., 2008a; Stone et al., 2010). These chemical classifications of the NPs are shown in Table 1.1.

Table 1.1 Chemical categories of nanoparticles.

Chemical categories	Sub-category	Materials
Carbon based materials	Nanotubes	Single-walled carbon nanotubes "SWCNTS"
		Multi-walled carbon nanotubes "MWCNTS"
	Fullerenes	$C_{60,}$ buckyballs
Metal based materials	Metals	Gold, silver, iron
	Metal oxides	Titanium dioxide, zinc oxide, silicon oxide
	Metal sulphides	Zinc sulphides, copper sulphides
	Nitrides of metals	Silicon, cadmium, tellurium
Organic	Polymers	Polyethyleneglycol, latex
	Dendrimers	Polyamidoamide
Composites	polymer nanocomposites	Multicomponent nanomaterial
	quantum dots	Multicomponent nanomaterial

1.2 Physico-chemical properties of nanoparticles

One of the main concerns about nanomaterials is that their novel properties will lead to new or unknown toxic effects. It is therefore critical to consider the physico-chemistry of NPs in toxicology (Lead and Wilkinson, 2006; Handy et al., 2008a; Landsiedel et al., 2010). There is much research to do on this aspect, but factors of concern include surface area, shape, crystal structure, surface reactivity and how aggregation chemistry influences toxicity (Handy et al., 2008a, Stone et al., 2010, Von der Kammer et al., 2012). NPs can show aggregation behaviour which partly depends on the large surface area proportional to their volume. Particles may form agglomerates (loosely bound particles) which bonded together by weak forces, such as Vander Waals forces, electrostatic forces and surface tension. Alternatively, particles may also form aggregates (groups of strongly connected particles) that are not easily redispersed mechanically (Handy et al., 2008a). These forces are explained by the DLVO theory which is named after Derjaguin and Landau, (1941), and Verwey and Overbeek, (1948). When the NPs aggregate in a solution they should be follow this theory i.e., remain as single particles in a solution, or form aggregates via particle-particle, particle-cluster

and cluster-cluster interactions (Handy et al., 2008a). The theory also predicts that ionic strength (e.g., changes in salinity), and the presence of cations such as Ca^{2+} (e.g., changes in water hardness), or other charged particles will influence this aggregation behaviour (Borm et al., 2006; Handy et al., 2008a, Von der Kammer et al., 2012). There are many physico-chemical properties to investigate in toxicology studies. So far, particular emphasis has been given to the surface area issue. The behaviour of NPs can be influenced by the increased specific surface area (SSA) proportional to the small size of NPs, and this may increase the bioavailability and toxicity of the NPs (Handy et al., 2008a). According to Oberdörster et al. (2007) the dose effect of NMs can be better explained based on the SSA rather than concentration, suggesting the former may be more important in the toxicity of NPs. Similar arguments have been made about surface reactivity, since it is this surface that presents toxic chemicals to the organism. A huge increase in a surface: volume ratio, and hence the presence of more surface molecules should result in more intrinsic toxicity of the materials (Donaldson and Tran, 2004), and for some particles there is evidence that toxicity may be a function of particle size rather than mass concentration (Oberdörster, 2000). Surface charge also is an issue, a study by Schaeublin et al. (2011) showed that gold NPs sized at 1.5 nm, either positively charged, neutral and negatively charged, cause disrupted to the morphology of human keratinocyte cell line (HaCaT); with cell death through apoptosis induced by charged NPs and cell necrosis by neutral NPs. Other studies on invertebrates also emphasized the differences in acute toxicity of NP is dependent on sample preparation and therefore the presence of small or larger aggregates in the test medium (Lovern and Klaper, 2006). The toxicity of NPs may be further influenced by the shape of the materials. Hamilton et al. (2009) showed that anatase nanobelt increased markers of the inflammation detected in bronchoalveolar lavage (BAL) of mice in comparison to those detected with TiO_2 nanospheres in treated animals.

1.3 Routes of exposure

The exposures of humans to manufactured NPs in the environment provide different routes to penetrate the human body, i.e. the skin (dermal penetration), respiratory tract (inhalation), and gastrointestinal tract (ingestion) (Hoet et al., 2004; Oberdörster et al., 2005b; Yah et al., 2012). Humans could also be exposed to NPs through other routes (medical devices, cosmetics, or clinical procedures using manufactured NMs, Nel et al., 2006; Arora et al., 2012). Another possible route of exposure is by parental administration of NPs in the case of biomedical applications like intravenous, intradermal and peritoneal exposures (Yah et al., 2012).

1.3.1 Skin

The skin is the largest organ of the body and interfaces with the environment. The skin is considered as the largest primary defence of the body against external interferences. The skin is directly exposed to NPs through the application of sunscreen creams, cosmetics, skin care products and drug treatments (Oberdörster et al., 2005b; Hagens et al., 2007). Then the NPs could penetrate into the deeper parts of the skin; and have been localized within the epidermal and dermal layers (e.g., Fullerene-based peptides, Rouse et al., 2006; TiO_2 NPs, Gontier et al., 2008).

1.3.2 Respiratory system

Inhalation is considered as the main route of exposure to NPs in humans and recently researchers found different pathogenic effects after inhalation of different manufactured NPs (Oberdörster et al., 2005a; Donaldson et al., 2006; Lam et al., 2006; Song et al., 2009). An *in vitro* study on the exposure of human bronchial epithelial cells (BEAS-2B) to different concentrations of SWCNT (0.06 mg ml^{-1}, 0.12 mg ml^{-1} or 0.24 mg ml^{-1}) for 18 h at 37 ºC showed that SWCNT caused structural and morphological changes, cellular toxicity, apoptosis and induced an oxidative stress effect in the lung (Shvedova

et al., 2003). Other studies showed that the absorption of NPs by the lung epithelium, primarily through the alveolar region, could reach different internal body systems or organs like the spleen, liver, bone marrow, lymph nodes, heart and brain via blood and lymph (Nemmar et al., 2001; Kreyling et al., 2002; Oberdörster et al., 2005a; Hagens et al., 2007).

1.3.3 Gastrointestinal tract (GIT)

Another important route of exposure to NPs is via ingestion. Gastrointestinal tract exposure to NPs could be happening either via an indirect route through the respiratory system after excretion of inhaled particles by the mucociliary escalator and then ingested into GIT (Oberdörster et al., 2005b; Hagens et al., 2007), or directly ingested via food, water, drugs, cosmetics and drug delivery devices (Oberdörster et al., 2005b; Arora et al., 2012; Yah et al., 2012). There is a wide concern about NPs toxicity through food (Tiede et al., 2008; Fröhlich and Roblegg, 2012). Weir et al. (2012) shows that body exposure to TiO_2 via food was on average between 1-3 mg TiO_2/Kg body weight /day depending on the age and dietary habits considered 36% of these particles in nanoscale range.

Absorption of NPs through the gut epithelium have been shown by some studies and with sometimes with evidence of translocatone into other internal organs (Jani et al., 1990; Borm and Kreyling, 2004; Oberdörster et al., 2005a; Oberdörster et al., 2005b; Chung et al., 2010). Koeneman et al. (2010) showed that TiO_2 NP at 10 $\mu g\ ml^{-1}$ and above could cross the human intestinal cell line (Caco-2) and penetrate through the cells via a transcellular vesicular trafficking pathway without disturbing junctional complexes.

Oral and dietary exposures to TiO_2 NPs *in vivo* show some toxic effects to the GIT in different organisms. A study by Wang et al. (2007) indicates some pathology in liver and kidney (hepatic injury and nephrotoxicity) of mice after single oral gavage of

TiO_2 NPs (25 or 80 nm) and observed Ti accumulation in spleen, kidney and lung. However, the dietary exposure of TiO_2 NPs showed less toxicity to the GIT and detected Ti accumulation in different organs (e.g., rat, Jani et al., 1994; fish, Ramsden et al., 2009).

1.4 Toxic effects of NPs on different organisms

Studies on the toxic effects of NPs have been applied to different groups of organisms including human, mammals, birds, fish, invertebrates, plants, as well as bacteria. A number of vertebrates (amphibians and reptiles) still lack information on NPs toxicity to date. Some key findings on different groups of organisms are summarised below.

1.4.1 Mammals and birds

There are many studies on NPs toxicity on mammals, and most of these studies have focused on the respiratory toxicity. Pathologies are observed in rodents after intratracheal instillation or aerosol inhalation of different NPs, including the formation of epithelial granuloma, fibrosis and inflammation according to the type of particle used (Bermudez et al., 2004; Lam et al., 2004; Warheit et al., 2004; Warheit et al., 2006). Lam et al. (2004) showed that exposure of mice to 0.5 mg/mouse of SWCNT induced 56% mortality with lung lesions, necrosis, macrophages and granulomas, interstitial and peribronchial inflammation.

Also, there is NP toxicity detected in liver, spleen, and kidney of mice after dietary exposures (Chen et al., 2006; Wang et al., 2006). Mice exposed to copper NPs via oral gavage demonstrated acute toxicity with pathological damage to kidney, liver and spleen compare to bulk copper; and observed colour changes (staining intensity) in both spleen and kidney with the atrophy of spleen after ingesting nano-copper particles (Chen et al., 2006). While the exposure of adult mice to nano-zinc suspensions showed the symptoms of lethargy, nausea, vomiting and diarrhoea (Wang et al., 2006). Liver

and heart damage, disturbances of energy and amino acid metabolism was observed after oral administration of TiO_2 NP in rats (Bu et al., 2010).

There is a very limited data on NP exposures to birds. All the studies have been focused on silver NPs with no significant effects shown for different parameters (white blood cells, blood enzymes, embryonic growth and development) in broiler chicken or chicken embryo (Grodzik and Sawosz, 2006; Sawosz et al., 2007; Ahmadi and Kurdestany, 2010; Pineda et al., 2012).

1.4.2 Fish, aquatic and terrestrial invertebrates

For the fishes, most of the studies have been on fresh water fish. There is evidence of a range of different toxic effects with some data on the accumulation of NPs in different organs (Oberdörster, 2004; Oberdörster et al., 2006; Federici et al., 2007; Smith et al., 2007; Ramsden et al., 2009; Wu et al., 2010; Fraser et al., 2011; Shaw and Handy, 2011; Jahanbakhshi et al., 2012). Aqueous exposure of rainbow trout (*Oncorhynchus mykiss*) to different sizes of Ag NPs for 10 days resulted in accumulation of silver in the gills and liver with oxidative stress effects found in the gills (Scown et al., 2010). The accumulation of silver in the liver was twice that found in the gills, which suggests that the important route of exposure and uptake of Ag NPs in fish may be via the gut epithelium (Scown et al., 2010).

There are lots of data available on fresh water invertebrates specially in *Daphnia magna* (Lovern and Klaper, 2006; Oberdörster et al., 2006; Lovern et al., 2007; Roberts et al., 2007; Gao et al., 2009). The exposure of *Daphnia magna* to 0.2-10 $mg1^{-1}$ of TiO_2 NPs (10-20 nm) for 48h showed 100 % mortality (Lovern and Klaper, 2006). *Daphnia magna* showed acute toxicity and biomodification when exposed to 20 $mg1^{-1}$ SWCNT (Lipid coated) (1.2 nm) and 100% mortality observed after 48 h (Roberts et al., 2007).

Only a few data have been collected on terrestrial invertebrates (Jemec et al., 2008; Drobne et al., 2009; Wang et al., 2009; Hu et al., 2010; Li et al., 2011). A study

by Li et al. (2011) showed that the exposure of earthworm *Eisenia fetida* to 1000 mg ZnO NP Kg^{-1} agar for short time (96 h) resulted in 100% mortality. However, using the filter paper method demonstrated highest mortality rate with lower concentrations (50 mg l^{-1}). This mortality seemed to decline with increasing exposure concentration (Li et al., 2011).

One study on the marine invertebrate (*Arenicola marina*) lugworm showed a significant decrease in casting rate, as well as increases in cellular and DNA damage after exposure to 1 g Kg^{-1} TiO_2 NP through natural sediments for 10 days. However, no significant effects were seen after exposed to 0.03 g Kg^{-1} SWNT (Galloway et al., 2010).

1.4.3 Plants

Only a few data are available on interaction of NPs with plants (Corredor et al., 2009; Wang et al., 2011; Lee et al., 2012). In a hydroponics study, a slight reduction on root elongation was found in presence of uncoated alumina NPs but not with phenanthrene coated NPs (Yang and Watts, 2005). One study on green algae showed some toxic effects, observed by a growth reduction after the exposure to TiO_2 NPs (Hund-Rinke and Simon, 2006). TiO_2 also induced a positive effect on the growth of spinach, when either administered to the seeds or sprayed onto the leaves (Zheng et al., 2005; Yang et al., 2006).

1.4.4 Bacteria

Toxicological studies of NPs are limited on bacteria, protozoa, and other microbes (Lyon et al., 2005; Adams et al., 2006; Zhu et al., 2006; Zhang et al., 2007; Pelletier et al., 2010). Zhu et al. (2006) showed that the uptake of CNTs by unicellular protozoans induced a dose-dependent growth inhibition. Inorganic NPs (TiO_2, SiO_2 and ZnO) had toxic effects on bacteria (*Escherichia coli* and *Bacillus Subtilis*) represented by

enhancing generation of reactive oxygen species associated with the inhibition of bacterial growth (Adams et al., 2006). In addition, the presence of light was a significant factor for increasing this toxicity (Adams et al., 2006).

1.5 Systemic toxicity

The toxicity of certain NPs could be reaching beyond the site of uptake to the major internal body systems. In most studies, the lethal dose (LD_{50}) may not be estimated because of the difficulty to achieve the high mg levels needed to achieve acute toxicity for many NPs (Handy et al., 2008a). For example, Chen et al. (2006) showed that the LD_{50} determined for 23.5 nm copper NPs and cupric ions in mice exposed via oral gavage were 413 and 110 mg kg^{-1} body weight, respectively. Lovern and Klaper (2006) also suggest that the medial lethal concentration (LC_{50}) level for 30 nm TiO_2 is 5.5 mg l^{-1} in *Daphnia magna*. It is therefore likely that the main concern for NPs will be sublethal effects on the physiology and biochemistry of the animals. Most of the literature on the body systems toxicity of NPs comes from mammalian studies mainly on respiratory exposure, or from *in vitro* cell studies (Handy and Shaw, 2007).

1.5.1 Respiratory system

There is an historic literature on respiratory exposure to ultrafine particles, and arguably, the respiratory route has been investigated the most. Exposure of the respiratory system to NPs has demonstrated lung injury, inflammation and possibly tumour formation in the lung in several studies (Bermudez et al., 2004; Lam et al., 2004; Warheit et al., 2004, 2006). Epithelial cells of the mammalian lung represent a typical mucous epithelial tissue, which is not fundamentally different to the structure of the epithelia of gill or gut of the aquatic organisms, or the body surface of earth worms (Handy et al., 2008b). There is also evidence of the similar epithelial injury observed in fish gill (Federici et al., 2007; Smith et al., 2007; Sun et al., 2009).

1.5.2 Gastrointestinal tract (GIT)

The gut is also an important epithelial tissue, and a potential route of uptake of toxic chemicals. The data on dietary exposure to NPs is currently limited (Panessa-Warren et al., 2006; Arora et al., 2012). However, exposure of mice to 5 g kg^{-1} of zinc NPs (58 nm) caused severe symptoms of lethargy, vomiting and diarrhoea for the first few days and two mortalities after the first week; the dead mice showed aggregation of Zn particles in the intestine (Wang et al., 2006). Federici et al. (2007) reported that the exposure of rainbow trout to 0.1-1 $mg1^{-1}$ of TiO_2 NPs (24 nm) for up to 14 days via the water (stress-induced by drinking contaminated water) caused injuries to the intestine including erosion of the villi, as well as fusion and vacuolation of the mucosa. Ramsden et al. (2009) showed an accumulation of Ti in gut after dietary exposure of rainbow trout to 10 or 100 mg kg^{-1} TiO_2 NPs. The accumulation of arsenic in the stomach and intestine of carp had been significantly increased by 132% in presence of 10 mg l^{-1} TiO_2 NPs after 25 days aqueous exposure (Sun et al., 2007). Effects on NPs on nutritional performance are not currently clear, and data on aspects such as growth rate, functions of digestive enzymes and absorption remain to be determined.

1.5.3 Integumentary system (skin)

There are limited *in vivo* studies that have been conducted on the cutaneous toxicity of NPS. Studies on skin cultures, subcutaneous implantation (1 and 4 weeks) in rats exposed to carbon nanofibers and carbon nanotubes (0.1 mg l^{-1}) observed foreign body granuloma (Sato et al., 2005; Yokoyama et al., 2005).

1.5.4 Cardiovascular and immunology system

Once the NP has crossed the lung (gill), gut or skin it will have access to the cardiovascular system and body fluids. There is little data on the cardiotoxicity of NPs. The heart is very sensitive to oxidative stress and low oxygen conditions (e.g., carbon

monoxide exposure, Patel et al., 2004), and this is a concern for NPs that may be oxidising agents. The administration by oral gavages of 5 mg kg^{-1} TiO_2 NPs (25 and 80 nm) in adult mice produced a significant enhancement of serum lactate dehydrogenase (LDH), and alpha-hydroxybutyrate dehydrogenase (HBDH) suggesting myocardial damage (Wang et al., 2007). The exposure of human red blood cells (cell culture) to 5 µg ml^{-1} ultrafine TiO_2 (30-40 nm) for 4-24 h showed by electronic microscope intracellular NPs aggregates (RBCs uptake) with no morphological changes (no cell damage) (Rothen-Rutishauser et al., 2006).

The intraperitoneal injection of male rats with 1 ml of different concentrations (25, 50 and 100 mg l^{-1}) of cerium oxide NPs showed an immune response to the NPs exposure indicated by the increase in number of white blood cells. Subsequently, increasing the exposure with 200 mg l^{-1} of cerium oxide NPs caused severely reduced numbers of white blood cells compared to the control and other lower exposure concentrations (Hamrahi-michak et al., 2012).

1.5.5 Brain and central nervous system

The effects of NPs on the brain and central nervous system are also a concern. The inhalation of 30 nm MnO_2 NP in rats was associated with elevated levels of Mn in the brain, including the frontal cortex, striatum and cerebellum (Elder et al., 2006). An *in vitro* study by Hussain et al. (2006) indicated the ability of manganese NPs to induce adverse effects in neuronal cells, including loss of cell viability, induction of oxidative stress, and dopamine depletion. Studies on trout brain showed pathological deformations including possible aneurisms or swellings on the ventral surface of the cerebellum after exposure to 0.25 mg l^{-1} SWCNT (Smith et al., 2007). Oberdörster (2004) showed a significant elevation of the lipid peroxidation in the brain after exposure of the juvenile largemouth bass to 0.5 mg l^{-1} C_{60} fullerenes for up to 48 h, but did not include a vehicle control in their experiment.

1.5.6 Internal organs (kidney, liver and spleen) and reproductive system

There is some information on the effects of NPs on internal organs. Exposure of mice to copper NPs (23.5 nm diameter), dosed with different concentrations (108, 158, 232, 341, 501, 736 and 1080 mg kg^{-1}) via oral gavage, induced toxicological effects indicated by significant injuries in the kidney, liver and spleen (Chen et al., 2006). In the kidney, the pathology included swelling of renal glomeruli, degeneration and irreversibly massive necrobiosis of epithelial cells of renal proximal convoluted tubules. In the liver, steatosis around the venae centrals of hepatic tissue was reported and atrophic changes in the spleen (Chen et al., 2006).

In fish, the exposure of rainbow trout to TiO_2 NPs or SWCNT showed minor fatty change and lipidosis in liver cells, and some hepatocytes showed condensed nuclear bodies (apoptotic bodies) (Federici et al., 2007; Smith et al., 2007). After aqueous exposure to 100 and 200 mg l^{-1} TiO_2 NPs for 20 days in carp, different pathologies was observed in the liver including necrotic and apoptosis hepatocytes with depletion of antioxidant enzymes activities and elevation of liver lipid peroxidation (Hao et al., 2009). Ti accumulations were observed in the liver and spleen after dietary exposure of 10 or 100 mg kg^{-1} TiO_2 NPs for up to 8 weeks (Ramsden et al., 2009).

Data on the effects of NPs on reproductive behaviours, gamete production, and reproductive success appear to be lacking. *In vitro* study by Komatsu et al. (2008) found effects on Leydig cells, including changes in cell viability and gene expression after expose of mouse Leydig TM3 cells to diesel exhaust NPs (DEPs), TiO_2 and carbon black (CB) NPs.

1.6 Titanium dioxide NPs (TiO_2)

TiO_2 is a non-combustible and odourless white powder which naturally exists in three mineral structures that include anatase, rutile and brookite crystal forms (Chen and Mao,

2007; Macwan et al., 2011). The anatase and rutile forms are manufactured commercially and both of them have a tetragonal crystal system, whereas the rutile form has a denser arrangement of atoms (Iavicoli et al., 2011). TiO_2 NPs are being used as a white pigment for a wide range of paints, paper, plastic, ceramics, and with the ability to absorb and reflect UV light, it has been used in sunscreens and cosmetics (Aitken et al., 2006; Hansen et al., 2008). These wide applications cause wariness about the ability of TiO_2 NPs to penetrate the human, or animal bodies, by different routes of exposure (Sayes et al., 2006; Wang et al., 2007; Warheit et al., 2007b; Xie et al., 2011) which raise the concern about the toxicity of TiO_2 NPs.

1.6.1 Toxic effects of TiO_2 NPs

Several studies in rodents and aquatic organisms have demonstrated some toxic effects of TiO_2 NPs. Examples of *in vivo* and *in vitro* toxicity data are shown in Table 1.2 and 1.3. Ultrafine-TiO_2 particles have been considered as more toxic than fine particles (Oberdörster et al., 1992; Bermudez et al., 2002; Bermudez et al., 2004; Warheit et al., 2007a). There may also be different biological effects of these materials such as inflammation and fibrosis of the lung (Oberdörster et al., 1992; Bermudez et al., 2004; Warheit et al., 2006), or even lung tumours after chronic exposures (Heinrich et al., 1995), see Table 1.2 and 1.3.

Both the anatase and rutile crystal forms of TiO_2 are toxic (Warheit et al., 2007b), but the anatase crystal form is considered as a superior catalysts, a better generator of reactive oxygen species (ROS), and therefore more cytotoxic compared to the rutile particle form (Uchino et al., 2002; Sayes et al., 2006). The data so far suggests that TiO_2 NPs may be toxic via several mechanisms.

Cytotoxicity of different concentrations of TiO_2 NP have been observed after exposure of the human bronchial epithelial cell line (BEAS-2B), which led to cell death, increases of reactive oxygen species (ROS), and decreased glutathione (GSH) (Park et

al., 2008). Alterations in thiobarbituric acid substances (TBARS), which indicates general changes in oxidative stress, were observed in tissues from trout after exposure to the TiO_2 NP (Federici et al., 2007). TiO_2 NPs in the anatase form produced the most ROS generation and the largest cytotoxic responses following *in vitro* exposures to human dermal fibroblasts or to human lung epithelial cells (Sayes et al., 2006).

TiO_2 NPs may also be neurotoxic. The exposure of mouse brain microglia cells (BV2 cells) to different concentrations of TiO_2 NPs (P25) stimulated the production of ROS by the microglia through an oxidative burst suggesting interference with mitochondrial energy production (Long et al., 2006). Exposure of mice to different concentrations of TiO_2 NP for 60 days via intragastric administration caused brain damage and a decline in behaviours associated with memory of spatial recognition (Hu et al., 2010).

DNA damage has also been observed in several studies (Gurr et al., 2005; Trouiller et al., 2009; Shukla et al., 2011), see Table 1.2 and 1.3. Vevers and Jha (2008) showed the induction of DNA strand breaks (including oxidative damage to the DNA) after the interactive toxic potential of TiO_2 NPs with ultraviolet radiation (UVA) and also lysosomal membrane integrity using neutral red retention (NRR) assay in an established fish cell line.

The exposure to TiO_2 NPs can influence the uptake of other pollutants. For example, there was a 146% increase in the accumulation of cadmium (Cd) in the presence of TiO_2 NPs compared with a control of Cd exposure alone in carp (Zhang et al., 2007) as well as *Daphnia magna* and *Lumbriculus variegatus* (Hartmann et al., 2012). Some of these effects may relate to the surface properties of NPs.

Table 1.2 Toxic effects of TiO_2 NPs *in vivo* on mammals and aquatic organisms.

TiO_2 NPs Information	Dose / Time	Exposure Route	Species	Toxic Effects	Author
Ultrafine TiO_2 average size 21 nm	0.5, 2.0 or 10mg m^{-3} for 6h/day for 5 days a week over 13 weeks	Aerosol inhalation	Mice, rats and hamsters	Pulmonary inflammation in rats and mice (increased number of macrophages and neutrophils) fibrosis in rats, elevated protein and lactate dehydrogenase levels. Bronchoalveolar hyperplasia and metaplasia, pulmonary tumorigenesis	Bermudez et al. (2004)
Ultrafine TiO_2 ~20 nm	104 µg or 200 µg for 24 h	Intra tracheal instillation	Rats	Ultrafine particles TiO_2 increased pulmonary toxicity, as indicated by increased alveolar epithelial permeability (protein leakage), and acute pulmonary inflammation and lung injury.	Oberdörster et al. (1992)
Ultrafine TiO_2 P25 or fine (25-300 nm)	10 mg m^{-3} for 24 months	Inhalation exposures	Rats	Chronic inhalation exposure to10 mg m^{-3} TiO_2 for 24 months causes pulmonary fibrosis and lung tumours.	Heinrich et al. (1995)
TiO_2, rods (~35 nm) and dots (~10 nm)	1 or 5 mg single dose exposure and the recovery up to 3 months	Intra tracheal instillation	Rats	The exposure to nanoscale TiO_2 rods or dots particles produced temporary lung inflammation and fibrosis with cell injury effects at 24 h of exposure. Dots exhibit moderate to severe aggregation while rods are individually separated with little or no aggregation.	Warheit et al. (2006)
Nano sized TiO_2 (25 and 80 nm)	5 g kg^{-1} for 2 weeks	Oral administration	Mice	TiO_2 (25 and 80 nm) groups showed acute toxicity indicated by high coefficients of liver with hepatic injury, nephrotoxicity, myocardial damage and accumulation of TiO_2 particles in spleen, kidney and lung tissue.	Wang et al. (2007)
TiO_2 (21 nm)	60–600 mg l^{-1} for 5 days	Orally via drinking water	Mice	Inflammation, oxidative stress and DNA damage in various tissues.	Trouiller et al. (2009)
TiO_2 (50-120 nm)	5 g kg^{-1} for 7 days	Oral administration	Mice	Liver and kidney damage only in combination with lead acetate.	Zhang et al. (2010)
TiO_2 (5 nm)	5–50 mg Kg^{-1} for 60 days	Intragastric administration	Mice	Brain damage morphological signs, neurobehavioral performance decline and damage of spatial recognition memory behavior.	Hu et al. (2010)

Table 1.2 Continued.

TiO_2 NPs Information	Dose / Time	Exposure Route	Species	Toxic Effects	Author
Ultrafine TiO_2 (21 nm) P25 75% anatase, 25% rutile.	0.1,0.5 or 1.0 mg l^{-1} for 14 days	Aqueous exposure	Rainbow trout (*Oncorhynchus mykiss*)	Mainly the anatase form: gill pathologies including oedema, thickening of the lamellae and injuries with respiratory toxicity and some irritation to the gut showing erosion of the villi tips, fusion and vacuolation of the mucosa epithelium.	Federici et al. (2007)
TiO_2 (50 nm)	0–250 mg l^{-1} for 20 days	Aqueous exposure	Juvenile Common carp (*Cyprinus carpio*)	Exposed the fish to 100 and 200 mg l^{-1} TiO_2 NPs for 20 days caused respiratory distress including oedema and thickening of gill lamellae, liver pathologies including necrotic and apoptosis hepatocytes and oxidative stress.	Hao et al. (2009)
TiO_2 (24 nm)	0-100 mg Kg^{-1} for 8 weeks	Dietary exposure	Rainbow trout (*Oncorhynchus mykiss*)	50% inhibition of Na+/K+-ATPase activity seen in the brain and a 50% reduction in thiobarbituric acid reactive substances (TBARS) in the gill and intestine with Ti accumulation in gill, gut, liver, spleen and brain.	Ramsden et al. (2009)
TiO_2 NPs 30 nm filtered / 100-500 nm unfiltered	0.2-10 mg l^{-1} for 48 h filtered / 50-500 mg l^{-1} unfiltered for 48 h	Aqueous exposure	*Daphnia magna*	100% mortality rate for the filtered and 9% mortality rate for the unfiltered TiO_2 NPs.	Lovern and Klaper (2006)

Table 1.3 Toxic effects of TiO_2 NPs *in vitro*.

TiO_2 NPs Information	Dose / Time	Exposure Route	Toxic Effects	Author
Ultrafine TiO_2 Anatase (10-20 nm) Rutile (200 nm)	10 µg ml^{-1} (about 1.77 µg cm^{-2}) for 1 h	Human Bronchial Epithelial Cells, BEAS-2B	The anatase form was much more toxic than the rutile form which caused DNA damage that detected in treatment with 10 µg ml^{-1} anatase TiO_2 10 nm particles but no damage was detected with 5 µg ml^{-1} anatase TiO_2 10 nm particles or with > 200 nm particles, lipid peroxidation and micronuclei formation (damage to nucleus).	Gurr et al. (2005)
Ultrafine TiO_2 Anatase form 30-40 nm	5 µg ml^{-1} suspension for 4-24 h	Human Red Blood Cells	Electron microscopy showed intracellular NPs aggregates (RBC uptake) with no morphological changes (no cellular damage).	Rothen-Rutishauser et al. (2006)
TiO_2 NPs different sizes	From 3-30 mg ml^{-1} for up to 48 h	Human Lung Epithelial Cells (A549 cells)	Dose-dependent decrease in cellular viability, some lactate dehydrogenase release from cells at the highest concentration. Inflammatory mediators (interleukin 8) induced at the highest concentration.	Sayes et al. (2006)
TiO_2 (˜20nm)	0.25-1.5 mg ml^{-1}	Human Fetal Lung Fibroblasts (HFL1)	Dose dependant manner toxicity effect, mitochondrial dysfunction, apoptosis and morphological modification.	Zhang et al. (2011)
TiO_2 (25 nm)	0.8 µg ml^{-1} and above for 6 h	Human Epidermal Cell Line (A431)	Demonstrate genotoxicity and cytotoxicity of epidermal cells by induces ROS and oxidative stress leading to oxidative DNA damage and micronucleus formation.	Shukla et al. (2011)
TiO_2 P25 (30 nm)	0.2, 2 and 20 mg /cm^{-2} for 24 h	Primary Human Foreskin Keratinocytes [PHFK]	Early keratinocyte differentiation related with decrease cell proliferation and altered the calcium homeostasis.	Simon et al. (2011)
TiO_2 NPs different sizes	10 g l^{-1} water suspension added to the MD exposure for 14-20 h at 36 ºC	*Escherichia coli* and *Bacillus subtilis* in Minimal Davis medium(MD)	Bacterial growth inhibition (increased in presence of light). E.coli showed 72% growth inhibition in cells exposed to 5000 ppm TiO_2, B.subtilis showed 75% growth inhibition with 1000 ppm TiO_2 and 99% growth reduction with 2000 ppm.	Adams et al. (2006)

1.6.2 Mechanisms of TiO_2 toxicity

In addition to surface area, and the chemical reactivity of particular crystal structures, there are several experiments that suggest the possible mechanisms of toxicity. TiO_2 may not be chemically modified inside organisms. For example, hydrophobic TiO_2 formulations are acutely toxic, but there is no significant difference in hydrophilic and hydrophobic functionalized TiO_2 after intratracheal instillation (Rehn et al., 2003). However, one basic toxic mechanism may involve the generation of reactive oxygen species (ROS). TiO_2 NPs have been shown to trigger ROS produced by alveolar macrophages, phagocytes and microglial cells (Olmedo et al., 2005; Long et al., 2006), whereas the ultrafine-TiO_2 (TiO_2 NPs) appears further enhance the formation of ROS in comparison to fine TiO_2 (Scherbart et al., 2011). Under ultraviolet (UV) light, TiO_2 may induce the formation of ROS such as hydrogen peroxide, hydroxyl radicals, and super oxides (Fig. 1.1). These oxygen species may lead to cellular toxicity (Blake et al., 1999) and observed DNA damage resulting in cell death after exposure to TiO_2 NPs (Trouiller et al., 2009; Shi et al., 2010). Apoptosis and cell necrosis have been also reported as cellular toxic effects of nanoscale TiO_2 which may be induced by the formation of ROS (Rahman et al., 2002; Braydich-Stolle et al., 2009; Lapied et al., 2011). This apoptosis that is induced by TiO_2 NPs has been suggested to involve the mitochondrial apoptosis pathway (Shi et al., 2010). Moreover, the phototoxic damage associated with a decrease in cell viability and an increase in the generation of ROS was also indicated after exposure of ARPE-19 cells to TiO_2 NPs under UV light (Sanders et al., 2012). Furthermore, the photocatalytic properties of TiO_2 mediating toxicity have been shown to eradicate cancer cells, and it is hypothesized that TiO_2 NPs accumulation on cell membranes may lead to cell rupture and then cell death (Thevenot et al., 2008).

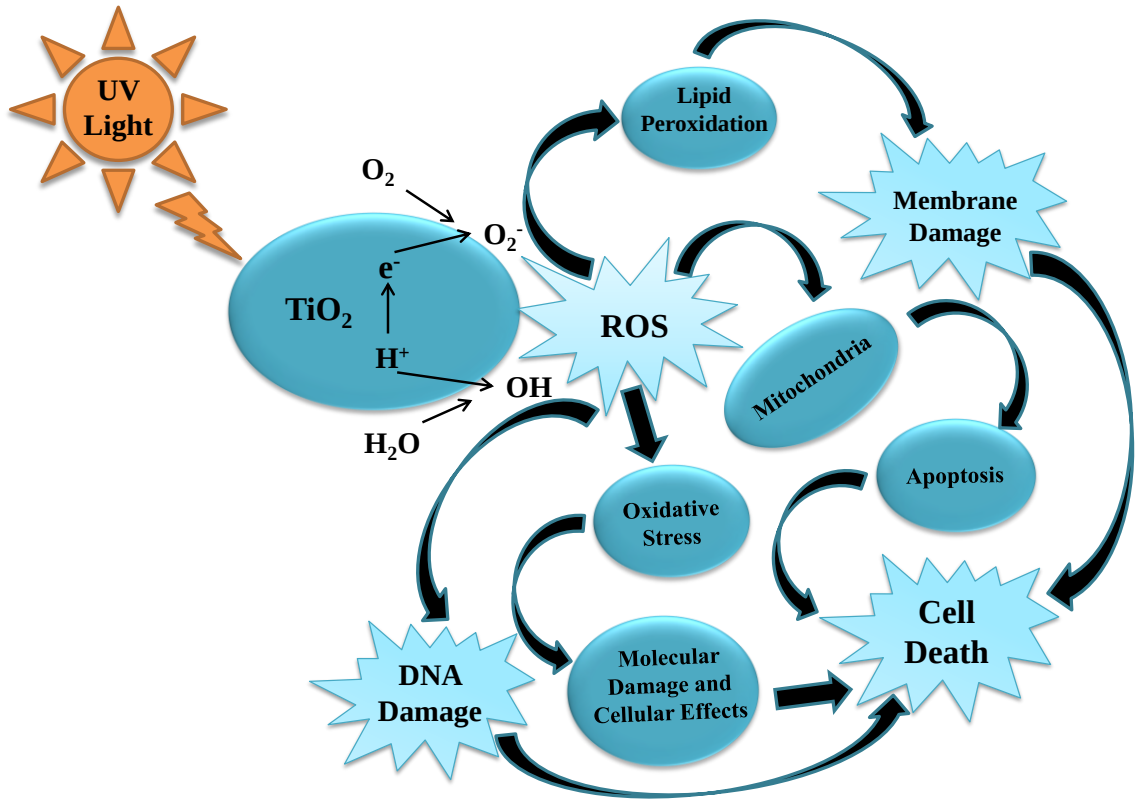

Figure 1.1 Possible toxic mechanisms of TiO_2 and the generation of ROS in the cells after been exposed to UV light, showing the pathways of these oxygen species which may lead to DNA damage, membrane damage and then cell death through different cellular toxic effects.

1.6.3 Oral uptake of TiO_2 NPs and dietary exposure

Bulk TiO_2 powders have been considered safe and used as a digestibility marker (an inert marker in the diet that is not appreciably absorbed) in nutrition studies on a range of animals including fish (Mamun et al., 2007). Recently the nanoscale versions of TiO_2 have been used in personal care products (lipstick, toothpaste, sunscreens) and food (food colours, packaging, food additives E171) (Fröhlich and Roblegg, 2012). This has led to some concerns about oral toxicity of TiO_2 NPs and their uptake through the gastrointestinal tract with potential for subsequent effects on the internal organs. Powell et al., (2010) estimated the intake of TiO_2 NPs through food at about 5 mg person^{-1} day^{-1}. Another estimation via the food by Weir et al. (2012) showed an average daily TiO_2 intake of 1-3 mg Kg^{-1} day^{-1}, about 36% of the TiO_2 was estimated to be in the nanoscale range. Clearly there is a concern that in the long term, this daily intake may cause persistent accumulation of TiO_2 NPs in the human body.

The mechanisms that are involved in the absorption, distribution, metabolism and excretion (ADME) of the NPs remain to be investigated (Handy et al., 2008a) and they are likely to be influenced by different parameters including the aggregation, agglomeration, dispersability, size, solubility, and surface area, charge and other physico-chemistry of the NPs (Stone et al., 2010). The physico-chemical properties of NPs may play an important role in their absorption. Absorption is the first step of biological uptake for substances (Handy and Eddy, 2004). For nanomaterials, the considerations include the aggregation or precipitation of NPs during their adsorption onto the exterior surface of the organisms. There is some reliable evidence that supports this notion through experimental observation, for example, the aggregation of the TiO_2 NPs around the microvilli of the lugworm gut epithelium cells (Galloway et al., 2010). The next step is the uptake of the NPs through the cell membrane and the mechanisms of this uptake are still unclear. The possible uptake mechanisms of NPs through the gut

epithelium are shown in (Fig. 1.2) which is modified from Handy et al. (2008b). The NPs are too large to be taken by ion transports across the cell membranes or by diffusion, however diffusion cannot be excluded for lipophilic NPs. Additionally, the diffusion through the paracellular route is difficult because of the ion-rich environment of the tight junctions with Ca^{2+} and Mg^{2+} which suggests that NPs would aggregate rather than diffuse. The movement of the NPs across the gut epithelium might occurby other processes like endocytotic transvesicular transport, and/or endocytosis by M-cells in the Peyer's patch (Mcclean et al., 1998; Des Rieux et al., 2007). The use of vesicular membrane trafficking systems is seemingly the most probable transport modes.

To date the information on the distribution of the NPs in the body and the target organs has yet to be established. However, the measurement of the NP concentrations in the tissue can be clarified by using inductively coupled plasma mass spectrometry (ICP-MS) (Zhang et al., 2010), and particles can also identify in the tissues using electron microscopy (Scown et al., 2009). So far there is no specific study regarding the metabolism or excretion of the NPs. However, the excretion of the NPs might occur via the process of exocytosis (Handy et al., 2008a). Simon et al. (2011) suggest that the exocytosis of TiO_2 NPs can be mediated by endosomes or other secretory vesicles.

Limited studies have been performed on the toxicity of TiO_2 NPs via oral exposure. Aqueous exposure of rainbow trout to 0 - 1.0 mg l^{-1} TiO_2 NPs for less than 14 days caused an increase in thiobarbituric acid reactive substances (TBARS) in the intestine that suggested the fish suffered from oxidative stress (Federici et al., 2007). Some irritation was observed in the gut showing erosion of the villi tips and also fusion and vacuolation of the mucosa epithelium. The fish with severe injuries showed mucous residue in the lumen with milky colouration, which raises the possibility of TiO_2 NPs causing toxic effects via oral exposure (Federici et al., 2007). The administration of 5 g kg^{-1} body weight of TiO_2 suspension by single oral gavage for 2 weeks in mice has

shown the ability of TiO_2 NPs (25 and 80 nm) to enter the blood circulation leading to damage in both the liver and kidneys with hepatic injury, nephrotoxicity, myocardial damage and accumulation of TiO_2 particles in spleen, kidney, lung tissue and even the brain (Wang et al., 2007). The same observation has been shown after dietary exposure (TiO_2 incorporated in food pellets) of juvenile rainbow trout to 10 or 100 mg kg^{-1} of TiO_2 NPs for 8 weeks which resulted in Ti accumulation in the gill, gut, liver, spleen and brain (Ramsden et al., 2009). All these findings support the potential of nanoscale TiO_2 to be absorbed via the gut epithelium and subsequently pass through to other internal organs after oral administration. An *in vitro* study by Koeneman et al. (2010) provided the evidence of the ability of TiO_2 NPs to cross the human intestinal cell line (Caco-2) at a level of 10 µg ml^{-1} and above. However, the precise mechanism of TiO_2 NPs transfer through the gastrointestinal tract remains to be clarified. Zhu et al. (2010) also raised concerns about potential food chain effects. Their study reported the transfer of TiO_2 NPs from *Daphnia magna* to zebrafish (*Danio rerio*) through dietary exposure.

1.7 In vitro techniques for studying metal uptake

There is a strong demand for the use of *in vitro* techniques in nanotoxicology and studying the uptake mechanisms of NPs. These techniques need to be scientifically robust and ethically sound by reducing the use of laboratory animals for toxicity testing. Low-cost, high throughput *in vitro* toxicity assays should allow detailed examination under controlled conditions of various factors involved in toxicity (Panessa-Warren et al., 2006; Kahru et al., 2008). This will enhance understanding the effects of NPs at the level of physiology and aid in predicting the human health hazards.

The REACH (Registration, Evaluation, Authorisation of Chemicals) legislation aims, since it came into force on the 1st June 2007, to improve the protection of human health and the environment by the better and earlier identification of the intrinsic

properties of chemical substances (Crane et al., 2008). One concern about REACH is that the novel and varied properties of NPs will generate a very large number of "new substances" that need testing. The increasing use of different NPs in a wide range of applications further highlights the need for rapid *in vitro* techniques for testing those NPs. An intelligent strategy of *in vitro* safety testing was proposed by Roszak et al. (2013) for evaluation and prediction of risk assessment of nanomaterials. This includes further steps to check cytotoxicity or genotoxicity potential of TiO_2 NPs. *In vivo* testing is a good starting point for the overall testing strategy, and could start with simple measurements such as an assessment of cell viability.

1.7.1 Perfused organ preparations

These preparations were developed to study physiology at the organ level, and have been used for the isolated perfused heart (Del Nido et al., 1998; Khairallah et al., 2004), isolated perfused liver (Strubelt, 1996; Whihelm et al., 1996), isolated perfused kidney (Frödin, 1975), isolated perfused head (gill) (Payan and Matty, 1975; Perry et al., 1984; Campbell et al., 1999) and isolated perfused intestine (Wapnir, 1991; Handy et al., 2000). Many of these isolated perfused preparations were originally used to study ion transport processes and have advantages over other techniques because the method is rapid, with the avoidance of long periods of ischemia. In addition, the volume of the external medium can be modest (e.g., 150 ml for gill perfusion, Perry et al., 1983; 500 ml for gut perfusion, Handy et al., 2000). These preparations have different layers of tissues, which mimics the situation *in vivo*, allowing the investigation of the uptake and metabolism of different materials. This may be particularly important for testing new substances like NPs. However, some difficulties are encountered with the perfusion techniques such as oedema, leakage of the perfusate and loss of the mucous constituents if the composition of the physiological saline is not carefully considered.

1.7.2 Metal uptake studies using isolated intestine preparations

The isolated gut sac preparation has been used to determine which sections of the gut are involved in metal uptake, and the perfused intestine has been used to measure the uptake kinetics and pharmacology of metal uptake (see Table 1.4). Gut sacs of oesophagus, stomach, pyloric caeca, mid and hind intestine were prepared from the whole gut and filled with the material under investigation and left for up to 4 h of exposure (Handy et al., 2000). The whole gut sac method allows a rapid way to determine in which part of the gut the metal uptake is happening. Studies on the uptake and accumulation of the metals along the gut sac showed that the main accumulation of metals was in the mid and hind intestine with 70% or more being accumulated in the mucosa rather than the underlying muscularis (e.g., copper, Handy et al., 2000; mercury, Hoyle and Handy, 2005).

The isolated perfused intestine technique has been used in both mammalian and fish physiology for many years to study the uptake of ions and water (e.g., Ando et al., 1986), and has also been used for measuring the uptake of toxic metals like copper and mercury (e.g., Handy et al., 2000). The approach involves removing the intestine from the animal, carefully turning it inside out (everted) so that mucosal epithelium is now on the "outside" and can be directly bathed in the external media (usually in a static, stirred bath of a gut saline and gassed with 95% O_2: 5% CO_2 at room temperature, for example, 22 ºC for catfish perfused intestine). This enables the experimenter to change the composition of the bath (i.e., the mucosal or luminal-side solution) so that uptake mechanisms can be investigated by adding, for instance, different concentrations of the test substance or inhibitors to the bath. Criteria for the viability of preparations are achieved by observing the normal morphology, steady appearance of the flow rate, low LDH leak and normal content of Na^+, K^+ and pH in the solution. Only those preparations showing normal contractions after 5-10 min resting in oxygenated saline

and with healthy morphology should be used. All these aspects (from the well preparation of the perfused intestine to good viability criteria with short time gaining results) indicate that perfusion techniques can be used effectively to study the physiology and the uptake mechanism of NPs.

Table 1.4 Uses of the perfused intestine preparations for investigating metal uptake

Perfused Intestine				
Chemical	Concentration	Species	Measured Factors	Author
Copper (Cu)	10, 50, 100 µmol l^{-1} for 2 h at 22 ºC	African walking catfish (*Clarias gariepinus*)	Intestinal Cu uptake, effects of ion-transport inhibitors and manipulating Cl^- gradient.	Handy et al. (2000)
Inorganic mercury (Hg)	0-100 µmol l^{-1} for 4 h	Rainbow trout (*Oncorhynchus mykiss*)	Regional intestinal uptake of Hg, effects of amiloride and Ca^{2+} chelators.	Hoyle and Handy (2005)
Methyl mercury $CH_3Hg(II)$	Different concentrations at 20 or 4 ºC for 1h and 45 min	Channel Catfish (*Ictalurus punctatus*)	Temperature sensitivity, transport mode (active/ passive process or energy dependent).	Leaner and Mason (2002)
Inorganic mercury (Hg) and methyl mercury CH_3Hg	50 ng ml^{-1} for 2 h	Blue crab (*Callinectes sapidus*)	Accumulation and transport mode of each form of mercury in intestine and gill.	Laporte et al. (2002)
Copper (Cu) and Sodium	Cu 31.5 µm (2 mg l^{-1}) in isotonic solutions	Rat	Effect of Na^+ addition on Cu retention, effects of amiloride and furosemide.	Wapnir (1991)
Cu and Competitor Zinc (Zn)/ L-histidine (His)	0.1 mM Cu for 2 h	Juvenile Rats	Effect of competitors (Zn / His group) on Cu absorption, effect of high Na^+ intake and regional accumulation.	Wapnir and Lee (1993)
Inorganic mercury (Hg) and cadmium (Cd)	20 µm Hg at 37 ºC for 0.5 or 3 min	Rat	Jejunal uptake of Hg and Cd, temperature sensitivity and mucosal permeability.	Foulkes and Bergman (1993b)

1.7.3 Human colon adenocarcinoma cell line (Caco-2 cells)

The most popular intestine cell line model is the Caco-2 which was originally obtained from a human colon adenocarcinoma and has several morphological and functional characteristics of the intestinal epithelium including the presence of tight junctions in highly polarised cells (Grasset et al., 1985) and a well differentiated brush border on the apical surface (Hauri et al., 1985). The Caco-2 cell line has been used in different metal studies to assess the uptake mechanisms and toxic effects (Reeves et al., 1998; Han and Wessling-Resnick, 2002; Zerounian et al., 2003).

The use of NPs as drugs and in food has increased interest in studying the transepithelial transport behaviours of Caco-2 cells. The ability of salmon calcitonin (sCT) with biodegradable poly (lactic-co-glycolic acid) (PLGA) NPs to transport from the apical side to the basolateral side and across the monolayer of the Caco-2 cells was shown in comparison with free sCT (Sang Yoo and Gwan Park, 2004). Varied uptake capacity has been observed with different concentrations of biodegradable lactic acid – glycolic acid copolymer (PLGA 75:25) NPs (over 25-800 μg ml^{-1}) and the maximum uptake rate occurred after 4 h exposures of Caco-2 cells (Katsikari et al., 2009). Exposure of the cells to quantum dots (QDs) coated with hydrophilic thioglycolate capping ligands at a concentration of 0.1 mg l^{-1} induced cell death along with disruption of the epithelium monolayer (Koeneman et al., 2009). After exposure of Caco-2 cells to 10 μg ml^{-1} and above of TiO_2 NPs, some alteration occurred to the microvillar organization on the apical surface and an elevation of the intracellular free calcium was noticed with no cell death found or any lethal effects (Koeneman et al., 2010).

1.8 Hypothesis

The hypothesis of this study is that TiO_2 NPs can cross the epithelial layer of the gastrointestinal tract and are then taken up to the blood side using a number of active transport modes (Fig. 1.2). This idea is supported firstly by the translocation of Ti in other systemic organs, with some gut pathology indicated in freshwater fish after *in vivo* aqueous exposure (Federici et al., 2007) and dietary exposure (Ramsden et al., 2009) to TiO_2 NPs, and secondly by the indication of the ability of TiO_2 NPs to penetrate and cross the epithelial lining of *in vitro* Caco-2 cells without disrupting junctional complexes (Koeneman et al., 2010).

In this thesis, the following hypotheses are tested:

i. Bulk TiO_2 and TiO_2 NPs will be uptake by the intestinal tissue through a form of diffusion. This could be tested by the dialysis experiment.

ii. TiO_2 particles might be bind to the strands of mucous in the intestine so that the surface binding experiment will be applied to investigate this process.

iii. Bulk TiO_2 and TiO_2 NPs will be uptake by the isolated perfused intestine of rainbow trout (*Oncorhynchus mykiss*) as well as by the human intestinal Caco-2 cells using an active mode of transport, either by vesicular transport of NPs or through M-cells (Fig. 1.2). Different inhibitors will be used to investigate on the uptake mechanisms mode of TiO_2.

iv. Uptake will occur without loss of tissue integrity. The viability of the perfused intestine can be examined using standard viability markers such as LDH activity, histopathology and flow rate of the perfusion along with the leak of K^+ and Na^+ ions.

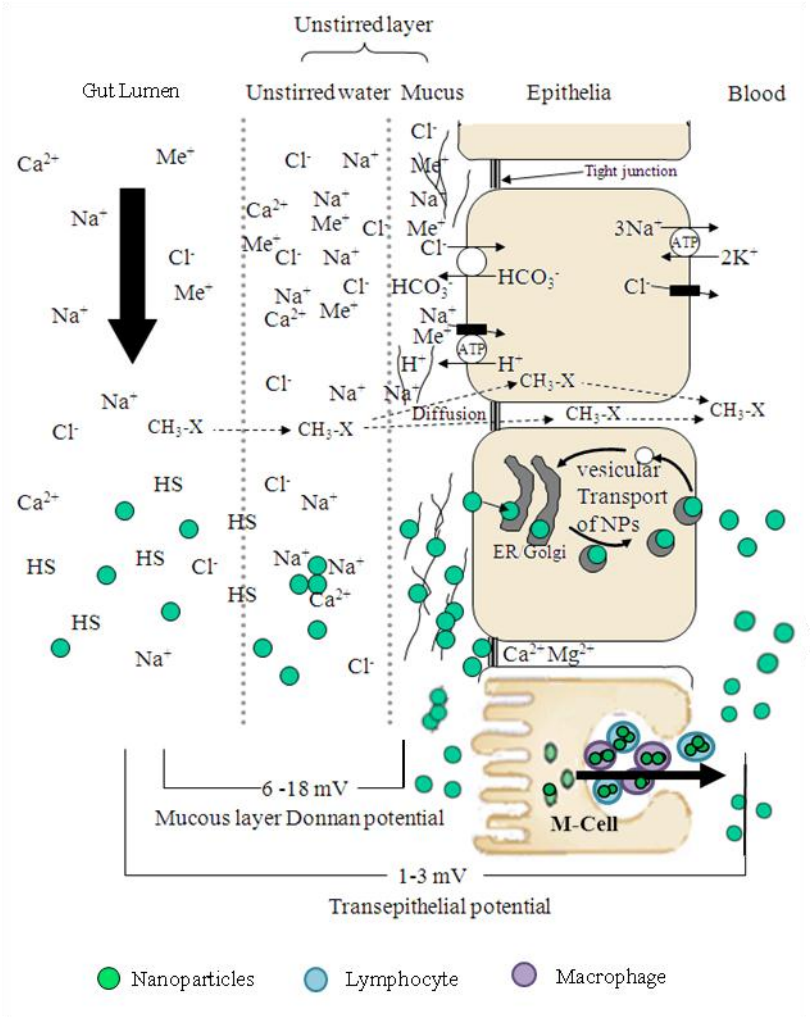

Figure 1.2 An idealised diagram of the freshwater fish gut, showing the mechanisms of uptake for electrolytes, toxic metal ions (Me^{+}), and small lipophilic organic chemicals (CH_3–X), compared to NPs. Modified from (Handy et al., 2008b). The substances in the gut lumen must diffuse into an unstirred layer (USL) comprising of water/mucus secretions, prior to transfer across the gut epithelium. The upper portion of the diagram shows electrolytes and toxic metals ions which diffuse into the USL, and may bind to strands of mucus (mostly polyanionic) where the exclusion of free anions like Cl^{-} from the mucus layer contributes to the Donnan potential at the apical surface. Electrolytes and toxic metal ions usually move through the cell using ion transport pathways. In contrast, small lipophilic organic chemicals can diffuse into the USL and then through the cells (transcellular diffusion), or between the cells via the tight junctions (paracellular diffusion). NPs are too large to be taken up by ion or other transporters on the cell membranes, and although diffusion cannot be excluded for lipophilic NPs. The Ca^{2+} and Mg^{2+} rich environment in the tight junctions suggest that NPs would aggregate rather than diffuse through the paracellular route. Diffusion of charged NPs into the USL will be affected by the Donnan and transepithelial potentials, in a similar way to other charged substances. NP uptake through vesicular transport and M-cells seems likely. The phagocytosis active transports are largely restricted to M-cells in Peyer's patch and play an important role in absorbed the larger particles (NPs aggregates).

1.9 Aims of the research

There is a lack of information on the uptake of NPs along with the mechanisms of this uptake through the gut epithelium of different organisms. The overall aim of this study is to assess the uptake of TiO_2 NPs across the gastrointestinal tract of rainbow trout and humans using the isolated perfused intestine and Caco-2 cells, respectively. TiO_2 NPs are selected because of the wide use of these particles in the food industry and because they are incorporated in many different healthcare products which are in daily contact with humans (Aitken et al., 2006; Weir et al., 2012). Furthermore, some investigations on the physiology, behaviour and possible toxic effects will be conducted to evaluate the hazards of human exposure to TiO_2 NPs.

The specific objectives of the study are:

i. The isolated perfused intestine and the whole gut preparation are suitable to be used in the study of nanoparticles.

ii. Determine which part of the gut is responsible for the TiO_2 uptake using the isolated whole gut sac preparation.

iii. Measure the uptake rate of TiO_2 across the intestinal epithelium of isolated perfused trout gut preparation.

iv. Determine by which mechanism the uptake is happening using different inhibitors.

v. Comparative study between different gas supplement effects on TiO_2 uptake across the intestinal epithelium.

vi. Comparative toxicity, how the above compare to human Caco-2 cells with the consequences for hazard and risk assessment in the environment and for human health by considering the important elements of the environmental risk assessments, including the exposure and the effects (hazard) assessments.

Chapter 2

General Methodology

2.1 Stock animals

Rainbow trout, *Oncorhynchus mykiss*, weighting 295 ± 10 g (mean ± S.E.M., n = 89), were collected from a commercial supplier (Torre Fisheries, Watchet, Somerset, UK). The fish were brought into the aquarium facility at Plymouth University and transported in water aerated with 100% O_2. Fish were then acclimatized in a recirculating system of approximately 6 m^3 of freshwater. Fish were kept in a photoperiod of 12 light:12 dark (on at 8 am and off at 8 pm) and held in dechlorinated Plymouth tap water with an ionic composition as following (mmol l^{-1}): Na^+, 0.43 ± 0.01; K^+, 0.03 ± 0.01; Ca^{2+}, 0.45 ± 0.01; Mg^{2+}, 0.07 ± 0.01 (mean ± S.E.M., n = 71), and the background Ti concentrations in the water was 1 ± 0.1 µg l^{-1} (mean ± S.E.M., n = 8). Water samples were checked daily (mean ± S.E.M., n = 85) for pH, 6.95 ± 0.05; temperature, 15.6 ± 0.3 °C and oxygen saturation, 100 ± 0.3% (HACH HZ40d multi meter); and monitored weekly (mean ± S.E.M., n = 10, in mg l^{-1}) for total ammonia, 0.12 ± 0.02 (HI95715, Hanna Instruments); total nitrite 0.06 ± 0.01 (HI93707, Hanna Instruments) and total nitrate, 3.63 ± 0.64 (HI93728, Hanna Instruments). Where necessary, a 10% trickle of new water was used to top up the recirculation system. Fish were initially fed with a food top dressed with ascorbic acid (vit C) on a normal salmonid commercial diet from EWOS. This was used in animal welfare to aid the recovery of the animals from any transport stress on arrival at the aquarium facility. Then the fish were feed twice daily with (EWOS sigma 50) which they contains: raw material (100 – 40% inclusion), fish meal (25 – 10% inclusion), fish oil 23%, protein 45%, fibre 1.0%, Ash 10%, wheat, soya bean meal, beans, wheat gluten, sunflower meal, vitamins (vit A, 10 000 IU kg^{-1}; vit D, 1750 IU kg^{-1} and vit E, 240 IU kg^{-1}), minerals, copper (Cupric sulphate 8 mg kg^{-1}) and ethoxyquin (an approved antioxidant). Before the experiments, all fish were starved for 48 h to let the gut empty of food and to facilitate the eversion of the gut.

2.2 Preparation of the isolated perfused intestine

Uptake in the preparation is generally recorded in two ways: (i) measurement of the test substance in the gut tissue at the end of the experiment, (ii) measurement of the appearance of test substance on the blood side of the preparation (i.e, in the serosal perfusate). In the latter, which represents transepithelial uptake across the gut into the blood, the perfusate is usually flows constantly in the preparation (via a peristaltic pump) to prevent the system from coming into a diffusional steady-state so that true uptake rates can be measured. In this study the isolated perfused intestine was prepared exactly according to Handy et al. (2000). The fish were humanely sacrificed by a blow to the head and the brain was pithed. The weight and total length of the fish was measured; then the entire intestinal tract (from pyloric caeca to the rectum) was quickly removed. The mass and length were also recorded for the mid and hind intestine together after cutting the tissue at the junction with the pyloric caeca. The gut was then everted, connected to the perfusion apparatus, and bathed in 500 ml of the physiological saline which contained (in mmol l^{-1}) according to Handy et al. (2000): NaCl, 117.5; KCl, 5.7; $NaHCO_3$, 25.0; $NaH_2PO_4 \cdot 2H_2O$, 1.2; $CaCl_2 \cdot 2H_2O$, 5.0; $MgSO_4$, 1.0; glucose, 5.0; mannitol, 23.0; osmolarity ~320 mosm (Osmomat 030, Gonotec) and adjusted to pH 7.4 (Hanna GLP Bench-top pH/mV/ISE/°C meter) with a few drops of 1 mol l^{-1} HCl, at 18°C (a constant room temperature), gassed with 95% O_2: 5% CO_2 (a standard gas mixture used for gut perfusion work, Handy et al., 2000) or with 99.5% O_2: 0.5% CO_2 ("low CO_2" gas mixture). The latter, being closer to the acid-base status of trout *in vivo* (Milligan et al., 1991; Goss et al., 1992). The intestine was serosally perfused (1 ml min^{-1} via an Ismatec peristaltic pump) using the gut saline described above for up to 4 h (Fig. 2.1). This physiological saline is a buffered salt solution which is used for the both sides of the tissue (symmetrical perfusion) and is sufficient to meet the ionoregulatory and acid-base needs of the tissue. Perfusions were conducted in pairs, with a control (no

added TiO_2) and treatment (e.g., + TiO_2 NP or bulk powder) performed each day (n = 6 perfusions per treatment; n = 7 perfusions for the control and TiO_2 NP treatment gassed with the standard gas mix). The eluted serosal perfusate was collected manually in 10 min fractions, and the volume determined gravimetrically. Five ml of the mucosal solution (bath samples) were collected every 30 min for TiO_2 analysis (see below), and the pH was checked. At the end of each experiment the gut was carefully washed in deionised water to remove excess TiO_2, and the surface area of the open gut was measured (manually using graph paper). Samples of each gut were taken for histopathology and electron microscopy. Then the gut was cut into mid and hind sections for trace metal analysis and moisture content (see below), while the perfusate and mucosal solutions were analysed for TiO_2 and biochemistry (see below) (Fig. 2.2).

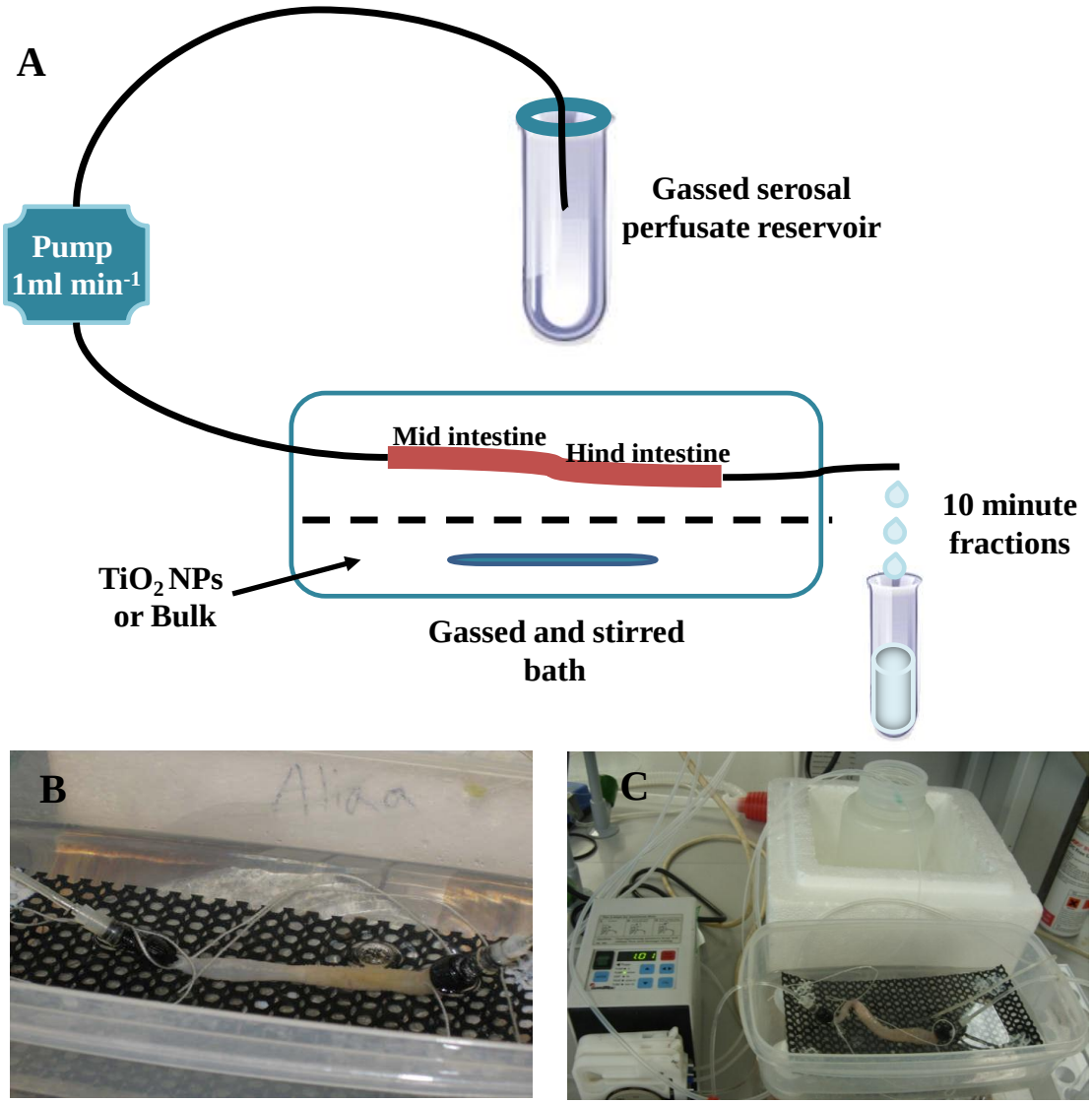

Figure 2.1 Diagram (A) showing the processing and the design of the isolated gut perfusion experiment. The images in (B and C) presents the everted mid and hind intestine bathed into 500 ml of the physiological saline, gassed with 95% O_2: 5% CO_2 or 99.5% O_2: 0.5% CO_2 and serosally perfused with another volume of physiological saline for up to 4 h.

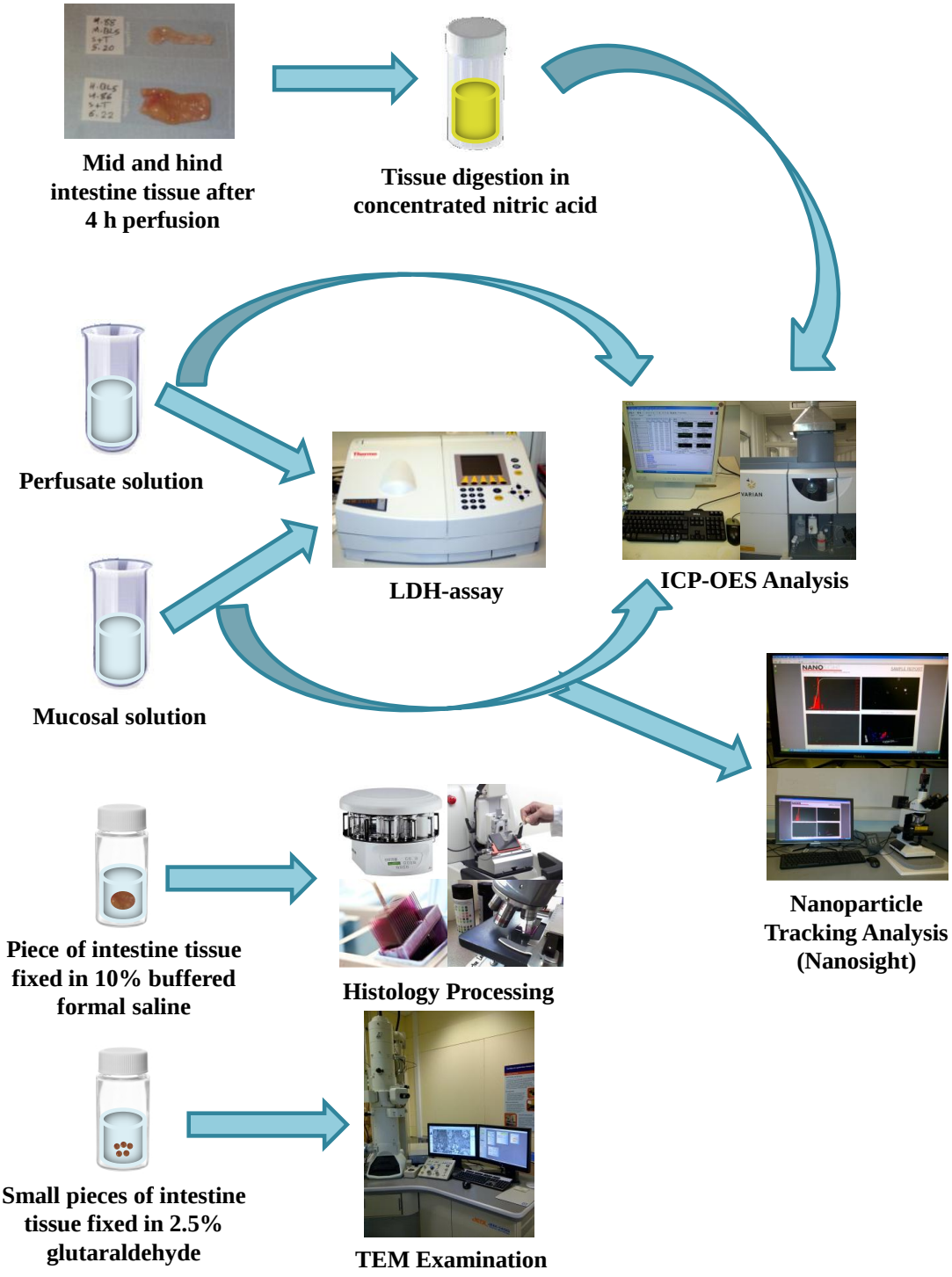

Figure 2.2 Experimental processing of the isolated perfused intestine after a 4 h perfusion. Mid and hind intestine were digested in a concentrated nitric acid and then analysed by the ICP-OES for the Ti and metal concentrations in the tissue. LDH assay was applied to investigate on any tissue damage by testing the perfusate and mucosal (bath) solutions and then those solutions were analysed by the ICP-OES for the Ti and metal concentrations. Distributions of the TiO_2 particles in the mucosal solution were further detected using the nanosight. A piece of intestinal tissue were taken from the middle part of the gut after 4 h perfusion for histopathology and a small pieces also taken from the same area for TEM examination.

2.3 Lactate dehydrogenase (LDH) assay

The routine viability criteria for the perfused intestine preparation are the presence of steady perfusate flow, net efflux of water across the gut in a freshwater fish (see Handy et al., 2000), as well as the LDH leak measurements. In the perfused intestine LDH leak from the tissue is usually low and negligible (Handy et al., 2000) and any elevation of this cytosolic enzyme can indicate tissue damage to the preparation. LDH measurements were done, along with perfusate flow and net water flux, to determine if these criteria also worked for perfusions with nanomaterials. After each experiment all the samples (perfusate and mucosal solutions) were analysed for the LDH activity. The LDH assay was determined by the disappearance of nicotine amide adenine dinucleotide (NADH) at 340 nm (Helios B, Spectrophotometer) resulting from NADH oxidation by pyruvate at 25°C and pH 7.4. According to Campbell et al. (1999), the reaction mixture contained: (i) 2.8 ml of 0.6 mmol l^{-1} pyruvate in 50 mmol l^{-1} phosphate buffers (pH 7.4); (ii) 0.1 ml of 0.6 mmol l^{-1} NADH solution; (iii) 0.1 ml of sample then mixed directly in a 3 ml cuvette. The reaction was allowed to proceed for 2 min and the LDH concentration calculated using an extinction coefficient of 6.3 for a path length of 10 mm. LDH activity is expressed as IU ml^{-1} (equal to µmol min^{-1} ml^{-1}) for individual samples and as IU (µmol min^{-1}) for the cumulative activity of the LDH. The samples and blanks were compared with an LDH standard (0.1 ml of 10.66 IU ml^{-1}). Typically, in perfused organ preparations from fish, the maximum LDH release into the media from a normal healthy tissue would not exceed 1 IU ml^{-1} and the data for all samples here were below this value (see results).

2.4 Trace metal analysis

The methodology for trace metal analysis in tissues was based on the original nitric acid digestion method of Handy et al. (2000) for fish intestine, but with some novel

modifications that enable detection of Ti from intact TiO_2 NPs dispersed in the tissue digest without the need for aggressive hydrofluoric acid or hot sulphuric acid digestion (see Lomer et al., 2000 for the traditional H_2SO_4 method for foods) to completely dissolve the Ti metal (Ramsden et al., 2012 in review, and patent pending, UK Patent application No: 1207745.9). The modification presented here involved adding Triton X-100 to a diluted the nitric acid digest, and with mixing/shaking it was possible to get good nebulisation of the sample in the spray chamber of the inductively coupled plasma optical emission spectrometer (ICP-OES, Varian 725 ES) to detect both the total Ti metal concentrations from the NP exposure and other dissolved trace metals in the sample. Briefly, tissues from all experiments were oven dried to a constant weight at 100 °C for up to 48 h (Gallenkamp Oven BS Model OV- 160), then the samples were transferred into 20 ml scintillation vials (VWR International Ltd, Poole, UK) and digested in 1 or 4 ml (depending on tissue weight) of concentrated nitric acid for 3 h at 70 °C in a water bath. The digested samples were allowed to cool, and then Triton X-100 was slowly added to each digested with Milli-Q water (ultra-pure ion free water) to achieve a final volume of 2% Triton X-100 in each sample. Typically this involved carefully adding around 3.2 or 0.8 ml of 10% Triton X-100 and diluting to a final volume of 16 or 4 ml (for tissue weights of ~1g or 0.1g respectively). Digests were then analysed for total Ti metal, Na^+, K^+, Ca^{2+} and Mg^{2+} concentrations by ICP-OES. Critically, samples were mixed immediately before introduction to the instrument (30 min, KS501 digital orbital shaker, IKA Labortechnik; set at 145 r min^{-1}, or vortexing for 10 s IKA MS2 Minishaker; set at 2500 r min^{-1}), depending on the size/shape of the test tubes used. The instrument detection limit (3 x standard deviation of the blank) for measuring the gut salines or matrix matched standards was calculated as 1.920 µg l^{-1} (equivalent to 0.04 µmol l^{-1} of Ti metal), and for the entire digestion protocol (procedural blank) was 4.925 µg l^{-1} (equivalent to 0.1 µmol l^{-1} of Ti metal, and for a

typical 0.5 g tissue sample equates to 0.0032 µmol Ti metal g^{-1} dry weight of tissue). The optimised protocol gave good spike recovery for fish tissue (e.g., mean ± SEM, *n* = 6-13; 97.5 ± 2.9% for spiking with Ti metal, and 92.2 ± 1.4% for spiking with TiO_2 NPs) and low coefficients of variation within and between tissue samples from different stock fish (around 5% or less for repeats of the entire protocol). Calibrations with different concentration of Triton-X100 in standards had a negligible effect (no problems with instrument calibration with metals standards or TiO_2 dispersions, Ramsden et al., in review).

Tissue Ti levels are reported as µmol of Ti metal g^{-1} dry weight, being converted to molar units in order to allow comparison with gut perfusion studies in the epithelial physiology literature and previous Ti measurements in trout tissue (see Federici et al., 2007). The bath solution was measured for Ti to confirm the TiO_2 dosing and for convenience the data are reported as mg l^{-1} of TiO_2 (for the bath solution only) after correcting the Ti metal data using the stoichiometry of the compound (Ti content of TiO_2 as 60% of the mass). All other data are reported as total Ti metal concentrations (in the tissues and eluted perfusates). The moisture content of tissues was determined by taking the weight of the tissue before and after oven drying and calculated as: ((wet weight – dry weight)/wet weight) x 100. The mucosal solutions from all experiments were also analysed using a flame photometer (Corning 480) for Na^+ and K^+ concentrations. The latter instrument burns the sample in an air/acetylene flame, and detects changes in absorbance due to the colour intensity of each element (Domingo and klyne, 1949). The absorbances are converted to metal concentrations by the software in the instrument using standards and the application of the Beer-Lambert law.

2.5 Preparation of titanium dioxide NP and bulk stock solutions

A 1 g l^{-1} dispersion of bulk TiO_2 was prepared from 1 g of TiO_2 powder (ACROS, Titanium (IV) oxide, New Jersey, USA; manufactures information: purity of 98.0-

100.5% TiO_2). The manufacturer's technical support indicated a crystal structure mixture of more anatase than rutile, but could not report the exact proportions. Counting of crystal shapes on our electron microscopy images (n = 10 random pictures) indicated 25.3% rutile and 74.7% anatase. The powder was dissolved and stirred (Stuart magnetic stirrer, set at half speed) in 1 litre of ultrapure Milli-Q for 20 minutes. The particle size was determined by two independent methods. First, sub samples of the 1 g l^{-1} stock dispersion in ultrapure Milli-Q water (stirred for 20 min) were examined using transmission electron microscopy (TEM, JEOL-JEM.1400) and examples of the particles are shown in (Fig. 2.3A) with a primary particle size measurement of 147 ± 9 nm (mean ± S.E.M., n = 148), while the aggregates viewed by electron microscopy were typically 1124 ± 331 nm (mean ± S.E.M., n = 9). The second approach for particle sizing was nanoparticle tracking analysis (NTA, using a Nanosight LM 10, Nanosight, Salisbury, UK, laser output set at 30 mW at 640 nm). In order to measure particle size distribution by NTA the initial stock dispersion (1 g l^{-1}) was diluted to 1 mg l^{-1} in the physiological saline used for gut perfusions (see below) to account for matrix effects on aggregation (0.5 ml of the initial stock into 500 ml of saline, stirred as above), and the resulting dispersion gave a mean values of (hydrated radius) 166 ± 20 nm for the average particle size and 84.7 ± 19.4 nm mean of the smallest size bin of the particles (mean ± S.E.M., n = 3) (Fig. 2.3C). The mucosal samples from the end of the experiments using 1 mg l^{-1} bulk TiO_2 were also analysed for Ti distribution using the Nanosight LM10 (see results, Fig. 2.3E).

The stock material of TiO_2 NP used here was the same as that used by Federici et al. (2007). The powder form of ultrafine titanium dioxide NP type "Aeroxide" P25 (DeGussa AG, supplied by Lawrence Industries, Tamworth, UK) with (revised manufactures information): a crystal structure of 25% rutile and 75% anatase TiO_2, purity was at least 99% TiO_2 (maximum impurity stated was 1% Si), the average

particle size was 21 nm with a specific surface area of 50 ± 15 m^2 g^{-1}. Chemical analysis of stock dispersions revealed no metal impurities (below the detection limit so the data are not shown), and the batch purity was high. A stock dispersion of 10 g l^{-1} TiO_2 NPs was made (no solvents) by dispersing the NPs in ultrapure Milli-Q water with sonication in a bath-type sonicator (500 ml of stock, 35 kHz frequency, Fisher brand FB 11010, Germany) for 6 h. A 1 g l^{-1} TiO_2 NPs stock solution was prepared from the stock above by diluting 10 ml to 100 ml in ultrapure Milli-Q water, and sonicated as above for 6 h. This second stock dispersion was used for dosing the perfusion bath. Transmission electron microscopy showed the structure and the measured primary particle size of 22.8 ± 0.6 nm (mean ± S.E.M., *n* = 169), while the mean size of aggregation of NPs were 121.7 ± 19.7 nm (mean ± S.E.M., *n* = 8; Fig. 2.3B) with similar crystals showing as the bulk TiO_2. These measurements were very similar to that reports for TiO_2 NPs in Federici et al. (2007). The dosing of the bath was as above for the bulk material, and the distribution of the 1 mg l^{-1} TiO_2 NPs in the physiological saline prior to the start of experiments was also confirmed by NTA. The mean values for particle size were 117 ± 17 nm and the smallest size bin of particles had a mean of 35 ± 5 nm (mean ± S.E.M., *n* = 3; Fig. 2.3D). The mucosal samples from the end of the experiments following expose to 1 mg l^{-1} TiO_2 NP were also analysed for Ti concentration using the Nanosight (Fig. 2.3F).

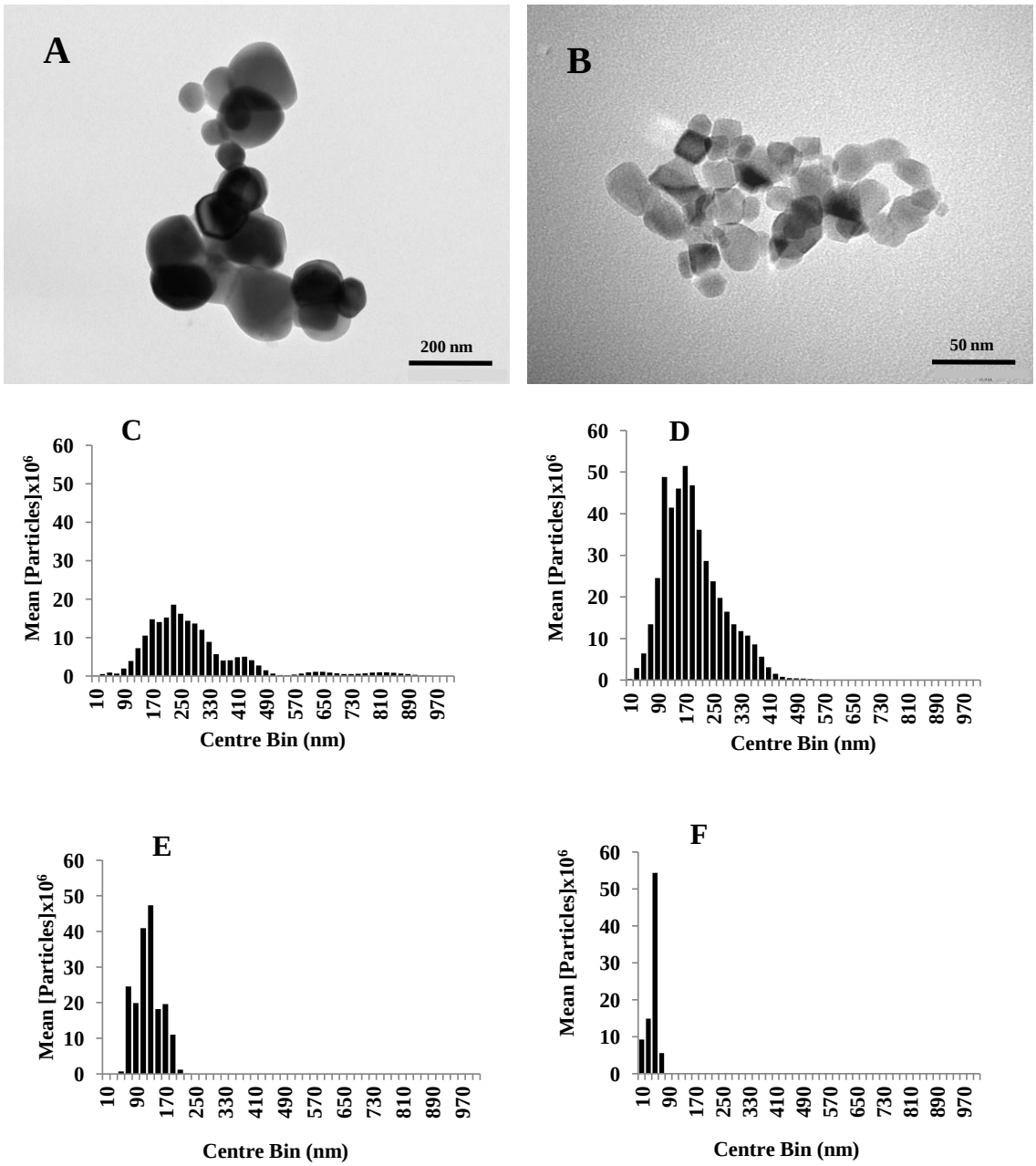

Figure 2.3 Electron micrographs showing (A) bulk and (B) nano TiO_2 particles in a 1 g l^{-1} stock dispersion. Particle size distributions measured by nanoparticle tracking analysis (NTA) are shown below; (C) bulk TiO_2 and (D) TiO_2 NPs in a 1 mg l^{-1} stock dispersion in physiological saline (without the gut present); (E) bulk TiO_2 and (F) TiO_2 NP in the same mucosal solution samples at the end of a 4 h intestinal perfusion, graphs are individual examples from triplicate measurements of each.

2.6 Histology and transmission electron microscopy

After each perfusion a piece of tissue from the middle of each preparation (so as to avoid the ends attached to the apparatus) was carefully collected for light microscopy (*n* = 6 perfusions per treatment; *n* = 7 perfusions for the control and TiO_2 NP treatment gassed with the standard gas mix). Histology was performed according to (Handy et al., 2002b). Briefly, tissues were rinsed and fixed in 10% buffered formal saline for at least 48 h, dehydrated in graded ethanol solutions to remove excess water, and cleared in three graded series of xylene for 1 h each prior to embedding in paraffin blocks. Dewaxed sections (8 μm) were stained with haematoxylin and eosin. Slides were examined using light microscopy (Olymus Vanox - TAH2) and photographs were taken using a digital camera (Olympus camedia C-2020 Z).

For the transmission electron microscope investigations, small fragments from mid and hind intestine (*n* = 3 per treatment) were fixed in glutaraldehyde (2.5%) at low temperatures (4 °C), buffered in 0.1 M sodium caodylate pH 7.2 and post-fixed in osmium tetra oxide 2% (OsO4). The pieces were then dehydrated in a graded series of ethanol and infiltrated with a graded series of Spur's resin. Embedding as a small capsule was performed using pure resin. Thin sections were cut and stained with 2% uranyl-acetate and lead citrate (Au et al., 1999), then examined by transmission electron microscope (TEM, JEOL-JEM.1400).

2.7 Calculations and terminology

All calculations on uptake rates were performed according to Handy et al. (2000). Briefly, data were graphically presented as the absolute cumulative appearance of Ti metal in the perfusate, plotted against exposure time for example perfusions; and with cumulative perfusate flow shown on the same graph. The absolute Ti content of each 10 min fraction (μg) was calculated by multiplying the total Ti metal concentration in each

tube (µg ml^{-1}) by the total volume of perfusate/tube (ml). Ti contents of each fraction were summed for the cumulative plots (reported as nmols absolute of Ti metal). The initial (first 10 min) and overall (240 min) net Ti flux rates ($J_{net,Ti}$, in nmol g^{-1} dry tissue h^{-1}) to the serosal perfusate were calculated from the perfusate Ti content (in nmol) divided by the tissue dry mass and corrected to 1 h, while the initial (first 10 min) and overall (240 min) net water flux rates ($J_{net,\ H2O,}$ in ml g^{-1} dry tissue h^{-1}) to the eluted perfusate were calculated from the differences between the rates of cumulative perfusate and effluent flow divided by the tissue dry mass and corrected to 1 h. In the present study, precise terminology were used for the absolute amounts of Ti metal in the perfusates (nmols, not a concentration), the concentration of total Ti metal in the tissue (µmol g^{-1} dry weight of Ti metal, not TiO_2 compound), and distinguish this from the mg l^{-1} of TiO_2 compound added to the bath when confirming the exposure. The phrase "total Ti metal concentrations" is used to mean the total mass concentration of Ti (not TiO_2 compound) in the tissue or relevant salines determined by ICP-OES, it does not infer anything about whether the Ti is present as particulate TiO_2 or as a dissolved Ti species. The term "Ti accumulation" is used to mean a net increase in the total Ti metal concentration in the tissue over time, determined by ICP-OES of the tissue digests. The phrase "Ti uptake" is used specifically to mean the net uptake of total Ti metal to the serosal compartment in relation to the flux calculations above. Again, this relates to ICP-OES measurements of Ti in the perfusates and does not infer anything about whether the Ti is taken up as particulate TiO_2 or as a dissolved Ti species. In relation to the dialysis experiments, the phrase "apparent total dissolved Ti" is sometimes used to mean the total Ti metal concentration in the aqueous phase of the beaker that has passed through the dialysis membrane. Dispersed TiO_2 particles are therefore distinguished from the apparent total dissolved Ti metal in the text.

2.8 Statistical analysis

All data were presented as mean ± S.E.M (standard error of mean) and analysed using Stat Graphics Plus Version 5.1 while figures were drawn using Excel or sigmaplot 12.0. The data (treatment and time effects) were tested after checking for kurtosis, skewedness, and unequal variance (Bartlett's test). Parametric data were tested by one-way ANOVA followed by the least squares difference multiple range test. Non-parametric data that could not be transformed were tested using the Kruskal–Wallis test (analysis by ranks) and differences were located using notched box and whisker plots. The Student's *t*-test was used as well to investigate the differences between pairs of data, or the Mann-Whitney U test where appropriate for non-parametric data. All statistical analysis used a 95% confidence limit, so that *P*-values equal to or greater than 0.05 were not considered statistically significant.

Chapter 3

Uptake of titanium from TiO_2 nanoparticle exposure in the isolated perfused intestine of rainbow trout, (*Oncorhynchus mykiss*) with novel CO_2 components

Abstract

In vivo studies have raised concerns that titanium dioxide nanoparticles (TiO_2 NPs) may be taken up across the gut of fish, but there are limited data on the uptake kinetics. Whole gut sacs and the isolated perfused intestine of rainbow trout (*Oncorhynchus mykiss*) were used to determine the parts of the gut involved in absorption, and the intestinal uptake rates of Ti from TiO_2 NPs across fish gut. Differences between bulk and nanoscale TiO_2, and the effects of varying the CO_2 content of the perfustae were also examined. Luminal exposure of whole gut sacs to 1 mg l^{-1} TiO_2 NP for 4 h caused accumulation of Ti in the hind and mid intestine, with 80% or more of the Ti in the mucosa, rather than underlying muscularis. Perfused intestines exposure to 1 mg l^{-1} TiO_2 NP or the equivalent bulk powder in the mucosal solution for 4 h gassed with 95% O_2 :5% CO_2 showed a time-dependent accumulation of Ti in the serosal perfusate with a maximum initial uptake rate (mean ± S.E.M., n = 6 for the bulk TiO_2; n = 7 for the control and TiO_2 NP treatment) of 1.55 ± 0.33, 0.98 ± 0.47, and 0.23 ± 0.16 nmol g^{-1} h^{-1} for TiO_2 NPs, bulk powder, and no-added Ti controls, respectively (statistically significant differences on all treatments, ANOVA or Kruskall-Wallis test, $P < 0.05$) demonstrating NP translocation across the gut into the blood side. Notably, there was at least a 10 fold increase in Ti from TiO_2 NPs uptake to 21.16 ± 18.9 nmol g^{-1} h^{-1} (mean ± S.E.M., n = 6) when the CO_2 content of the perfusate gas was reduced to 0.5% (statistically significant, t-test, $P < 0.05$). In conclusion, the TiO_2 NPs are mostly absorbed across the mid and hind intestine, the uptake rate for Ti from TiO_2 NPs across the intestine being much faster than the bulk powder, and the uptake mechanism(s) involve a CO_2 sensitive component across the mucosal membrane.

3.1 Introduction

The wide applications of TiO_2 NPs in food and different consumer products arise from the unique physico-chemical properties of TiO_2 at the nanoscale including its stability, photocatalytic properties, and bright whiteness as a pigment (e.g., Allen et al., 2002; Krischok et al., 2002). The respiratory toxicity of TiO_2 NPs is relatively well established in mammals (Bermudez et al., 2004; Warheit et al., 2006) and waterborne exposure of fish gills to metallic NPs also causes pathology of the respiratory epithelium (TiO_2 NPs, Federici et al., 2007; Cu NPs, Griffitt et al., 2009).

For exposure via the gut, fish that drink water containing 1 mg l^{-1} TiO_2 NP show irritation to the gut mucosa with erosion of the villi tips, fusion and vacuole formation in the mucosal epithelium (Federici et al., 2007). However, dietary exposures to TiO_2 NPs in the food are much less toxic, and trout readily eat diets containing 10 or 100 mg kg^{-1} of TiO_2 NPs for 8 weeks with a normal growth rate and haematology (Ramsden et al., 2009). The latter study also showed Ti accumulation in some of the internal organs, suggesting dietary uptake across the intestinal epithelium of either Ti metal or TiO_2 NPs. This internal uptake suggests that TiO_2 NPs do cross the gut. The uptake of TiO_2 NP across gills and gut epithelium had also been suggested from the appearance of metal from metallic NPs in waterborne studies (Federici et al., 2007; Griffitt et al., 2008; Hao et al., 2009), supports the notion of possible NP transfer across gill epithelia with the ability of NPs to cross cell membranes (Geiser et al., 2005) and penetrate into and through the cells without disrupting junctional complexes (Koeneman et al., 2010). Metallic NPs have also been located on or in gill epithelial cells of trout using coherent anti-Stokes Raman scattering (CARS) (Johnston et al., 2010). However, precise information on the rates of uptake of TiO_2 NPs across epithelia is lacking, especially for the intestine.

The aim of current study was to determine which part of the gut was involved in the Ti accumulation from an exposure to TiO_2 NPs by using isolated whole gut sacs (Hoyle and Handy, 2005), and then to measure the total Ti uptake rates based on total metal concentrations in perfusates using the isolated perfused intestine (Handy et al., 2000). These long-established *in vitro* preparations of intact intestinal tissue allow easy manipulations of the external media to measure concentration-dependent uptake. An additional aim was also to demonstrate the utility of the perfused intestine preparation for studies with manufactured NPs, and to show that viability criteria and other measurements relating to physiological function could be met. Finally, the work also aimed to explore changes of the composition of the media for NP studies by using different gas mixtures to reveal a CO_2-sensitive component to metal uptake from particle exposure that has not been previously reported.

3.2 Methodology

3.2.1 Preparation of the whole gut sacs

Whole gut sacs were used to determine which parts of the gastrointestinal tract are mainly involved in Ti absorption from TiO_2 exposure and prepared according to Hoyle and Handy (2005) derived from the original method of Handy et al. (2000). This well-established physiological technique involves removing the whole gut from the animal, filling the lumen (according to the size of the gut trying not tighten the pressure inside the gut) with the test substance of interest, and then suturing closed the different anatomical parts of the gut so that regional uptake into the tissue can be measured over a few hours (Fig. 3.1). Fish were humanely sacrificed by a blow to the head and the brain was pithed. The weight and total length of the fish was measured; then the entire gastrointestinal tract was carefully removed, washed and flushed through with the physiological saline (described below). The gut was sutured closed at the posterior end,

and the lumen filled with 1 mg l^{-1} TiO_2 (NP, Bulk, or no added TiO_2 control as appropriate) in physiological saline which contained (in mmol l^{-1}): NaCl, 117.5; KCl, 5.7; $NaHCO_3$, 25.0; $NaH_2PO_4 \cdot 2H_2O$, 1.2; $CaCl_2 \cdot 2H_2O$, 5.0; $MgSO_4$, 1.0; glucose, 5.0; mannitol, 23.0; osmolarity ~320 mOsm (Osmomat 030, Gonotec) and adjusted to pH 7.4 with a few drops of 1 mol l^{-1} HCl, at 18 °C, gassed with 95% O_2: 5% CO_2. The concentration of 1 mg l^{-1} TiO_2 was chosen because it may be physiologically relevant and to compare it with previous work on TiO_2 by Federici et al. (2007). Then the gut was closed with a suture around the upper end of the oesophagus, and further sutures applied to separate each region of the gut (oesophagus, stomach, pyloric caeca, mid and hind intestine) according to Hoyle and Handy (2005). The gut was then bathed with 500 ml of the same physiological saline (no added TiO_2). The bath (serosal side) was continuously stirred and gassed with 95% O_2: 5% CO_2 at 18 °C for 4 h. The 4 h duration time for this experiment was chosen following the previous metal perfusion studies which indicated saturable uptake within 4 h (e.g. Cu in catfish gut, Handy et al., 2000; Hg in trout gut, Hoyle and Handy, 2005). After each experiment the gut was carefully opened and washed with deionised water to remove excess TiO_2, then divided into sections of intact oesophagus, stomach, pyloric caeca, mid and hind gut for metal analysis and histology (see below). In some experiments, each part of the gut was further divided longitudinally into two equal parts; one part was stripped of the mucosa, while the other part was left whole, to enable calculation of the relative proportion of Ti in the mucosa and underlying muscularis (Hoyle and Handy 2005).

A full description of the isolated perfused intestine, LDH assay, trace metal analysis, and the stock TiO_2 solution preparations, stock animals, histology with TEM, calculations and statistical analysis were found and explained in details in Chapter 2.

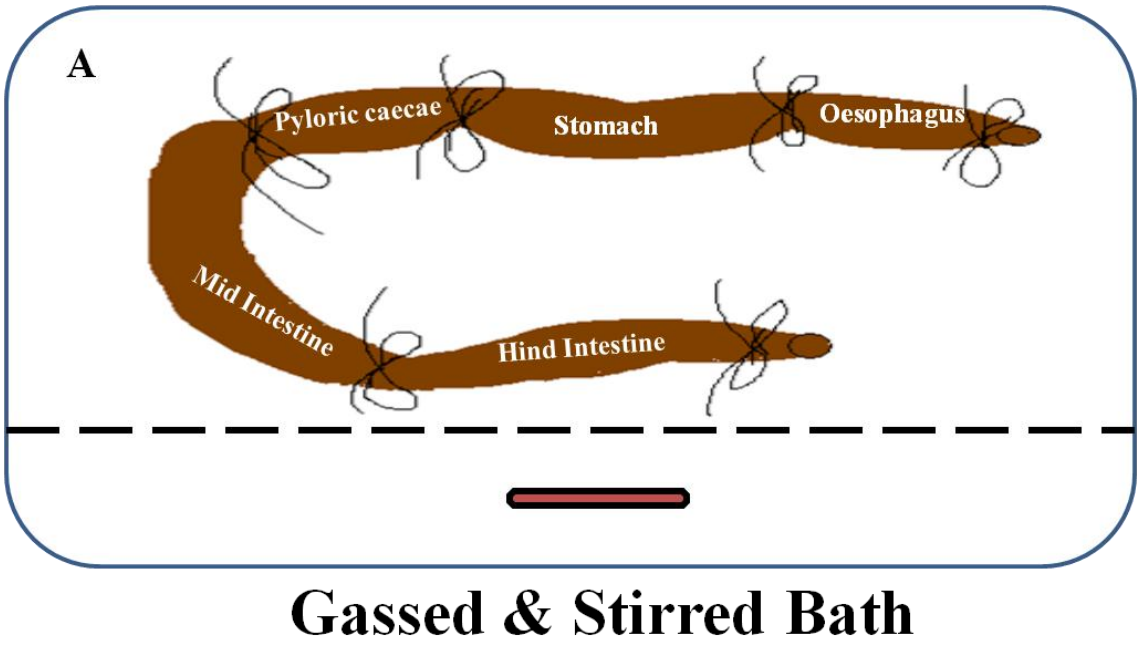

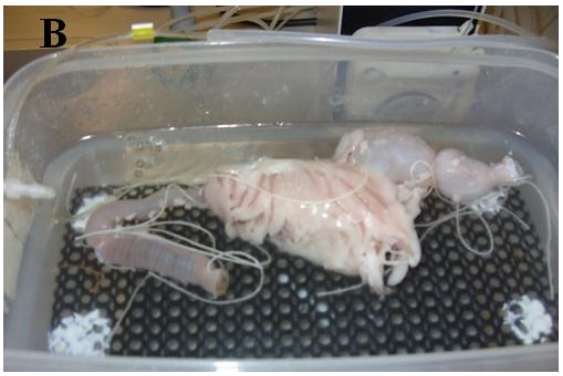

Figure 3.1 An ideal diagram of the whole gut sac preparation technique (A). The images (B and C) shows the different parts of the gut filled with the exposure material, sutured close each part separately and bathed into 500 ml of physiological saline, continuously stirred and gassed with 95% O_2: 5% CO_2 for up to 4 h incubation.

3.3 Results

3.3.1 Ti accumulation by whole gut sacs experiment

The whole gut sac preparation was used to determine which regions of the gut were accumulating Ti from TiO_2 exposures (Table 3.1). All regions of the intact gut showed statistically significant elevations of total Ti metal concentrations in the tissues from exposure to the bulk TiO_2 compared to the unexposed control, with the greatest increases in the mid and hind intestine (Kruskal-Wallis test, P = 0.009 and 0.006 for mid and hind intestine respectively, Table 3.1). Elevations of total Ti metal concentrations in the tissues were also observed for nanoscale TiO_2 exposures in all regions of the gut, and unlike the bulk material there were no statistically significant differences between the regions of the gut in the TiO_2 NP treatment (ANOVA, P = 0.25, Table 3.1). Within each region of the gut there was no material-type effect (comparison of bulk versus nano treatment, ANOVA or Kruskal-Wallis test, $P > 0.05$) on the tissue total Ti metal concentration. Comparison of the proportions of total Ti metal concentrations in the mucosa and underlying muscularis of stripped gut confirmed that most (74% or more) of the background Ti in the gut of control animals was in the mucosa. Similar observations were made for guts exposed to TiO_2 NPs and bulk TiO_2 (Table 3.2). However, for bulk TiO_2 the proportion of Ti in the mucosa of the mid intestine was only 54% and even less for the hind intestine; both gut regions being much lower than the TiO_2 NP treatment which showed 71% or more of the tissue total Ti metal concentration in the mucosa.

3.3.2 Electrolyte composition and moisture content of whole gut sac experiments

There were some regional differences in the electrolyte composition of the gut as expected (Table 3.1). However, there were no treatment-dependent effects of either bulk or nanoscale TiO_2 on the Na^+, K^+, Ca^{2+}, or Mg^{2+} concentrations in the whole gut sacs. A

slight increase in the concentrations of K^+ and Na^+ was detected in some regions of the gut but this increase was not significantly different (ANOVA or Kruskal-Wallis test, $P > 0.05$) compared to the control values. A depletion in the concentrations of Ca^{2+} and Mg^{2+} was founded in all regions of the gut exposed to TiO_2 (NP or bulk) compared to the controls; with a statistically significant difference found only in the mid intestine (ANOVA or Kruskal-Wallis test, $P < 0.05$, Table 3.1). An increase in the moisture content was found in all region of the gut except for the oesophagus compared to the controls after exposure to bulk or TiO_2 NPs with a statistically significant difference found in the mid intestine (ANOVA or Kruskal-Wallis test, $P < 0.05$, Table 3.1).

Potassium concentration in the stripped (muscularis) was higher than that found in the mucosa (Table 3.3) in all gut regions, except for the oesophagus which showed lower values of K^+ than the mucosa. Sodium concentration in mucosa was mainly higher than the stripped one after exposed to TiO_2 NPs (66% or more) indicated by a significantly difference (ANOVA or Kruskal-Wallis test, $P < 0.05$) compared to the control or bulk treatment in mid and hind intestine (Table 3.3). Calcium and magnesium concentrations were accumulated in the mucosa more than the stripped gut after exposure to TiO_2 NPs for all regions of the gut; with values for the magnesium being significantly higher than either the control or bulk in the mucosa of mid and hind intestine (ANOVA or Kruskal-Wallis test, $P < 0.05$, Table 3.3).

3.3.3 Histopathology of the whole gut sac experiment

Morphological examination of the whole gut sac after 4 h incubation with 1mg l^{-1} TiO_2 NPs or bulk resulted in normal gut morphology with no pathologies detected in gut tissue. However, a minor effect was observed in the pyloric caeca represented by the appearance of vacuoles in just one out of six fish examined from one treatment (Fig. 3.2-i).

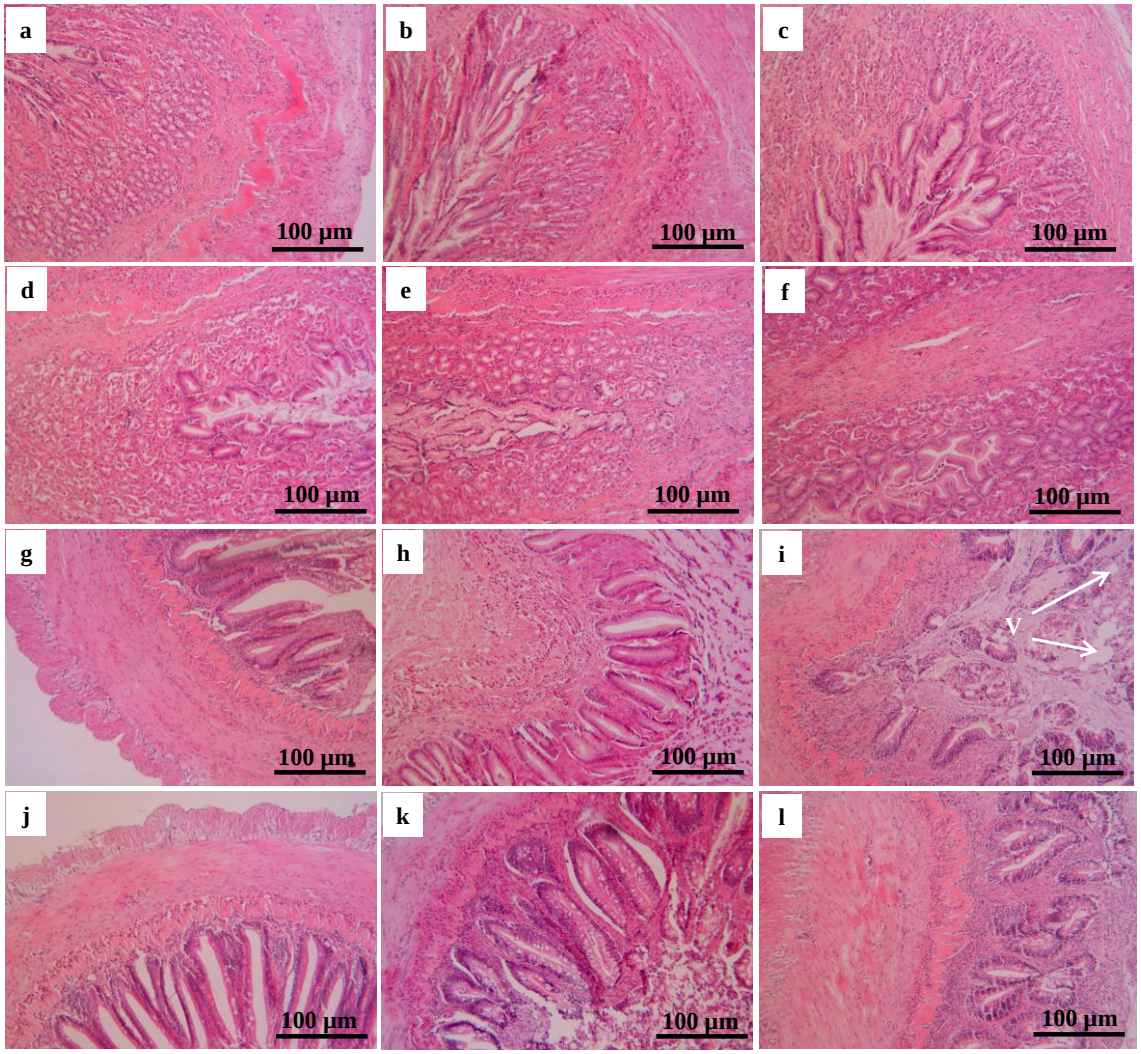

Figure 3.2 Histology of the whole gut sac after 4 h experiment. (a) control oesophagus, (b) 1 mg l^{-1} bulk TiO_2 oesophagus, (c) 1 mg l^{-1} TiO_2 NP oesophagus showing normal tissue. (d) control stomach, (e) 1 mg l^{-1} bulk TiO_2 stomach, (f) 1 mg l^{-1} TiO_2 NP stomach showing normal tissue. (g) control pyloric caeca, (h) 1 mg l^{-1} bulk TiO_2 pyloric caeca, (i) 1 mg l^{-1} TiO_2 NP pyloric caeca showing appearance of vacuoles (V). (j) control intestine, (k) 1 mg l^{-1} bulk TiO_2 intestine, (l) 1 mg l^{-1} TiO_2 NP intestine showing normal tissue. Scale bar = 100 µm, sections were 8 µm thickness and stained with haematoxylin and eosin (n = 6 fish per treatment).

Table 3.1 Total Ti metal, K^+, Na^+, Ca^{2+} and Mg^{2+} concentrations of gut tissue segments from whole gut sacs following exposure to 1 mg l^{-1} of TiO_2 in the gut lumen for 4 h.

		[Metal] µmol g^{-1} dry mass				
Parameter		Oesophagus	Stomach	Pyloric caeca	Mid intestine	Hind intestine
[Ti]						
	Control	< 0.003^{a}	0.003 ± 0.001^{a}	< 0.003^{a}	0.004 ± 0.001^{b}	0.006 ± 0.004^{a}
	Bulk TiO_2	0.033 ± 0.009^{ab,*}	0.029 ± 0.007^{a,*}	0.016 ± 0.003^{a,*}	0.062 ± 0.018^{b,*}	0.041 ± 0.011^{ab,*}
	TiO_2 NP	0.027 ± 0.009^{a,*}	0.017 ± 0.003^{a}	0.015 ± 0.003^{a,*}	0.027 ± 0.005^{a,*}	0.030 ± 0.006^{a,*}
[K^+]						
	Control	158.4 ± 16.8^{ab}	168.4 ± 23.2^{a}	87.5 ± 7.9^{b}	224.5 ± 35.1^{a}	274.6 ± 71.4^{a}
	Bulk TiO_2	126.7 ± 18.8^{ab}	175.8 ± 13.7^{b}	81.4 ± 10.4^{a}	248.7 ± 15.7^{c}	239.4 ± 29.3^{c}
	TiO_2 NP	221.5 ± 86.3^{a}	184.7 ± 22.2^{ad}	80.5 ± 5.8^{b}	203.1 ± 25.9^{cd}	239.3 ± 11.1^{c}
[Na^+]						
	Control	245.9 ± 21.6^{a}	219.6 ± 27.1^{a}	121.8 ± 16.8^{b}	245.3 ± 44.7^{a}	286.4 ± 54.7^{a}
	Bulk TiO_2	207.8 ± 25.9^{a}	253.3 ± 12.7^{a}	114.9 ± 9.1^{b}	353.6 ± 75.3^{a}	290.3 ± 53.0^{a}
	TiO_2 NP	311.2 ± 114.8^{a}	207.5 ± 23.2^{ac}	102.1 ± 7.1^{b}	269.7 ± 38.1^{c}	305.9 ± 58.9^{ac}
[Ca^{2+}]						
	Control	17.2 ± 2.2^{a}	16.8 ± 2.9^{a}	10.9 ± 2.8^{b}	22.1 ± 8.5^{ab}	23.9 ± 9.2^{ab}
	Bulk TiO_2	12.6 ± 1.7^{ab}	15.6 ± 1.3^{b}	8.9 ± 1.5^{a}	21.6 ± 2.9^{c,*}	15.9 ± 1.4^{b}
	TiO_2 NP	18.8 ± 7.4^{a,*}	12.7 ± 1.7^{a}	6.2 ± 0.5^{b}	14.9 ± 1.8$^{ac,\#}$	17.9 ± 2.4^{c}
[Mg^{2+}]						
	Control	15.9 ± 1.3^{a}	15.4 ± 1.7^{a}	9.5 ± 0.8^{b}	18.6 ± 3.2^{a}	22.3 ± 5.1^{a}
	Bulk TiO_2	13.0 ± 1.7^{a}	16.3 ± 0.5^{ad}	8.7 ± 0.9^{b}	20.9 ± 1.5^{c}	18.8 ± 2.0^{cd}
	TiO_2 NP	22.4 ± 8.7^{a}	15.6 ± 1.4^{ac}	8.4 ± 0.4^{b}	17.4 ± 1.9^{ac}	19.5 ± 0.7^{c}
Moisture (%)						
	Control	80.2 ± 2.6^{a}	77.5 ± 1.8^{a}	62.6 ± 7.2^{b}	74.5 ± 1.8^{a}	78.2 ± 2.9^{a}
	Bulk TiO_2	75.9 ± 0.8^{ab}	79.6 ± 0.7^{a}	68.6 ± 6.2^{b}	83.1 ± 1.4^{a,*}	80.1 ± 1.3^{a}
	TiO_2 NP	76.1 ± 0.5^{a}	78.7 ± 0.8^{a}	66.3 ± 5.8^{b}	78.4 ± 2.2^{a,*}	81.7 ± 0.7^{a}

Values are means ± S.E.M. (n = 6 for each group) expressed as µmol g^{-1} dry mass of intestinal tissue, except moisture content (%) = ((wet weight – dry weight)/wet weight) x 100. Whole gut sacs were filled with physiological saline (control), 1 mg l^{-1} bulk TiO_2 and 1 mg l^{-1} TiO_2 NP at laboratory temperature (18°C) for 4h. * Statistically significant difference from control values within columns and electrolytes (ANOVA or Kruskal-Wallis test, $P < 0.05$). # Statistically significant difference from bulk TiO_2 value within columns and electrolytes (ANOVA or Kruskal-Wallis test, $P < 0.05$). Different letters (within rows) indicate a statistically significant difference between regions of the gut (ANOVA or Kruskal-Wallis test, $P < 0.05$).

Table 3.2 Total Ti metal concentrations in stripped portions of gut and the corresponding mucosa following exposure of isolated whole gut sacs to 1 mg l^{-1} TiO_2 in the gut lumen for 4 h.

			[Ti] µmol g^{-1} dry mass			
			Oesophagus	Stomach	Mid intestine	Hind intestine
Treatments	Control	Stripped	$< 0.003^{a}$	$< 0.003^{a}$	0.004 ± 0.001^{a}	0.005 ± 0.002^{a}
		Mucosa	0.018 ± 0.009^{a}	0.010 ± 0.005^{a}	0.012 ± 0.008^{a}	0.019 ± 0.012^{a}
		% in mucosa	90.0 ± 14.5^{a}	83.3 ± 18.3^{a}	75.0 ± 16.9^{a}	79.2 ± 16.8^{a}
	BulkTiO_2	Stripped	$0.018 \pm 0.003^{a,*}$	0.030 ± 0.009^{a}	$0.135 \pm 0.039^{ab,*}$	0.252 ± 0.131^{b}
		Mucosa	$0.128 \pm 0.039^{a,*}$	$0.065 \pm 0.019^{a,*}$	$0.159 \pm 0.049^{a,*}$	$0.148 \pm 0.035^{a,*}$
		% in mucosa	87.7 ± 6.6^{a}	68.4 ± 5.9^{a}	54.1 ± 3.1^{b}	37.0 ± 10.8^{b}
	TiO_2 NP	Stripped	$0.019 \pm 0.005^{a,*}$	$0.021 \pm 0.004^{ac,*}$	$0.056 \pm 0.010^{b,*}$	$0.040 \pm 0.011^{bc,*}$
		Mucosa	$0.174 \pm 0.019^{a,*}$	$0.060 \pm 0.006^{b,*}$	$0.136 \pm 0.025^{a,*}$	$0.165 \pm 0.026^{a,*}$
		% in mucosa	90.2 ± 2.1^{ac}	74.1 ± 4.3^{bc}	70.8 ± 4.1^{b}	80.1 ± 2.9^{c}

Values are means ± S.E.M. (n = 6 for each group) expressed as total Ti metal concentration in µmol Ti g^{-1} dry mass of intestinal tissue. Whole gut sacs were filled with physiological saline (control), or the saline containing 1 mg l^{-1} Bulk TiO_2 or 1 mg l^{-1} TiO_2 NP at laboratory temperature (18°C) for 4h. The mucosa was stripped off each section of gut so that the mucosa and underlying sub-mucosa/muscularis (stripped gut) separately analysed for total Ti metal concentration. % Ti in the mucosa is calculated for each region of the gut, % Ti in mucosa= [Ti] mucosa/([Ti] stripped + [Ti] mucosa) x 100. * Statistically significant difference from control values within columns (ANOVA or Kruskal-Wallis test, $P < 0.05$). Different letters (within rows) indicate a statistically significant difference between regions of the gut (ANOVA or Kruskal-Wallis test, $P < 0.05$). There was no material-type effect (bulk versus nano treatment) within each region of the gut for the tissue Ti concentrations.

Table 3.3 Total K^+, Na^+ Ca^{2+} and Mg^{2+} concentrations in stripped portions of gut and the corresponding mucosa following exposure of isolated whole gut sacs to 1 mg l^{-1} TiO_2 in the gut lumen for 4 h.

			[Metal] µmol g^{-1} dry mass			
Parameters			Oesophagus	Stomach	Mid intestine	Hind intestine
Potassium	Control	Stripped	154.03 ± 13.02^{a}	219.29 ± 16.43^{ab}	247.64 ± 43.49^{b}	201.01 ± 35.76^{ab}
		Mucosa	201.58 ± 52.72^{a}	164.73 ± 48.37^{a}	092.72 ± 22.09^{a}	159.80 ± 7.90^{a}
		% in mucosa	52.5 ± 6.7^{a}	39.2 ± 5.4^{ab}	27.6 ± 5^{b}	46.5 ± 4.5^{a}
	Bulk TiO_2	Stripped	141.55 ± 12.91^{a}	209.97 ± 24.23^{ab}	276.31 ± 16.83^{b}	308.14 ± 63.70^{b}
		Mucosa	267.92 ± 83.12^{a}	172.09 ± 34.56^{a}	151.30 ± 20.96^{a}	206.89 ± 30.20^{a}
		% in mucosa	59.8 ± 6.8^{a}	44.5 ± 4.2^{ab}	34.8 ± 2.9^{b}	42.5 ± 6.6^{b}
	TiO_2 NP	Stripped	155.76 ± 15.31^{a}	204.54 ± 8.48^{b}	230.74 ± 16.40^{c}	197.41 ± 12.36^{bc}
		Mucosa	241.83 ± 31.36^{ac}	118.11 ± 15.65^{b}	212.13 ± 41.20^{ab,*}	326.88 ± 40.27$^{c,*\#}$
		% in mucosa	59.9 ± 4.7^{a}	35.9 ± 2.6^{b}	46.2 ± 3.5^{b}	61.3 ± 3.9^{a}
Sodium	Control	Stripped	253.18 ± 39.47^{a}	245.68 ± 16.23^{a}	220.82 ± 30.35^{a}	217.07 ± 20.15^{a}
		Mucosa	424.30 ± 79.28^{ab}	461.25 ± 149.63^{a}	182.22 ± 31.90^{b}	217.07 ± 46.28^{ab}
		% in mucosa	60.3 ± 6.2^{a}	59.4 ± 5.8^{a}	44.9 ± 6.8^{a}	47.9 ± 5.7^{a}
	Bulk TiO_2	Stripped	222.97 ± 019.95^{a}	240.64 ± 027.00^{ab}	333.00 ± 76.18^{ab}	343.65 ± 47.26^{b,*}
		Mucosa	542.83 ± 119.89^{a}	692.06 ± 177.26^{a}	380.72 ± 117.03^{b}	400.78 ± 147.91^{b}
		% in mucosa	67.5 ± 5.1^{a}	71.6 ± 4.2^{a}	51.2 ± 2.9^{b}	48.4 ± 7.5^{b}
	TiO_2 NP	Stripped	213.63 ± 13.01^{a}	215.54 ± 05.20$^{a,\#}$	224.85 ± 15.76^{a}	231.61 ± 36.90$^{a,\#}$
		Mucosa	516.71 ± 85.86^{a}	422.99 ± 56.36^{a}	444.52 ± 44.42$^{a,*\#}$	528.76 ± 171.66$^{a,*\#}$
		% in mucosa	69 ± 3.4^{a}	64.9 ± 3.2^{a}	65.8 ± 2.4^{a}	66.2 ± 3.4^{a}
Calcium	Control	Stripped	17.20 ± 2.89^{a}	15.97 ± 1.91^{a}	21.02 ± 4.35^{a}	21.88 ± 7.85^{a}
		Mucosa	24.69 ± 5.42^{a}	22.74 ± 6.06^{a}	9.57 ± 1.28^{b}	12.71 ± 2.60^{b}
		% in mucosa	56.3 ± 6.2^{a}	55.4 ± 4.3^{a}	34.2 ± 5.6^{b}	41.1 ± 6.7^{ab}
	Bulk TiO_2	Stripped	33.09 ± 18.85^{a}	15.59 ± 1.19^{b}	27.02 ± 3.92^{a}	29.55 ± 7.41^{a}
		Mucosa	33.23 ± 7.72^{a}	33.16 ± 7.07^{a}	18.30 ± 4.11^{b}	16.32 ± 4.28^{b}
		% in mucosa	58.6 ± 5.7^{a}	66 ± 3.7^{a}	39.6 ± 2.9^{b}	38.5 ± 9.7^{b}
	TiO_2 NP	Stripped	22.99 ± 9.76^{a}	13.68 ± 1.61^{a}	17.95 ± 1.76^{a}	15.26 ± 2.18^{a}
		Mucosa	28.85 ± 3.92^{a}	23.48 ± 3.75^{a}	18.60 ± 2.02^{a,*}	23.57 ± 6.30^{a}
		% in mucosa	60.7 ± 5.6^{a}	61.8 ± 4.6^{ab}	50.7 ± 2.9^{b}	57.9 ± 4.7^{ab}

Table 3.3 continued

			[Metal] µmol g^{-1} dry mass			
Parameters			Oesophagus	Stomach	Mid intestine	Hind intestine
Magnesium	Control	Stripped	14.74 ± 0.96^{a}	18.08 ± 1.52^{a}	18.54 ± 2.81^{a}	16.66 ± 2.55^{a}
		Mucosa	29.43 ± 7.62^{a}	33.03 ± 11.13^{a}	11.93 ± 2.71^{b}	16.35 ± 1.88^{b}
		% in mucosa	61.9 ± 5.8^{a}	58.6 ± 6.2^{a}	38.7 ± 6.5^{b}	50.2 ± 3.9^{ab}
	Bulk TiO_2	Stripped	4.52 ± 0.92^{a}	16.61 ± 1.51^{a}	20.98 ± 1.77^{a}	24.27 ± 4.85^{b}
		Mucosa	40.71 ± 13.70^{a}	37.34 ± 10.32^{a}	19.40 ± 3.08^{b}	19.46 ± 2.74^{b}
		% in mucosa	67.4 ± 6.2^{a}	65.6 ± 4.9^{a}	47.2 ± 4.3^{b}	46.4 ± 6.8^{b}
	TiO_2 NP	Stripped	15.60 ± 1.31^{a}	17.26 ± 0.76^{a}	17.08 ± 1.25^{a}	15.54 ± 0.90^{a}
		Mucosa	32.74 ± 3.31^{a}	23.95 ± 2.82^{a}	$27.71 \pm 3.92^{a,*\#}$	$31.79 \pm 3.79^{a,*\#}$
		% in mucosa	67.2 ± 3.2^{a}	57.2 ± 2.8^{b}	61 ± 2.5^{ab}	66.2 ± 3.1^{a}

Values are means ± S.E.M. (n = 6 for each group) expressed as total electrolytes concentration in µmol g^{-1} dry mass of intestinal tissue. Whole gut sacs were filled with physiological saline (control), or the saline containing 1 mg l^{-1} TiO_2 NP or 1 mg l^{-1} Bulk TiO_2 at laboratory temperature (18 ºC) for 4h. The mucosa was stripped off each section of gut so that the mucosa and underlying sub-mucosa/muscularis (stripped gut) separately analysed for total electrolytes concentration. % electrolytes in the mucosa is calculated for each region of the gut, % electrolytes in mucosa= [electrolytes] mucosa / ([electrolytes] stripped + [electrolytes] mucosa) x 100. * Statistically significant difference from control values or # Statistically significant difference from Bulk TiO_2 value (ANOVA or Kruskal-Wallis test, $P < 0.05$) (within columns). Different letters (within rows) indicate a statistically significant difference between regions of the gut.

3.3.4 The effect of TiO_2 on the viability of the perfused intestine

All the viability criteria of the perfused intestines were good in general and met in all treatments. Measured by the morphological examination of the intestine (light microscopy of fixed wax sections), LDH activity for both the perfusate and mucosal solution (bath samples), as well as the mucosal solution [K^+], [Na^+], and pH.

3.3.4.1 Histopathology

The histological examination of the perfusate intestine after 4 h showed normal gut morphology (Fig. 3.3). The addition of 1mg l^{-1} TiO_2 NP or bulk to the mucosal solution had only minor effects on the epithelium regardless of the gas mixture and only observed in one or two out of six animals in total, with no clear treatment-related effect. These included some slight swelling of the occasional goblet cells (in one out of six animals per treatment), minor lifting of the epithelial cell (in two out of six animals per treatment) and appearance of vacuoles (in two out of six animals per treatment).

3.3.4.2 LDH measurements

The LDH activity in all experiments (n = 6 per treatment; n = 7 for the control and TiO_2 NP treatment gassed with the standard gas mix) in both perfusate and mucosal solutions remained low and within the viability criteria for the preparation (< 1 IU ml^{-1}). The maximum individual perfusate LDH concentrations reached for control, bulk TiO_2 and TiO_2 NP gassed with standard mix gas were 0.71, 0.73 and 0.79 IU ml^{-1} respectively. For the low CO_2 experiments, LDH activity also remained low with the maximum individual LDH activity reached in the perfusates being 0.76, 0.78 and 0.79 IU ml^{-1} for control, bulk TiO_2 and TiO_2 NP respectively. However, statistically significant lower values of the cumulative LDH activity for TiO_2 NP (t-test, P = 0.001, Fig. 3.4 A and B) were observed compared to the standard gas mix group, and the same situation was seen with the bulk TiO_2 treatment (t-test, P = 0.006). For the mucosal LDH, the maximum

individual values reached for the control, bulk TiO_2 and TiO_2 NP gassed with standard gas mix were 0.54, 0.65 and 0.47 IU ml $^{-1}$ respectively; while it was 0.35, 0.42 and 0.35 IU ml $^{-1}$ gassed with the low CO_2. Bulk TiO_2 showed statistically significant lower mucosal LDH values than the bulk TiO_2 with standard gas mix (*t*-test, $P = 0.026$, Fig. 3.5 A and B). The cumulative LDH activity for both perfusate and mucosal solutions showed a linear and steady increase over time for all gas mixtures. In the perfusate for the standard gas mixture, the bulk TiO_2 treatment showed a statistically lower cumulative LDH activity by the end of the experiment compared to either control or TiO_2 NP treatments (Kruskal-Wallis test, $P = 0.001$, Fig. 3.4 A). The same situation was seen with the low CO_2 treatments (Kruskal-Wallis test, $P = 0.003$, Fig. 3.4 B). There were no statistically significant differences between treatments in the cumulative LDH in the mucosal solutions with either gas mixture (ANOVA, $P > 0.05$, Fig. 3.5 A and B), except for the bulk TiO_2 gassed with standard gas mix at 240 min, a statistically significant increase in the cumulative LDH was detected in compare to the control and TiO_2 NP (Kruskal-Wallis test, $P = 0.032$, Fig. 3.5 A). Additionally, a statistically lower of the cumulative LDH was noticed for the TiO_2 NP at 120 min gassed with the standard gas mix compared to the control and bulk TiO_2 (Kruskal-Wallis test, $P = 0.02$, Fig. 3.5 A).

3.3.4.3 Effects of TiO_2 on the mucosal solution [K^+], [Na^+], and pH

There were no TiO_2-treatment dependent effects on [K^+], [Na^+], or pH of the mucosal solution for most experiments (Table 3.4 and 3.5), which indicate that the intestine was normal with no measurable leak of electrolytes. The measured levels of [K^+], [Na^+] and pH in the fresh physiological saline used in the experiments were 5.86, 146 mmol l^{-1} and 7.4, respectively, and in comparison there were only micromolar increases in electrolytes above this background concentration in all experiments. For example, the average increase (grand means of both control and treatments) in the [K^+], [Na^+] in the

mucosal solution gassed with low CO_2 were 0.14 ± 0.03 and 0.79 ± 0.19 mmol l^{-1} respectively (mean ± S.E.M., *n* = 12 experiments) over 4 h, while the increase in the mucosal solution gassed with the standard gas mix over 4 h were 0.27 ± 0.04 and 4.49 ± 0.41 mmol l^{-1} respectively (mean ± S.E.M., *n* = 14 experiments). The grand mean change in pH for the standard gas mixture for all experiments was 0.39 ± 0.03, indicating the expected normal base secretion of the intestine. However, in the standard gas mix experiments there was slightly more (statistically significant, ANOVA, *P* = 0.03, Table 3.4) base secretion in the nano treatment compared to bulk or controls (mean ± S.E.M., *n* = 20 experiments; increases of pH; 0.29 ± 0.07, 0.43 ± 0.02 and 0.48 ± 0.04 for control, bulk TiO_2 and TiO_2 NPs, respectively). There were no treatment-dependent changes in net acid excretion into the mucosal solution for the 0.5% CO_2 treatment (Table 3.5), with a grand mean changes of 0.81 ± 0.02 pH units for all treatments combined (mean ± S.E.M., *n* = 18 experiments). However, compared to the standard gas mixture, the 0.5% CO_2 had larger increases in pH; 0.83 ± 0.05, 0.82 ± 0.03 and 0.79 ± 0.03 for control, bulk TiO_2 and TiO_2 NPs, respectively (mean ± S.E.M., *n* = 18 experiments) indicated that the pH was more stable with standard gas mix experiment than that found with low CO_2 one.

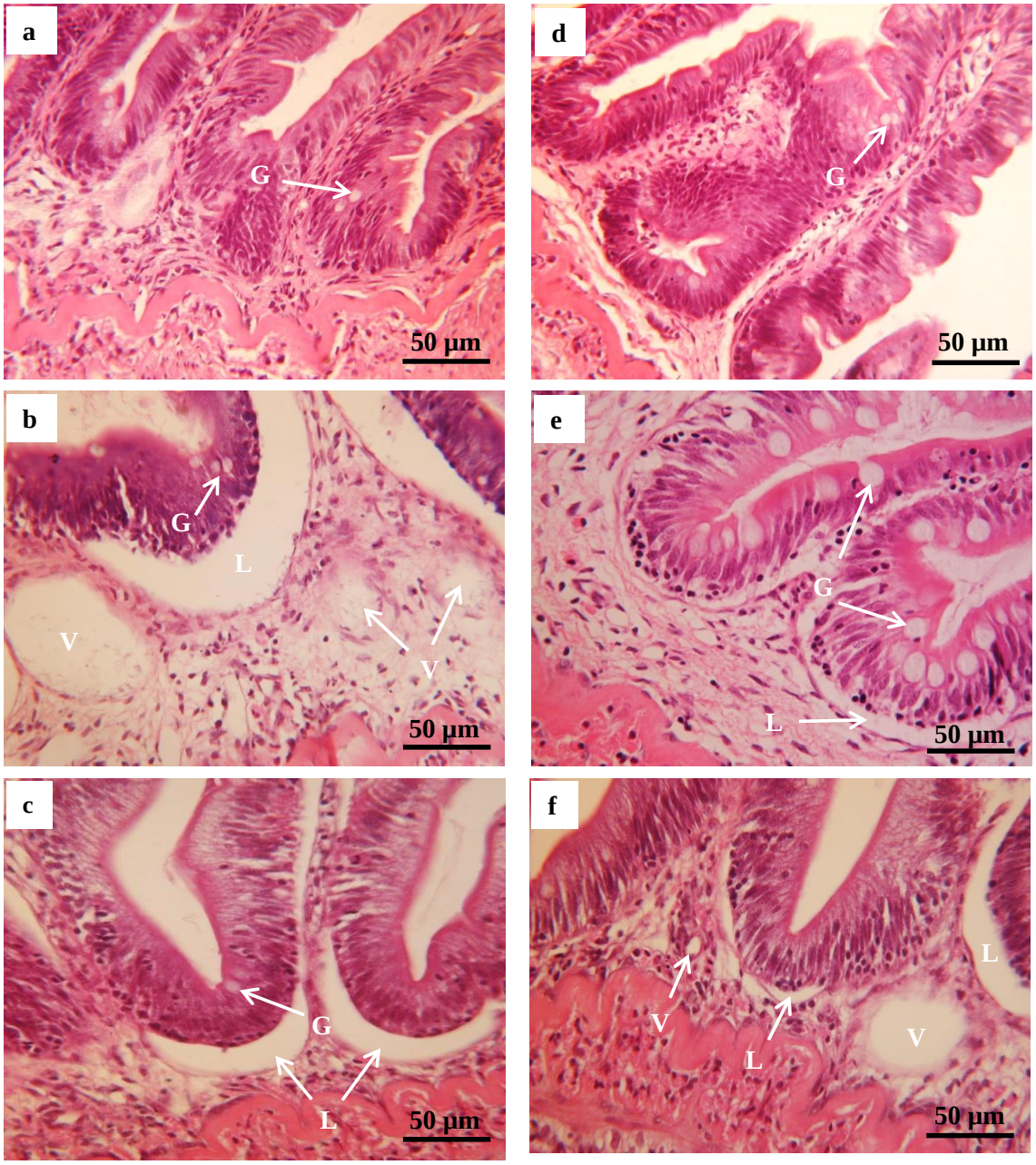

Figure 3.3 Histology of the perfusate intestine after 4 h perfusion. (a) Control gassed with standard gas mix showing normal intestine with goblet cells (G), (b) 1 mg l^{-1} bulk TiO_2 gassed with standard gas mix showing appear of vacuoles (V) and lifting epithelium (L), (c) 1 mg l^{-1} TiO_2 NP gassed with standard gas mix showing lifting of epithelial cell (L), (d) Control gassed with low CO_2 showing normal tissue, (e) 1 mg l^{-1} bulk TiO_2 gassed with low CO_2 showing minor lifting epithelium (L), and swelling of the goblet cells (G), (f) 1 mg l^{-1} TiO_2 NP gassed with low CO_2 showing appear of vaculation (V) and lifting of epithelial cell (L). Scale bar = 50 µm, sections were 8 µm thickness and stained with haematoxylin and eosin (n = 6 per treatment; n = 7 for the control and TiO_2 NP treatment gassed with the standard gas mix).

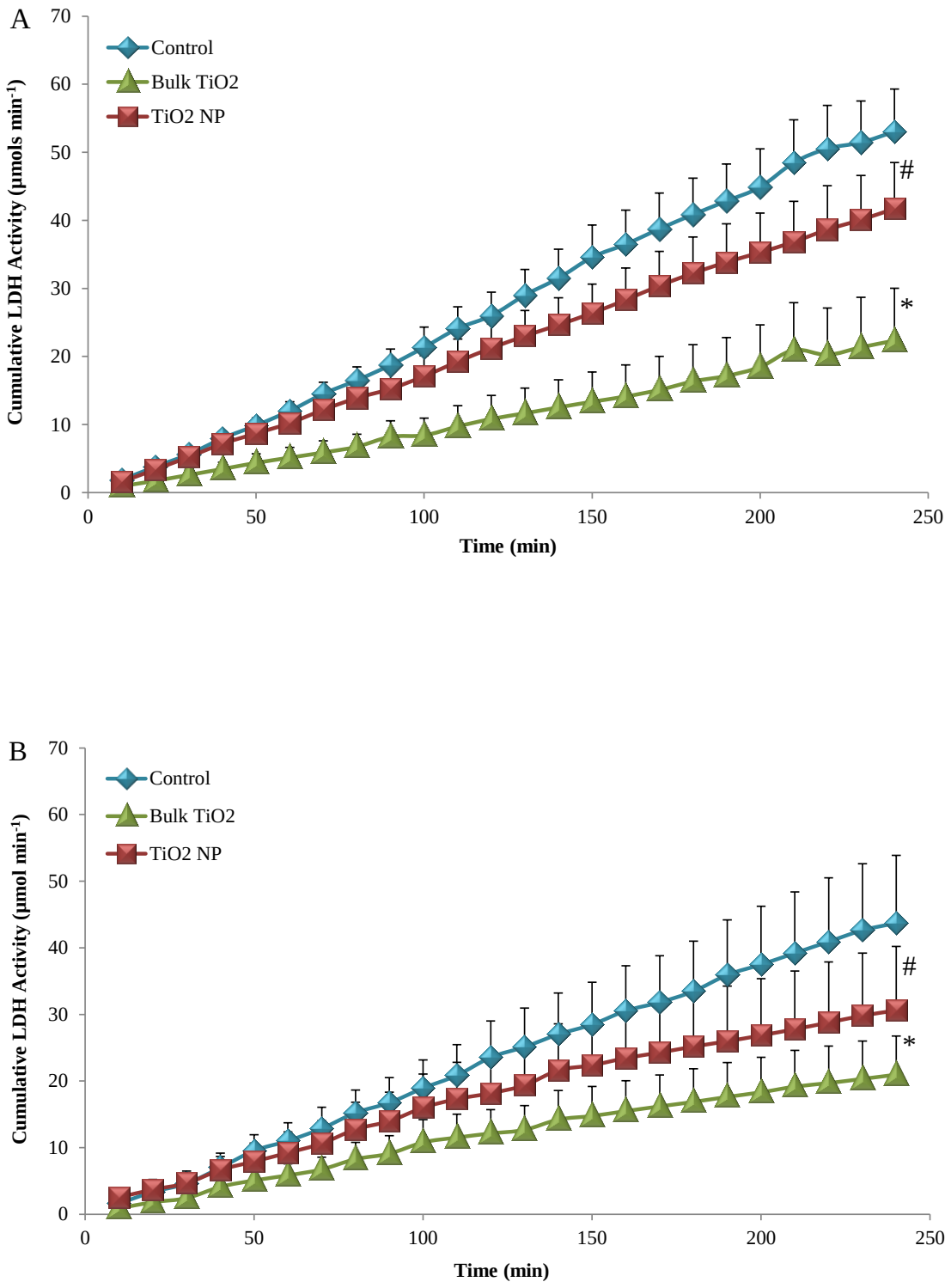

Figure 3.4 The effect of 1 mg l^{-1} TiO_2 exposure on the cumulative perfusate LDH activity (cumulative sum of international units of LDH activity per minute) over 4 h in perfused intestine at 18°C, (A) control, bulk TiO_2 and TiO_2 NP gassed with standard gas mix, (B) Control, bulk TiO_2 and TiO_2 NP gassed with low CO_2. Values are means ± S.E.M (n = 6 per treatment; n = 7 for the control and TiO_2 NP treatment gassed with the standard gas mix). *Statistically significant difference from the control value (ANOVA or Kruskal-Wallis test, $P < 0.05$). # Statistically significant difference from bulk TiO_2 value (ANOVA or Kruskal-Wallis test, $P < 0.05$).

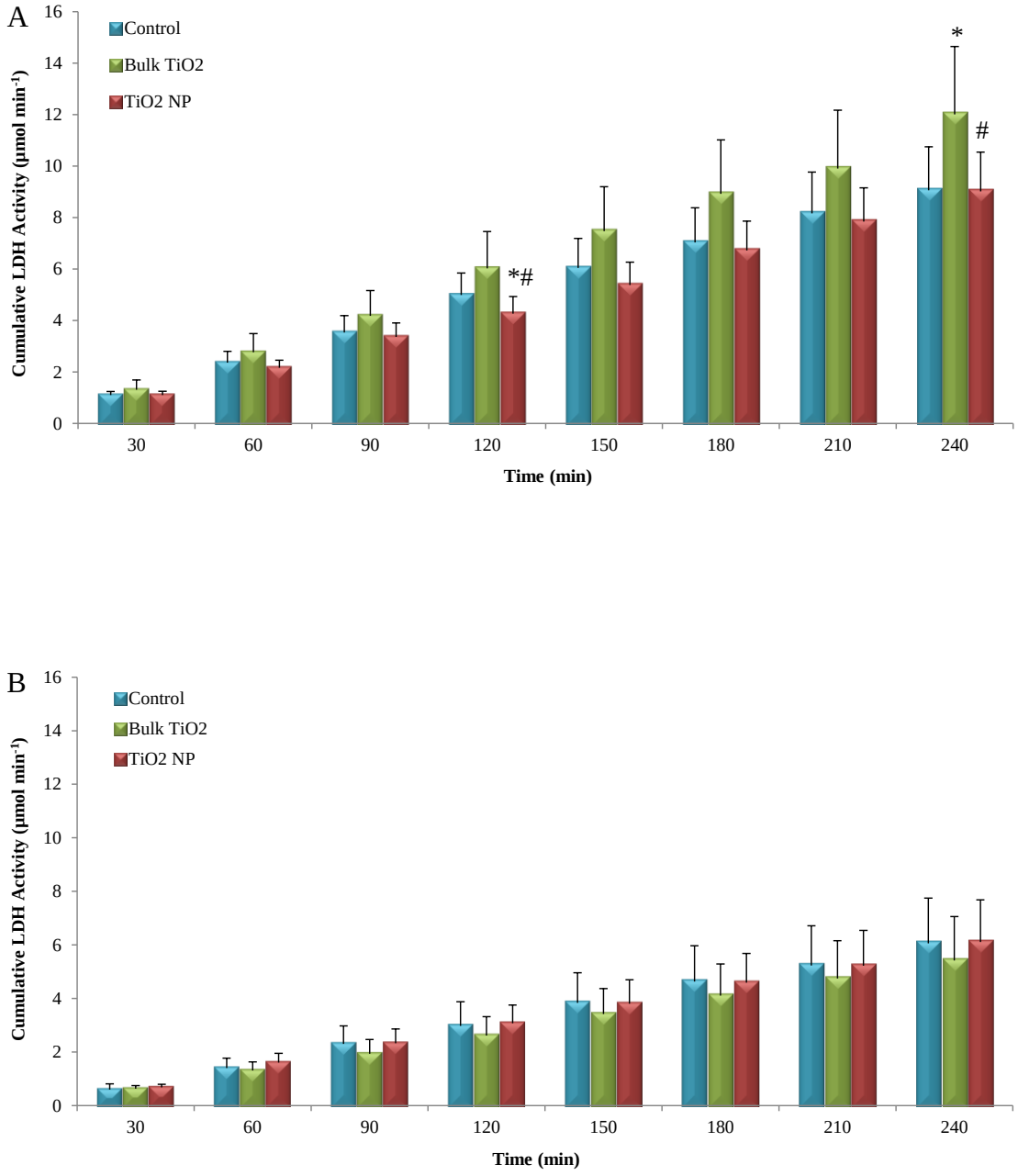

Figure 3.5 The effect of 1 mg l^{-1} TiO_2 exposure on the cumulative mucosal solution (bath) LDH activity (cumulative sum of international units of LDH activity per minute) over 4 h in perfused intestine at 18°C, (A) control, bulk TiO_2 and TiO_2 NP gassed with standard gas mix, (B) Control, bulk TiO_2 and TiO_2 NP gassed with low CO_2. Values are means ± S.E.M (n = 6 per treatment; n = 7 for the control and TiO_2 NP treatment gassed with the standard gas mix). * Statistically significant difference from control values (ANOVA or Kruskal-Wallis test, $P < 0.05$) within each time point. # Statistically significant difference from bulk TiO_2 value (ANOVA or Kruskal-Wallis test, $P < 0.05$) within each time point.

Table 3.4 Total pH, Na^+ and K^+ concentrations in the mucosal solution after exposure of the isolated perfused intestine to 1 mg l^{-1} TiO_2 gassed with 95% O_2: 5% CO_2 for up to 4h.

Time (min)	Control			TiO_2 NP			Bulk TiO_2
	pH	Bath Na^+ (mmol l^{-1})	Bath K^+ (mmol l^{-1})	pH	Bath Na^+ (mmol l^{-1})	Bath K^+ (mmol l^{-1})	pH
30	7.6 ± 0.06	148.8 ± 0.58	5.9 ± 0.03	7.8 ± 0.03*	147.4 ± 0.6	5.89 ± 0.03	7.8 ± 0.02*
60	7.6 ± 0.06	149.2 ± 0.66	6.1 ± 0.05	7.8 ± 0.04*	148.8 ± 0.97	5.97 ± 0.03	7.8 ± 0.02*
90	7.7 ± 0.07	150.8 ± 1.02	6.2 ± 0.05	7.8 ± 0.04	149.8 ± 0.37	6.02 ± 0.02*	7.8 ± 0.02
120	7.7 ± 0.07	149.6 ± 0.40	6.1 ± 0.07	7.9 ± 0.04	149.8 ± 0.85	6.05 ± 0.06	7.8 ± 0.02
150	7.7 ± 0.08	153.4 ± 2.46	6.3 ± 0.13	7.9 ± 0.05*	150.3 ± 0.48	6.08 ± 0.04	7.8 ± 0.02
180	7.7 ± 0.08	151.4 ± 0.75	6.3 ± 0.11	7.9 ± 0.05	153.3 ± 2.63	6.22 ± 0.16	7.9 ± 0.02
210	7.7 ± 0.08	151.2 ± 0.73	6.3 ± 0.09	7.9 ± 0.05*	150.8 ± 0.95	6.13 ± 0.07	7.9 ± 0.02
240	7.8 ± 0.08	152.2 ± 0.66	6.4 ± 0.11	7.9 ± 0.04	151.0 ± 0.71	6.17 ± 0.08	7.9 ± 0.02

Values are means ± S.E.M. (n = 6 for the bulk TiO_2; n = 7 for the control and TiO_2 NP treatment) expressed as mmol l^{-1} for both Na^+ and K^+ in the mucosal solution (bath solution). * Statistically significant difference from control values (Kruskal-Wallis test or t-test, $P < 0.05$) (within rows).

Table 3.5 Total pH, Na^+ and K^+ concentrations in the mucosal solution after exposure of the isolated perfused intestine to 1 mg l^{-1} TiO_2 gassed with 99.5% O_2: 0.5% CO_2 for up to 4h.

Time (min)	Control			TiO_2 NP			Bulk TiO_2
	pH	Bath Na^+ (mmol l^{-1})	Bath K^+ (mmol l^{-1})	pH	Bath Na^+ (mmol l^{-1})	Bath K^+ (mmol l^{-1})	pH
30	7.92 ± 0.08	145.7 ± 0.88	5.87 ± 0.04	7.92 ± 0.08	146.7 ± 0.33	5.92 ± 0.02	7.98 ± 0.07
60	8.07 ± 0.08	146.0 ± 0.58	5.90 ± 0.02	8.05 ± 0.07	145.7 ± 0.33	5.89 ± 0.01	8.10 ± 0.06
90	8.17 ± 0.06	146.3 ± 0.33	5.92 ± 0.03	8.13 ± 0.03	146.7 ± 0.33	5.93 ± 0.02	8.17 ± 0.02
120	8.23 ± 0.07	146.3 ± 0.33	5.94 ± 0.03	8.20 ± 0.04	146.3 ± 0.33	5.92 ± 0.03	8.21 ± 0.04
150	8.30 ± 0.04	147.3 ± 0.33	5.97 ± 0.02	8.25 ± 0.02	146.3 ± 0.33	5.93 ± 0.02	8.25 ± 0.02
180	8.35 ± 0.04	148.0 ± 0.00	6.10 ± 0.06	8.30 ± 0.03	147.3 ± 0.33	6.05 ± 0.08	8.33 ± 0.02
210	8.38 ± 0.05	147.7 ± 0.33	6.17 ± 0.17	8.33 ± 0.02	147.3 ± 0.33	6.05 ± 0.08	8.33 ± 0.02
240	8.42 ± 0.04	148.0 ± 0.00	6.23 ± 0.19	8.36 ± 0.02	147.0 ± 1.00	6.14 ± 0.18	8.38 ± 0.02

Values are means ± S.E.M. (n = 6 for each group) expressed as mmol l^{-1} for both Na^+ and K^+ in the mucosal solution (bath solution). There was no statistically significant difference (Kruskal-Wallis test or t-test, $P > 0.05$) between groups (control, bulk or nano) within each time point over 4 h perfusion.

Table 3.6 Total TiO_2 concentration in the mucosal solution after exposure of the isolated perfused intestine to 1 mg l^{-1} TiO_2 for up to 4h.

Time (min)	Mucosal TiO_2 (mg l^{-1})					
	Gassed with 95% O_2: 5% CO_2			Gassed with 99.5% O_2: 0.5% CO_2		
	Control	Bulk TiO_2	TiO_2 NP	Control	Bulk TiO_2	TiO_2 NP
30	< 0.004	0.37 ± 0.05*	0.10 ± 0.02#	< 0.004	0.16 ± 0.01*	0.18 ± 0.07*
60	< 0.004	0.32 ± 0.03*	0.19 ± 0.07*	< 0.004	0.08 ± 0.03*	0.21 ± 0.13*
90	< 0.004	0.36 ± 0.02*	0.12 ± 0.04*#	< 0.004	0.09 ± 0.03*	0.21 ± 0.12*
120	< 0.004	0.34 ± 0.04*	0.17 ± 0.05*#	< 0.004	0.08 ± 0.03*	0.13 ± 0.08*
150	< 0.004	0.35 ± 0.03*	0.18 ± 0.10*#	< 0.004	0.05 ± 0.02*	0.05 ± 0.03*
180	< 0.004	0.34 ± 0.04*	0.09 ± 0.02*#	< 0.004	0.03 ± 0.01*	0.07 ± 0.03*
210	< 0.004	0.35 ± 0.02*	0.14 ± 0.04*#	< 0.004	0.03 ± 0.01*	0.07 ± 0.03*
240	< 0.004	0.38 ± 0.01*	0.16 ± 0.05*#	< 0.004	0.02 ± 0.01	0.06 ± 0.03*

Values are means ± S.E.M. (n = 6 per treatment; n = 7 for the control and TiO_2 NP treatment gassed with the standard gas mix) expressed as mg l^{-1} for TiO_2 in the mucosal solution (bath solution) gassed with 95% O_2: 5% CO_2 and 99.5% O_2: 0.5% CO_2. * Statistically significant difference from control values or # Statistically significant difference from Bulk TiO_2 value (ANOVA or Kruskal-Wallis test, $P < 0.05$) (within columns).

3.3.5 TiO_2 Distribution in the mucosal solution

The dispersion of TiO_2 was confirmed by the nanoparticles tracking analysis system (Nanosight LM 10) which analysed the mucosal solution samples that taken at the beginning (at 30 min) and at the end (at 240 min) of the experiments. The bulk TiO_2 material remained stable over the 4 h perfusions, at the start of experiments the bulk TiO_2 had a mean particle size of 301.50 ± 43.47 nm, with the smallest size bin in the distributions being 70.61 ± 14.79 nm (mean ± S.E.M., n = 6, Fig. 3.6. C). The mean values for the bulk TiO_2 at the end of the experiments were 236.67 ± 24.05 nm, with the smallest size bin of 61.5 ± 7.10 nm (mean ± S.E.M., n = 6, neither being statistically different from the start of the experiment, t-tests, $P > 0.05$, Fig. 3.6. D). TiO_2 NP showed statistically significant lower mean particle size values (t-tests, $P < 0.05$) compared to the bulk TiO_2 treatment at each time point. The mean size of the TiO_2 NP at the beginning of the experiment and after 4 h perfusion were 169.43 ± 18.77 nm and 140.18 ± 15.85 nm (mean ± S.E.M., n = 10, t-test, P = 0.84), respectively, while the smallest size bin of particles had a mean of 50.10 ± 3.71 nm and 46.93 ± 1.88 nm (mean ± S.E.M., n = 10, t-test, P = 0.66), at the start and end of the experiment respectively (see Fig. 3.6. A and B).

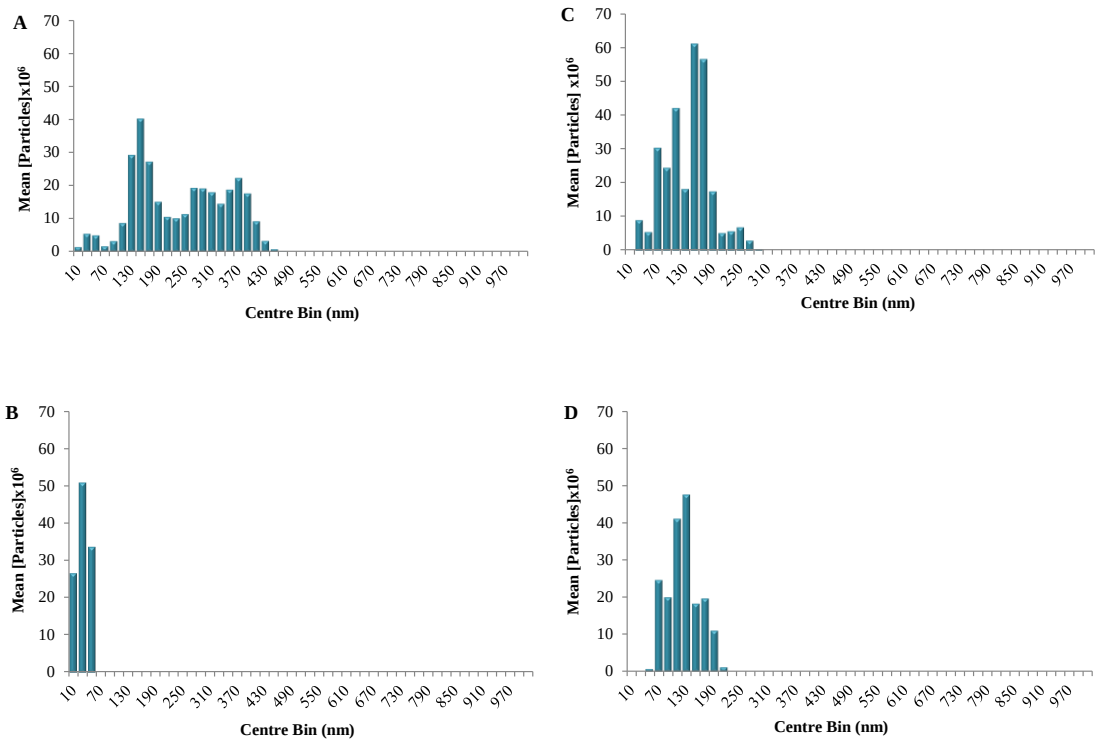

Figure 3.6 The dispersion of 1 mg l^{-1} TiO_2 in the mucosal solution. Nanosight graphs are represent examples of individual samples from replicated experiments (TiO_2 NP, *n* = 10 and Bulk TiO_2, *n* = 6). (A) TiO_2 NP distribution in mucosal solution at the beginning of the experiment (at 30 min), mean are 103 nm, started with 26 nm primary particle size. (B) TiO_2 NP distribution in mucosal solution at the end of the experiment (at 240 min), mean are 81 nm, with 28 nm primary particle size. (C) Bulk TiO_2 in mucosal solution at the beginning of the experiment (at 30 min), mean are 136 nm and 36 nm primary particle size. (D) Bulk TiO_2 in mucosal solution at the end of the experiment (at 240 min), mean are 122 nm with 65 nm primary particle size.

3.3.6 Ti uptake from TiO_2 by the perfused intestine

3.3.6.1 Titanium accumulation from TiO_2 exposures in the perfused intestine

The accumulation of Ti from TiO_2 in the tissue during the perfusions is shown in Fig. 3.7. As expected, total Ti metal concentrations in the tissues were higher in both of the TiO_2 treatments compared to the no added TiO_2 control. However, there were differences between the mid and hind gut depending on both types of TiO_2 treatment, and the gas supplement used. In general, there was a material-type effect, with TiO_2 NP treatment showing lower total Ti metal concentrations in the tissue than the equivalent bulk treatment when using the standard gas mixture (Fig. 3.7. A). The hind gut also generally accumulated less Ti than the mid gut within treatment (statistically significant, *t*-tests, $P < 0.05$, Fig. 3.7. A). For the mid gut gassed with standard gas mix the total Ti metal concentrations in control, bulk TiO_2 and TiO_2 NP groups were < 0.004, 0.094 ± 0.041 and 0.019 ± 0.004 μmol g^{-1} dry weight of tissue, respectively (mean ± S.E.M., n = 6 perfusions for the bulk TiO_2; n = 7 perfusions for the control and TiO_2 NP treatment, Kruskal-Wallis test, P = 0.002). In the hind gut the total Ti metal concentrations in control, bulk TiO_2 and TiO_2 NP groups were 0.003 ± 0.001, 0.022 ± 0.005 and 0.009 ± 0.003 μmol g^{-1} dry weight of tissue, respectively (mean ± S.E.M., n = 6 perfusions for the bulk TiO_2; n = 7 perfusions for the control and TiO_2 NP treatment, Kruskal-Wallis test, P = 0.02). Bulk TiO_2 showed significantly higher values than that found in both control and TiO_2 NP groups for either mid or hind gut.

The addition of low CO_2 into the mucosal solution changed the Ti accumulation in the tissue compared to the standard gas mix groups (Fig. 3.7. B); showing higher Ti accumulation with TiO_2 NP treatment than the equivalent bulk treatment. The Ti concentration from TiO_2 in the mid gut for control, bulk TiO_2 and TiO_2 NP groups were 0.002 ± 0.001, 0.013 ± 0.005 and 0.029 ± 0.009 μmol g^{-1} dry weight of tissue, respectively (mean ± S.E.M., n = 6, Kruskal-Wallis test, P = 0.003). The hind gut Ti

concentrations were 0.002 ± 0.001, 0.009 ± 0.002 and 0.023 ± 0.009 μmol g^{-1}dry weight of tissue in control, bulk TiO_2 and TiO_2 NP groups respectively (mean ± S.E.M., n = 6, Kruskal-Wallis test, P = 0.003). The TiO_2 NP treatment was significantly higher than the bulk TiO_2 one. No significantly differences were found for the Ti concentration between the mid and hind intestine (t-test, $P > 0.05$) in all treatment groups.

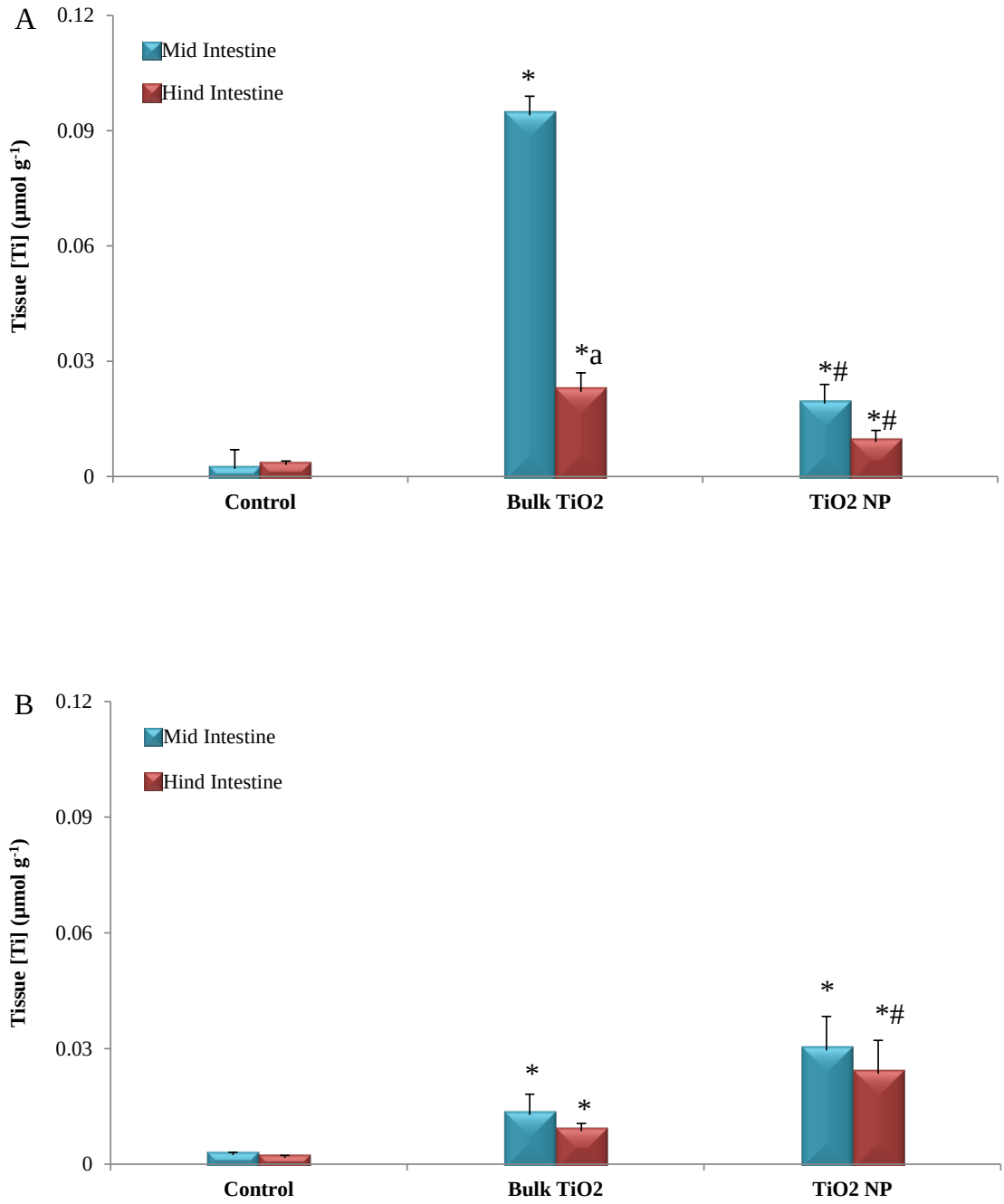

Figure 3.7 Total Ti metal concentrations in the tissues determined by ICP-OES in the mid (blue bars) and hind gut (red bars) after 4 h perfusions with a concentration of 1 mg l^{-1} TiO_2 (bulk or NP) added to the mucosal solution gassed with standard gas mix (A) or low CO_2 (B). Data are means ± S.E.M. (n = 6 perfusions per treatment; n = 7 perfusions for the control and TiO_2 NP treatment gassed with the standard gas mix). * Statistically significant difference from control values (ANOVA or Kruskal-Wallis test, $P < 0.05$). # Statistically significant difference from bulk TiO_2 treatment (ANOVA or Kruskal-Wallis test, $P < 0.05$). Letter (a) indicates statistically significant differences between mid and hind intestine (t-test, $P < 0.05$).

3.3.6.2 Net Ti flux to the serosal compartment

The cumulative Ti metal uptake across the intestine into the serosal perfusate for individual experiments at different size (NP and Bulk) and different gas supplement (standard gas mix and low CO_2) are shown in Fig. 3.8. There was a steady appearance of Ti in the eluted perfusate over time in the treated animals compared to controls (Fig. 3.8). There was also a substantial difference between the TiO_2 NP accumulations in the perfusate associated with the type of gas mixture. Changing from the standard gas mixture to the low CO_2 gas mixture greatly enhanced the appearance of Ti in the serosal perfusate from both the bulk and nano TiO_2 exposures (compare bulk, Fig. 3.8.B and E; compare nano, Fig. 3.8.C and F). The maximum initial uptake rate of NP into the serosal perfusate with standard gas mix showed a lower values by 13 folds than the low CO_2 being 1.55 ± 0.33 and 21.16 ± 18.90 nmol g^{-1} h^{-1} (mean ± S.E.M., n = 6 perfusions per treatment; n = 7 perfusions for the control and TiO_2 NP treatment gassed with the standard gas mix), respectively. The bulk TiO_2 showed low content of Ti in the serosal perfusate being 0.98 ± 0.47 nmol g^{-1} h^{-1} for the standard gas mix (mean ± S.E.M., n = 6) and 3.42 ± 0.74 nmol g^{-1} h^{-1} for the low CO_2 (mean ± S.E.M., n = 6). Ti content in the serosal perfusate from bulk TiO_2 represented a significantly lower values than Ti from TiO_2 NP group for both standard gas mix (t-test, P = 0.04) and low CO_2 (t-test, P = 0.001). However, reduce the appearance of the Ti in the serosal perfusate did not compromise the steady perfusate flow (one of the viability criterion for the preparation).

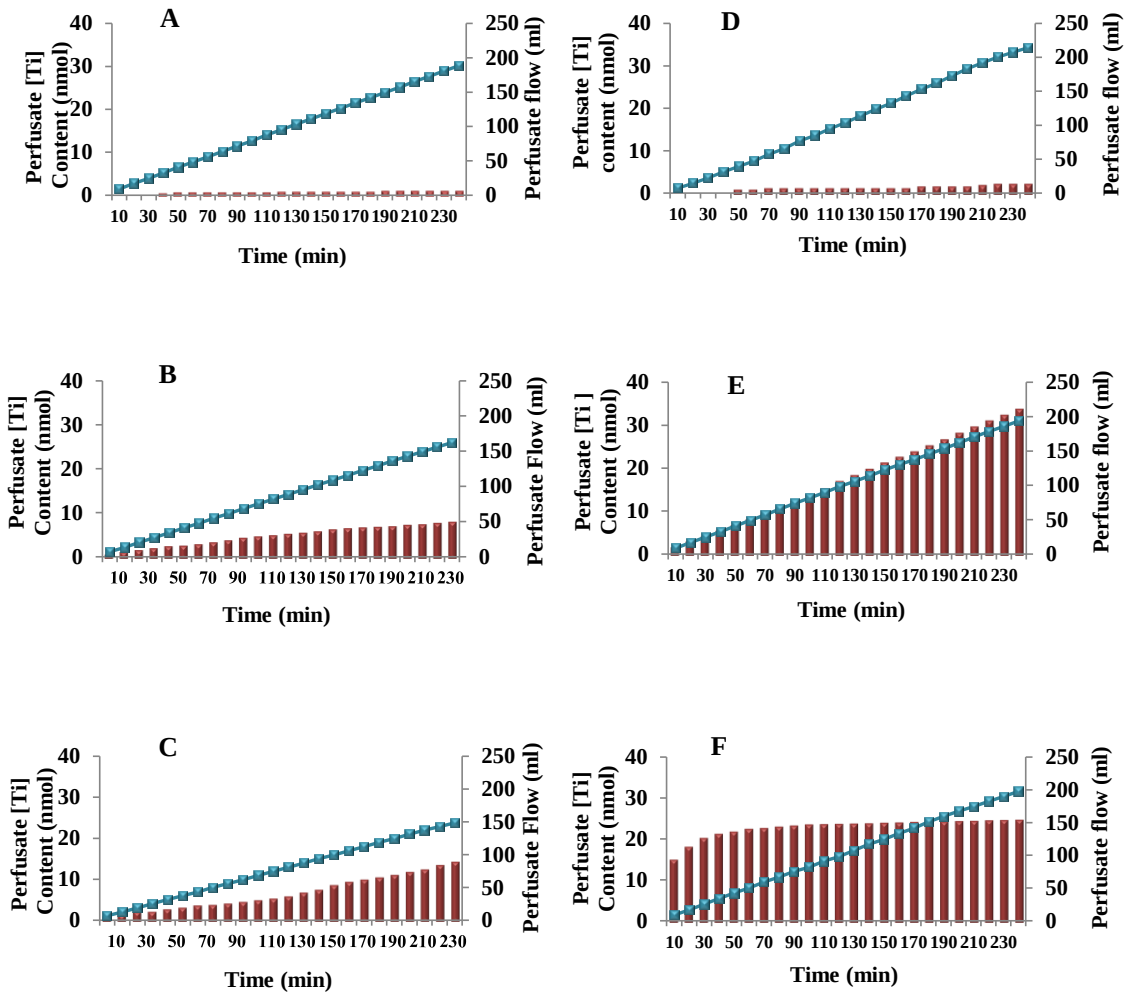

Figure 3.8 The cumulative appearance of total Ti metal in the serosal compartment (red bars, nmol Ti metal) of perfused intestine preparations from rainbow trout exposed to 1 mg l^{-1} of TiO_2 in the mucosal saline. Cumulative perfusate flow (blue diamonds, ml) is also shown. Graphs are representative examples of individual perfusions from replicated experiments (n = 6 perfusions per treatment; n = 7 perfusions for the control and TiO_2 NP treatment gassed with the standard gas mix). (A) Control with no added TiO_2, (B) bulk TiO_2, (C) TiO_2 NPs, (D) control gassed with low CO_2, (E) bulk TiO_2 gassed with low CO_2; (F) TiO_2 NPs gassed with low CO_2. Fish weights in the examples are 307, 136.3, 249.9, 229.8, 648.9 and 140.3g, respectively.

3.3.6.3 Perfusate Ti from TiO_2 and water uptake rates

Calculated net Ti from TiO_2 uptake rates and water flux across the intestine are shown (Table 3.7). When using the standard gas mixture, both bulk and nano TiO_2 treatments showed a trend of higher net fluxes compared to the no-added TiO_2 controls. However, only the TiO_2 NP treated showed a statistically significant higher net flux to the serosal compartment (7 and 9 fold higher than controls for initial and overall flux rates respectively, Table 3.7). For the standard gas mixture, there were no differences between the initial and overall Ti flux rates, indicating that the flux measurements were not hampered by saturation of the Ti electrochemical gradient (still movement of Ti across the tissue). Importantly, these net fluxes of Ti were in the opposite direction to the net water flux across the tissue (not explained by passive solvent drag). Both the bulk and TiO_2 NP treatments increased the net outward flux of water across the intestine compared to the control, and there was a statistically significant material-type effect with the bulk treatment causing more net water efflux than the nano treatment for both initial and overall rates (Kruskal-Wallis test, $P < 0.05$, Table 3.7).

3.3.7 Tissue electrolytes and moisture content of perfused intestine

Tissue electrolytes concentrations and moisture content of the perfused intestine are shown (Table 3.8). Using the standard gas mixture, there was generally no TiO_2 treatment effect on tissue Na^+ concentrations, but there was a statistically significant increase (Kruskal-Wallis test, $P < 0.05$) in tissue K^+, Mg^{2+} (in both the mid and hind intestine), and Ca^{2+} (just in the hind intestine) for the bulk TiO_2 in comparison with the control; and compared to TiO_2 NP treatments indicating a material-type effect (Table 3.8). The moisture content of the intestine was not affected by any treatment (Table 3.8).

3.3.8 Effects of lowering CO_2 to 0.5%

Some of the largest changes in total Ti metal concentration in the tissues and Ti uptake observed in these experiments were due to changing the gas mixture for the standard 95% O_2: 5% CO_2 to 99.5% O_2: 0.5% CO_2. In general, the effect of using the lower CO_2 mixture was to cause large increases in the net Ti flux to the serosal compartment (Table 3.7, Fig. 3.8), associated with either depletion (bulk material) or elevation (nano material) of the total Ti metal concentration in the tissue compared to the standard gas mixture (Fig. 3.7B). Most notably for the TiO_2 NP treatment, the initial Ti flux rate increased from 1.6 to 21.2 nmol g^{-1} h^{-1} (13 fold increase) when the lower CO_2 mixture was used (Table 3.7). This was accompanied by an increase in the total Ti metal concentration in the tissue in the 0.5% CO_2 treatment containing TiO_2 NPs (mean ± S.E.M., n = 6, mid intestine, 0.03 ± 0.01; hind intestine, 0.02 ± 0.01 μmol g^{-1}dry weight, Fig. 3.7) equating to about a 1.5 and 2.5 fold increase in these tissue respectively due to the lower CO_2 gas mixture.

There was a strong effect associated with the type of material and the increase in the initial flux rate, due to changing the gas mixture, for the bulk material was from 0.98 to 3.4 nmol g^{-1} h^{-1} (Table 3.7). This represents a 3.5 fold increase in net Ti flux, but even this is small compared to the 13 fold increase with the equivalent nanomaterial treatment (statistically significant material-type effect, Table 3.7). For the bulk material, unlike the nano scale TiO_2, the CO_2 mixture effect was to decrease the total Ti metal concentration in the tissue (e.g., a 7.2 fold decrease in the mid intestine, Fig. 3.7B). Changing the gas mixture had no effect on unexposed control intestines, and there were no anatomical regional differences for the gut in terms of the Ti accumulation response to the 0.5% CO_2 gas mixture (*t*-test, $P > 0.05$, Fig. 3.7B).

Altering the gas mixture had no statistically significant effects on net water fluxes in the intestines from control fishes, or from guts in the bulk TiO_2 treatment.

Unlike the standard gas mix the large rise in net water efflux associated with exposure to the TiO_2 NP material (Table 3.7), indicating a material-type effect of the CO_2 manipulation on water fluxes.

Changing the gas mixture generally had no effect on the electrolytes in the intestines from unexposed control animals, but did cause an increase (not significantly difference) of K^+, Ca^{2+} and Mg^{2+} concentrations in the mid intestine from the TiO_2 NP treatment, but notably in this treatment, the hind intestine also showed depletion of the same electrolytes (Table 3.8). Changing the gas mixture in the bulk TiO_2 treatment generally caused much larger increases in tissue Na^+, K^+ and Ca^{2+} concentrations than the equivalent nano treatment (combined gas and material-type effect on tissue electrolytes, Table 3.8). Moisture content and Mg^{2+} concentrations were generally unaffected by changing the gas mixture (Table 3.8).

3.3.9 Presence of particles within the gut mucosa

Transmission electron microscopy images of the gut epithelium from control, bulk and TiO_2 NP treated fish are shown in Fig. 3.9 and 3.10. For all treatments, except the no added particle control, electron dense particles are observed inside the epithelial cells with some of the particles observed inside vesicles, or associated with tight junctions (Fig. 3.9 and 3.10). Damage of the mitochondria (Fig. 3.10) was shown in the gut tissue after exposure to the bulk TiO_2 represented by degradation with lose of the structure of the mitochondria. The damaged mitochondria after exposure to TiO_2 NP were exhibited by a loss of the structure of the cristae inside the mitochondria. Degeneration of the microvilli was also noted in the epithelial cells after being exposed to both bulk and TiO_2 NP treatments (Fig. 3.9).

Table 3.7 Effects of exposure to 1mg l^{-1} TiO_2 with/without different gases on the Ti and water fluxes across the isolated perfused trout intestine.

Mucosal [TiO_2] (1mg l^{-1}) and Drugs Concentration	Net Ti flux, $J_{net,Ti}$ (nmol g^{-1} h^{-1})		Net water flux, $J_{net,H2O}$ (ml g^{-1} h^{-1})	
	Initial rate	Overall rate	Initial rate	Overall rate
Control	0.23 ± 0.16	0.26 ± 0.04	-6.22 ± 0.85	-7.50 ± 1.18
Bulk TiO_2	0.98 ± 0.47	0.85 ± 0.32	-26.28 ± 2.52*	-28.54 ± 3.19*
TiO_2 NP	1.55 ± 0.33*#	2.38 ± 0.68*#	-17.56 ± 4.00*#	-18.01 ± 4.16*#
0.5% CO_2 Control	0.51 ± 0.14	0.06 ± 0.03	-3.42 ± 1.71	-3.97 ± 0.97
0.5% CO_2 Bulk TiO_2	3.42 ± 0.74*‡	3.18 ± 0.42*‡	-7.05 ± 2.29‡	-8.95 ± 1.78*‡
0.5% CO_2 TiO_2 NP	21.16 ± 18.90*#‡	3.27 ± 1.60*[a]	-17.13 ± 2.37*#	-22.30 ± 6.40*#

Values are means ± S.E.M. (n = 6 perfusions per treatment; n = 7 perfusions for the control and TiO_2 NP treatment gassed with the standard gas mix). expressed per gram dry mass of intestine per hour. Negative values indicate a net loss from the serosal solution, initial and overall rates data were calculated from cumulative perfusate data at 10 min and 4 h, respectively.* Statistically significant difference from the relevant control values within columns (ANOVA or Kruskal-Wallis test, $P < 0.05$), # Statistically significant difference from bulk TiO_2 value within columns (ANOVA or Kruskal-Wallis test, $P < 0.05$) and ‡ Statistically significant difference from the standard gas mix group values within columns (ANOVA or Kruskal-Wallis test, $P < 0.05$). Letter (a) within rows indicates a statistically significant difference between initial and overall rates (t-test, $P < 0.05$).

Table 3.8 Total K^+, Na^+, Ca^{2+}, and Mg^{2+} Concentrations of gut tissue following exposure of isolated perfusate trout intestine to 1 mg l^{-1} TiO_2 for 4 h.

Mucosal [TiO_2] (1mg l^{-1})	Tissue [Metal] µmol g^{-1} dry mass				
	Na^+	K^+	Ca^{2+}	Mg^{2+}	Moisture %
Mid Intestine					
Control	145.5 ± 11.9	142.9 ± 16.0	17.0 ± 4.5	14.0 ± 1.7	81.0 ± 1.8
Bulk TiO_2	156.1 ± 24.3	212.0 ± 15.8*	18.6 ± 3.5	20.2 ± 1.7*	78.4 ± 2.1
TiO_2 NP	162.8 ± 34.6	136.1 ± 18.3#	12.5 ± 1.3	12.1 ± 1.2#	82.3 ± 1.7
0.5% CO_2 Control	127.8 ± 11.5	145.6 ± 14.2	15.1 ± 3.8	13.0 ± 0.9	80.5 ± 1.2
0.5% CO_2 Bulk TiO_2	329.1 ± 26.1*	283.3 ± 13.8*	35.2 ± 3.1*	16.3 ± 1.7	82.6 ± 0.8
0.5% CO_2 TiO_2 NP	118.8 ± 17.9#	161.9 ± 24.6#	22.9 ± 9.7#	14.3 ± 2.6	83.4 ± 1.8
Hind Intestine					
Control	117.4 ± 7.6	127.2 ± 7.9	9.5 ± 0.6	10.8 ± 0.4	81.6 ± 1.4
Bulk TiO_2	116.5 ± 7.6	168.3 ± 5.9*	18.0 ± 4.2*	15.8 ± 0.7*	81.5 ± 1.8
TiO_2 NP	98.7 ± 9.5	121.0 ± 7.1#	7.9 ± 0.5#	9.9 ± 0.6#	80.9 ± 1.4
0.5% CO_2 Control	109.3 ± 8.8	135.1 ± 13.1	9.6 ± 0.9	11.0 ± 0.9	81.1 ± 1.6
0.5% CO_2 Bulk TiO_2	399.7 ± 25.8*	293.3 ± 11.1*	21.1 ± 2.4*	17.9 ± 1.1	84.4 ± 0.6
0.5% CO_2 TiO_2 NP	75.1 ± 8.6#	107.8 ± 17.8#	14.5 ± 5.0	9.5 ± 1.3#	78.5 ± 3.5

Values are means ± S.E.M. (n = 6 perfusions per treatment; n = 7 perfusions for the control and TiO_2 NP treatment gassed with the standard gas mix). expressed as µmol g^{-1} dry mass of intestinal tissue, except for moisture content (%) = ((wet weight – dry weight)/wet weight) x 100. * Statistically significant difference from control values within columns (ANOVA or Kruskal-Wallis test, $P < 0.05$), # Statistically significant difference from bulk TiO_2 value within columns (ANOVA or Kruskal-Wallis test, $P < 0.05$).

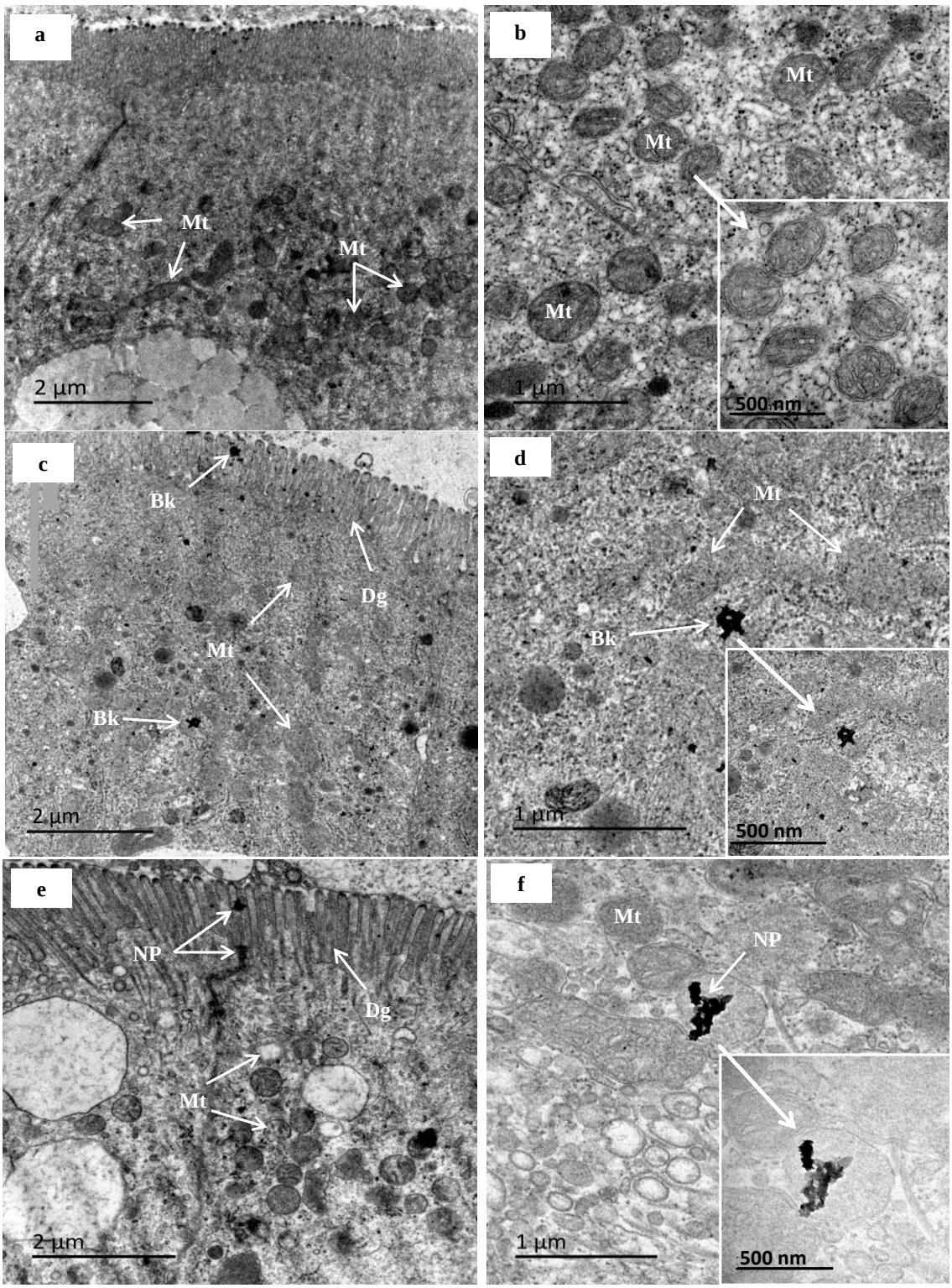

Figure 3.9 TEM images of rainbow trout gut epithelium cells. (a,b) control showing normal structure of the mitochondria (Mt); (c,d) 1 mg l^{-1} bulk TiO_2 showing accumulation of assumed bulk TiO_2 particles (Bk) and some damaged mitochondria (Mt); (e,f) 1 mg l^{-1} TiO_2 NP show examples of assumed TiO_2 nanoparticles (NP) inside the vacuoles and near to the tight junction with some damaged mitochondria (Mt). (c) and (e) Images show some occasional fusion or degeneration of parts of the villi (Dg). Scale bar = 2 µm in (a, c and e) and 1 µm in (b, d and f) as well as 500 nm, (n = 3 per treatment). Composition of the particles was not confirmed in the electron micrographs.

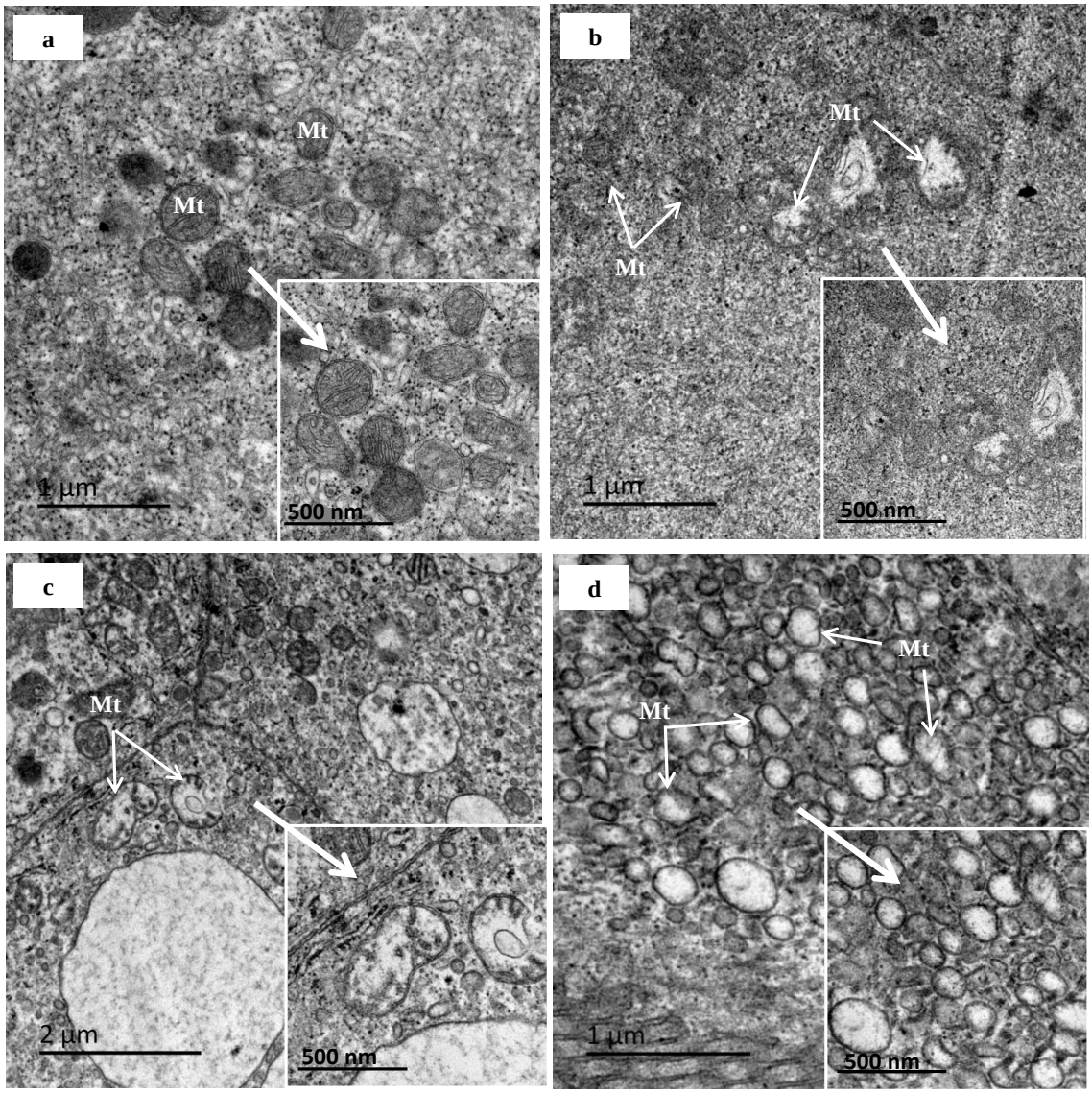

Figure 3.10 TEM images of rainbow trout gut epithelium cells (a) control showing normal structure of mitochondria (Mt), (b) 1 mg l^{-1} bulk TiO_2 showing some damaged mitochondria (Mt) represented by degradation with lose of the structure of the mitochondria, (c) and (d) 1 mg l^{-1} TiO_2 NP showing some damaged mitochondria (Mt) represented loss of the structure of the cristae inside the mitochondria. Scale bar = 1 µm in (a, b and d) as well as 500 nm, and 2 µm in (c), (*n* = 3 per treatment).

3.4 Discussion

This is the first reports on transepithelial uptake of NPs by the gut of rainbow trout, using the isolated gut perfusion technique. TiO_2 is one of the most widely used NPs and this is the first study designed to show how particles cross the gut, after the evidence of Ti accumulation in the gut, liver, gill, brain and spleen of trout (Federici et al., 2007; Ramsden et al., 2009).

3.4.1 Where is the TiO_2 NP absorbed along the gut?

Previous studies have shown Ti accumulation in rainbow trout gut from ingested water containing TiO_2 NPs during aqueous exposure studies (Federici et al., 2007) and from dietary inclusions of TiO_2 NPs (Ramsden et al., 2009). In rodents, Ti accumulation from oral exposure to bulk TiO_2 has also been reported. For example, oral gavage of high mg doses (12.5 mg kg^{-1}) of the rutile TiO_2 form of the bulk material (500 nm size) in rats causes Ti metal accumulation in the internal organs, and notably in the gut associated lymphoid tissue (Jani et al., 1994). However, to our knowledge the regional differences in total Ti metal concentrations in the tissue associated with exposure to TiO_2 particles in the gut have not been previously reported in fish. In this study following treatment with either the bulk or nanomaterial, Ti accumulated in all the regions of the gut from the oesophagus to the hind intestine. For the bulk material treatment, most of the Ti accumulation was in the intestinal regions rather than the stomach (Table 3.1), with the mid intestine having the highest total Ti metal concentrations. However, the situation was different for the TiO_2 NP treatment which showed an even accumulation of Ti in the different parts of the gut, but with a tendency for the total Ti metal concentrations to be higher in the mid and hind gut (not statistically different between gut regions, Table 3.1). There were no major fluid shifts within the gut tissue, with normal water content (66 – 81%) in the different regions of the gut and the absence of disturbances to the major electrolyte levels, especially Na^+ which is crucial to osmoregulation in the tissue

(Table 3.1). This confirms the tissue was not leaking and that the Ti accumulation cannot be explained by osmotic solvent drag. Overall, these data suggest the intestine is more important for Ti uptake from TiO_2 exposures than other parts of the gut, although the form of the accumulated Ti (as particles and/or dissolved Ti) cannot be determined from the tissue concentration measurements alone. Nonetheless, the involvement of the intestine more than other regions of the gut is consistent with reports on many other trace metals (Handy et al., 2000; Hoyle and Handy, 2005). Notably, for both experimental treatments of TiO_2, the measured total Ti metal concentrations were higher in the mucosa, rather than the muscularis (Table 3.2). This suggests a specific accumulation of either Ti metal and/or TiO_2 particles into the epithelial cells (see below). The proportions of the total Ti metal concentration in the mucosa (typically 70% or more) are broadly similar to previous reports for trace metals in fish gut (e.g. Cu in catfish gut, Handy et al., 2000; Hg in trout gut, Hoyle and Handy, 2005).

3.4.2 Viability of the perfused intestine

The viability criteria normally employed for the perfusion techniques (Handy et al., 2000). In the present study, the histology integrity of the gut as a barrier, perfusate and mucosal LDH activity, leak of ions into the mucosal solutions ($[K^+]$, $[Na^+]$) and perfusate flow were used to assess the viability. These parameters are essential to evaluate the viability criteria of the perfusion techniques (Perry et al., 1983; Perry et al., 1984; Handy et al., 2000), and the accepted results should be obtained only from those perfusions which passed all these checks. Current results from this study indicate the suitability of using the perfusion technique with the NPs which is met with the viability criteria of the preparation.

3.4.2.1 Histopathology

Histological examinations of guts after exposure to either bulk or nano TiO_2 showed normal tissue for the all gut regions. However, some minor effects on gut morphology

were shown in one or two animals considered by minor lifting of epithelium, swelling of the goblet cells and occasional appearance (occurring at infrequent parts of the tissue) of some vacuoles which would not compromise the intestinal barrier (Fig. 3.3).

3.4.2.2 LDH measurement

One of the most sensitive indicators of cell injury is the LDH activity and the amount of LDH in the normal cells (no damage) compared to that present in the blood stream (Moss and Henderson, 1986; Lott and Nemensanszky, 1987). In trout, the blood normally contains about 1 IU ml^{-1} LDH *in vivo* (Hille, 1982). In the perfusate, LDH activity is considered as a very sensitive viability indicator (Campbell et al., 1999; Handy et al., 2000), and in this study the LDH activity was far below that found *in vivo* (< 1 IU ml^{-1}) in all experiments, in perfusates (Fig. 3.4) and mucosal solutions (Fig. 3.5). The low LDH leak was evident even when the gas mixture was changed (5% or Low CO_2).

3.4.2.3 [K+], [Na+] and pH content in the mucosal solution

Leak of electrolytes from the tissue was negligible showed only micromolar changes in mucosal solution K^+, and Na^+ concentration comparing to controls (Table 3.4 and 3.5). The steady rates of eluted perfusate flow suggested good viability of the preparations (Fig. 3.8). Taken together, the good perfusate flow, low LDH leak, and normal electrolytes suggests that the preparations were of good viability and has a utility for measuring the uptake of Ti from both bulk and nano forms of TiO_2.

In the normal medium (5% CO_2), the steady mucosal solution pH and no leakage of the electrolytes also suggests no acidification of the tissue (see Handy et al., 2000; Holye and Handy, 2005). However, decreasing the gas supplement to 0.5% CO_2 caused an elevation of the pH in the mucosal solution from [insert pH] of 7.4 to about pH 7.9, suggesting either the uptake of H^+ ions by the tissue, or the efflux of bicarbonate to

result in a more alkaline pH. The secretion of bicarbonate by fish, resulting in decreased serosal HCO_3^- concentration (Grosell et al., 2005), may explain the pH change here. It is interesting that the role of this bicarbonate secretion in fish is to ensure the precipitation of magnesium and calcium carbonates (e.g., $MgCO_3$), which functions to maintain the outward diffusion gradients for divalent ions (Grosell et al., 2005). The generation of CO_3 may also occur by a spontaneous chemical reaction on the surface of the nanoparticle when the CO_2 interacts with the alkali atoms on TiO_2 (Krischok et al., 2002). This could therefore alter, the HCO_3^- equilibrium across the tissue, and therefore explain the effect of lowering the CO_2 in the presence of TiO_2 NPs.

3.4.3 Ti exposure and the distribution of the TiO_2 in the mucosal solution

The exposure to TiO_2 was confirmed by applying different processes to measure the mass concentration of TiO_2 and particle size distributions in the mucosal solution by using nanoparticle tracking analysis (NTA, Fig. 3.6), the appearance of particulate material in the mucosa by electron microscopy (Fig. 3.9 and 3.10), as well as total Ti metal concentration in the intestinal tissue (Fig. 3.7 A and B). NTA measurements were made at 30 and 240 minutes during the experiments using a triplicate samples for each time. In general, the distribution of NP and bulk TiO_2 was good, with the mean particle diameter changing from only 301 to 236 nm for the bulk material, and from 169 to 140 nm for the NPs. The distribution of particles moving towards slightly smaller sizes in the mucosal solution, are probably just a reflection of the faster settling of larger aggregates as proposed by other studies (Keller et al., 2010), and should not be interpreted as selective uptake of larger particles by the tissue. The concentration of TiO_2 in the mucosal solution was 0.35 and 0.14 mg l^{-1} of bulk and TiO_2 NPs, respectively (Table 3.6) after 4 h perfusions and exposure to 1 mg l^{-1} of TiO_2 suggesting loss of metal and/or particles from the mucosal solution. This phenomena is well known for dissolved metals where the intestinal bioavailability is a fractions of the exposure

dose, and is associated with the normal protective role of mucus secreted by the preparation which will chelate then precipitate metal ions (e.g., for Cu perfusions, 77% of the added Cu is lost at exposures of 100 µmol l^{-1}, Handy et al., 2000). Obvious clumps of white-coloured mucous precipitate appeared in the bath over time (as observed with gill mucus during waterborne exposures with TiO_2, Federici et al., 2007); suggesting precipitation of particles with the mucus.

3.4.4 The uptake of Ti from TiO_2 by the perfused intestine

3.4.4.1 Tissue TiO_2 uptake

The increase of measured total Ti metal concentrations in the tissue following exposure to either the bulk or nano form of TiO_2 confirmed that the exposure took place, and that Ti (the form cannot be identified from the total tissue Ti measurements) was presents in/on the gut tissue after 4 h perfusion. Most of the metal was internalised with the mid gut generally accumulating more Ti than the hind gut (Fig. 3.7 A and B). Particulate material was also observed inside the epithelial cells using electron microscopy (Fig. 3.9 and 3.10). Similar observations have been made in rat gut associated lymphoid tissue with measurable Ti metal from rutile TiO_2 appearing in/on the tissue (500 nm, dose 12.5 mg kg^{-1} for 10 days, Jani et al., 1994). Galloway et al. (2010) also recently reported particles from TiO_2 NP exposures in close association with the microvilli in marine polychaete worms.

The intestinal Ti accumulation was greater from the bulk TiO_2 compare to nano exposure in both mid and hind intestine with different gas supplements; suggesting that the bulk TiO_2 was accumulated in the tissue rather than diffuse to the serosal side. However, this does not imply a "nano effect" on tissue Ti accumulation *per se*. This result could be explained by the fact that the bulk material maintained a slightly higher concentration in the mucosal solution than the nano form, or that particle for particle, more Ti on a mass basis is inevitably moved into the tissue by uptake of a bulk particle

compared to a smaller nano one. Regardless of any nano effect, the fact that Ti accumulates in the intestine suggests that the efflux of Ti from the gut to the blood must be slower than the mucosal (apical) uptake in order to achieve net accumulation in the tissue.

3.4.4.2 Serosal TiO_2 uptake

In all experiments, there was a cumulative increase of total Ti metal in the serosal perfusate suggesting transepithelial absorption of either Ti metal and/or particulate TiO_2. The nano form of TiO_2 showed higher values compare to bulk TiO_2 in the serosal perfusate content which indicated the transfer of the NP into the serosal perfusate rather than accumulation in the intestinal tissue (i.e., more transepithelial uptake of the nanoform). The steady, and sometimes saturable, appearance of Ti in the eluted perfusate over time (Fig. 3.8), suggests a carrier-mediated mechanism(s). This hypothesis is supported by net water flux being in the opposite direction to net Ti fluxes (Table 3.7) and the absence of dilution of electrolytes in the tissue (Table 3.8); excluding passive solvent drag or leak (see Handy et al., 2000) of any (theoretically) dissolved Ti.

3.4.4.3 Perfusate Ti from TiO_2 and water uptake rates

The differences between the initial and overall TiO_2 uptake rates (Table 3.7) indicate that the serosal solution was at equilibrium with TiO_2 during the experiments. However, this is not simply explained by diffusion process associated with solvent drag of water across the epithelium. First of all this is not a valid scientific argument as NPs are not in solution, but in suspension. There is no logical reason why solvent drag would occur. Also, the water fluxes are in the opposite direction to the Ti fluxes. The latter is best explained by a carrier-mediated process, not by the solvent drag. The same suggestion

has been made by Handy et al. (2000) after exposure of the perfused intestine to dissolved copper.

3.4.5 Effects of altering the gas composition on Ti uptake

Interestingly, the largest increase of net Ti uptake to the serosal compartment was caused by changing the gas mixture from 95% O_2: 5% CO_2 to 99.5% O_2: 0.5% CO_2. It seems unlikely that the small 4% increase in O_2 content is physiologically important, since the tissue is already saturated with oxygen. The maximum amount of the oxygen in fresh water at air saturation (21% oxygen) is about 10 mg l^{-1} (Eddy and Handy, 2012) and the gut tissue in the isolated perfused experiment was in direct contact with 99.5% of O_2 which means it is given at least five times the amount of the O_2 in fresh water. However, a change of CO_2 from 5 to 0.5% represents a profound change in acid-base balance for a freshwater fish (review, Goss et al., 1992). It is common practise in fish cell culture, and with perfused organ methods to use 95% O_2: 5% CO_2 as a standard gas mixture for *in vitro* preparations. In this experiment, changing the gas mixture to 99.5% O_2: 0.5% CO_2 (10 fold reductions in CO_2 content) caused a 13-fold increase in the initial Ti uptake rate in the TiO_2 NP exposed intestines (Table 3.7). A statistically significant effect was also noted for the bulk material, with a 3-fold increase in the initial Ti uptake with the 0.05% CO_2 gas mixture (Table 3.7).

This unexpected finding represents an important nano effect on bioavailability (10 fold elevation in Ti uptake with the nano treatment compared to the bulk treatment) that may also be of profound importance in real ecosystems because it is related to the partial pressure of gases in the external medium. The mechanisms involved require further investigation, but there are several possible explanations for this effect. One biological explanation is that the 5% CO_2 in the standard gas mixture for *in vitro* studies represents a severe acidosis for a freshwater fish (which normally have blood pCO_2 ten times lower than mammals, Eddy, 1977; Goss et al., 1992). Thus, lowering the CO_2 to

0.5% is simply moving it closer to *in vivo* values, and the Ti transport mechanism(s) are just recovering their normal (higher) transport rate following acidosis. This argument would work well for fish gill, but not the gut mucosa which can see some high CO_2 levels during digestive processes, and has sufficient carbonic anhydrase activity to convert CO_2 to bicarbonate (Grosell et al., 2009). In the present experimental conditions, the elevation of Ti uptake rate with decreasing CO_2 content of the gas mixture occurred with the expected changes of pH in the external medium associated with normal net base excretion in the intestine (> by about 0.4 pH units in the standard CO_2 mixture, and about 0.8 units in the 0.5% CO_2 mixture). The pCO_2 effect on Ti uptake can be explained by acid-base toxicity in the intestine.

An alternative explanation is that one of the mechanisms of Ti movement across serosal membrane is HCO_3^--sensitive. Anion-dependent metal efflux pathways are known including a DIDS (4,4'-diisothiocyano stilbene-2,2'-disulfonic acid) and Cl^- sensitive Cu efflux in fish intestine (Handy et al., 2000), a Mg-anion transporter in mammalian cardiac muscle (Ödblom and Handy, 1999), and uptake of anionic Zn species on the Cl^-/HCO_3^- exchanger in red blood cells (Torrubia and Garay, 1989). In the saline conditions of natural seawater Ti is almost exclusively present as $TiO(OH)_2$ (Van Den Berg et al., 1994), and water soluble forms of Ti readily form anion complexes with anions like citrate (Deng et al., 2007). It therefore seems theoretically possible that anion complexes of Ti could be exported to the blood on a basolaterally-located anion-exchanger, using the downward serosal to apical HCO_3^- gradient (low external CO_2) as a driving force.

The gas mixture effect is not easily explained by the chemical reactivity of TiO_2 with CO_2. Carbon dioxide gas spontaneously reacts on the surface of TiO_2 particles in the presence of alkali metals (e.g., Na^+ K^+, present in the gut at mmolar levels) to form carbonate ions (Krischok et al., 2002), that would be rapidly converted to HCO_3^- ions in

the gut lumen by carbonic anhydrase activity. The reaction on the crystal surface of the metal oxide normally uses oxygen from water molecules, but can utilise surface oxygen atoms from the TiO_2, especially where there are point defects in the crystal structure (Linsebigler et al., 1995). Thus a reaction of the crystal surface with CO_2 could liberate Ti ions as the oxygen atoms in the TiO_2 structure are used up. However, decreasing CO_2 in the medium would be expected to slow this reaction and therefore the availability of Ti ions in solution (less Ti dissolution). This is not consistent with the observed increase in Ti uptake at the lower CO_2 content (Fig. 3.8; Table 3.7). However, lowering the CO_2 would decrease external HCO_3^- generated by this reaction in the gut lumen and would drive some of the metal-anion transporters above. The gas mixture-dependent increase in Ti uptake was also observed with the bulk powder treatment, but to a lesser extent than the nano treatment. This is not necessarily a nano size effect, as numerous aspects of the crystal structure and spatial arrangement of particle surfaces will alter the CO_2 reaction outline above (Linsebigler et al., 1995), but clearly the gas mixture effect was stronger with nano compared to bulk material treatment in the experimental conditions used here.

3.4.6 Is there a material-type effect on tissue electrolytes in the perfused intestine?

There are some differences of Ti accumulation and uptake rates between bulk and nano treatments of TiO_2 in the perfused intestine (Fig. 3.7A and B; Table 3.7), but whether or not this translates into a nano effect of functional significance to the gut as an important osmoregulatory organ is less clear. Exposure to either material increased net water efflux across the intestine (Table 3.7, standard gas mix), but the bulk TiO_2 treatment caused a greater net water efflux than the nano treatment (Table 3.7) without dehydrating the tissue or altering tissue Na^+ (Table 3.8). This suggests the bulk material was better at promoting physiological flux of water to the gut lumen, which would be an osmoregulatory advantage for a freshwater fish living in a very dilute environment

(Eddy, 2009). The bulk material also caused Mg^{2+} retention in the gut that was not observed in the nano treatment (Table 3.8), suggesting some material-specific effects on magnesium homeostasis. In the hind intestine, this was also accompanied by elevation of tissue Ca^{2+} due to treatment with the bulk material only (Table 3.8), implying some regional effect on calcium homeostasis. Similar observations were made for K^+ in the mid intestine (Table 3.8). The depolarising effect of increased tissue K^+ (i.e., more positive mucosal membrane potential) might also contribute to the difference in Ti uptake rate between the bulk and nano forms in this experiment (positive potential slowing Ti influx). The experiment with the 0.5% CO_2 gas mix also revealed a bulk material-specific elevation of tissue electrolytes compared to all other treatments, especially on tissue Na^+ (Table 3.8). The reasons for this are unclear, but for example, bulk material interference with sodium carbonate co-transport is worthy of investigation.

Some mitochondrial damaged was found in the gut tissue after been exposed to both bulk and TiO_2 NP (Fig. 3.9 and 3.10). This damage included some degradation of the mitochondrial structure and swelling with the loss of definition of the cristae in the mitochondria. This observation is consistent with some oxidative injury of some of the mitochondria. The same mitochondrial damaged in the gut was shown in earthworms treated with 5 g kg^{-1} of TiO_2 NPs (Hu et al., 2010), the authors reported disorganization, fracture and reduction (in size) of the mitochondria, and loss of the structure of the cristae. The physiological significance of these phenomena relates to the absorptive function of the epithelium. For example, during active trace element absorption from the food, trout intestinal epithelial cells show intact mitochondria which are aligned directly under the microvilli on the apical surface (Kamunde et al., 2003), apparently to provide energy for forming absorptive vesicles containing the micronutrients. Disrupted mitochondria would be less able to perform such functions.

Conclusions

This study shows that the isolated perfused intestine preparation works with NPs, and the viability criteria remain good with these materials. Additionally, this work demonstrates that Ti from TiO_2 can cross the vertebrate intestine to appear in the serosal compartment, and there is a material-type effect with much faster net uptake of Ti from the nano form. Ti absorption from both bulk TiO_2 and nano form is time-dependent, saturable and the uptake mechanism is affected by the gas mixture used. All these factors suggest an active absorption mechanism happened. Therefore, from a regulatory perspective, a dietary exposure hazard to ecosystems and human health should be considered in risk assessments. The net uptake rates reported here for Ti are approximately 1-3 nmol g^{-1} h^{-1}, identical to those for copper (Handy et al., 2000), but about 10 fold less than Hg uptake rates (40-50 nmol g^{-1} h^{-1} for 0.2-2 mg l^{-1} of Hg metal, Hoyle and Handy, 2005) in the perfused intestine. The oral uptake hazard for Ti is therefore of a similar magnitude to other metals (see also Ramsden et al., 2009). The fact that the nano form is taken up faster than bulk TiO_2 also implies that risk assessments based on the bulk material will underestimate the nano accumulation hazard. The assumption that the traditional bulk forms of TiO_2 powders are not appreciably absorbed via the gut should also be reconsidered. Notably, the gas mixture effect observed in the present study, adds a new dimension to hazard assessment not previously considered for metals or NMs. For ecosystems this could include considering changes in environmental pCO_2 associated with the exposure to TiO_2.

Chapter 4

Behaviour of TiO_2 NPs in the gut lumen and pharmacological studies on the uptake mechanism across the isolated perfused intestine of rainbow trout: nystatin and vanadate sensitive components

Abstract

There is limited information on the uptake mechanism of NPs and their pathway(s) across the gastrointestinal tract. In this study, different kinds of inhibitors (pharmacology treatments) were used to determine the pathway(s) for the uptake of Ti from TiO_2 exposures across the gut epithelium of the isolated gut perfusion of rainbow trout (*Oncorhynchus mykiss*). Pharmacological investigations of the uptake mechanism(s) of the Ti from TiO_2 NPs in perfusions gassed with 95% O_2: 5% CO_2 showed that addition of 10 mmol l^{-1} potassium cyanide (KCN) to the mucosal and serosal solutions caused an elevated accumulation of Ti in the tissue, but this did not stop transepthelial uptake into the serosal compartment with 2.56 ± 0.65 nmol g^{-1} h^{-1} of Ti from the TiO_2 NPs (mean ± S.E.M., n = 6). The addition of 100 µmol l^{-1} sodium orthovanadate, a P-type ATPase inhibitor, to the serosal solution increased the initial net uptake rate of Ti from TiO_2 NPs by 1.5 fold to 2.29 ± 0.64 nmol g^{-1} h^{-1} (mean ± S.E.M., n = 6) compared to the TiO_2 NP treatment without vanadate. However, the overall net uptake in 4 h of Ti to the serosal compartment was reduced by 2.8 fold after vanadate additions. In contrast, adding 120 IU ml^{-1} nystatin, an endocytosis inhibitor, to the mucosal solution completely blocked the uptake of Ti from both TiO_2 NPs and the bulk powder. The pharmacological responses with TiO_2 NPs showed some differences compared to their responses with bulk powder. We conclude that the uptake mechanism(s) involve a nystatin-sensitive endocytosis across the mucosal membrane.

4.1 Introduction

The precise mechanism(s) of NP uptake across the epithelia of fish (and mammals) remains controversial (Handy et al., 2008b; Shaw and Handy, 2011). Handy et al. (2008b) argues that apical entry of intact NPs into the epithelial cells of fish (gills, gut) is unlikely to occur via the traditional ion transport pathways (e.g., by diffusion through epithelial ion channels), because the NPs are simply far too large, but uptake into the cells by endocytosis remains possible. Similar arguments have been made for the mammalian gut (Panessa-Warren et al., 2006), and the cells of invertebrates (Moore, 2006). The diffusion of intact NPs through the paracellular route (e.g., via tight junctions) into the blood also seems unlikely (Handy et al., 2008b), due to the Ca^{2+} and Mg^{2+}-rich microenvironment of the tight junctions which may lead the NPs forming aggregates. It seems more likely that most uptakes would be trans-cellular. However, it remains unknown whether any NPs taken up by putative endocytosis from the mucosal solution would be exported into the blood as intact particles or broken down to free metal ions. Information on the NPs transfer across epithelia is still unclear, relative to our knowledge on traditional dissolved metals (e.g., Foulkes and Bergman, 1993a; Handy et al., 2002a review).

The aim of this study was to pharmacologically investigate the uptake mechanisms of NPs using the isolated perfused intestine (Handy et al., 2000), and to also interpret any uptake in the context of particle behaviour in the gut lumen as well as surface bindings on the intestinal mucosa. The pharmacological investigations here involved using: (i) potassium cyanide (KCN) which is a general inhibitor of aerobic metabolism and often reduces the availability of ATP in cells for energy-dependent processes such as active ion uptake or movement of the cytoskeleton (endocytosis, cell volume control, etc.,); (ii) sodium orthovanadate which is a P-type ATPase inhibitor which non-specifically blocks the ATPase family of ion pumps including the Na^{+}-K^{+}

ATPase, Ca^{2+}-ATPase, and Mg^{2+}-ATPase; (iii) nystatin, a putative inhibitor of the lipid raft-caveolae endocytosis pathway in animal cells. To interpret whether apparent uptake had any surface-bound components of Ti, some rapid solution dipping experiments were done to measure the instantaneous adsorption of TiO_2 to the intestine. In addition, and the possibility of free metal ion dissolution from the particles was explored using a dialysis method to aid interpretation of particle versus free metal ion absorption.

4.2 Methodology

4.2.1 Surface binding experiment

To aid data interpretation on Ti accumulation in the mucosa, some rapid solution dipping experiments were done to quantify surface binding of Ti. The approach followed a well-established method for fish tissue (Handy and Eddy, 2004) which is also well known for metal salts (Shaw and Handy, 2011). The technique involves allowing the tissue to instantaneous adsorb metal onto the surface of the epithelium over a few seconds (i.e., before true uptake can occur) and then determining the metal concentration on/in the tissue. Measurements were made on both mid and hind intestine. Briefly, fish were sacrificed and the intestinal tract was quickly removed, everted, and then rinsed in clean saline (see Chapter 3). Pieces of mid or hind intestine (n = 6 fish per treatment) were then dipped (mucosa facing the solution) in 500 ml of fresh physiological saline for 15 sec (control dip to equilibrate the surface of the tissue with the saline), then dipped in to 1 mg l^{-1} of TiO_2 NPs or bulk TiO_2 in 500 ml physiological saline for 30 sec. Finally, tissues were rinsed of excess TiO_2 by dipping in two consecutive 500 ml beakers of clean physiological saline (total of 15 seconds rinsing) (Fig. 4.1). Tissues were then digested in nitric acid and analysed for total Ti metal concentrations as described in Chapter 2.

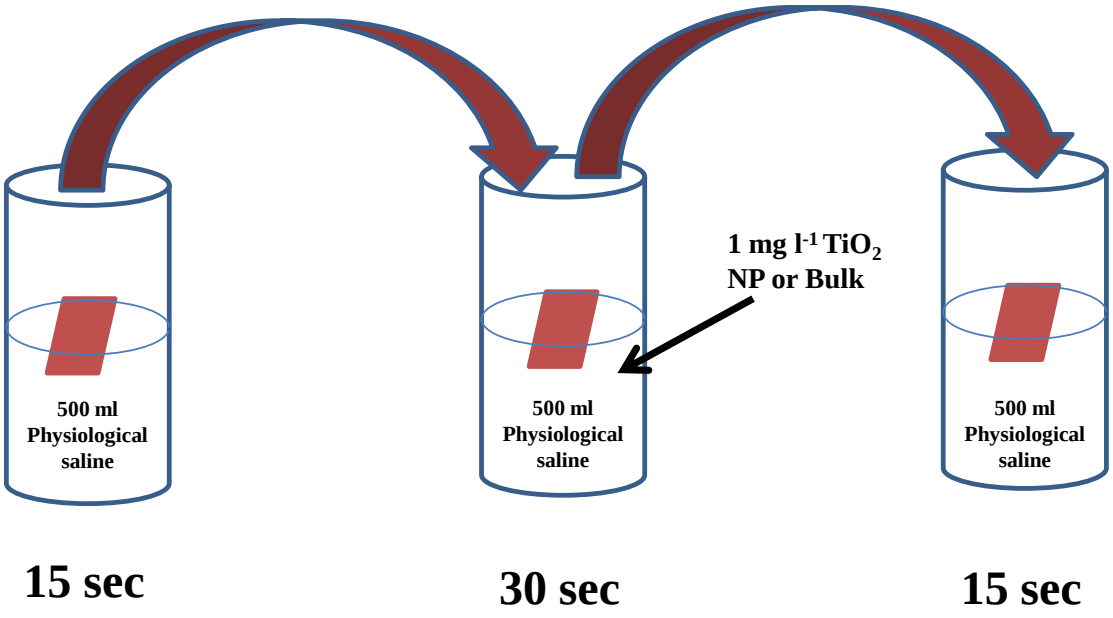

Figure 4.1 Method of the surface binding tissue experiment showing the processing of the everted tissue dipping first in 500 ml of clean physiological saline for 15 sec then exposed the tissue to the 1 mg l^{-1} of TiO_2 for up to 30 sec and finally dipped in same clean saline for 15 sec rinsing.

4.2.2 Dialysis experiments

These experiments were conducted to determine whether an apparent dissolved Ti metal fraction could be released from the TiO_2 NPs or the bulk material contained within dialysis tubing in the experimental conditions used for the gut perfusions. The rates of appearance of total apparently dissolved Ti (i.e., measured total Ti that could pass through the dialysis membrane into the external media) from the TiO_2 NPs or bulk TiO_2 in the physiological saline (described in Chapter 2) was determined using the standard gas mix and the low CO_2 gas mixture, at pH 7.4. In addition, a saline mimicking intracellular conditions (Handy et al., 1996) was also tested, which contained (in mmol l^{-1}): KCl, 140; NaCl, 10; HEPES, 10 and adjusted to pH 7.2 to represent cytosolic intracellular pH. The intracellular saline was also made at pH 3, to determine whether an extremely acidic pH in an intracellular compartment (e.g., lysosomes) would cause the release of apparently dissolved Ti through the dialysis tubing. All glassware was acid washed (5% nitric acid) and triple rinsed in ultrapure Milli-Q water. The dialysis method is based on Handy et al. (1989) with modifications for NMs. Briefly, 8 ml of 100 mg l^{-1} of TiO_2 NPs, bulk TiO_2 stock dispersions made in the appropriate saline, or a control (the appropriate saline with no added TiO_2) were placed carefully into dialysis bags (7 cm long x 25 mm wide, dialysis tubing product code: D9777, cellulose membrane with a molecular weight cut off at 12,000 Da, Sigma-Aldrich, St. Louis, USA) and the ends closed with Medi-clips to prevent any leakage. The bags were immediately dialysed in a glass beaker containing 492 ml of the appropriate saline (bringing the total volume to 500 ml). Care was taken to use beakers of identical shape/size for the experiments, and each experiment was performed in triplicate (3 separate beakers) for each material and external medium (intracellular saline pH 7.2 and pH 3, physiological saline with standard gas mix and low gas mixture). The solutions in the beakers were gently agitated with a multipoint magnetic stirrer (RO 15P power, Ika-

Werke GmbH & Co. KG, Staufen, Germany) for 24 h at room temperature (21 °C). Samples of the external media (4.5 ml) were taken from each beaker at 0, 0.5, 1, 2, 3, 4, 6, 8 and 24 h, the pH of the samples was recorded at each time point. At the end of experiment, the remaining contents of the dialysis bag were also collected. All samples were then analysed by ICP-OES for total Ti metal concentration.

4.2.3 Preparation of the isolated perfused intestine

The preparation of isolated perfused intestine was performed exactly as described in Chapter 2 with some additions. Briefly, a series of perfusions were used to investigate the effects of inhibitors (n = 6 perfusions per treatment for each inhibitor). These included experiments with 10 mmol l^{-1} cyanide (KCN) added to both the perfusate and mucosal solutions to determine whether Ti uptake from exposure to TiO_2 NP had an energy-dependent component. Then in experiments using TiO_2 or bulk powder, the effects of adding 100 µmol l^{-1} sodium orthovanadate (Na_3Vo_4, an ATPase transporter inhibitor, Campbell et al., 1999; Handy et al., 2000) to the serosal solution was tested to explore whether ion transport was involved in Ti export from the gut cells to the blood. In separate experiments, additions of the endocytosis inhibitor, 120 IU ml^{-1} nystatin (dose to produce 100% inhibition, Lewis et al., 1977), was added to the mucosal solution only.

The stock animals, preparations of the TiO_2 stock solutions and trace metal analysis, histology, calculations and statistical analysis were described in details in Chapter 2.

4.3 Results

4.3.1 Ti accumulation by surface binding experiment

Measurements from the rapid solution dipping protocol to determine surface-bound Ti on the mid and hind intestine revealed low concentrations of Ti metal. The total Ti metal concentration of dipped mid intestine was (means ± S.E.M., n = 6); 0.007 ± 0.001, 0.014 ± 0.005 and 0.012 ± 0.002 μmol g^{-1} for control, bulk and TiO_2 NP exposures, respectively. The values for the TiO_2 treatments were not statistically different from the control (Kruskal-Wallis test, P = 0.47, Fig. 4.2), indicating negligible surface binding, and tissue concentrations were also significantly lower than those reported in the whole gut sacs or perfused intestine (t-tests, P values all < 0.05). Total Ti metal concentration in dipped hind intestine was (mean ± S.E.M., n = 6); 0.006 ± 0.001, 0.014 ± 0.002 and 0.008 ± 0.002 μmol g^{-1} for control, bulk and TiO_2 NP exposures, respectively, with only the bulk being significantly higher than both control and NPs (ANOVA, P = 0.04, Fig. 4.2). Total Ti metal concentrations in the hind gut from the surface binding experiments were also significantly lower than the values reported in the whole gut sacs or intestinal perfusions (t-tests, P values all < 0.05), with the later representing (at the most) 27 and 26% of the total Ti reported for intact hind gut tissue in Table 3.1.

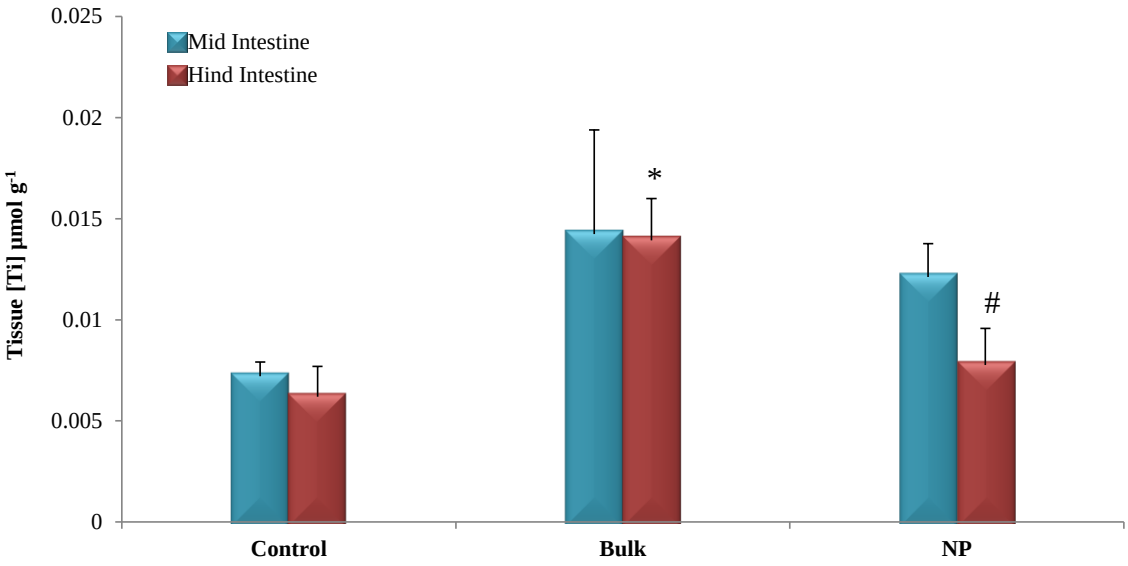

Figure 4.2 Total Ti metal concentrations in the tissues determined by ICP-OES in the dibbed mid (blue bars) and hind intestine (red bars) after exposed to 1 mg l^{-1} TiO_2 (bulk or NP). Data are means ± S.E.M. (n = 6 perfusions per treatment). * Statistically significant difference from control values (ANOVA or Kruskal-Wallis test, $P < 0.05$). # Statistically significant difference from bulk TiO_2 tretment (ANOVA or Kruskal-Wallis test, $P < 0.05$). There is no significant difference found between mid and hind intestine (t-test, $P > 0.05$).

4.3.2 Apparent total dissolved Ti from dialysis experiments with the mucosal solution and with intracellular salines

Dialysis experiments confirmed no measurable appearance of apparent total dissolved Ti metal from either the bulk or nano TiO_2 in the physiological saline used for the mucosal solution, indicating that the tissue was probably only exposed to particles. There were no measurable increases in the total Ti metal concentrations in any of the beakers from the dialysis experiments with physiological saline over 24 h (concentrations below detection limit, all < 1 µg l^{-1}), regardless of the gas mixture (stand gas mix, or low CO_2 mix) or the type of particles added (the same finding for bulk and nano, data not shown). However, this was not the case for salines mimicking the intracellular environment.

Unlike the mucosal solution, the dialysis experiments using salines representing the intracellular ionic environment did show some appearance of measurable total Ti metal in the beakers from dialysis bags containing either the bulk or nano forms of TiO_2. In the pH 3 experiment (representing the low pH of vesicular compartments such as lysosomes) there was a small but detectable increase in apparent total dissolved Ti in the external media (beakers) after 3h in the TiO_2 treatments. Calculated cumulative Ti releases over 24 h were < 0.45 (values below detection in controls), 1.15, and 2.25 µg of Ti metal (mean of the triplicate measurement, absolute amount released) in to each dialysis bag for control, bulk and nano TiO_2, respectively. The rate of appearance of total metal in the external media in the beakers was much greater for the intracellular solution at pH 7.2 (i.e., representing the general cytosolic pH) with a clear time-dependent cumulative increase of the apparent total dissolved Ti concentrations in the beakers (Fig. 4.3). The maximum rates of appearance of cumulative total metal in the beakers (steepest part of the curves, not at equilibrium) were 9.7 and 6.9 µg Ti metal h^{-1} (or 26 and 18 nmols Ti metal h^{-1}) for the bulk and nano TiO_2, respectively (control, at or

below detection limit). The beakers reached a steady-state maximum release of 46.0, and 34.7 µg Ti metal over the 24 h for the bulk and TiO_2, respectively (Fig. 4.3).

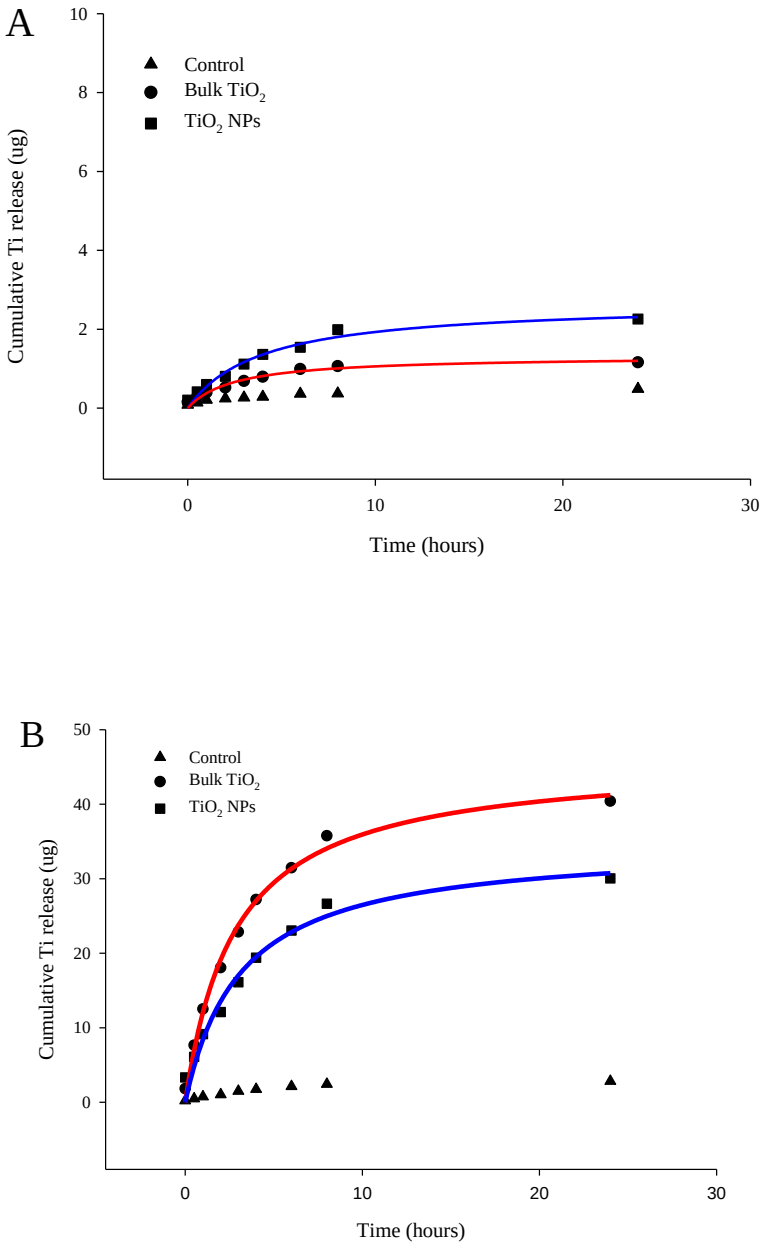

Figure 4.3 The cumulative appearance of total Ti metal through dialysis tubing into the external medium of beakers for dialysis bags containing either bulk or nano TiO_2 using a saline mimicking the intracellular environment at pH 3 and pH 7.2. The data points are mean values derived from triplicate measurements (n = 3 beakers per treatment). Curves are fitted to the data points shown using a rectangular hyperbole function (one site, ligand binding to saturation) in SigmaPlot version 12. At pH 3, the bulk: y = 1.32*abs(x)/(2.51 + abs(x)), r^2 = 0.96. For TiO_2 NPs: y = 2.68*abs(x)/(3.90 + abs(x)), r^2 = 0.97. At pH 7.2, the bulk: y = 46.04*abs(x)/(2.815 + abs(x)), r^2 = 0.99, and TiO_2 NPs: y = 34.74*abs(x)/(3.126 + abs(x)), r^2 = 0.99. The controls were at or below detection limits, and so a curve is not fitted, but data points are shown for convenience (i.e., cumulative sum of detection limit values). The standard errors were too small to be visible on the figures.

4.3.3 Effects of inhibitors on the TiO_2 NP treatment

In general, the additions of inhibitors decreased the cumulative uptake of Ti to the serosal compartment, but without compromising perfusate flow in the preparations (examples in Fig. 4.4). This was confirmed for the TiO_2 NP treatment by a statistically significant decrease in the overall Ti net flux in the presence of 10 mmol l^{-1} cyanide, 100 µmol l^{-1} vanadate or 120 IU ml^{-1} nystatin compared to the no added Ti control, or the bulk material alone (Kruskal-Wallis test, $P < 0.05$). Notably, nystatin completely abolished the Ti flux associated with the TiO_2 NP treatment. The effects of all these drugs on the TiO_2 NP treatment was accompanied by a statistically significant reduction in net water flux compared to the equivalent no-added drug TiO_2 treatment, but the water fluxes were still higher than the resting values from control intestines (Table 4.1) indicating that that additions of inhibitors did not reverse the effects of TiO_2 on net water efflux across the gut.

Despite some marked reductions in the net Ti flux associated with TiO_2 NPs exposure in the presence of inhibitors (Table 4.1), the effects of inhibitors on tissue total Ti metal concentrations during the TiO_2 NP exposures were modest. Serosal and mucosal applications of 10 mmol l^{-1} cyanide (KCN) did not stop Ti accumulation in the tissue for the TiO_2 NP treatment, but instead, increased the total Ti metal concentration in the tissue. Values were 0.08 ± 0.01 and 0.03 ± 0.01 µmol g^{-1} dry weight for the mid and hind intestine, respectively with cyanide (mean ± S.E.M., $n = 6$ for each, Fig. 4.5), being 4.1 and 1.4 fold higher than their respective tissue concentration in the presence of TiO_2 NPs without cyanide (statistically significant cyanide effect, *t*-tests, $p = 0.001$ and 0.035, respectively). For the TiO_2 NP treatment with vanadate (Fig. 4.5), some Ti accumulation in the tissue was observed in mid and hind intestine (total Ti metal concentrations in the tissue, mean ± S.E.M., $n = 6$; 0.033 ± 0.005 and 0.013 ± 0.004 µmol g^{-1} dry weight, respectively), representing a small 1.7 fold increase in Ti in the

mid intestine compared to the TiO_2 treatment without the vanadate for the mid intestine (not statistically significant, *t*-test, $P = 0.06$), and a 0.4 fold decrease in the hind intestine (not statistically significant, *t*-test, $P = 0.45$). In the case of nystatin additions, the situation was similar with measurable Ti accumulation in the tissue (Fig. 4.5, 0.017 ± 0.004 and 0.007 ± 0.002 μmol g^{-1} dry weight in the mid and hind intestine, respectively), but being only 10% and 68% lower than the respective values without the drug with TiO_2 NPs (*t*-tests, $P = 0.26$ and 0.39, mid and hind intestine, respectively).

Metabolic and ion transport inhibitors are expected to cause some dissipation of electrolyte gradients across tissues, all three inhibitors (cyanide, vanadate, and nystatin) caused statistically significant elevation of tissue Na^+ and Ca^{2+} concentrations, and depletion of K^+ in mid intestine, compared to the appropriate drug-free control (Table 4.2). For example the TiO_2 NP treatment with cyanide (mean ± S.E.M., $n = 6$, mid intestine) showed Na^+, Ca^{2+} and K^+ concentrations of 405.2 ± 54.7, 66.5 ± 11.1 and 73.1 ± 10.9 μmol g^{-1} dry weight for each electrolyte, respectively. The same situation found in hind intestine, just for the K^+ concentrations in vanadate and nystatin groups which appear significantly higher than TiO_2 NP drug free control. There were no drug effects on Mg^{2+} concentrations or tissue moisture content for both mid and hind intestine (Table 4.2).

4.3.4 Effects of inhibitors on the bulk TiO_2 treatment

The inhibitory effects of drugs on net Ti fluxes for the bulk material treatment were similar to those for the TiO_2 NPs (Table 4.1), with the drugs also abolishing or reducing the Ti net flux. There was a notable material-type effect on the vanadate-sensitive Ti flux (Table 4.1), with the Ti flux associated with the bulk material treatment being completely abolished, compared to only partial inhibition in the nano treatment (i.e., different sensitivities of the Ti flux associated with the bulk and nano treatments to vanadate). The total Ti metal concentrations in tissues following drug treatments in the

bulk TiO_2 exposure, showed statistically significant reductions in tissue Ti compared to the no-added drug Ti control (Fig. 4.5). For example, the addition of 100 µmol l^{-1} vanadate to the perfusate solution showed total Ti metal concentrations associated with the bulk Ti treatment in the mid and hind intestine of 0.028 ± 0.006 and 0.007 ± 0.001 µmol g^{-1}dry weight of tissue, respectively (mean ± S.E.M., n = 6 for each), being 6.6 and 1.5 fold less than in the TiO_2 bulk treatment without drugs for mid and hind intestine, respectively (t-tests, $P < 0.05$). For the 120 IU ml^{-1} nystatin, a similar effect on tissue total Ti metal concentrations was observed with Ti from the bulk Ti treatment with nystatin in the mid and hind intestine being 0.031 ± 0.004 and 0.008 ± 0.001 µmol g^{-1}dry weight of tissue, respectively (mean ± S.E.M., n = 6 for each), 6.3 and 1.4 fold less than that in the TiO_2 bulk treatment without drugs for mid and hind intestine, respectively (t-tests, $P < 0.05$). The tissue electrolyte response to inhibitors was similar to that described for the nano TiO_2 treatment above (Table 4.2), just for the Mg^{2+} concentrations with drug treatments which appear significantly lower than TiO_2 bulk drug free control for both mid and hind intestine (Table 4.2).

4.3.5 Histopathology

The histological examination of the perfusate intestine after 4 h perfusion with 1 mg l^{-1} TiO_2 NPs or bulk using different inhibitors showed some minor injuries in the intestinal tissue (Fig. 4.6 and 4.7), the addition of 10 mmol l^{-1} potassium cyanide to the serosal and mucosal solution showed some abnormal structure of the mucosal layer in compare to TiO_2 NP drug free control in five out of six animals. There were also some lesser effects with additions of 120 IU ml^{-1} of nystatin to the mucosal solution in both bulk and nano TiO_2 which showed in three out of six animals per treatment. Serosal addition of 100 µmol l^{-1} of sodium vanadate showed fusion of the occasional intestinal villi with the occasional appearance (in one part of the tissue) of vacuoles in the villi with TiO_2

NPs and shown in two out of six animals, but with the bulk TiO_2 the effects was minor, just a slight appearance of lifting epithelium which showed in one out of six animals.

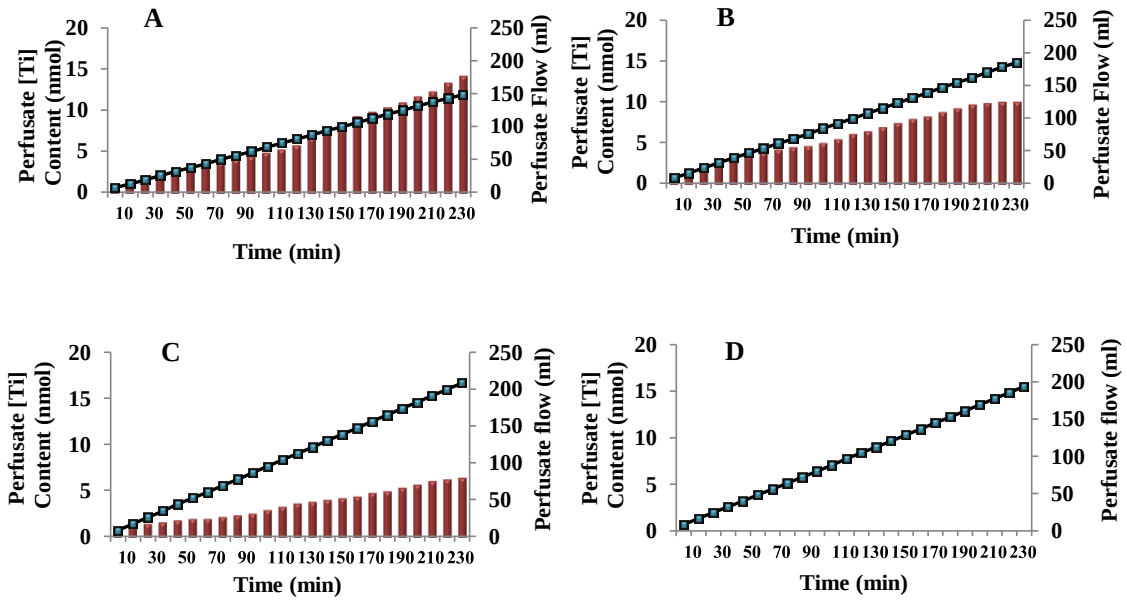

Figure 4.4 The cumulative appearance of total Ti metal in the serosal compartment (red bars, nmol Ti metal) of perfused intestine preparations from rainbow trout exposed to 1 mg l^{-1} of TiO_2 in the mucosal saline. Cumulative perfusate flow (blue diamonds, ml) is also shown. Graphs are representative examples of individual perfusions from replicated experiments (n = 6 perfusions per treatment; n = 7 perfusions for the control TiO_2 NP treatment), gassed with 95% O_2: 5% CO_2. (A) TiO_2 NPs as a control without drugs, (B) 10 mmol l^{-1} cyanide exposure with TiO_2 NP, (C) 100 µmol l^{-1} sodium vanadate exposure with TiO_2 NP, (D) 120 IU ml^{-1} nystatin exposure with TiO_2 NP. Fish weights in the examples are 249.9, 360.7, 137 and 273.9 g, respectively.

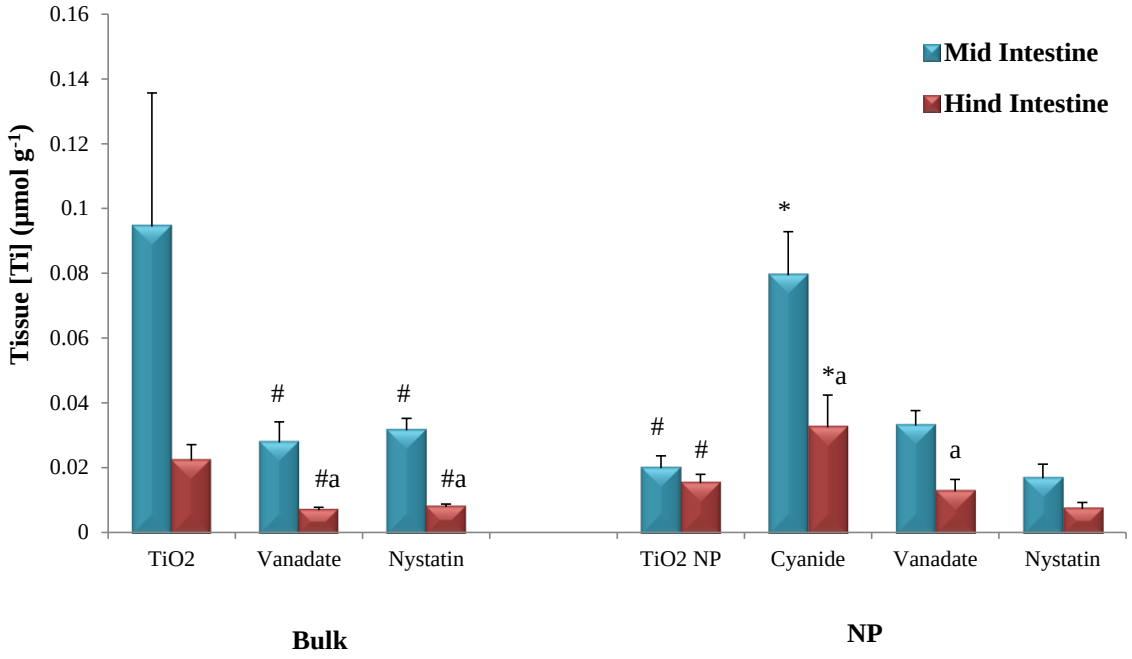

Figure 4.5 Total Ti metal concentrations in the tissues determined by ICP-OES in the mid (blue bars) and hind intestine (red bars) of rainbow trout after 4 h perfusions with a mucosal side exposure to 1 mg l^{-1} of bulk TiO_2 or TiO_2 nanoparticles (NP). The appropriate TiO_2 was added to the mucosal solution in the presence of the standard gas mixture (95% O_2: 5% CO_2), and in the presence of inhibitors: 120 IU ml^{-1} nystatin (putative endocytosis inhibitor), 100 µmol l^{-1} sodium vanadate (an ATPase inhibitor) and 10 mmol l^{-1} cyanide (general inhibitor). Data are means ± S.E.M (n = 6 perfusions per treatment; n = 7 perfusions for the control TiO_2 NP treatment). * Statistically significant difference from the TiO_2 NPs drug free control (ANOVA or Kruskal-Wallis test, $P < 0.05$), # statistically significant difference from the bulk TiO_2 drug free control (ANOVA or Kruskal-Wallis test, $P < 0.05$). Letter (a) indicates statistically significant difference between mid and hind intestine (t-tests, $P < 0.05$).

Table 4.1 Effects of exposure to 1 mg l^{-1} TiO_2 with/without drugs on the Ti and water fluxes across the isolated perfused trout intestine.

Mucosal [TiO_2] (1 mg l^{-1}) and Drugs Concentration	Net Ti flux, $J_{net,Ti}$ (nmol g^{-1} h^{-1})		Net water flux, $J_{net,H2O}$ (ml g^{-1} h^{-1})	
	Initial rate	Overall rate	Initial rate	Overall rate
Bulk TiO_2	0.98 ± 0.47	0.85 ± 0.32	-26.28 ± 2.52	-28.54 ± 3.19
TiO_2 NP	1.55 ± 0.33#	2.38 ± 0.68#	-17.56 ± 4.00#	-18.01 ± 4.16#
Bulk TiO_2 vanadate	< 0.004#	< 0.004#	-13.57 ± 1.83#	-38.41 ± 0.07#a
Bulk TiO_2 nystatin	< 0.004#	< 0.004#	-09.97 ± 2.05#	-31.66 ± 0.08a
TiO_2 NP cyanide	2.56 ± 0.65*	0.85 ± 0.17*	-13.40 ± 3.66*	-44.51 ± 2.76*a
TiO_2 NP vanadate	2.29 ± 0.64*	0.83 ± 0.22*	-16.26 ± 2.66*	-49.17 ± 3.88*a
TiO_2 NP nystatin	< 0.004*	< 0.004*	-13.96 ± 2.29*	-36.42 ± 2.03*a

Values are means ± S.E.M. (n = 6 perfusions per treatment; n = 7 perfusions for the control TiO_2 NP treatment) expressed per gram dry mass of intestine per hour. Negative values indicate a net loss from the serosal solution, initial and overall rates data were calculated from cumulative perfusate data at 10 min and 4 h, respectively.* Statistically significant difference from TiO_2 NP drug free control values within columns (ANOVA or Kruskal-Wallis test, $P < 0.05$), # Statistically significant difference from bulk TiO_2 drug free control values within columns (ANOVA or Kruskal-Wallis test, $P < 0.05$). Letter (a) within rows indicates a statistically significant difference between initial and overall rates (t-test, $P < 0.05$). Drug concentrations were 120 IU ml^{-1} nystatin, 10 mmol l^{-1} cyanide, or 100 µmol l^{-1} vanadate (see text for details).

Table 4.2 Total Na^+, K^+, Ca^{2+}, and Mg^{2+} concentrations of gut tissue following exposure of isolated perfusate trout intestine to 1 mg l^{-1} TiO_2 and different drugs for 4 h.

Mucosal [TiO_2] (1 mg l^{-1})	Tissue [Metal] µmol g^{-1} dry mass				
	Na^+	K^+	Ca^{2+}	Mg^{2+}	Moisture %
Mid Intestine					
Bulk TiO_2	156.09 ± 24.33	212.02 ± 15.78	18.64 ± 3.45	20.15 ± 1.66	78.36 ± 2.14
TiO_2 NP	162.80 ± 34.59	136.07 ± 18.25#	12.51 ± 1.34	12.06 ± 1.24#	82.26 ± 1.72
Bulk TiO_2 vanadate	258.92 ± 13.52#	158.47 ± 11.76#	33.35 ± 6.50	13.69 ± 0.85#	81.82 ± 1.23
Bulk TiO_2 nystatin	253.28 ± 15.29#	138.97 ± 11.53#	36.69 ± 8.16#	12.11 ± 0.49#	80.65 ± 1.38
TiO_2 NP cyanide	405.20 ± 54.74*	73.09 ± 10.96*	66.48 ± 11.06*	10.87 ± 1.70	88.33 ± 1.09
TiO_2 NP vanadate	427.10 ± 50.53*	160.08 ± 32.49	56.90 ± 10.23*	17.17 ± 2.51	84.94 ± 2.61
TiO_2 NP nystatin	229.45 ± 21.40*	117.95 ± 10.51*	25.90 ± 5.47*	10.91 ± 0.86	84.54 ± 0.93
Hind Intestine					
Bulk TiO_2	116.48 ± 7.57	168.29 ± 5.93	18.00 ± 4.17	15.83 ± 0.69	81.54 ± 1.80
TiO_2 NP	98.65 ± 9.46	121.03 ± 7.05#	7.98 ± 0.49#	9.99 ± 0.59#	80.85 ± 1.39
Bulk TiO_2 vanadate	237.76 ± 8.87#	164.60 ± 4.42#	13.23 ± 0.33	13.49 ± 0.28#	82.08 ± 0.42
Bulk TiO_2 nystatin	222.63 ± 13.25#	146.59 ± 5.74	15.30 ± 0.98	11.50 ± 0.46#	80.65 ± 1.49
TiO_2 NP cyanide	342.82 ± 26.38*	84.52 ± 8.99	47.57 ± 9.32*	10.05 ± 0.53	88.11 ± 1.05
TiO_2 NP vanadate	251.57 ± 27.68*	174.39 ± 18.22*	19.18 ± 3.59*	14.53 ± 1.29	82.02 ± 2.16
TiO_2 NP nystatin	219.43 ± 11.66*	156.27 ± 7.17*	13.93 ± 0.45	12.60 ± 0.48	85.24 ± 1.34

Values are means ± S.E.M. (n = 6 perfusions per treatment; n = 7 perfusions for the control TiO_2 NP treatment) expressed as µmol g^{-1} dry mass of intestinal tissue, except for moisture content (%) = ((wet weight – dry weight)/wet weight) x 100. * Statistically significant difference from TiO_2 NPs drug free control values within columns (ANOVA or Kruskal-Wallis test, $P < 0.05$), # Statistically significant difference from bulk TiO_2 drugs free control values within columns (ANOVA or Kruskal-Wallis test, $P < 0.05$).

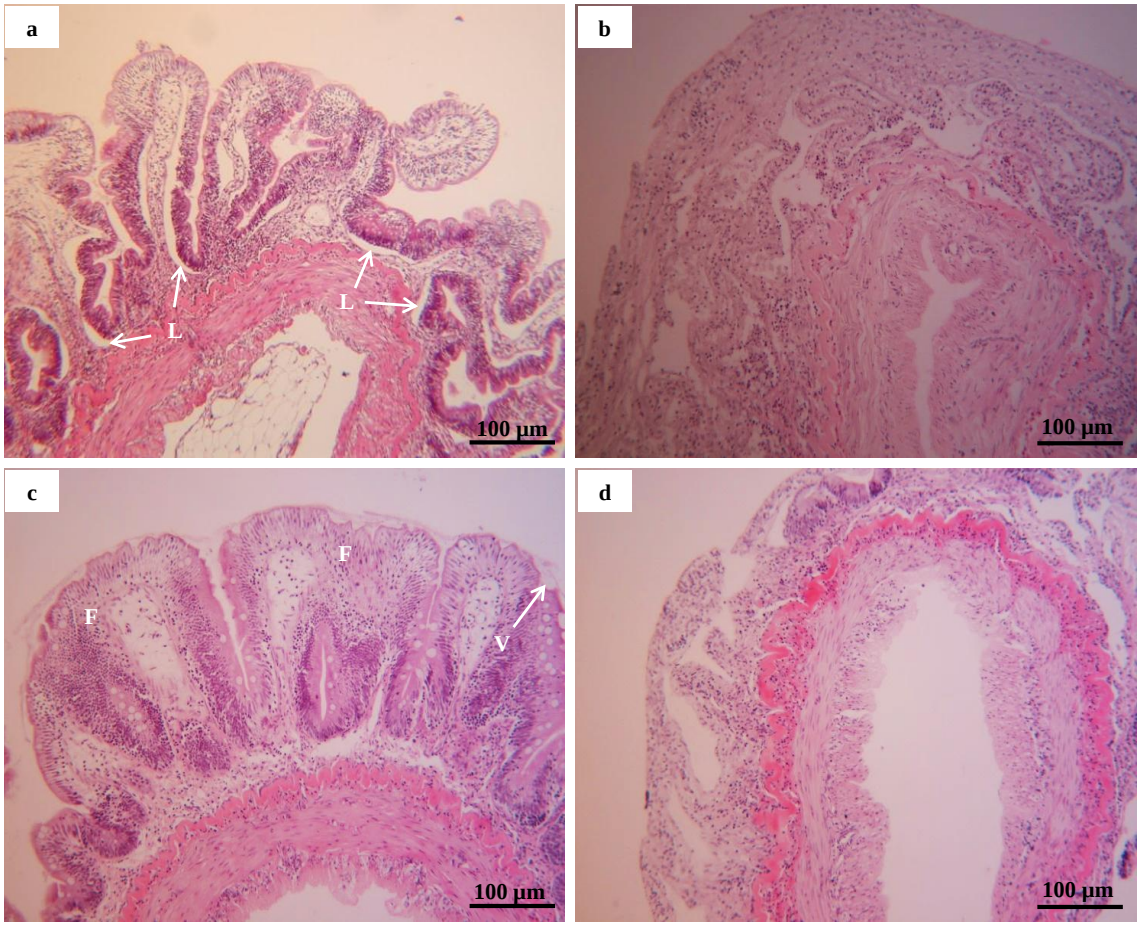

Figure 4.6 Histology of the perfusate intestine after 4 h perfusion gassed with standard gas mix. (a) 1 mg l^{-1} TiO_2 NPs drug free control showing lifting of epithelial cell (L), (b) 1 mg l^{-1} TiO_2 NPs with 10 mmol l^{-1} potassium cyanide showing abnormal structure of the mucosal layer (in five out of six animals), (c) 1 mg l^{-1} TiO_2 NPs with 100 µmol l^{-1} sodium vanadate showing fusion of the intestinal villi (F), and appear of vacuoles (V) (in two out of six animals), (d) 1 mg l^{-1} TiO_2 NPs with 120 IU ml^{-1} nystatin showing abnormal structure of the mucosal layer (in three out of six animals). Scale bar = 100 µm, sections were 8 µm thickness and stained with haematoxylin and eosin (n = 6 per treatment).

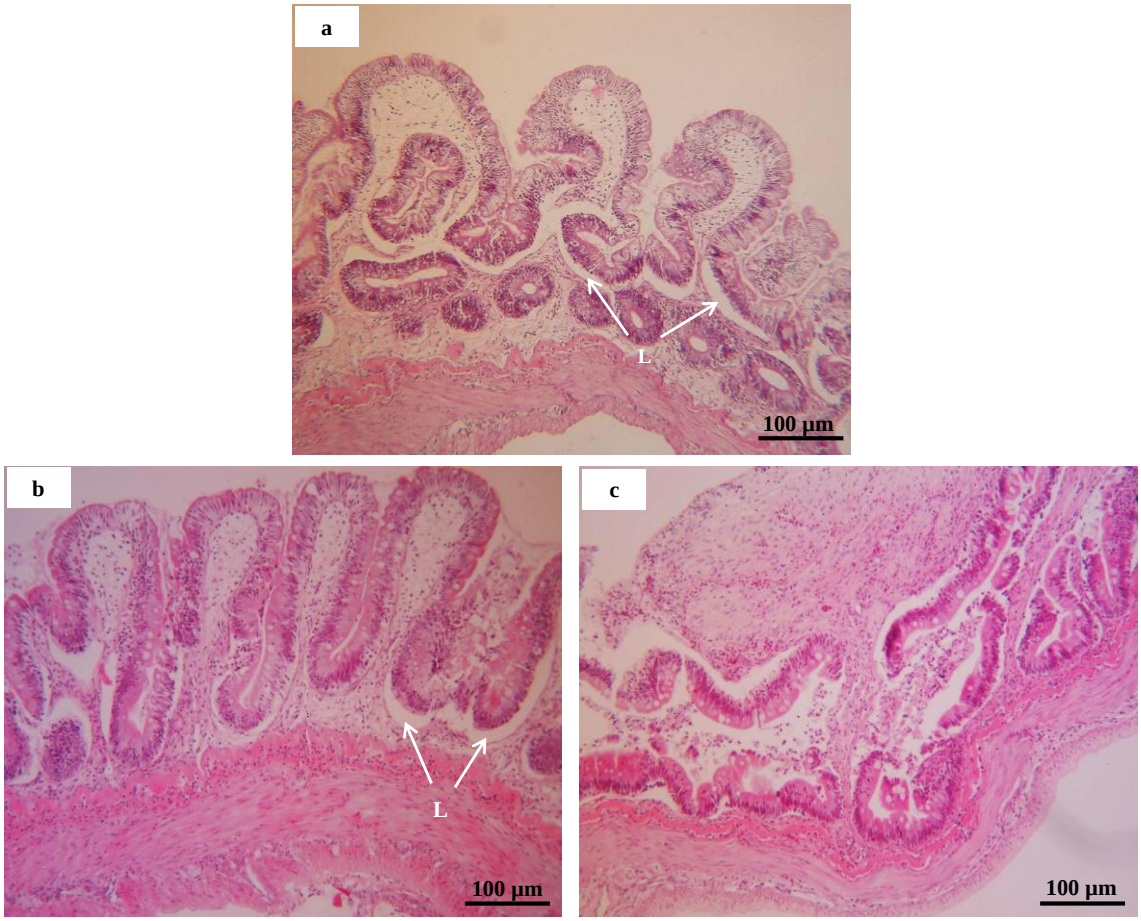

Figure 4.7 Histology of the perfusate intestine after 4 h perfusion gassed with standard gas mix. (a) 1 mg l^{-1} bulk TiO_2 drug free control showing lifting of epithelial cell (L), (b) 1 mg l^{-1} bulk TiO_2 with 100 µmol l^{-1} sodium vanadate showing lifting of epithelial cell (L) (in one out of six animals), (c) 1 mg l^{-1} bulk TiO_2 with 120 IU ml^{-1} nystatin showing abnormal structure of the mucosal layer (in three out of six animals). Scale bar = 100 µm, sections were 8 µm thickness and stained with haematoxylin and eosin (n = 6 per treatment).

4.4 Discussion

This is the first report on the uptake kinetics of NPs across the gut of rainbow trout using the isolated gut perfusion technique. Mechanism(s) uptake pathway of Ti from both bulk and nano forms of TiO_2 showed the effects of nystatin on the uptake, suggest at least part of the mucosal influx step is by endocytosis in the intestine. However, the effect of solute transport inhibitors also suggests a dissolved Ti component involved in Ti export from the tissue to the blood for bulk and nano TiO_2. Further investigations using the rapid dipping solution experiment observed an apical uptake of the particles and the exposure is took place.

4.4.1 TiO_2 uptake through intestinal tissue

The both forms of TiO_2 showed that the Ti was accumulated in the mucosa, rather than the underlying muscularis (see Chapter 3, Table 3.2). The observed increases in total Ti metal concentrations in the mucosa are not easily explained by surface-binding (i.e., assumed adsorption) of TiO_2 (and/or Ti metal) to the exterior of the gut, with the rapid solution dipping experiments showing only about one fifth of the measured Ti being on the exterior within 30 sec (Fig. 4.2). There is usually some time dependence of surface-binding in such experiments, but only for the first 90 sec (Handy and Eddy, 2004). A longer "dip" in the physiological saline of 60 sec might show slightly higher tissue Ti metal concentrations, suggesting more instantaneous binding of TiO_2 and/or Ti metal. However the instantaneous surface binding, of dissolved metals at least, is not linear over time with most of the binding occurring in the first 30 sec (Handy and Eddy, 2004) and a longer dip would at most add a further fifth (bring the total surface binding to $2/5^{th}$ of the overall tissue metal concentration). This would still leave more than half the measured total Ti metal concentration representing internalised metal in the whole gut sac experiments. After 90 sec, radiotracer studies show that dissolved metals can be detected in the blood of trout (indicating transepithelial uptake, Handy and Eddy, 2004)

and within 5 min the apparent accumulation is dominated by internal uptake of the metal. It would therefore seem logical that a 4 h exposure would give mostly internalisation (measured total Ti metal on the inside) rather than on the outside of the tissue.

4.4.2 Dissolution of Ti from both bulk and nano TiO_2 in different salines

The dialysis experiments showed that there was no appreciable dissolution of dissolved Ti metal from the mucosal saline in 24 h (gassed with 95% O_2: 5% CO_2 or 99.5% O_2: 0.5% CO_2), so the situation here is likely to be associated with the binding and settling of particulate TiO_2 with the secreted mucus. The notion of some small fraction of dissolved Ti ions in the cell is supported by the dialysis experiments, where the appearance of total Ti measured in the beaker outside the dialysis bag increased over time, but only when using the intracellular saline at pH 7.2 (Fig. 4.3B). This observation could be interpreted as a tiny fraction of dissolved Ti metal being released by dissolution from the particles, and subsequently diffusing through the dialysis membrane into the external media of the beaker. The rate of appearance of total metal in the external media in the beakers (18-26 nmol Ti metal h^{-1} depending on particle type) represents about 0.01% loss of metal from the particles every hour. If this interpretation is correct, this rate of release also represents the maximum dissolution rate of Ti metal from the particles in these specific experimental conditions. The dissolution of aqueous Ti metal species from TiO_2 particles has not been previously investigated in a high KCl media typical of the intracellular environment. However, Schmidt and Vogelsberger, (2009) recently investigated Ti dissolution from TiO_2 NPs (including P25 and anatase forms) in 0.1 mol l^{-1} NaCl solution. These experiments were conducted over the whole pH range (pH 1-13) and for long durations (up to 1200 h), much longer than the 4 h perfusion here; but showed that TiO_2 will release metal ions by dissolution in NaCl solutions under certain conditions. At pH 3 or less, they detected dissolved Ti (around

0.1 and 1µmol l^{-1} Ti for pH 3 and pH 1, respectively). This observation tentatively suggests that TiO_2 NPs might also dissolve very slowly over several days in very acidic intracellular compartments (e.g., lysosomes). Schmidt and Vogelsberger, (2009) also measured the equilibrium solubility (at 500 h) of TiO_2 particles by absorptive stripping voltammetry, and showed that at pH 7, the P25 TiO_2 had a solubility of approximately 10^{-9} mol l^{-1}. This is a tiny amount of dissolved Ti from a physical chemistry perspective, but biologically, this would be a very relevant free ion concentration for metal homeostasis in cells. Schmidt and Vogelsberger, (2009) also calculated that this dissolved Ti would be present mainly as the dissolved Ti(OH)4 species at neutral pH, with the Gibbs free energy in favour of dissolution (overall solubility product, $10^{-9.05}$). There are some major differences between the dialysis experiments in this study and the work of Schmidt and Vogelsberger, (2009). The present study used much shorter durations (24 h for dialysis experiments) and so one might expect less dissolution of Ti in this experiments. However, KCl was also used instead of NaCl, and this seems to be important. The rate of release of apparent total dissolved Ti during dialysis was much faster in KCl solution (the intracellular saline, Fig. 4.3B) compared to the NaCl-rich mucosal saline. This may interpreted as an apparent difference in Ti dissolution rates between Na- and K-containing media. This needs further investigation, but may be due to the relative depolarising effect of K^+ or its greater diffusion coefficient (i.e., more mobile) compared to Na^+ (Robinson and Stokes, 1968). Regardless, considering that trace metal homeostasis in cells operates at infinitely small free ion concentrations (e.g., Cu, maximally 10^{-18} moles $cell^{-1}$, Rae et al., 1999), the apparent total dissolved metal release rates in KCl-containing media here would be more than enough Ti release to enable Ti transport. Alternative explanations of the dialysis experiments, such as the NPs breaking up inside the dialysis bag (not observed) to release ~1 nm particles that might fit through the pore structure of the dialysis tubing cannot be completely excluded

in this experiment, but seems very unlikely given the KCl-effect above. It is also hard to imagine how primary particles of ~24 nm could weather to ~1-2 nm in 24 h without releasing significant quantities of metal ions. Notably, particles of a few nm wide were not observed in the electron micrographs of the original stock dispersions.

4.4.3 How does titanium associated with titanium dioxide particle exposures across the apical brush boarder membrane?

The discussion on events at the mucosal (apical) membrane of epithelia has focused on whether or not metallic NPs will be taken up directly across the apical membrane of epithelial cells as particles, and/or as dissolved metal (review, Shaw and Handy, 2011). In the present study the dialysis experiments showed that the appearance of total Ti metal in the mucosal solution was below the detection limits of ICP-OES, suggesting no measurable dissolution of dissolved Ti from the particles in the mucosal solution. The additions of nystatin (high dose, selected to completely inhibit endocytosis) caused about a 50 – 60% block of tissue Ti accumulation (depending on gut region and material, Fig. 4.5). Most of the apparent residue total Ti metal concentration in the tissue after nystatin treatment may simply represent the small amount of surface bound total Ti (regardless of form) detected in the solution dipping experiments (discussed above). Together, these observations argue in favour of some direct particle uptake at the mucosal membrane. However, the unstirred layer on the surface of epithelia is often a different chemical environment to that of the surrounding media (Handy and Eddy, 2004; Shaw and Handy, 2011) and the possibility of some dissolution of dissolved Ti metal from the particles in direct contact with the membrane cannot be excluded. Unfortunately the apical solute transport mechanisms for Ti metal are poorly understood, but the ionic radius of Ti^{2+} is about 1 Ångstrom (similar to Na^{+} and Ca^{2+} ions, (crystaline values, 0.95 and 0.99, Robinson and Stokes, 1968). A theoretical possibility of facilitated diffusion through epithelial ion channels therefore exists (see Handy et al.,

2002a). Facilitated diffusion would also be supported by the cyanide effect in the present study (Fig. 4.5), which did not prevent metal accumulation in the tissue, suggesting a passive uptake component across the mucosal membrane down the electrochemical gradient (as observed for Hg, Hoyle and Handy, 2005). A transferrin-like receptor mediated endocytosis (well known for Fe transport, see Bury and Handy, 2010), or non-specific uptake on divalent metal ion transporter 1 (Gunshin et al., 1997) are also theoretical possibilities. Furthermore, the reduction of net Ti uptake from TiO_2 NPs in the presence of cyanide (Fig. 4.4B) which was also sensitive to serosal additions of vanadate (Fig. 4.4C), suggests an energy-dependent efflux of Ti metal ions on a basolaterally-located ATPase into the blood as the most likely mechanism. There is no evidence in the literature of vanadate-sensitive ATPases being involved in exocytosis of particulate material from the gut mucosa to the blood at the serosal membrane. However, metal transporting ATPases are known to be involved in loading metal ions into vesicles. For example, it is well known that Cu ions are loaded into the Golgi compartment of cells via a Cu-ATPase (Dameron and Harrison, 1998), which is followed by subsequent vesicular trafficking of Cu to the serosal membrane (Handy et al., 2000). It remains possible that Ti could cross the cell using a similar ATPase-dependent trafficking system to the well-known Cu pathway, which is also known to be hijacked by other non-essential toxic metals like mercury (Hoyle and Handy, 2005). Tentatively, if particles are taken up into the tissue, it therefore implies that some dissolution of Ti from the materials was occurring in order to enable the vanadate-sensitive serosal efflux to occur. A separate nystatin-sensitive exocytosis pathway for particles to move from the epithelial cell to the blood is unlikely as nystatin completely abolished transepithelial uptake of both materials (e.g., Fig. 4.4D for TiO_2 NPs), but further research is needed on this aspect.

4.4.4 Intestine tissue structure after drug exposures

Some injuries were observed in the gut tissue after exposed to different inhibitors, mainly shown in the mucosal layer, and without effects on the muscularis indicating the intestinal barrier was not compromised. The histological observations were limited, and with no clear TiO_2-dependent effects with the drugs present, and in only a few specimens. Potassium cyanide is considered as toxic via its interference with the electron transport train in mitochondria, preventing the tissue from using the oxygen (Eisler, 1991; Yamamoto, 1989). A localised subsequent hypoxia with metabolic acidosis could affect the structure of the mucosal layer. The distribution of the lipid rafts in the cell membranes could be altered by nystatin (Semis et al., 2012). It may, in theory, be possible for the membrane to be more vulnerable during lipid raft formation, and the oxidation potential of nystatin as a foreign substance has not been examined. Further work is needed to understand the effects of nystatin on the appearance of the mucosal layer in the intestine. For TiO_2 NPs, the vanadate treatment showed some vacuole formation with appearance of the occasional villi fusion. This was the same injury (but to a much lesser extent) to that observed by Federici et al. (2007), suggesting that the damage was caused by TiO_2 NPs exposure not by the vanadate. The bulk TiO_2 treatment showed a normal tissue appearance after exposure to vanadate with some minor lifting of epithelium (likely processing artefact) which appeared to be the same as the bulk TiO_2 (drug free control). Overall, this suggests no effects of vanadate on intestinal tissue integrity.

Conclusions

The present study indicates that the uptake of Ti from both bulk and nano TiO_2 had occurred across the intestine. This uptake was interpreted in the context of limited surface binding of Ti metal on the intestinal tissue. The dialysis investigation of the role

of dissolved Ti ions tentatively suggests that some limited role in the uptake inside the cells. Further evidence of the mechanisms of uptake was found by testing inhibitors of the main uptake pathways in the gut; which indicated both nystatin-sensitive and vanadate-sensitive Ti uptake associated with TiO_2 exposures. This suggests that both particulate and dissolved metals components are involved in the overall uptake. This implies that environmental regulation for TiO_2 NPs cannot simply use the existing dissolved metal paradigm (Shaw and Handy, 2011), but a modification for particle uptake at the mucosal surface should be included in any biotic ligand model (BLM) for TiO_2 NPs. Further investigations on the mechanism of uptake are recommended using other inhibitors of endocytosis to determine, the sub-types of vesicular trafficking involved in the overall uptake.

Chapter 5

The uptake of different crystal structures of TiO_2 nanoparticles by Caco-2 intestinal cells

Abstract

The proposed uses of nanomaterials in food and different healthcare products heights the possibility of their uptake through the gastrointestinal tract in humans. The current study was applied to investigate the possible uptake of different forms of TiO_2 and their pathways for uptake into Caco-2 cells. Four different forms of 1 mg l^{-1} TiO_2 were used: (i) TiO_2 NPs as P25 with a composition of 75% anatase and 25% rutile, (ii) bulk TiO_2 with the same crystal structure as the P25, (iii) nano anatase TiO_2 and (iv) nano rutile TiO_2. The bulk TiO_2 showed the greatest uptake rate, being 14.1 nmol mg^{-1} protein, while the nano rutile TiO_2 presents the lowest uptake rate, being 6.9 nmol mg^{-1} protein. Another series of experiments investigated the mechanism of uptake of TiO_2 using two kinds of inhibitors, (i) 120 IU ml^{-1} nystatin, an endocytosis pathway inhibitor and (ii) 100 µmol l^{-1} sodium orthovanadate, a P-type ATPase inhibitor. Both vanadate and nystatin produced an increase in Ti accumulation from different forms of TiO_2. It is hypothesized that these drugs interfere with one of the endocytosis pathways. The results shows that 1 mg l^{-1} TiO_2 is actively taken up by Caco-2 cells with rates being influenced by the crystal structure and behaviour of TiO_2. The electrolyte concentrations in Caco-2 cells showed normal concentrations of Na^+ and K^+, but with an elevation in Mg^{2+} and Ca^{2+} concentration after exposure to different forms of TiO_2; suggesting specific material-type effects on electrolytes homeostasis .

5.1 Introduction

Growing advances in nanotechnology have stimulated the development of many products in areas such as biomedicine, food, and cosmetics which may deliver chemicals or nutrients in a targeted and controlled manner to human beings. Titanium dioxide (TiO_2) is amongst the most widely used of metal oxide nanoparticles (NP) and is found in a variety of applications ranging from toothpastes to water treatment (Aitken et al., 2006; Fröhlich and Roblegg, 2012) and especially applications of TiO_2 NPs in cosmetics as transparent sunscreen blockers (Calzolai et al., 2012). Bulk TiO_2 is broadly used in food as a food colouring agent (normal white colour), food additives (E171) and in food packaging with daily ingestion estimated to be between 5 and 50 mg in the USA and Europe (Powell et al., 2010; Weir et al., 2012). According to Weir et al. (2012), 36% of the particles in E171 may be considered to be nano TiO_2 and its ingestion could have potentially toxic effects.

TiO_2 crystal structure and surface chemistry has been found to influence its toxicity (Chen and Mao, 2007). TiO_2 exists in three distinct forms brookite, anatase, and rutile, the latter two being more commonly produced (Chen and Mao, 2007). Studies have shown that anatase is more toxic than the rutile form with regards to its reactive oxygen species (ROS) promoting ability. This increased capacity for ROS generation compared to rutile TiO_2 has been shown to elicit cell damage and morphological changes (Sayes et al., 2006; Shi et al., 2007; Wang et al., 2008).

The pathways of inorganic NPs into and out of the cell membrane are still poorly understood. Dombu et al. (2010) suggested both endocytosis and exocytosis are involved in NP transport through epithelial cells. A study by Ryabachikova et al. (2010) examined the MDCK cells under electron microscope after exposure to different crystal forms of TiO_2 NPs. After 1 h, TEM images showed direct contact of NPs with the cell and NP filled and coated vesicles inside the membrane suggesting the

possibility of receptor-mediated endocytosis (Ryabachikova et al., 2010). Only one study by Koenman et al. (2010) has been applied on Caco-2 human intestinal cell line exposure to TiO_2 NPs. Exposure of the cells to 10 or 100 μg ml^{-1} of TiO_2 NPs did not cause death to the cells or disruption of junctional complexes, TiO_2 appeared in the cells and underneath the cells suggesting that NPs transport through individual epithelial cells by transepithelial uptake is likely (Koenman et al., 2010). This has prompted research into which mechanisms are responsible for TiO_2 cell internalisation through the intestinal epithelium.

The overall aims of current study was to demonstrate the utility of the Caco-2 cell line for accumulation studies with TiO_2 NPs and then to compare the uptake of Ti from the bulk and nano forms (size effect), as well as the effects of different crystal structures (anatase and rutile). The approach included detailed pharmacological investigations of solute transport pathways for metals, as well as pharmacological studies to establish whether the different sizes or forms of TiO_2 were using different pathways to enter the cells. Finally, measurements of electrolytes in the cells, biochemical measurements on cell integrity, and electron microscopy investigations were made in the experiments to understand the physiological basis of any differences observed.

5.2 Methodology

Several experiments were performed using confluent monolayers of Caco-2 cells in culture medium (see below). The first series determined the Ti accumulation in confluent Caco-2 cells exposed to 1 mg l^{-1} of different forms of TiO_2 (bulk, nano, nano anatase or nano rutile) over 24 h, and also the effects of the TiO_2 exposure on cell viability (LDH release, cell morphology) and electrolyte concentrations. The second series of experiments involved pharmacological investigations to determine whether or

not the observed Ti accumulation involved either solute transport or endocytosis-related pathways for uptake at the mucosal (apical) membrane. All data on Ti was normalized to nmol [Metal] mg^{-1} cell protein (see below).

5.2.1 Cell culture

A human intestinal cell line, Caco-2 (brush border expressing, European collection of cell cultures) were routinely incubated in 75 cm^2, 200 ml flasks (Sterilin, Newport, UK) containing 15 ml of Dulbecco's modified eagle medium (DMEM) supplemented with 10% fetal bovine serum (FBS), 1% glutamine and 1% penicillin-streptomycin (100 IU Penicillin-100 μg ml^{-1} Streptomycin), at 37 ºC and gassed with 95% air: 5% CO_2, all the equipment (DMEM, FBS, glutamine and penicillin-streptomycin) was obtained from (Lonza, B-4800 Verviers, Belgium). For routine maintenance, the medium was changed every 48 h and the cells were sub-cultured by trypsination. Experiments were conducted on cells between passage 60 - 75 (cells were purchased at passage 45) and antibiotic were withdrawn to avoid possible interference with ion transport at least 2 passages before seeding the cells into 6-well plates (Sterilin, Newport, UK) for experiments. Preliminary trials were conducted to determine the optimum seeding density and time to confluence of the cells in 6-well plates by measuring the electrical resistance of the epithelium using an xCelligence real time label free cellular analysis system (Real-Time Cell Analyzer (RTCA), Roche Applied Science). In brief, the instrument monitors the electrical resistance of the cells grown on gold-coated wells, as cells adhere the resistance of the plate increases until confluence is reached, whereupon the relative resistance (cell index) remains constant. A seeding density of 5 x 10^4 cells/ cm^2 produced confluence by 24 h (Fig. 5.1). Subsequently for all experiments, cells were seeded at 5 x 10^4 cells/cm^2 in the 6-well plates and after an initial 24 h of growth, the cells were left for a further 48 h to ensure both 100% confluence and that the cells were rested. The cells were also visually inspected (Phase contrast microscope,

Olympus/CK30-F200, Japan) each day until they became confluent, a description of general experimental methodology shown in Fig. 5.3 and 5.4. Cell viability was also checked by trypan blue exclusion, prior to seeding the flasks and 6-well plates, less than 90% viability was discarded. LDH was also checked in the external and internal cell cultures (see below) to measure the cell membrane integrity and the cytotoxic effects of different TiO_2 in compare to control LDH leak.

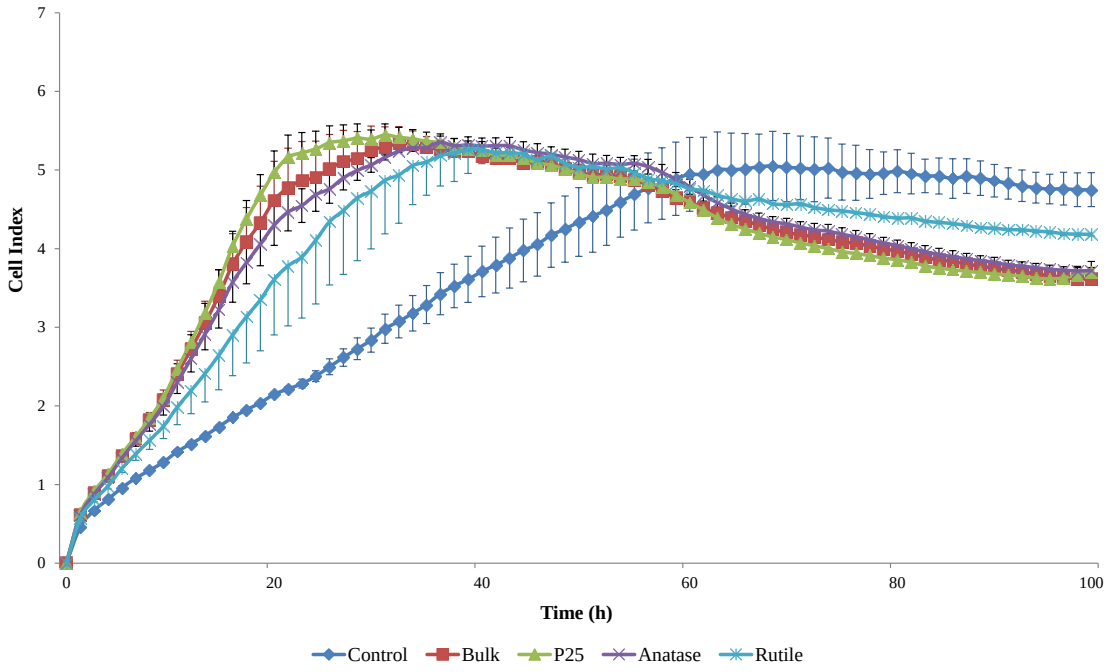

Figure 5.1 The cell index of Caco-2 cells after exposed to 1 mg l^{-1} of different forms of TiO_2 showing the optimum seeding density of the cells at the 24 h of the exposure. Values are means ± S.E.M (n = 4 plates per treatment).

5.2.2 Stock dispersions and materials characterisation

Four different types of TiO_2 were used (manufacturer's information): (i) bulk TiO_2 powder (ACROS, Titanium (IV) oxide, New Jersey, USA), with an unspecified mixture of anatase and rutile (but see below), with a purity of 98.0-100.5% TiO_2. (ii) Ultrafine TiO_2 NP type "Aeroxide" P25 (DeGussa AG, supplied by Lawrence Industries, Tamworth, UK) with a crystal structure of 25% rutile and 75% anatase TiO_2, purity was at least 99% TiO_2 (maximum impurity stated was 1% Si), the average particle size was 21 nm. (iii) Anatase TiO_2 NP form (US Research Nanomaterials, Inc, Houston, Texas, USA) with purity of 99% and 10-25 nm average particle size. (iv) Rutile TiO_2 NP form (US Research Nanomaterials, Inc, Houston, Texas, USA) with high purity, 99.9% and 30 nm average particle size. A stock solution of 500 mg l^{-1} for each type of TiO_2 was made (no solvents) by dispersing the particles in ultrapure Milli-Q water with manually vigorous shaking for 1-2 min. Preliminary studies identified the materials as source of bacterial infection to cell cultures (data not shown) and subsequently all stock dispersions and the dry powder were gamma irradiated to sterilise them (Red Perspex, Turntable Irradiation Geometry, Becton Dickinson, Belliver Industrial Estate, Plymouth, England). The radiation dose was 36.42 - > 40.72 kGy for 10 h to ensure sterility before starting cell culture experiments, and optimised to ensure the radiation did not interfere with the crystal structure of the materials.

The particle characterisation followed the similar protocol in Chapter 2. Briefly, the particle sizes were reported by using two methods. First, sub samples of the 500 mg l^{-1} stock dispersion were examined using transmission electron microscopy (TEM, JEOL-JEM.1400) (Fig. 5.2). The primary particle size measurement of 103.2 ± 16 nm (mean ± S.E.M., n = 7), 22.8 ± 0.6 nm (mean ± S.E.M., n = 169), 16.4 ± 2.4 nm (mean ± S.E.M., n = 6) and 30.8 ± 2.5 (mean ± S.E.M., n = 7) for bulk, P25, anatase and rutile, respectively, with the aggregates (viewed by electron microscopy) measuring 1162.8 ±

428.6 nm (mean ± S.E.M., *n* = 6), 121.7 ± 19.7 nm (mean ± S.E.M., *n* = 8), 106.8 ± 27.1 (mean ± S.E.M., *n* = 6) and 115.1 ± 17.9 (mean ± S.E.M., *n* = 3), respectively.

The second method was to analyse the dispersion and distribution of TiO_2 in the medium by using nanoparticle tracking analysis (NTA, using a Nanosight LM 10, Nanosight, Salisbury, UK, laser output set at 30 mW at 640 nm). The media (DMEM) alone was filled with particles (29 nm smallest particle size and 156 nm mean values) so ultrapure Milli-Q water was used instead. TiO_2 was prepared by vigorous shaking instead of sonication and this may leave the stock full with aggregates particles, for this reason the concentration used here was 10 mg l^{-1} to assess the measuring. The dispersion results gave a mean values of 179.3 ± 13.7, 7.1 ± 4.1, 142.3 ± 14.4 and 88.3 ± 34.1 nm (mean ± S.E.M., n = 3), for bulk, P25, anatase and rutile, respectively, While the mean of the smallest particles were 38.7 ± 3.5, 7.5 ± 1.2, 6.7 ± 1.2 and 7.7 ± 0.3 nm (mean ± S.E.M., *n* = 3), respectively (Fig. 5.2).

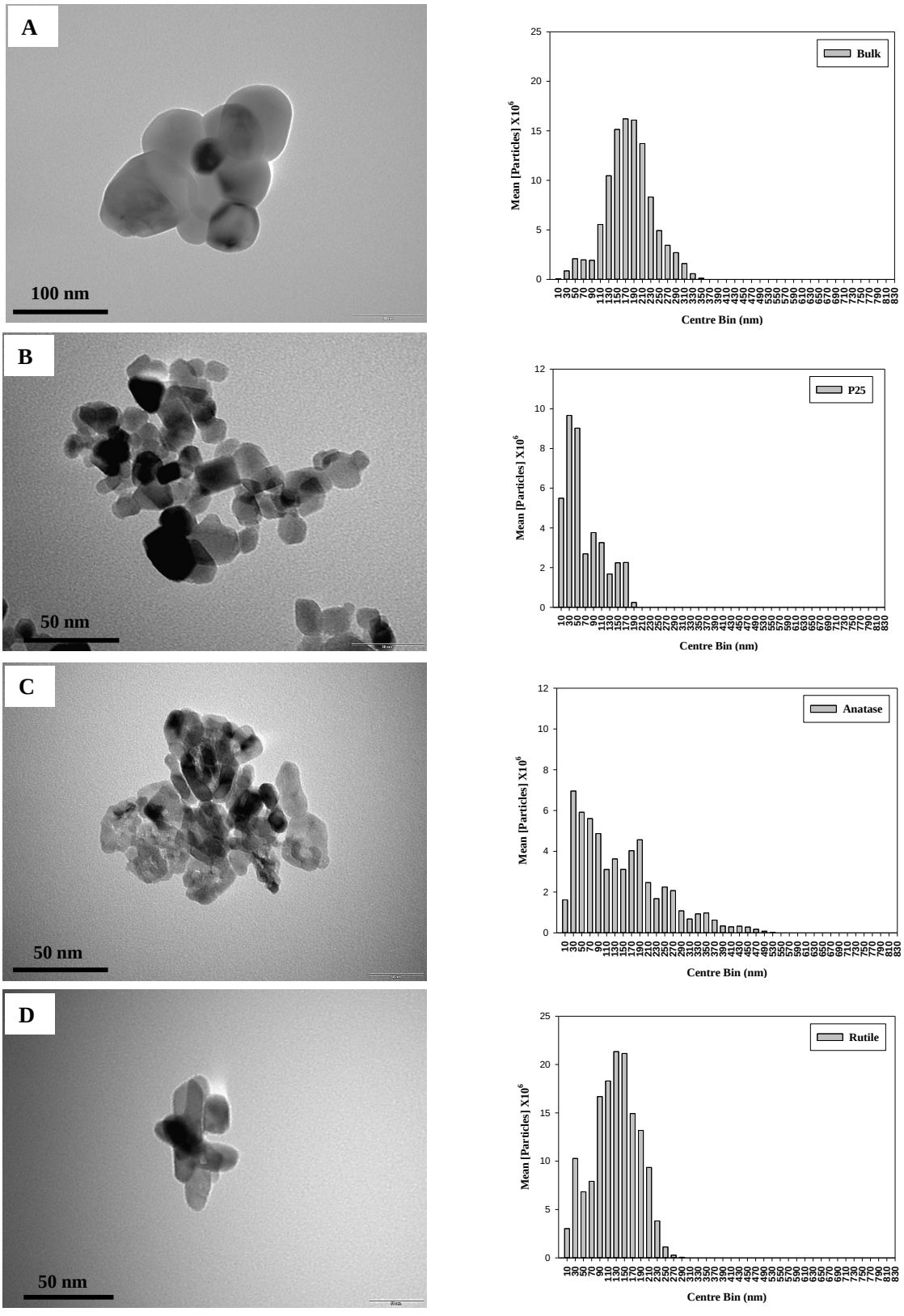

Figure 5.2 Electron microscope (EM) images showing (A) bulk TiO_2 particles (B) P25 (C) nano anatase and (D) nano rutile in 500 mg l^{-1} stock solution (Milli-Q water). The images shows individual examples from triplicates (n = 7, 169, 6 and 7 for bulk, P25, anatase and rutile, respectively). Nanosight graphs showing the distribution of bulk TiO_2, P25, nano anatase and nano rutile in 10 mg l^{-1} stock solution, graphs are individual examples from triplicate meaurements (n = 3).

5.2.3 Experiment 1: Time course of Ti accumulation from different forms of TiO_2

This experiment determined the time course of Ti accumulation from the different forms of TiO_2 in Caco-2 cells over 24 h. Confluent cells (72 h after seeding, as above) were exposed to the cell culture media (as above minus antibiotics) containing 1 mg l^{-1} of either no added TiO_2 (control), bulk, P25, anatase or rutile forms of TiO_2. Dosing of the wells was performed as follows: Media was made fresh on the day, TiO_2 (different forms) stock solutions were diluted with sterile distilled water from 500 mg l^{-1} to a concentration of 10 mg l^{-1} and then performing a 1: 10 dilution with cell culture media (1 ml stock: 9 ml media) to obtain a final concentration of 1 mg l^{-1} TiO_2 exposure. Cells were exposed for 24 h to each material, and then the cell mixture after scraped from the flasks was tested (see Fig. 5.3 and 5.4). Six plates per treatment at each time point: 0, 2, 4, 6, 8 and 24 h were analysed for Ti, electrolytes, LDH leak, and cell morphology (see below).

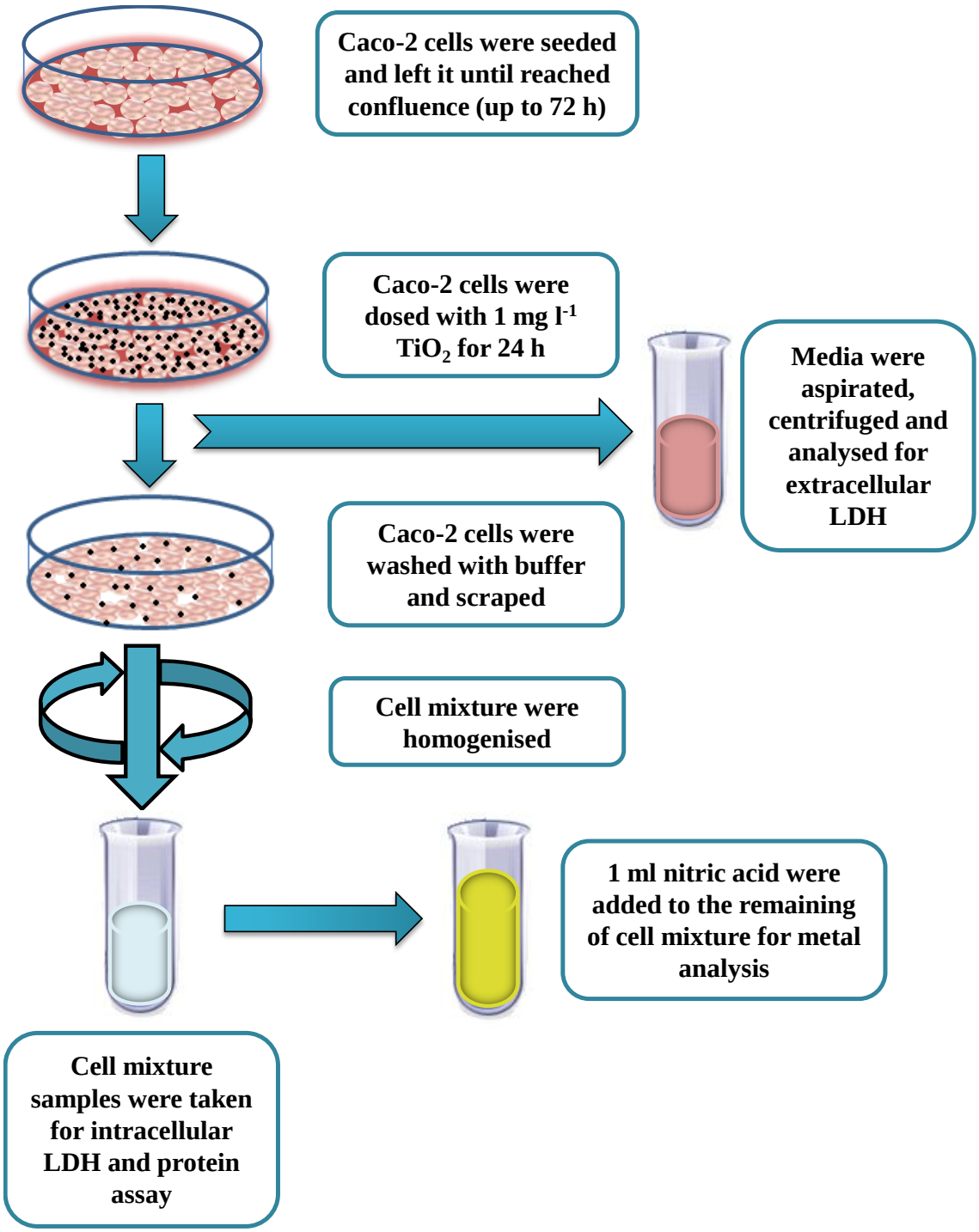

Figure 5.3 General experimental methods showing the processes of the experiment from seeding the cells till the analysis of samples. In all experiments, the cells were seeded in 6-well plates (two controls and different forms of TiO_2) and conducted in replicates (n = 6 plates per treatment). For the control, follow the same pattern of the experiment method with no exposure to TiO_2.

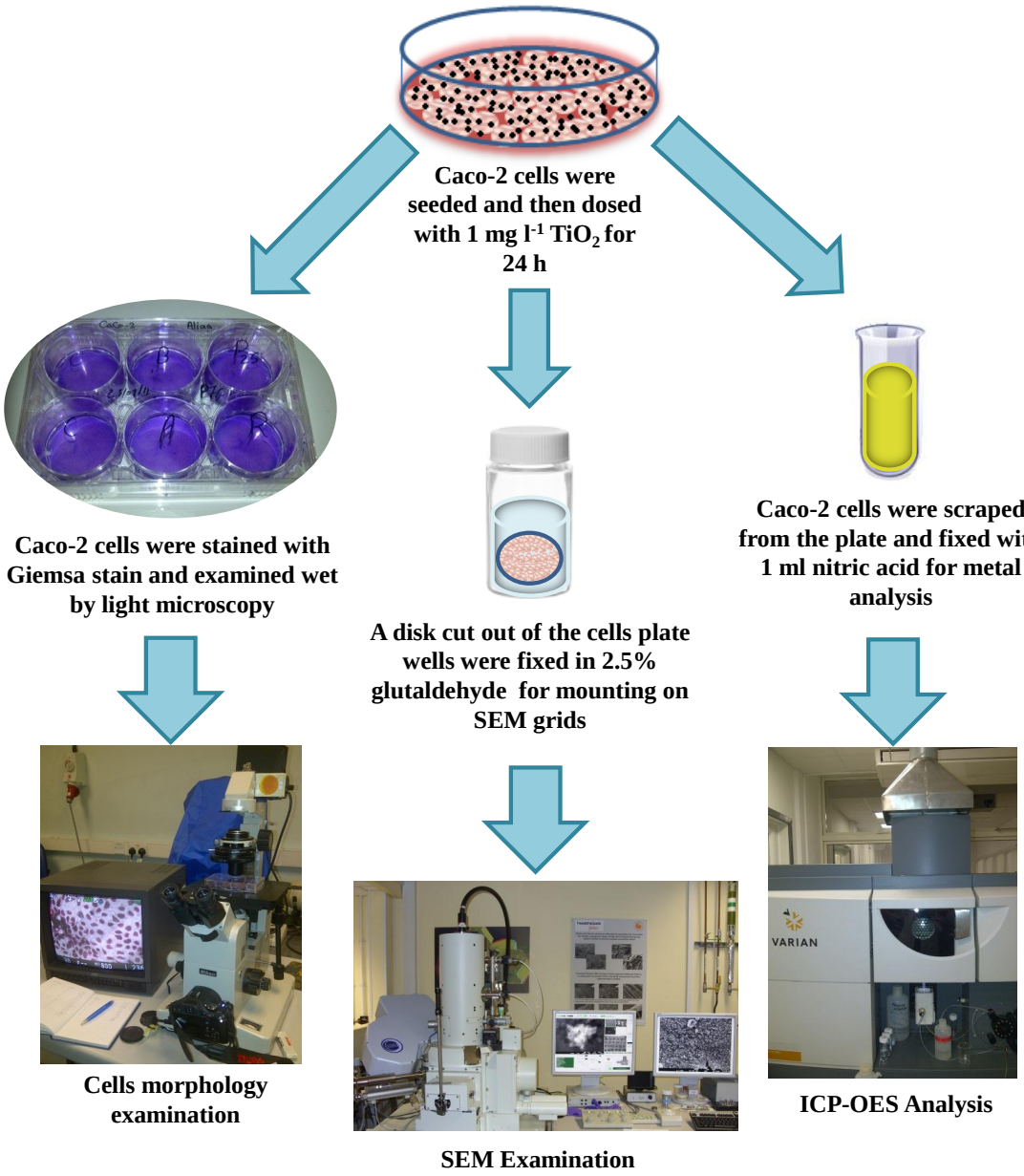

Figure 5.4 Experimental processing of the Caco-2 cells after been exposed the cells to 1 mg l^{-1} TiO_2 for 24 h. The cells were stained with Giemsa stain for the morphology examination (n = 3 plates per treatment). SEM grids of Caco-2 cells plate wells were obtained for the SEM examination (n = 3 plates per treatment). Caco-2 cells were fixed in a concentrated nitric acid and then analysed by the ICP-OES for the Ti and metal concentrations (n = 6 plates per treatment).

5.2.4 Experiment 2: The effect of nystatin and vanadate incubation on Ti accumulation

Having established the time course of Ti accumulation in Caco-2 cells from exposure to the different forms of TiO_2 the next stage was to assess the effect of mucosal (apical) additions of nystatin (a putative, endocytosis inhibitor, Iversen et al., 2011) and sodium orthovanadate (a P-type ATPase inhibitor, Cantley et al., 1978) on Ti accumulation. Cells were grown and dosed with 1 mg l^{-1} of the forms of TiO_2 as above, except that 1 h prior to dosing, cells were pre-incubated with either 120 IU ml^{-1} of nystatin (dose to produce 100% inhibition, Lewis et al., 1977), or 100 µmol l^{-1} sodium orthovanadate (enough to block metal transport in the intestine, Handy et al., 2000), compared to drug-free controls with and without added TiO_2. Both inhibitors were dissolved in 500 ml culture media (DMEM) to produce the appropriate concentration (see above) and pre-incubated for 1 h. This pre-incubation enabled the drugs to have direct contact with the cells without the risk of interference from the test materials (i.e., loss of bioavailable drug due to adsorption onto particles). The inhibitors remained in the media throughout the experiment, and the appropriate TiO_2 dose was simply added to the media after the initial 1h pre-incubation. Six plates per treatment for each inhibitor were conducted and after 24 h the cells was analysed as above.

5.2.5 Titanium determination and electrolytes in cells

In all experiments following TiO_2 exposure media was aspirated and centrifuged for 1 min (~160 *g*, Heraeus instruments, Biofuge *pico*, Germany) and collected for extracellular LDH analysis (see below). The cells were then collected to confirm Ti and/or electrolyte composition, the cells were washed twice with 2 ml of a sucrose washing buffer (300 mmol l^{-1} sucrose, 0.1 mmol l^{-1} ethylenediaminetetraacetic acid (EDTA), 20 mmol l^{-1} 4-(2-hydroxyethyl)-1-piperazineethanesulfonic acid (HEPES), buffered to pH 7.4 with a few drops of 2 mol l^{-1} Trizma base. Cells were scraped off the

dish (Fisher scientific cell scraper, 250 mm handle, 18 mm blade) and resuspended in 1 ml of a sucrose lysis buffer (the recipe above, but hypo-osmotic with only 30 mmol l^{-1} sucrose). The cell solution was sonicated (power 100 Watt, setting 8/ speed 22.5 kHz, Misonix incorporated, XL2000-010, New York) for 30 seconds to ensure the lysed sample was well mixed, centrifuged and a 200 µl aliquot fresh for LDH activity and protein determination (see below). For metal analysis, 1 ml of concentrated nitric acid was added to the remaining 800 µl of the cell homogenate for total Ti, Na^+, K^+, Ca^{2+} and Mg^{2+} determination by (ICP-OES, Varian 725 ES). The standards used for ICP-OES calibrations were between 0-1, 0-20 and 0-200 mg l^{-1} for Ti, K^+ and Na^+, respectively and between 0-40 mg l^{-1} for both Ca^{2+} and Mg^{2+}. All standards showed linear calibration with regression coefficient correlation of 0.99. To ensure acidity of the samples did not interfere with ICP- OES readout two sets of standards were made. One set were matrix matched and made in 30% nitric acid, the other made in 2% nitric acid. For the spike recovery test, samples (cell mixture) were spiked with 1 mg l^{-1} of different forms of TiO_2 and showed a good recovery of Ti metal measurement from the TiO_2 in different forms with 80.4 ± 4.2, 82.2 ± 1.5, 76.3 ± 4.7 and 75.7 ± 1.8% for bulk TiO_2, P25, anatse and rutile respectively (mean ± S.E.M, n = 6 for each material type). Both sets of standards and spikes showed low coefficients of variation within and between samples (< 5%).

5.2.6 Lactate dehydrogenase and protein determination

Lactate dehydrogenase activity was measured in the cell culture media ("extracellular" LDH, n = 6 per treatment) and in the cell homogenates ("intracellular" LDH, n = 6 per treatment). For the former, 200 µl of cell culture media from each well was gently centrifuged for 1 min to remove any cell debris/turbidity (~160 *g*, Heraeus instruments, Biofuge *pico*, Germany) and 100 µl of the resulting supernatant was used in the LDH assay. For the cell homogenate, 200 µl were sonicated, centrifuged (see above) and then

100 µl of the resulting homogenate was used in the LDH assay using the method of Plummer, (1971), full description found in Chapter 2. LDH activity is expressed as µmol min^{-1} ml^{-1} of media, or µmol min^{-1} mg^{-1} cell protein as appropriate. For calculation of the % LDH leak from the cells, cells were lysed for total LDH (lysate + Media LDH) and then media LDH was calculated as a percentage of the total, % LDH leak = (100 X extracellular LDH) / (intracellular LDH).

LDH activity in cell homogenates was normalised for cell protein content, and protein was measured in triplicate using the bicinchoninic acid (BCA) method (MC155208, Pierce, Rockford, USA). The BCA reagent is a mixture of two reagents, reagent A, containing sodium carbonate, sodium bicarbonate, bicinchoninic acid and sodium tartrate in 0.1 M sodium hydroxide; and reagent B, containing 4% cupric sulphate. These two reagents were mixed in a ratio of 50:1 of reagent A: B. Briefly, 15 µl of sample was added to 300 µl of the BCA reagent and the absorbance read at 570 nm in 96-well plates (VERSA max, Molecular Devices, Berkshire, UK) against bovine serum albumin standards. Calibrations spiked with and without 1 mg l^{-1} TiO_2 showed no interfere with the assay or colour reagent.

5.2.7 Cell morphology and scanning electron microscopy

Cell morphology was examined by light and electron microscopy during the cell culture, and prior to scraping the dishes at the end of the experiments. Briefly, cells were washed *in situ* on the cell culture dish with Dulbecco's phosphate buffered saline (DPBS) without calcium and magnesium (Lonza, B-4800 Verviers, Belgium), then fixed with 5 ml of 100% fresh methanol for 5 minutes, prior to staining with Giemsa (Giemsa's stain solution, IVD, England). Plates were examined wet using light microscopy (Nikon, 803923-Japan) and photographs taken using a digital camera (Pentax, K-X).

For scanning electron microscopy (SEM), the cells were fixed *in situ* on the culture plates and a disk cut out of the plate wells for mounting on SEM grids. Briefly, cells were washed in sucrose wash buffer (above) and fixed in 2.5% glutaldehyde in cacodylate buffer (0.2 M Sodium Cacodylate in water adjusted to a pH of 7.4) for 1 h. The cells were then washed twice in cacodylate buffer prior to being dehydrated in a graded series of ethanol. Cells were critically point dried and carbon coated (EMITECH-K850, K450X). Samples were imaged and elementally analysed (SEM, JEOL / JSM-7001F, Oxford Instruments INCA X-ray analysis system) using a 10 KV accelerating voltage, at a working distance of 10 mm.

5.2.8 Statistics

All data were statistically analysed used Stat Graphics Plus Version 5.1 and shown as means ± S.E.M (standard error of mean), while Figures were drawn using Excel and Sigma Plot Version 12.0, full description in details found in Chapter 2. In the time course experiment, two-way ANOVA was used to determine treatment x time effects and the curve fitting for time-effects were done using Sigma Plot Version 12.0, and curves were fitted to the raw data, although graphs show the mean values for convenience.

5.3 Results

5.3.1 Cell health and viability

The control Caco-2 cells (not exposed to TiO_2 or treated with drugs) showed normal morphology during the experiments with the cells remained confluent and well attached to the dishes (Fig. 5.5a). This was also supported by the LDH activity which remained at around 0.1 IU ml^{-1} or less of cumulative LDH release over the 24 h duration of the experiments (Fig. 5.6). The control Caco-2 cells also showed normal electrolyte levels with negligible variation in cell electrolyte concentrations. For example, in the time course experiment (triplicate plates/treatment) the electrolyte levels in control cells were (in nmol mg^{-1} protein); 6859.2 ± 237.6, 867.0 ± 26.3, 16.0 ± 4.1 and, 48.0 ± 0.9 for Na^+, K^+, Ca^{2+} and Mg^{2+}, respectively (mean ± S.E.M, n = 6), representing a within experiment variation of 1 - 20% depending on the analyte. The controls were also reproducible across experiments (and batches of cells). For example, the control cells in the second experiment showed cumulative LDH values in the media of 0.1 IU ml^{-1} or less, and the electrolyte concentrations in these controls were (in nmol mg^{-1} protein); 4518.6 ± 160.9, 718.9 ± 14.2, 10.6 ± 1.2 and 42.6 ± 1.1 for Na^+, K^+, Ca^{2+} and Mg^{2+} (mean ± S.E.M, n = 6). Overall across all experiments, the between experiment variation for electrolyte concentrations in cells from the unexposed/untreated controls was 10 - 30% depending on the analyte, (sodium and calcium varying the most) with cumulative LDH activity in the media remaining low (0.1 IU ml^{-1} or less).

The morphology of the Caco-2 cells after incubating with different forms of TiO_2 over 24 h exposure showed normal cells with good confluent and well attached to the wells in compare to control (Fig. 5.5b, c, d and e). Cumulative LDH activity release in the external media over 24 h remained low with 0.1 IU ml^{-1} or less for all different forms of TiO_2 (Fig. 5.6), the bulk showed the lowest LDH release with 0.04 IU ml^{-1} in compare to other forms of TiO_2. The percentage LDH leak through the Caco-2 cells

after exposed to different forms of TiO_2 was not significantly difference in compare to controls (ANOVA or Kruskal-Wallis test, $P > 0.05$, Table 5.1) indicating that the cell membrane integrity was not affected by different forms of TiO_2.

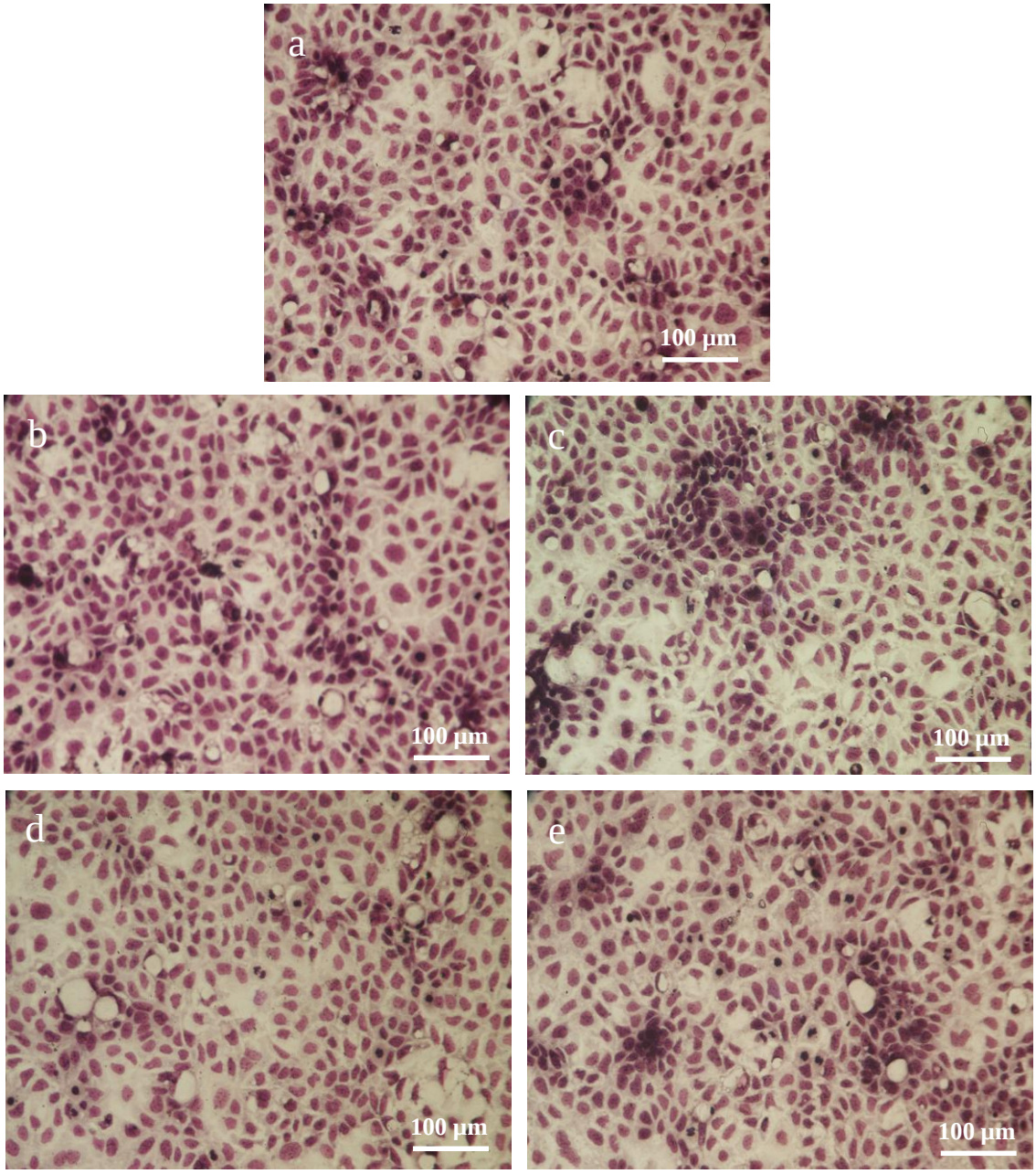

Figure 5.5 Morphology of the Caco-2 cells after 24 h exposure. (a) control (b) 1 mg l^{-1} bulk TiO_2 (c) 1 mg l^{-1} P25 (d) 1 mg l^{-1} nano anatase (e) 1 mg l^{-1} nano rutile showing normal morphology and well confluent of the cells in control and all treatment groups (n = 3 plates per treatment). Scale bar = 100 µm, stained with Giemsa's stain.

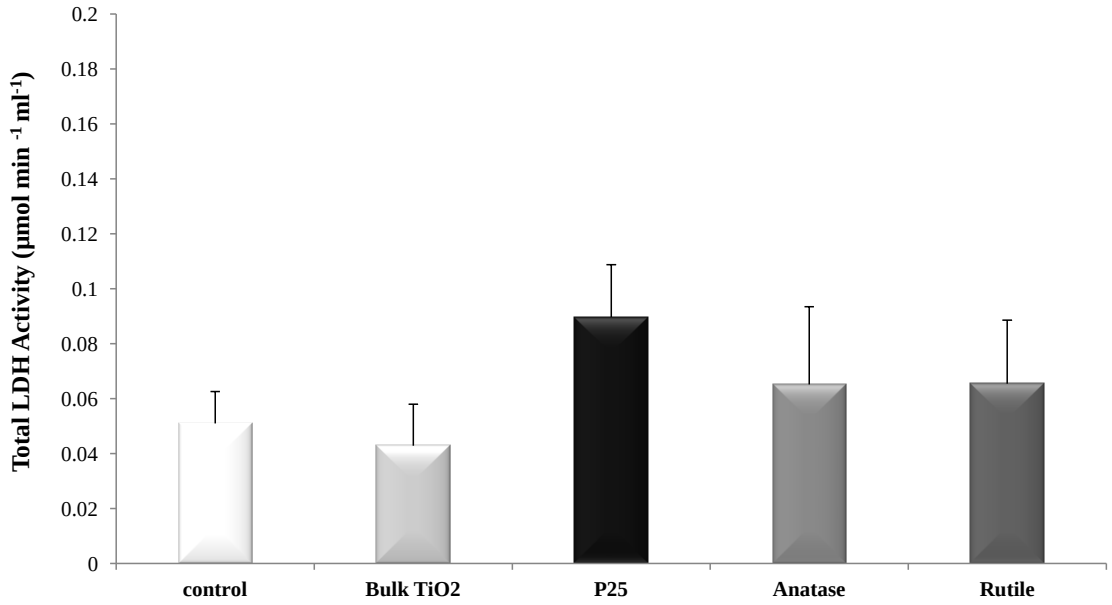

Figure 5.6 The effect of 1 mg l^{-1} different forms of TiO_2 exposure on the LDH release in external media (extracellular LDH) over 24 h in Caco-2 cells. Values are means ± S.E.M (n = 6). There were no statistically significant differences (ANOVA or Kruskal-Wallis test, $P > 0.05$) between groups (control, different forms of TiO_2).

Table 5.1 LDH leak in Caco-2 cells over 24 h after incubation with different forms of TiO_2.

TiO_2 1 mg l^{-1}	Total LDH activity (µmol min^{-1} ml^{-1})				
	Control	Bulk TiO_2	P25	Anatase	Rutile
Extracellular LDH	0.05 ± 0.01	0.04 ± 0.02	0.09 ± 0.02	0.06 ± 0.03	0.06 ± 0.02
Intracellular LDH	0.63 ± 0.02	0.61 ± 0.06	0.58 ± 0.07	0.56 ± 0.02	0.60 ± 0.03
% LDH Leak	7.32 ± 1.67	6.57 ± 2.52	13.18 ± 1.70	9.52 ± 3.96	9.16 ± 3.07

The effects of 1 mg l^{-1} different forms of TiO_2 exposure on the total LDH activity release after 24 h in Caco-2 cells. Values are means ± S.E.M. (n = 3-6). % LDH leak = (100 X extracellular LDH) / (intracellular LDH). There were no statistically significant differences (ANOVA or Kruskal-Wallis test, $P > 0.05$) between groups (control, different forms of TiO_2).

5. 3.2 Experiment 1: Time course of Ti accumulation from different forms of TiO_2

The time course of Ti accumulation for the different forms of TiO_2 are shown in Fig. 5.7, the unexposed control cells remained at a background level of around 2 nmol Ti mg^{-1} cell proteins throughout the experiment. However, all the TiO_2 treatments showed a non-linear hyperbolic rise in the Ti concentration in the cells, which achieved steady-state concentrations by 24 h. This saturable rise in net Ti accumulation by the cells occurred without similar elevations of cell Na^+ or K^+ concentrations in all treatments. The Na^+ and K^+ concentrations remained between 558 - 668 and 779 - 814 nmol mg^{-1} protein, respectively; indicating that the Ti response was Ti-specific and not an artefact of general electrolyte changes in the cells (not observed). There were some differences in the time courses of Ti accumulation for the different forms of TiO_2 (Fig. 5.7), and these were not explained by osmotic disturbances in the cells (no statistical differences by TiO_2 forms in the cell electrolyte contents, Table 5.2) or by differences in membrane permeability across the treatments. For the latter, the cumulative LDH leak by 24 h remained low at around 0.1 IU ml^{-1} (not statistically different from the control, and no material-type effect, ANOVA, P = 0.066 Table 5.1). The net Ti accumulation by 24 h was in the following order by material type: bulk, P25, anatase, rutile and unexposed controls. The bulk material and P25 showed the largest net Ti accumulation in 24 h, saturating at 14.4 ± 1.7 and 12.9 ± 0.4 nmol mg^{-1} protein respectively, but were not statistically different from each other (*t*-test, P = 0.473). The anatase form showed lower values with approximately 40% less Ti accumulation than either the P25 or bulk material (statistically different by 24 h, Kruskal Wallis test, P = 0.004). There were also some differences in Ti accumulation from the pure anatase and rutile forms, with the latter showing saturation at a slightly lower Ti concentration (Fig. 5.7). However, there was no statically significantly different showed between the anatase and rutile at 24 h (*t*-test, P = 0.295). The initial Ti accumulation rates calculated from the curves followed a

similar pattern with Ti accumulation from the bulk and rutile being faster than those from anatase or P25 (Fig. 5.7) and were 5.3, 3.73, 3.58 and 4.48 nmol mg^{-1} protein hr^{-1} for bulk, P25, anatase and rutile, respectively. The 50% saturation of Ti from different forms of TiO_2 were 7.1 nmol mg^{-1} protein at 1 h and 48 min, 6.82 nmol mg^{-1} protein at 2 h and 42 min, 4.26 nmol mg^{-1} protein at 1 h and 30 min and 3.47 nmol mg^{-1} protein at 30 min for bulk, P25, anatase and rutile, respectively. The plateau for the Ti accumulation from both bulk and P25 were at 8 h with 13.0 and 11.6 nmol mg^{-1} protein, respectively. Anatase was plateauing at 4 h with 6.78 nmol mg^{-1} protein while the rutile was the most rapid one which plateauing at 2 h and 30 min with 6.08 nmol mg^{-1} protein. At 24 h, the Ti from all different forms of TiO_2 exhibited statistically significant accumulation relative to control values (ANOVA or Kruskal-Wallis, $P < 0.05$) demonstrated a saturable time dependent response to 1 mg l^{-1} different forms of TiO_2.

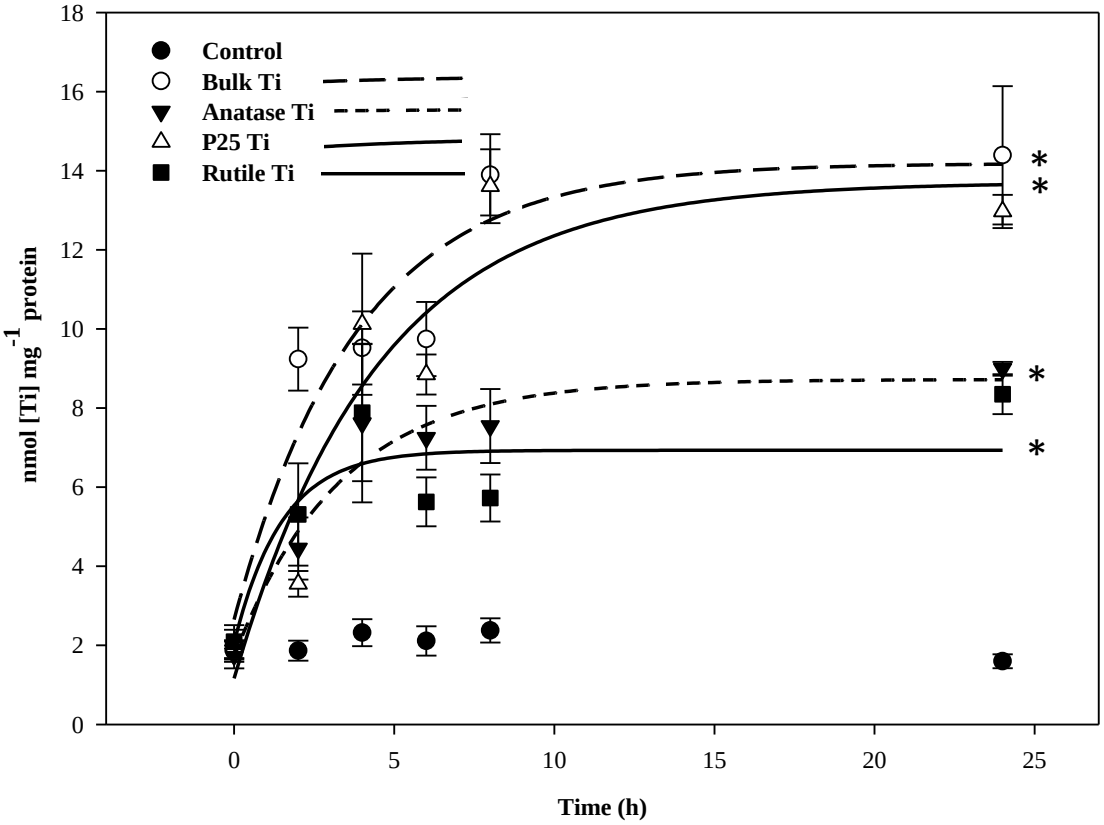

Figure 5.7 Titanium uptake in Caco-2 cells incubated with 1 mg l^{-1} different forms of TiO_2 for 24 h. The data points are mean values derived from triplicate measurements (n = 6 plates per treatment for each time point) and are expressed as nmol [Ti] mg^{-1} protein. Curves are fitted to the data points shown using hyperbolic exponential rise to the maximum (single, 3 parameters) in SigmaPlot version 12. The bulk: y = 2.65+11.54*(1-exp (-0.26*x)), r^2 = 0.90, P25: y = 1.16+12.54*(1-exp (-0.22*x)), r^2 = 0.86, anatase: y = 1.71+7.01*(1-exp (-0.30*x)), r^2 = 0.95 and rutile: y = 2.07+4.86*(1-exp (-0.67*x)), r^2 = 0.73. * Statistically significant difference from control values (ANOVA, P < 0.05). The control values were significantly lower than the treatment forms and so the curve is not fitted, but data points are shown for convenience.

5.3.3 Effects of TiO_2 exposure on intracellular electrolytes over 24 h

Caco-2 cells after exposed to 1 mg l^{-1} of different forms of TiO_2 over 24 h exhibited different effects on cell electrolytes. Intracellular potassium significantly decrease in all treatments groups relative to controls (ANOVA, P = 0.001, Table 5.2). The lowest value of K^+ was seen after rutile exposure, which dropped by 107 nmol mg^{-1} protein compared to the control.

Intracellular magnesium significantly increased in all treatments groups in comparison to the control (ANOVA, P = 0.0003, see Table 5.2). P25 caused the highest effects on Mg^{2+} levels relative to other treatment groups, showing 10.8 nmol mg^{-1} protein increases in comparison to the control magnesium level.

Calcium levels rose significantly in cells exposed to different forms of TiO_2 in comparison to the control (Kruskal-Wallis test, P = 0.04, Table 5.2). P25 caused the largest increase in intracellular calcium with a 24 nmol mg^{-1} protein rise compared to the control. The exposure of different forms of TiO_2 had no statistically significant effects on intracellular sodium levels relative to the control (Kruskal-Wallis test, P = 0.30, Table 5.2). However, changes in electrolyte levels were against the electrochemical gradient indicating that the membrane remained operative and did not passively leak electrolytes throughout the duration of the experiments.

5.3.4 Experiment 2: The effect of nystatin and vanadate incubation on Ti accumulation

Caco-2 cells were pre-incubated with 120 IU ml^{-1} nystatin to establish endocytosis inhibition or 100 µmol l^{-1} vanadate (a P-type ATPase inhibitor) to enhance blocking of any Ti metal transport through intestine. Nystatin and vanadate treatments showed significantly increased levels of bulk Ti accumulation compared to the control (ANOVA, P = 0.0002, Fig. 5.8). Bulk Ti accumulation increased by 3 nmol mg^{-1} protein compared to the control (10.76 nmol mg^{-1} protein) when incubated with nystatin, reaching a final concentration of 13.76 nmol mg^{-1} protein at 24 h. Incubating with vanadate further increased bulk Ti accumulation to 20.10 nmol mg^{-1} protein at 24 h, an increase of 10 nmol mg^{-1} protein compared to the control.

Nystatin caused an increase in P25 Ti accumulation (14.36 nmol mg^{-1} protein), 4 nmol mg^{-1} greater than the control (9.89 nmol mg^{-1} protein). Incubating with vanadate caused additional Ti accumulation reaching a final concentration of 22.26 nmol mg^{-1} protein, an increase of 12 nmol mg^{-1} protein compared to the control with a significant increase for both drugs (Kruskal-Wallis test, P = 0.0005, Fig. 5.8).

Anatase Ti accumulation were significantly increased when the cells were incubated with nystatin or vanadate (Kruskal-Wallis test, P = 0.0015, Fig. 5.8). Incubating with nystatin caused a 2 nmol mg^{-1} protein increase in accumulation compared to the control (9.47 nmol mg^{-1} protein). Incubating with vanadate further increased anatase Ti accumulation to 22.04 nmol mg^{-1} protein, an increase of 12 nmol mg^{-1} protein compared to the control.

Rutile Ti accumualation did not follow the same pattern in comparison with the other forms of TiO_2. Nystatin incubation showed a significant increase in Ti accumulation from exposure to the rutile form (ANOVA, P = 0.004, Fig. 5.8), by a 4 nmol mg^{-1} protein increase in compare to the control (5.38 nmol mg^{-1} protein).

Vanadate caused just a 0.9 nmol mg^{-1} increases in Ti accumulation, however this was not deemed statistically significant in comparison to the control (*t*-test, $P = 0.1602$).

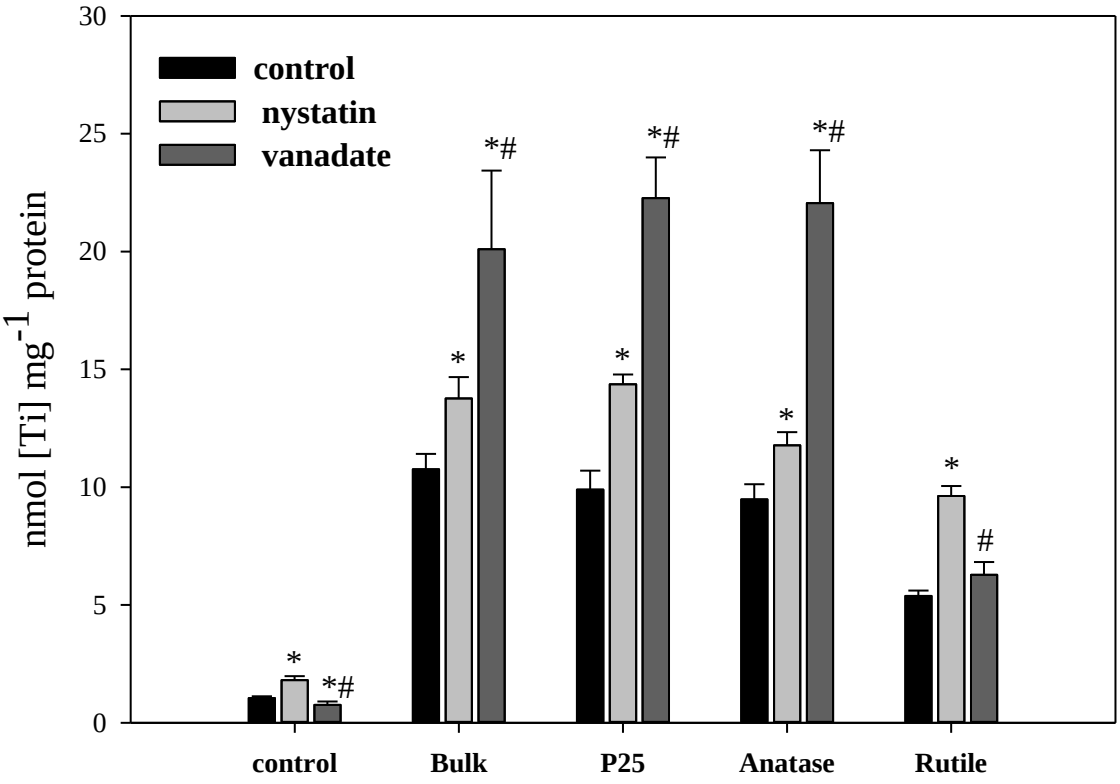

Figure 5.8 Drug effects on Ti accumulation in Caco-2 cells incubated with 1 mg l^{-1} different forms of TiO_2 over 24 h. Data are means ± S.E.M ($n = 6$) and expressed as nmol [Ti] mg^{-1} protein. * statistically significant difference from the no drug control values (ANOVA or Kruskal-Wallis test, $P < 0.05$). # statistically significant difference from the nystatin values (ANOVA or Kruskal-Wallis test, $P < 0.05$).

5.3.5 Effect of nystatin and vanadate exposure on intracellular electrolytes over 24 h

The electrolyte levels in Caco-2 cells varied in response to drug incubation and remained consistent within TiO_2 treatments. Electrolyte levels in nystatin controls were 6303.7 ± 468.1, 927.9 ± 50.9, 25.7 ± 9.5 and 56.2 ± 2.9 nmol mg^{-1} protein for Na^+, K^+, Ca^{2+} and Mg^{2+}, respectively (mean ± S.E.M, n = 6). Additions of different forms of TiO_2 to Caco-2 cells incubated with 120 IU ml^{-1} nystatin had no effects on intracellular Na^+, K^+ and Mg^{2+} levels relative to the no TiO_2 positive control (ANOVA or Kruskal-Wallis test, $P > 0.05$, Table 5.2). However, Ca^{2+} values were significantly decreased in comparison to the no TiO_2 positive control (Kruskal-Wallis, $P = 0.04$). Cells incubated with nystatin exhibited a significant increase in intracellular potassium with all the different forms of TiO_2 relative to the no drug controls (ANOVA or Kruskal-Wallis test, $P < 0.05$, Table 5.2) and similar to the equivlaentexposures without drugs. The level of K^+ decreased with all forms of TiO_2 in comparison to control values with nystatin present (see Table 5.2). Intracellular magnesium showed significantly increased levels for all the different forms of TiO_2 relative to their no drug controls (ANOVA or Kruskal-Wallis test, $P < 0.05$), except in cells exposed to P25 which were found not to be significantly different from the no drug control. Nystatin had no effects on intracellular calcium or sodium levels in compare to the no drug control (ANOVA or Kruskal-Wallis test, $P > 0.05$).

Electrolytes levels in the vanadate controls showed lower values than the nystatin controls (above) being 3632.0 ± 427.1, 466.9 ± 43.8, 20.9 ± 3.6 and 30.9 ± 3.4 nmol mg^{-1} protein for Na^+, K^+, Ca^{2+} and Mg^{2+}, respectively in vanadate-treated cells (mean ± S.E.M, n = 6). K^+ and Mg^{2+} levels in all TiO_2 forms incubated with vanadate showed a significantly lower values relative to the nystatin in all different forms of TiO_2 (ANOVA or Kruskal-Wallis test, $P < 0.05$). Caco-2 cells incubated with 100 µmol l^{-1} vanadate and different forms of TiO_2 displayed significantly decreased levels of

intracellular potassium in all TiO_2 forms relative to the no drug controls (ANOVA or Kruskal-Wallis test, $P < 0.05$), but there were no effects found on potassium levels in all TiO_2 forms relative to the no TiO_2 positive control (ANOVA, $P = 0.91$, Table 5.2). Cells incubated with vanadate cause a significant decrease in intracellular magnesium in all different forms of TiO_2 relative to the no drug controls (ANOVA or Kruskal-Wallis test, $P < 0.05$), but showed a significantly increase of Mg^{2+} level in the anatase and rutile groups comparing to the no TiO_2 positive control (ANOVA, $P = 0.047$). Calcium levels increased significantly in cells after incubated with vanadate in both bulk and rutile groups relative to the no drug controls (ANOVA or Kruskal-Wallis test, $P < 0.05$). There was no effects on calcium levels in all different forms of TiO_2 in presence of vanadate relative to the no TiO_2 control (ANOVA, $P = 0.48$). For the intracellular sodium levels, there was no significant effect found in compare to no drug control or no TiO_2 control (ANOVA or Kruskal-Wallis test, $P > 0.05$).

Table 5.2 Total Na^+, K^+, Ca^{2+} and Mg^{2+} nmol [Metal] mg^{-1} protein concentration in Caco-2 cells after exposed to 1mg l^{-1} different forms of TiO_2 over 24 h.

TiO_2 1 mg l^{-1}		Electrolytes (nmol mg^{-1} protein)			
		Na^+	K^+	Ca^{2+}	Mg^{2+}
No drugs	Control	4518 ± 160	718.8 ± 14.2	10.6 ± 1.2	42.6 ± 1.1
	Bulk TiO_2	4666 ± 576	663.9 ± 28.3*	14.3 ± 7.0	47.8 ± 2.2
	P25	4793 ± 231	643.8 ± 19.6*	28.0 ± 12.4*	53.4 ± 2.7*
	Anatase	5109 ± 624	637.9 ± 27.6*	20.8 ± 5.4*	49.8 ± 1.4*
	Rutile	4319 ± 350	611.1 ± 11.4*	19.1 ± 8.2*	50.7 ± 1.5*
Nystatin	Control	6303 ± 468#	927.9 ± 50.8#	25.7 ± 9.4#	56.2 ± 2.9#
	Bulk TiO_2	5253 ± 445	828.8 ± 62.3#	19.8 ± 2.2*#	55.3 ± 2.8#
	P25	5144 ± 308	815.7 ± 30.0#	27.8 ± 5.7	55.0 ± 1.8
	Anatase	5748 ± 455	822.7 ± 57.9#	14.4 ± 4.6*	56.2 ± 4.4#
	Rutile	5202 ± 417	807.1 ± 41.2#	17.7 ± 3.1*	55.0 ± 3.1#
Vanadate	Control	3632 ± 427†	466.8 ± 43.8†~	20.9 ± 3.6~	30.9 ± 3.4†~
	Bulk TiO_2	4246 ± 406	479.6 ± 36.9†~	25.2 ± 4.6~	38.9 ± 3.1†~
	P25	3982 ± 311	469.3 ± 26.9†~	18.0 ± 7.2	39.4 ± 2.7†~
	Anatase	4457 ± 216†	513.3 ± 16.9†~	18.7 ± 4.1	43.8 ± 2.3†*~
	Rutile	4534 ± 568	490.7 ± 37.1†~	29.1 ± 2.4~	40.9 ± 2.8†*~

Data are expressed as means ± S.E.M (n = 6 for each group). * statistically significant difference from the control values within columns, treatments and electrolytes (ANOVA or Kruskal-Wallis test, $P < 0.05$). # statistically significant difference of nystatin values relative to the no drug trials within columns, treatments and electrolytes (ANOVA or Kruskal-Wallis test, $P < 0.05$). ~ statistically significant difference of vanadate values relative to the no drug trials within columns, treatments and electrolytes (ANOVA or Kruskal-Wallis test, $P < 0.05$). † statistically significant difference of vanadate values relative to nystatin values within columns, treatments and electrolytes (ANOVA or Kruskal-Wallis test, $P < 0.05$).

5.3.6 Presence of particles within the Caco-2 cells

Scanning electron microscopy (SEM) of the Caco-2 cells was employed to investigate the presence, condition and organization of microvilli on the apical surface of control cells compared to cells exposed to the different forms of TiO_2 (Fig.5.9), and also to explore the presence of the TiO_2 particles in/on the cells by using the X-ray microanalysis detector (Fig. 5.10 and 5.11). Control cells showed good microvilli growing on the surface of the cultured cells after 96 h incubation. The exposure of Caco-2 cells to 1 mg l^{-1} of different forms of TiO_2 for 24 h showed different effects on the microvilli growth; bulk and anatase have a good development of the microvilli growth which showed similar organization to control cells. P25 and rutile seems to have the lowest microvilli growth density with the decreased numbers of the microvilli appearance on the apical surface of the cells relative to the no treated control cells (Fig. 5.9). For all TiO_2 forms, the Ti was detected by pinpoint X-ray analysis which observed the Ti particles in/on the Caco-2 cells and appear to be penetrate the cells and made a contact with the cell membrane (Fig. 5.10), some of the particles are suggest to be translocated in the nucleus (Fig. 5.11d-f) and other particles have been shown on the cell surface (Fig. 5.11a-c).

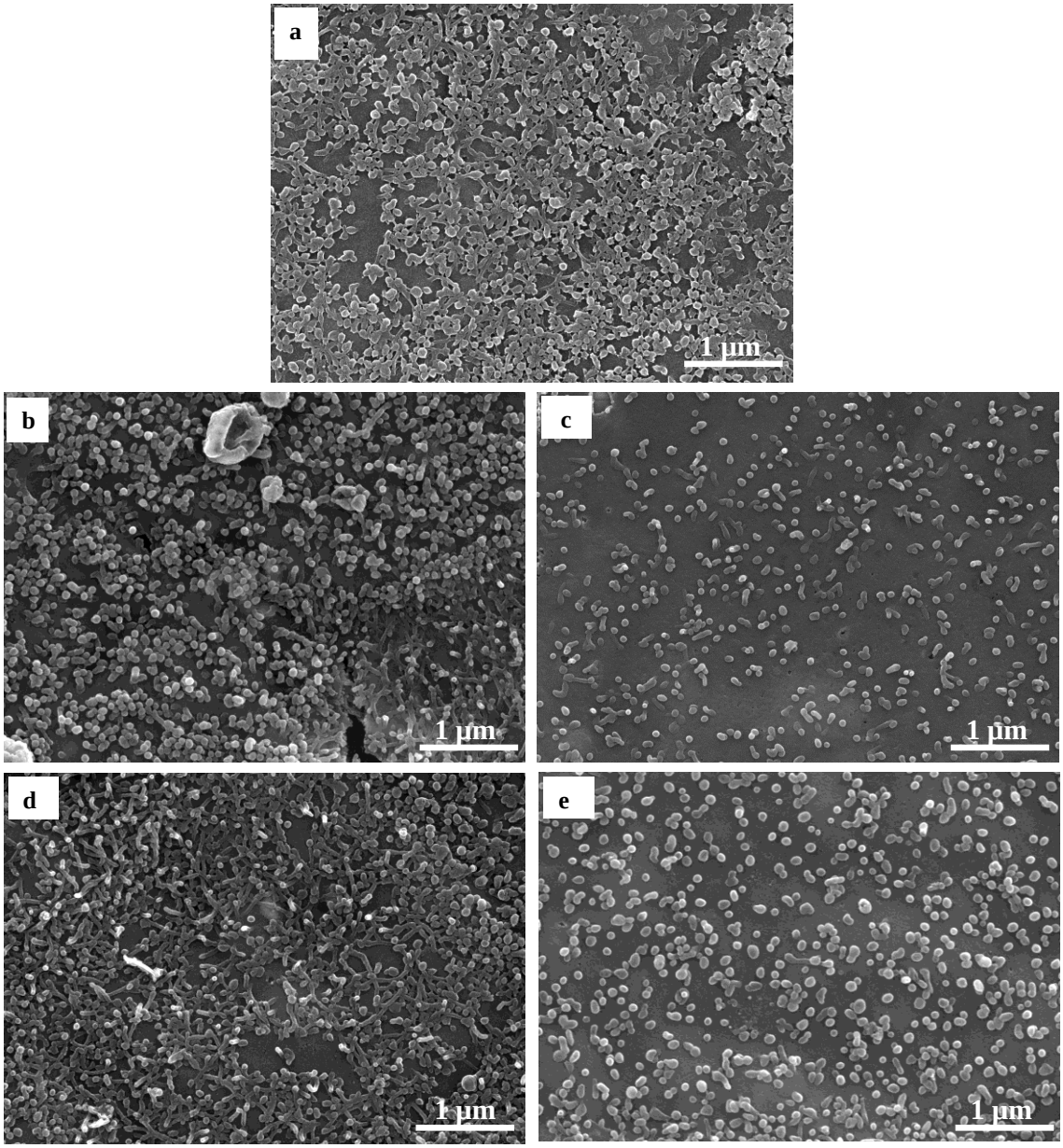

Figure 5.9 Scanning electron microscopy of Caco-2 cells after 96 h incubation showing the microvilli growth density on the apical surface of the cells after exposed to 1 mg l^{-1} different forms of TiO_2 for 24 h. (a) control, (b) bulk, (c) P25, (d) anatase and (e) rutile. Scale bar = 1 µm (*n* = 3 per treatment).

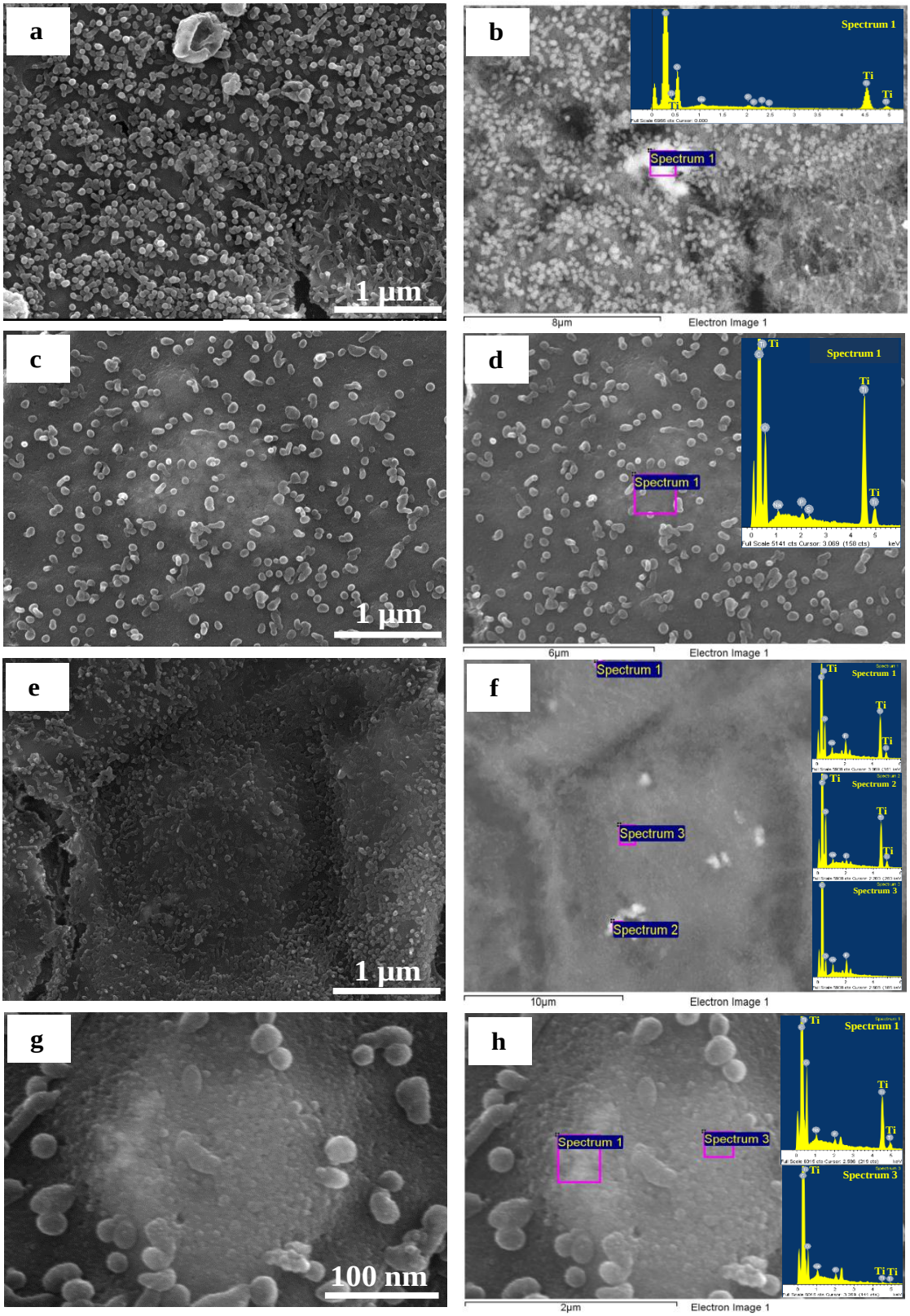

Figure 5.10 Scanning electron microscopy of Caco-2 cells after 96 h incubation showing presence of the Ti particles underneath the cells after exposed to 1 mg l^{-1} different forms of TiO_2 for 24 h (*n* = 3 per treatment). (a) Secondary electron image (SEI) of the bulk cell surface, scale bar = 1 µm; (b) Backscatter image (BSI) of 'a' image showing subsurface Ti with xrma spectra; (c) SEI of the P25 cell surface, scale bar = 1 µm; (d) BSI of 'c' image; (e) SEI of the anatase cell surface, scale bar = 1 µm; (f) BSI of 'e' image, (g) SEI of the rutile cell surface, scale bar = 100 nm; (h) BSI of 'g' image.

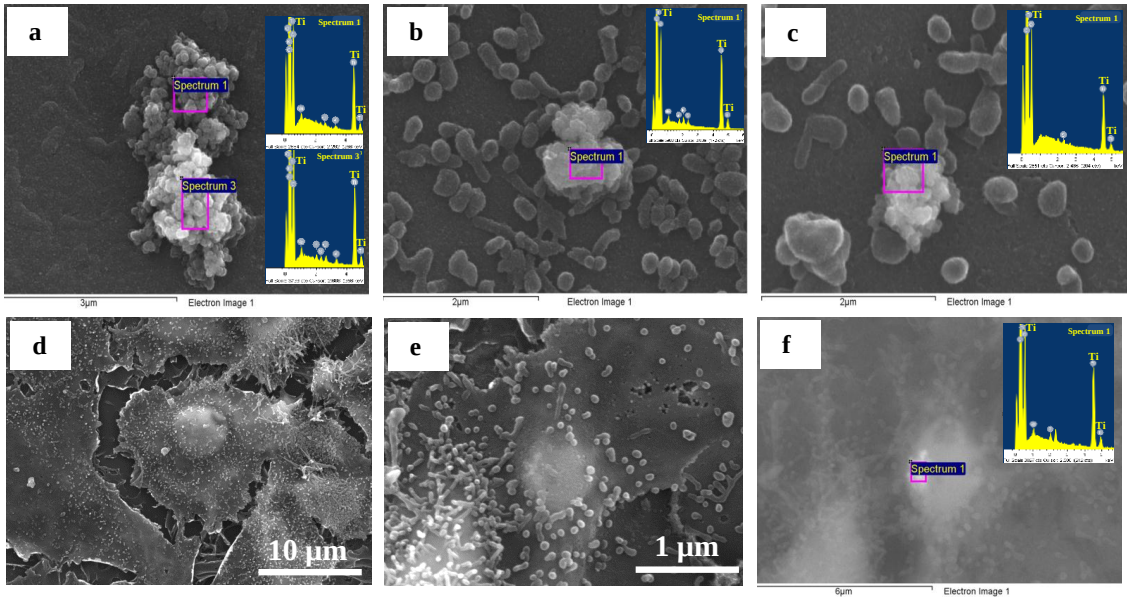

Figure 5.11 Scanning electron microscopy of Caco-2 cells after 96 h incubation showing presence of the Ti particles on the surface of the cells after exposed to 1 mg l^{-1} different forms of TiO_2 for 24 h (*n* = 3 per treatment). (a) Surface bound of P25 with spectra, scale bar = 3 µm; (b) Surface bound anatase with associated spectra, scale bar = 2 µm; (c) Surface bound rutile with associated spectra, scale bar = 2 µm; (d) SEI image of the cell surface exposed to P25. The yoke like structure in the centre is the nucleus, scale bar = 10 µm; (e) SEI image of the cell surface exposed to rutile showing the nucleus in the centre, scale bar = 1 µm; (f) A high magnification BSI of 'e' highlighting a Ti dense region within the left side of the nucleus.

5.4 Discussion

This experiment investigated the processes involved in the uptake and accumulation of different forms of TiO_2 using Caco-2 cells. The main findings were that Ti uptake rates from bulk TiO_2 were greater than that from the different nano forms of TiO_2, which indicated a material-type effect towards uptake of TiO_2 in Caco-2 cells. Following nystatin (an endocytosis inhibitor) and vanadate (a P-type ATPase inhibitor) incubation, an explanation of the data is that the mechanisms of TiO_2 uptake are likely mediated by endocytic mechanisms. Furthermore, exposure to different forms of TiO_2 (bulk and nano) altered cell electrolyte homeostasis.

5.4.1 Cell health and viability

The morphology of Caco-2 cells in the control and in all forms of TiO_2 was good in general, with normal morphology and well-confluent cell appearance (Fig. 5.5). There was no effect on the cell structure after exposure to different forms of TiO_2 in comparison with controls. The present findings seem to be consistent with other research which found no alteration in the morphology or density of the Caco-2 cells after exposure to 100 μg ml^{-1} TiO_2 NPs for 4 h, 24 h and 72 h compared to control cells (Fisichella et al., 2012).

The LDH activity was performed to ensure that the cell membrane integrity had been preserved throughout the experiments. There was no LDH leakage shown in either the controls or after exposing the cells to 1 mg l^{-1} of different forms of TiO_2. Control Caco-2 cells showed normal electrolyte levels, with negligible variation in electrolyte concentrations after exposure to different forms of TiO_2. Taken together, the normal morphology of the cells, negligible LDH leak, and normal electrolyte concentrations in Caco-2 cells indicate that cells were in good viability and have the utility for measuring the accumulation of Ti from different forms of TiO_2.

5.4.2 Uptake and accumulation of Ti from different forms of TiO_2 by Caco-2 cells

Ti uptake from different forms of TiO_2 in Caco-2 cells showed a steady, saturable, time dependent appearance over the 24 h experiment. This most likely indicates that Ti uptake involves active transport by endocytosis mechanism(s), which are influenced by particle characteristics, resulting in the nonlinear (saturable) uptake curves observed (Fig. 5.7), so the passive diffusion through the cell membrane or leakage of dissolved Ti seems unlikely. This is also indicated by Brun et al. (2011), who argue that no partial dissolution occurs for NPs after the Ti is internalised in Caco-2 cells as the nanoparticulate state. However, details of their solution preparation, exposure conditions, replication and controls were not fully documented in this preliminary conference report. Fröhlich and Roblegg (2012) also suggested that endocytosis is the most likely mechanism for the uptake of NP into intestinal epithelial cells.

The net uptake rate of Ti from bulk TiO_2 in Caco-2 cells was greater than the other NP forms of TiO_2. A possible explanation for this might be that the larger particles of the TiO_2 remained within the submucosa of the intestine and colon (Jani et al., 1990) or this might be related to the behaviour of bulk TiO_2 in the culture media. Bulk TiO_2 and the P25 were quickly dispersed in the culture media when prepared for the cell exposure, which may have improved cell surface contact and subsequent uptake. Anatase and rutile were individually aggregated quickly in the culture media. This possibly reduced the particle surface area available, and consequently decreases the cell surface contact. This is in agreement with Ryabchikova et al. (2010) who showed that TiO_2 crystal structure alters particle membrane interactions which can either increase or decrease particle internalisation. They hypothesised that the NPs may alter the function of the plasma membrane with simple mechanical binding to membrane macromolecules. Furthermore, the behaviour of TiO_2 in culture media might be related

to increased ionic strength from high salt concentrations in the culture media, which may lead to aggregation of a portion of NPs (Koeneman et al., 2010).

5.4.3 Effects of the different forms of TiO_2 on Caco-2 cells electrolytes

Despite the fact that cell culture media is enriched with magnesium and calcium, exposure of Caco-2 cells to different forms of TiO_2 caused an increase in cellular magnesium and calcium concentrations and a decrease in potassium concentration in cells compared with the controls (Table 5.2). The increase in Mg^{2+} level was not observed after bulk TiO_2 exposure; this elevation in Mg^{2+} level was just seen after exposure to different forms of TiO_2 NPs suggesting a specific material effect on Mg homeostasis. Increase the accumulation of cellular Mg^{2+} requires proper distributions of the ions across the cell membrane and any changes in the membrane potential especially in the polarized epithelia like intestine as well as changes in pyridine nucleotide levels will promote cellular Mg^{2+} accumulation (Romani, 2011). This suggests that the exposure to TiO_2 may result in changes in the membrane potential. Additionally, the decrease of the potassium concentration in cells exposed to different forms of TiO_2 could be related to this change in the membrane permeability associated with the mechanical interaction of TiO_2 and membrane macromolecules (Ryabchikova et al., 2010). This potassium reduction might also be happening through the activation of single stretch-activated potassium channels which are more permeable than other ion channels in the intestinal epithelium (Chang and Loretz, 1992). The same situation as Mg^{2+} was seen with the concentration of Ca^{2+} in the cells, where the bulk TiO_2 did not cause a marked increase in Ca^{2+} concentration compared to that caused by different forms of TiO_2 NPs. Scherbart et al. (2011) suggests that calcium influxes after exposure to different particle size of TiO_2 are nanoparticle type specific. Differences between bulk and nano TiO_2 could be based on the cell sensitivity to specific material effects on the calcium homeostasis. This intracellular calcium homeostasis might be related to the

over expression or under expressoin of calcium-binding proteins (Fisichella et al., 2012). The highest concentration of Ca^{2+} was observed with P25 exposure (Table 5.2), which was associated with the altered structural organisation of the cell surface villi (Fig. 5.9). The same alteration in villi structure has been noticed by Koeneman et al. (2010) who relate this effect to the increase in free cellular calcium concentration.

5.4.4 How does the Ti from different forms of TiO_2 can be taken up by Caco-2 cells?

Caco-2 cells were pre-incubated for 1 h with either 120 IU ml^{-1} nystatin (an endocytosis inhibitor) or 100 µmol l^{-1} sodium orthovanadate (P-type ATPase inhibitor) prior to being dosed with 1 mg l^{-1} of different forms of TiO_2 for 24 h. These inhibitors were applied to investigate whether TiO_2 uptake is a cholesterol-dependent endocytic mechanism or an energy-dependent process.

The nystatin exposure resulted in increased cellular Ti concentrations from all forms of TiO_2 in Caco-2 cells (Fig. 5.8). Nystatin is one of the endocytosis inhibitors which inhibit the lipid-raft mediated endocytosis including the caveolae by depleting the cholesterol from the plasma membrane (Nabi and Phuong, 2003; Ragnarsson et al., 2008). Endocytosis inhibition can reduce the transport of particles across the cell monolayer (Ragnarsson et al., 2008). Increased cellular Ti concentrations may indicate that endocytosis of TiO_2 is cholesterol independent, and uptake of TiO_2 particles could be mediated by another mode of endocytosis. Exposure of prostate PC-3M cells to TiO_2 NPs indicates that cell internalization could be via clathrin-mediated endocytosis, caveolin-mediated endocytosis and macropinocytosis (Thurn et al., 2011). Ryabchikova et al. (2010) showed clusters of TiO_2 NPs within large folds of the plasma membrane in TEM images from MDCK cells, suggesting possible uptake by macropinocytosis as well as clathrin-mediated endocytosis.

The increase in cellular Ti concentration from TiO_2 in cells incubated with nystatin (Fig. 5.8) can be attributed to the blocking of some exocytosis pathways that

are cholesterol dependent. This is because the cholesterol depletion increased NP uptake by 300% (Dombu et al., 2010) and this could be also explained by the fact that cholesterol depletion is totally blocking NP exocytosis (Dombu et al., 2010). However, the exocytosis mechanism of the NPs is still not well studied. Simon et al. (2011) suggests that TiO_2 NPs can enter the cell through different internalization pathways which interact with the golgi apparatus, and can be extruded from the cell by exocytosis via endosome or secretory vesicles.

Caco-2 cells after exposed to vanadate showed further elevation in cellular Ti concentration after exposure to all forms of TiO_2 with the exception of the rutile TiO_2 (Fig. 5.8). This could be due to inhibition of the active ATP metabolism in Caco-2 cells, which is required for transport of NPs through endocytic mechanism (Rangnarsson et al., 2008). Furthermore, inhibition of ATP-ase may result in inhibition of the GTP-ase binding protein Rac-1 to the plasma membrane that stimulates the actin filament and membrane ruffling (Ridley, 2001), that essential for the macropinocytosis mechanism (Grimmer et al., 2002). Moreover, the vanadate may interrupt TiO_2 efflux by inhibiting Rho GTPases which play an important role in exocytosis through the organization and dynamics of the actin cytoskeleton (Cobbold et al., 2002). Further investigation is required to fully characterise the exact endocytic/exocytic pathways that are interfered with through vanadate application.

5.4.5 Effects of nystatin and vanadate on Caco-2 cells electrolytes

Caco-2 cells pre-incubated with nystatin and then exposed to different forms of TiO_2 showed an increase in cellular potassium and magnesium concentrations in comparison to the no drug TiO_2 controls (Table 5.2). As mentioned above, nystatin is a cholesterol depletion drug and changing the cholesterol content in the plasma membrane may cause an alteration in the membrane permeability (Rodal et al., 1999). Since the effect of TiO_2 in the cells is to reduce the level of K^+ concentration, the elevated levels of K^+ in the

cells after exposed to nystatin suggest that this elevation is solely caused by the nystatine incubation. For the Mg^{2+}, the elevation after exposure to nystatin was more than that after TiO_2 exposure without drugs. This suggests that the elevated level of Mg^{2+} may interfere with the effects of nystatin by altering the cell electrolytes homeostasis after cholesterol depletion.

Cells incubated with vanadate showed a decrease in both potassium and magnesium cellular concentrations compared to the no drug TiO_2 controls (Table 5.2), but an elevation was noticed in cellular Ca^{2+} concentration. This could be explained by the structural differences in the protein and crystallite. E2 was designated for the low energy phosphoenzyme which includes the Na^+, K^+, ATPase, Mg^{2+} ATPase and Ca^{2+}-ATPase (Rice et al., 2001). Vanadate is a P-type ATPase inhibitor which inhibits both the Na^+, K^+, ATPase (Cantly et al., 1978) and Mg^{2+} ATPase (Rice et al., 2001) by making the transition state for phospholyration-dephospholyration mimic the state in E2. Ca^{2+}-ATPase has different crystallite structure that required EGTA (Stokes and Lacapere, 1994), this may lead to more stability of these crystals which are not affected by vanadate inhibitor.

5.4.6 Presence of particles within the Caco-2 cells

The different forms of TiO_2 showed different effects on the microvilli growth on the cell surface (Fig. 5.9) indicated by a lower density of the microvilli after exposure to both P25 and rutile. The same observation was reported by Koeneman et al. (2010) who suggested that the increase in free cellular Ca^{2+} concentration was the reason for the alteration of the microvilli organisation. The current study showed the same increase in Ca^{2+} concentration after exposure to P25 (Table 5.2). The alteration in the microvilli organisation may be related to the effects of Ca^{2+} elevation on the villin, a Ca^{2+} regulated actin binding protein that is associated with the brush border microvilli cytoskeleton (Bretscher and Weber, 1980). This effect is caused by the P25, a mixture

of anatase and rutile, rather than the individual crystal forms indicating that P25 is more toxic than the other forms of TiO_2.

The images from the SEM study showed clearly the penetration of the Ti from different forms of TiO_2 which was observed underneath the cells and in contact with the cell membrane (Fig. 5.10) and sometimes near to the nucleus (Fig. 5.11). This suggests that the NPs have the ability to enter the cells by an active transport mode which is mediated by a form of endocytic pathways. The same suggestion was made by Brun et al. (2011) after observing the appearance of TiO_2 NPs by TEM images in Caco-2 cells after 24 h exposure. They reported anecdotally, particles mainly grouped together inside the cells into heterogeneous clusters of 1-2 μm, and hypothesised that the NPs internalization occurred through macropinocytosis.

The intracellular trafficking of NPs towards the nucleus might be happening by microtubules mostly through dynein-dependant of the endosomes processing (Panariti et al., 2012). Additionally, the shape and charge may play an important role in localization of the NPs near to the nucleus. Rode shape NPs are likely to be moved towards the nucleus via microtubules (Xu et al., 2008). Furthermore, positively charged NPs are more easily approach the nucleus (Yue et al., 2011).

Conclusions

This study shows that Ti uptake in Caco-2 cells from different forms of TiO_2 was steady, saturable and time dependent over the period of 24 h exposure; this indicates that an active absorption mechanism has occurred. The highest uptake rate was observed with the bulk TiO_2 which was about 2 fold more than that indicated by the *in vivo* study on rats (Jani et al., 1994). The direct contact of Ti from different forms of TiO_2 with the cell membrane, results in localisation of Ti inside the cell both close to the membrane and also in the cytoplasm. This suggests that the mechanism of TiO_2

uptake involves a number of different active endocytic pathways. Increased cellular Ti concentration after exposure to both nystatin and vanadate may also be related to interference with the endocytic processes. The nano form of TiO_2 showed an alteration in cell electrolytes homeostasis. P25 produced the highest increase in cell Ca^{2+} concentration which altered the microvilli organisation on the cell surface. This raises the concern that P25 toxic effects should be considered as a potential hazard to human health.

Chapter 6

General Discussion

Currently there is a very limited data on the uptake of TiO_2 NPs via intestine, the mechanisms of their uptake, and the material-type effects on Ti uptake (differences between bulk and nano). This thesis aimed to give a better understanding of the TiO_2 NPs uptake by the intestine and the possible mechanisms involved, leading to a better understanding of the hazard and risk assessment of TiO_2 NPs intake by food.

This work reports regional differences in Ti accumulation from both bulk and nano forms of TiO_2 by vertebrate intestine (Chapter 3), and demonstrates the uptake of Ti from TiO_2 particles across the gut of rainbow trout using the isolated gut perfusion technique (Chapter 3). The main findings are that Ti from TiO_2 particles (bulk or nano) are mainly absorbed in the mid and hind regions of trout intestine, with the Ti accumulating in the mucosa rather the underlying muscularis. This uptake of the Ti from TiO_2 leads us to further investigate on the possible mechanism uptake. The effects of nystatin which inhibits the uptake of Ti from TiO_2, suggest at least part of the mucosal influx step is by endocytosis for both bulk and nano forms of TiO_2 (Chapter 4). However, the effect of solute transport inhibitors also suggests a dissolved Ti component involved in Ti export from the tissue to the blood for bulk and nano TiO_2 (Chapter 4). There was also a material-type effect where Ti from NPs crossed the gut faster than Ti from the bulk powder, and uptake from the nano form was more sensitive to nystatin treatment as well as changes in the gas mixture in the media. A novel effect of the partial pressure of carbon dioxide (pCO_2) on Ti uptake is also proposed, with several possible mechanisms by which CO_2 might modulate Ti uptake from particles (Chapter 3).

In human intestinal epithelial cell line (Caco-2 cells), the Ti from all different forms of TiO_2 were uptake by the cells and the accumulation of Ti was effected by the material-type and crystal structures (Chapter 5). Bulk TiO_2 shows the greater uptake rates relative to the other forms of TiO_2. Cells incubated with nystatin or vanadate

demonstrate further increases in cellular Ti concentration from all forms of the TiO_2 (Chapter 5) which indicate a different situation from the intestinal tissue (Chapter 4).

Histopathology and ultrastructural (TEM and SEM) studies of the intestine for both cell and tissue provided an indicator of the uptake of Ti from different forms of TiO_2 (Chapter 3-5).

6.1 Correlation steps between the in vivo and the in vitro methods

In vivo studies are complicated by a number of considerations during dietary exposure, such as the interaction of NPs with the food components, the transit time from the mouth through the GIT, and the varying conditions between each part of the gut (pH, enzymes, gas partial pressures and composition of the digesta). All these factors could be reasonably controlled to investigate Ti uptake using *in vitro* methods.

In this study, different *in vitro* methods with different organisms were used to evaluate them with the *in vivo* studies. The studies try to mimic the conditions in real organisms and offer a direct contact between particles and intestinal epithelium. The isolated perfused intestine method is closest to the *in vivo* condition by having four layers of the intestine tissue (from the mucosa to the serosa), as well as a good viability criteria of the tissue outside the living organisms. Human intestinal Caco-2 cell is another *in vitro* method used to improve our knowledge on the uptake of NPs across a monolayer intestinal cell.

The results from both *in vitro* methods in this study gives some similarities to the results of *in vivo* studies, from the uptake of bulk TiO_2 by rat intestine (Jani et al., 1994), TiO_2 NP uptake by intestine in mice (Wang et al., 2007) and the Ti accumulation in the gut from TiO_2 NPs exposure in rainbow trout fish (Ramsden et al., 2009). However, some differences were also noticed between the *in vitro* and *in vivo* methods especially for the electrolyte concentration. Both *in vitro* methods showed alteration in

gut electrolyte homeostasis which is different from what was reported by *in vivo* studies. For example, Ramsden et al. (2009) did not report any effects of TiO_2 exposure on tissue electrolytes (Na^+, K^+ and Ca^{2+}).

6.2 Uptake and accumulation of Ti from TiO_2 exposure by the perfused intestine and Caco-2 cells

Both *in vitro* methods showed that intestinal Ti accumulation from the bulk TiO_2 was greater than the other TiO_2 nano forms. For the perfused intestine, the bulk material accumulation in the tissue was greater by 7 and 2 folds for the mid and hind intestine respectively compared to the TiO_2 NP (P25) over 4 h exposure (Chapter 3, Fig. 3.7). This was expected; the results from the serosal perfusate indicated a slower efflux of the Ti from the bulk TiO_2 across the gut to the blood side relative to the P25 resulting in Ti accumulated in the tissue. The same situation was shown in Caco-2 cells; bulk TiO_2 showed greater accumulation by 2, 6 and 8 folds compared to P25, anatase and rutile, respectively over 24 h exposure (Chapter 5, Fig. 5.7). This matches the result from the hind intestine in the perfusion experiments, in which the accumulation of bulk TiO_2 was 2 fold greater than that of the P25.

The accumulation of the Ti metal from TiO_2 exposure in gut epithelium is explained by apical uptake of the Ti in the particulate form rather than the dissolved Ti metal from different types of TiO_2. This is supported by low proportion of the surface-bound total Ti metal on the gut mucosa that represented by rapid solution dipping experiment (Chapter 4, Fig. 4.3), and also by the measurable appearance of apparent dissolved total Ti metal from TiO_2 shown by the dialysis experiment with the normal physiological saline (mucosal solution). Furthermore, the particles in both methods were observed inside the epithelial cells using the TEM for perfused intestine and SEM for the Caco-2 cells.

For the Caco-2, the SEM work was supported by using the x-ray energy dispersive spectrophotometry (EDS) measurements which detected the Ti particles in/on the cells and within the nucleus of the cells (Chapter 5, Fig. 5.9, 5.10 and 5.11). The EDS measurement with the monolayer cells is much easier to detect the particles inside the epithelial cells rather than the folded tissue layers of the intestine.

For the gut perfusion tissue, the EDS measurements can detect Ti metal in large aggregates of TiO_2 on the surface of tissues (e.g., energy dispersive x-ray on top of rodent skin, Adachi et al., 2010), but these techniques have limitations for NPs *inside* cells (see review, Handy et al., 2012). In traditional fixed TEM specimens, there is a limitation of EDS represented by the energy beam which can only penetrate about 2-300 nm into the tissue, detection limit of EDS compared to the concentrations of the TiO_2 used here (1 mg l^{-1}, even if it was all absorbed into the cells) would still be far below the mass detection limit against the high carbon background in the specimen (e.g., even using 10% TiO_2, the carbon peaks in Adachi et al. 2010 are off the scale compared to the much smaller, variable, Ti peaks in the spectra). A further limitation of EDS is the minimum area or cluster size to reliably detect chemical composition of the particles relative to the size of the beam (spot size between 1-50 µm). Given these technical limitation we did not observe large enough aggregates in the cells, close enough to the surface, to make reliable Ti composition measurements by EDS. However, TEM instruments especially adapted with new field emission guns for EDS are now becoming available that can achieve beams in the nm range (as used by Michel-Jeanjean et al., 2012 on skin explants), albeit with the risk that the high brightness needed may damage the specimen. Nonetheless, like previous studies with electron microscopy images of putative TiO_2 NPs inside cells without EDS measurements (e.g., Galloway et al., 2010; Powell et al., 2010) inferences may be made from particle morphology.

In the TEM images of the gut perfusion tissue, some electron dense particulate materials was detected inside the epithelial cells and sometimes located within a vesicle. These particles represent a similar morphology to the particles in the TiO_2 NPs or bulk (Chapter 3, Fig. 3.9 and 3.10), the distinct shape and size of these particles with their absence from the controls (no indication of the same particles appearance) suggesting they were a TiO_2 particles from the exposures. This observation suggests that TiO_2 NPs or bulk could enter the cells through a form of endocytosis.

6.3 Possible mechanism uptake of Ti from TiO_2 across the intestinal epithelium

The mechanism uptake of metals and metal oxide NPs is likely by endocytosis and an active uptake. The main mechanisms are clathrin-mediated and caveolae-mediated endocytosis in addition to phagocytosis and macropinocytosis (Fig. 6.1) (Iversen et al., 2011; Fröhlich and Roblegg, 2012). The endocytosis of NPs is depending on the size, shape and the charge of the NPs, as well as on the cell type (Thurn et al., 2007). The general diameter of the clathrin-coated vesicles is nearly to 120 nm, while the caveosomes range between 50 and 80 nm (Johannes et al., 2002). Thus, it is likely for the NPs to be uptake by one of these endocytic mechanisms. Macropinosomes are the largest one with a range of diameter between 500 to 2000 nm (Johannes et al., 2002) which is possible for the bulk particles and the big aggregations of the NPs to be uptake by this mechanism.

The different crystal forms with so many shapes and sizes of the TiO_2 NPs possibly affecting on the endocytic pathways of its uptake which is not yet to be fully understandable. Also, the differences between the monolayer cells and the gut tissue are playing an important role in the particles uptake.

The present study indicated that the mechanism uptake of TiO_2 NPs across the epithelial cell of intestine involved one of the possible endocytic mechanisms

mentioned above (Fig. 6.1) after the sensitive responses towards the nystatin and vanadate inhibitors. Nystatin is a cholesterol depletion component via the lipid rafts and the TiO_2 NPs here acts differently towards the nystatin in the perfused intestine and Caco-2 cells. For the perfused intestine, the mechanism uptake of TiO_2 NPs could be through caveolae disturbance by cholesterol reduction and this could increase the uptake of NPs by the clathrin pathway. Thurn et al. (2011) demonstrated that uptake of TiO_2 NPs in prostate cancer PC-3M cells involved the endocytic pathways via clathrin-mediated endocytosis, caveolin-mediated endocytosis, and macropinocytosis.

In Caco-2 cells, cholesterol could be implied in the exocytosis of NPs, and for this reason the accumulation of the TiO_2 was increased after the cells were exposed to the nystatin. The cholesterol via lipid rafts may play an important role in the regulation of the exocytosis (Salaun et al., 2004; Chintigary et al., 2006). In addition, caveolae-mediated endocytosis has been suggested to play a role in the uptake of NPs (Thurn et al., 2011), but if this uptake is reduced by cholesterol-depleting agents and these agents may also affect the other endocytic mechanisms (Doherty et al., 2009). These results were agreed with the study by Dombu et al. (2010) which showed clearly the implied of the cholesterol in NP exocytosis.

Exposure to nystatin and vanadate completely abolished the uptake of the bulk TiO_2 by the perfused intestine. This made a suggestion of the possible phagocytosis involvement in the endocytic uptake of the big particles of TiO_2 by phagocytic cells like macrophages (Fig. 6.1) or by the macropinocytosis within the early endosome.

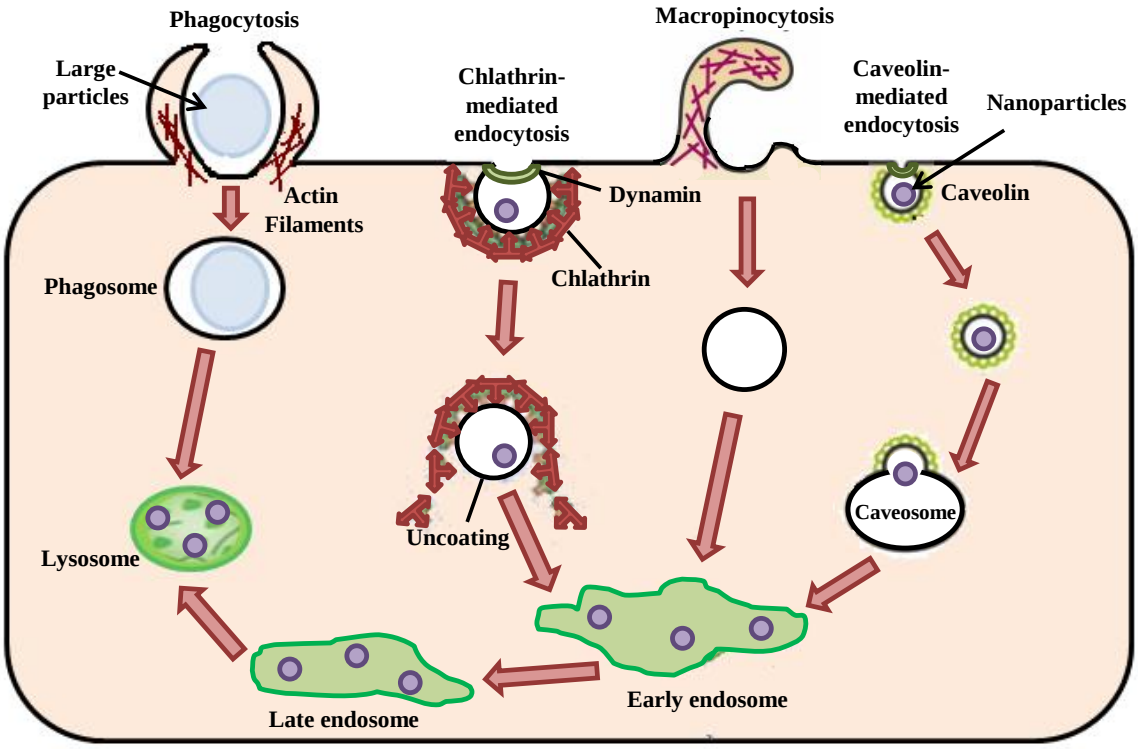

Figure 6.1 The possible endocytic mechanisms uptake of TiO_2 NPs (purple dots) or bulk TiO_2 (light blue dots) showing the process of their taken up by endocytosis within the early endosome or the phagosome and both of them are then combine with the lysosome. Four active mechanisms uptake via transcellular pathway are shown in the diagram. Phagocytosis is depends on the actin filaments as a receptor mediated and largely district to M cells of Peyer's patches. This process is used for the uptake of large particles. Clatherin-mediated endocytosis is a dynamin-dependent mechanism which is also a receptor mediated uptake process. Macropinocytosis is an active, actin-dependent process used to internalize the fluid surrounding the cell containing particles then taken up altogether and located inside the cell. Caveolin-mediated endocytosis is associated with protein caveolin which is essential for the endocytosis uptake by pinch off from the membrane of the intestinal epithelium.

6.4 Material-type effects on the electrolytes of the intestinal tissue and cell

The exposure to bulk and nano TiO_2 caused some effects on intestinal electrolytes homeostasis (Mg^{2+}, Ca^{2+} and K^{+}). Tissue and cell electrolytes showed difference effects between the perfused intestine and Caco-2 cells methods. For the isolated perfused intestine, the bulk TiO_2 caused an alteration in tissue electrolytes homeostasis (Chapter 3, Table 3.8). This was different for the Caco-2 cells, mainly all TiO_2 nano forms was responsible for the alteration of the cell electrolytes homeostasis (Chapter 5, Table 5.2). These effects should be studied carefully which may indicate that Ti metal may interfere with the endogenous electrolytes homeostasis, especially for the Ca^{2+} which raise the concern of the ability of Ti metal to interfere with the calcium homeostasis. Further investigations on the precise mechanisms of TiO_2 induced changes in electrolyte homeostasis are required.

6.5 Hazard screening of the TiO_2 uptake by food to the GIT tract

Little is known about the potential risk of nanotechnology applications to the human body, especially within the gastrointestinal tract which is a target system for food applications. The bulk and nano TiO_2 are metal oxides that are used, or proposed, for many applications, especially in the food sector. There is also a concern that environmental releases of TiO_2 NPs may enter the food chain and reach higher trophic levels including humans. The concentrations of TiO_2 NPs in surface water have been reported to reach 0.02 µg l^{-1}, while the concentration in the sewage treatment water was 4 µg l^{-1} (Gottschalk et al., 2009). For the intake of TiO_2 by food, Powell et al. (2010) estimate ingestion of 5 mg TiO_2/person/day with an unknown part of it in nanoform. Total dietary intake only of nano-TiO_2 is estimated to be 2.5 mg/individual/day (Lomer et al., 2000). Recently, Weir et al. (2012) reported that daily intake of TiO_2 by food is between 1-3 mg/Kg body weight/day, with 36% of the particles in nanoscale form.

Consequently, this daily intake raises the concern about the expected of chronic effects rather than acute toxic effects on humans (Weir et al., 2012).

The present thesis highlights the possibility of hazard via the food, as relevant TiO_2 NPs uptake within the intestinal epithelium has been demonstrated. The results indicated the ability of the Ti metal from TiO_2 exposure to across the intestine, with some material-type effects on the Ti metal uptake and accumulation from TiO_2 exposure (both bulk and nano treatment); and evidence of Ti appearance inside the intestinal epithelial cells. This raises the hazard potential of the Ti accumulation from nano TiO_2 exposure which should be reconsidered in risk assessments, in addition to that based only on the bulk material. The Ti metal uptake rates from TiO_2 exposure in present study are identical to other metals like Cu (Handy et al., 2000) but it is lower by 10 fold than the Hg uptake in the perfused intestine (Holye and Handy, 2005). Thus the absorption hazard of TiO_2 is similar to Cu but potentially less toxic than Hg.

Furthermore, the effects of CO_2 in the uptake of the TiO_2 NPs through intestine also need to be considered for the risk assessment purposes especially for the human health and the pCO_2 effect on Ti uptake can be explained by acid-base toxicity in the intestine. Carbonated fizzy drinks which contain large amount of CO_2, when combined with food intake, may accelerate the uptake of NPs through the intestine. In addition, the role of the CO_2 in elevating the uptake rate of Ti metal from TiO_2 NPs represents an important effect of these NPs in real ecosystems, associated to the partial pressure of the gasses in external medium which raise the concern of the environmental hazard from TiO_2 exposure. All the results in this study indicate an active absorption mechanism for TiO_2 in the intestinal epithelium, and this should be considered in risk assessments and dietary exposure to the TiO_2 NPs for both the ecosystems and human health. However, further investigations on the TiO_2 effects on food-related risk assessments and NPs hazards are advisable.

6.6 Future work

A number of areas of work require further investigation, and some suggestions are indicated below.

- Further investigation is required on the mechanism uptake of TiO_2 NPs by using other inhibitors of endocytic pathways. Chlorpromazine is mainly used as an inhibitor of clathrin-mediated endocytosis and known to function as a calmodulin antagonist. To further elucidate if the uptake of NPs is by a macropinocytosis pathway which is an actin-dependent mechanism, amiloride and calmodulin is often used to repress this process. Caveolae-mediated endocytosis can be inhibited by using tyrosine kinase inhibitors like genistein. More investigations on the precise endocytic/exocytotic mechanisms in conjunction with the sub cellular distribution are in demand.
- Gut rat perfusion is an ideal model to achieve our findings from the gut fish perfusion which represent a comparative study between lower vertebrates and mammals. Different concentrations of the TiO_2 (higher and lower than the 1 mg l^{-1}) are recommended, to learn more about the cellular uptake and intracellular transport of TiO_2 NPs across the gastrointestinal tract. Other approaches are needed to investigate more deeply about the material-type effects (particle size and/or crystal structure) on the uptake of TiO_2 by the intestinal epithelium. More knowledge on this aspect is important to determine the bioavailability of the ingested Ti from both bulk TiO_2 and the nano forms.
- To obtain more information about the uptake of TiO_2 NPs across epithelium tissue and subsequent biological effects, using the gill perfusion *in vitro* model in order to interpret and aid our data from the gut perfusion. This will enable further understanding on the uptake and behaviour of these particles by studying different parameters like the presence of organic matter such as dissolved

organic matter (DOM) which could affect NP aggregation. The salinity and hardness of the water may also alter the bioavailability and therefore the uptake of NPs. For example, the additions of Ca^{2+} to water will increase the hardness of water and that may affect the uptake and transport of NPs by influencing the aggregation of NPs, an effect which could be removed by using the Ca^{2+} chelator (+EGTA). Furthermore, the addition of NaCl will alter the ionic strength and may cause particle aggregation (reduced bioavailability). The influence of altering the water pH should be also addressed carefully, for at pH 5 the chemistry of the water and the aggregation of NPs may be different compared with pH 7.

- To assess our information about the uptake of TiO_2 NPs in either Caco-2 cells or gut tissue, it will be very useful to study molecular gene expression changes and identify the role of individual genes involved in the uptake of TiO_2 NPs. The genes that may interpret the TiO_2 uptake by gastrointestinal tract are dynamin 1, caveolin-1 and PTRF (cavin). This will provide a better understanding on the uptake mechanisms for NPs across the gut epithelium.

Research in all these aspects will increase our understanding on TiO_2 toxicity.

References

Adachi K, Yamada N, Yamamoto K, Yoshida Y and Yamamoto O 2010. *In vivo* effect of industrial titanium dioxide nanoparticles experimentally exposed to hairless rat skin. *Nanotoxicology* 4:296–306.

Adams LK, Lyon DY and Alvarez PJJ 2006. Comparative eco-toxicity of nanoscale TiO_2, SiO_2, and ZnO water suspensions. *Water Research,* 40**,** 3527-3532.

Ahmadi F and Kurdestany AH 2010. The Impact of silver nano particles on growth performance, lymphoid organs and oxidative stress indicators in broiler chicks. *Global Veterinaria 5,* 6**,** 366-370.

Aitken RJ, Chaudhry MQ, Boxall ABA and Hull M 2006. Manufacture and use of nanomaterials: current status in the UK and global trends. *Occupational Medicine (Lond),* 56**,** 300-306.

Allen NS, Edge M, Ortega A, Liauw CM, Stratton J and Mcintyre RB 2002. Behaviour of nanoparticle (ultrafine) titanium dioxide pigments and stabilisers on the photooxidative stability of water based acrylic and isocyanate based acrylic coatings. *Polymer Degradation and Stability,* 78**,** 467-478.

Ando M 1990. Effects of bicarbonate on salt and water transport across the intestine of the seawater eel. *Journal of Experimental Biology,* 150**,** 367-379.

Ando M, Sasaki H and Huang KC 1986. A new technique for measuring water transport across the seawater eel intestine. *Journal of Experimental Biology,* 122:257–268.

Arora S, Rajwade JM and Paknikar KM 2012. Nanotoxicology and *in vitro* studies: The need of the hour. *Toxicology and Applied Pharmacology,* 258**,** 151-165.

Au DWT, Wu RSS, Zhou BS and Lam PKS 1999. Relationship between ultrastructural changes and EROD activities in liver of fish exposed to Benzo[a]pyrene. *Environmental Pollution,* 104**,** 235-247.

Berkowitz BA 1996. Adult and newborn rat inner retinal oxygenation during carbogen and 100% oxygen breathing. Comparison using magnetic resonance imaging delta Po_2 mapping. *Investigative Ophthalmology and Visual Science,* 37**,** 2089-98.

Bermudez E, Mangum JB, Asgharian B, Wong BA, Reverdy EE, Janszen DB, Hext PM, Warheit DB and Everitt JI 2002. Long-term pulmonary responses of three laboratory rodent species to subchronic inhalation of pigmentary titanium dioxide particles. *Toxicological Sciences,* 70**,** 86-97.

Bermudez E, Mangum JB, Wong BA, Asgharian B, Hext PM, Warheit DB and Everitt JI 2004. Pulmonary responses of mice, rats, and hamsters to subchronic inhalation of ultrafine titanium dioxide particles. *Toxicological Sciences,* 77**,** 347-357.

Blake DM, Maness PC, Huang Z, Wolfrum EJ, Huang J and Jacoby WA 1999. Application of the photocatalytic chemistry of titanium dioxide to disinfection and the killing of cancer cells. *Separation and purification methods,* 28**,** 1-50.

Borm PJA and Kreyling W 2004. Toxicological hazards of inhaled nanoparticles - Potential implications for drug delivery. *Journal of Nanoscience and Nanotechnology,* 4**,** 521-531.

Borm PJA, Robbins D, Haubold S, Kuhlbusch T, Fissan H, Donaldson K, Schins R, Stone V, Kreyling W, Lademann J, Krutmann J, Warheit D and Oberdörster E 2006. The potential risks of nanomaterials: a review carried out for ECETOC. *Particle and Fibre Toxicology,* 3**,** 11.

Braydich-Stolle L, Schaeublin N, Murdock R, Jiang J, Biswas P, Schlager J and Hussain S 2009. Crystal structure mediates mode of cell death in TiO_2 nanotoxicity. *Journal of Nanoparticle Research,* 11**,** 1361-1374.

Bretscher A and Weber K 1980. Villin is a major protein of the microvillus cytoskeleton which binds both G and F actin in a calcium- dependent manner. *Cellular and Molecular Life Sciences,* 20**,** 839-847.

Brun E, Jugan ML, Herlin-Boime N, Jaillard D, Fayard B, Flank AM, Mabondzo A and Carrière M 2011. Investigation of TiO_2 nanoparticles translocation through a Caco-2 monolayer. *Journal of Physics: Conference Series,* 304**,** 012048.

Bu Q, Yan G, Deng P, Peng F, Lin H, Xu Y, Cao Z, Zhou T, Xue A, Wang Y, Cen X and Zhao YL 2010. NMR-based metabonomic study of the sub-acute toxicity of titanium dioxide nanoparticles in rats after oral administration. *Nanotechnology,* 21**,** 125105.

Burke J and Handy RD 2005. Sodium-sensitive and -insensitive copper accumulation by isolated intestinal cells of rainbow trout *Oncorhynchus mykiss*. *Journal of Experimental Biology,* 208**,** 391-407.

Bury NR and Handy RD 2010. Copper and iron uptake in teleost fish. In: Surface chemistry, bioavailability and metal homeostasis in aquatic organisms : an integrated approach. *Essential reviews in experimental biology, vol. **2***. London: Society for Experimental Biology.

Calzolai L, Gilliland D and Rossi F 2012. Measuring nanoparticles size distribution in food and consumer products: a review. *Food Additives and Contaminants: Part A,* 29**,** 1183-1193.

Campbell HA, Handy RD and Nimmo M 1999. Copper uptake kinetics across the gills of rainbow trout (*Oncorhynchus mykiss*) measured using an improved isolated perfused head technique. *Aquatic Toxicology,* 46**,** 177-190.

Cantley LC, Cantley LG and Josephson L 1978. A characterization of vanadate interaction with (Na,K)-ATPase: Mechanistic and recgulatory implications. *The Journal of Biological Chemistry,* 25**,** 7361-7368.

Chanc W and Loretz CA 1992. Activation by membrane stretch and depolarization of an epithelial monovalent cation channel from teleost intestine..*Journal of Experimental Biology,* 169**,** 87-104.

Chen X and Mao SS 2007. Titanium dioxide nanomaterials: Synthesis, properties, modifications, and applications. *Chemical Reviews,* 107**,** 2891-2959.

Chen Z, Meng H, Xing G, Chen C, Zhao Y, Jia G, Wang T, Yuan H, Ye C, Zhao F, Chai Z, Zhu C, Fang X, Ma B and Wan L 2006. Acute toxicological effects of copper nanoparticles *in vivo*. *Toxicology Letters,* 163**,** 109-120.

Chintagari NR, Jin N, Wang P, Narasaraju TA, Chen J and Liu L 2006. Effect of cholesterol depletion on exocytosis of alveolar type 2 cells. *American journal of respiratory cell and molecular biology*, 34, 677 - 687.

Chung I-S, Lee M-Y, Shin D-H and Jung H-R 2010. Three systemic argyria cases after ingestion of colloidal silver solution. *International Journal of Dermatology,* 49**,** 1175-1177.

Cobbold C, Ponnambalam S, Francis MJ and Monaco AP 2002. Novel membrane traffic steps regulate the exocytosis of the Menkes disease ATPase. *Human Molecular Genetics,* 11, 2855-2866.

Corredor E, Testillano P, Coronado M-J, Gonzalez-Melendi P, Fernandez-Pacheco R, Marquina C, Ibarra MR, De La Fuente J, Rubiales D, Perez-De-Luque A and Risueno M-C 2009. Nanoparticle penetration and transport in living pumpkin plants: in situ subcellular identification. *BMC Plant Biology,* 9**,** 45.

Crane M, Handy RD, Garrod J and Owen R 2008. Ecotoxicity test methods and environmental hazard assessment for engineered nanoparticles. *Ecotoxicology,* 17**,** 421-437.

Dameron C and Harrison M 1998. Mechanisms for protection against copper toxicity. *The American Journal of Clinical Nutrition,* 67**,** 1091S-1097S.

Del Nido PJ, Glynn P, Buenaventura P, Salama G and Koretsky AP 1998. Fluorescence measurement of calcium transients in perfused rabbit heart using rhod 2. *American Journal of Physiology - Heart and Circulatory Physiology,* 274**,** H728-H741.

Deng Y-F, Jiang Y-Q, Hong Q-M and Zhou Z-H 2007. Speciation of water-soluble titanium citrate: Synthesis, structural, spectroscopic properties and biological relevance. *Polyhedron,* 26**,** 1561-1569.

Derjaguin BV and Landau LD 1941. Theory of the stability of strongly charged lyophobic sols and of adhesion of strongly charged particles in solutions of electrolytes. *Acta Physicochim,* 14**,** 733-762.

Des Rieux A, Fievez V, Théate I, Mast J, Préat V and Schneider Y-J 2007. An improved *in vitro* model of human intestinal follicle-associated epithelium to study nanoparticle transport by M cells. *European Journal of Pharmaceutical Sciences,* 30**,** 380-391.

Doherty GJ and McMahon HT 2009. Mechanisms of endocytosis. *Annual Review of Biochemistry,* 78, 857–902.

Dombu CY, Kroubi M, Zibouch R, Matran R and Betbeder D 2010. Characterization of endocytosis and exocytosis of cationic nanoparticles in airway epithelium. *Nanotechnology,* 21, 8.

Domingo WR and Klyne W 1949. A photoelectric flame photometer. *Biochemistry Journal,* 45, 400-408.

Donaldson K, Aitken R, Tran L, Stone V, Duffin R, Forrest G and Alexander A 2006. Carbon nanotubes: A review of their properties in relation to pulmonary toxicology and workplace safety. *Toxicological Sciences,* 92**,** 5-22.

Donaldson K and Tran CL 2004. An introduction to the short-term toxicology of respirable industrial fibres. *Mutation Research-Fundamental and Molecular Mechanisms of Mutagenesis,* 553**,** 5-9.

Drobne D, Jemec A and Pipan Tkalec Ž 2009. *In vivo* screening to determine hazards of nanoparticles: Nanosized TiO_2. *Environmental Pollution,* 157**,** 1157-1164.

Eddy FB 1977. Oxygen uptake by rainbow trout blood, *Salmo gairdneri*. *Journal of Fish Biology,* 10**,** 87-90.

Eddy FB 2009. Regulation of sodium in the body fluids of teleost fish in response to challenges to the osmoregulatory system. *In:* Handy RD, Bury N and Flik G (eds.) *Osmoregulation and Ion Transport: Integrating Physiological, Molecular and Environmental Aspects.* Essential Reviews in Experimental Biology, Vol 1, Society for Experimental Biology Press, London.

Eddy FB and Handy RD 2012. Ecological and environmental physiology of fishes. *In:* Burggren W (ed.) *Ecological and environmental physiology series.* Vol 4, University Press, Oxford.

Eisler R 1991. Cyanide hazards to fish, wildlife, and invertebrates: a synoptic review. Washington, D.C.: Patuxent Wildlife Research, Center, U.S. Department of the Interior, Fish and Wildlife Service 85(1.23).

Elder A, Gelein R, Silva V, Feikert T, Opanashuk L, Carter J, Potter R, Maynard A, Finkelstein J and Oberdörster G 2006. Translocation of inhaled ultrafine manganese oxide particles to the central nervous system. *Environmental health perspectives,* 114**,** 1172-1178.

Federici G, Shaw BJ and Handy RD 2007. Toxicity of titanium dioxide nanoparticles to rainbow trout (*Oncorhynchus mykiss*): Gill injury, oxidative stress, and other physiological effects. *Aquat Toxicolo,* 84**,** 415-430.

Fisichella M, Berenguer F, Steinmetz G, Auffan M, Rose J and Prat O 2012. Intestinal toxicity evaluation of TiO_2 degraded surface-treated nanoparticles: a combined physico-chemical and toxicogenomics approach in caco-2 cells. *Particle and Fibre Toxicology,* 9**,** 18.

Foulkes EC and Bergman D 1993. Inorganic mercury absorption in mature and immature rat jejunum: transcellular pathways *in vivo* and in everted sacs. *Toxicology and Applied Pharmacology,* 120**,** 89-95.

Fraser TWK, Reinardy HC, Shaw BJ, Henry TB and Handy RD 2011. Dietary toxicity of single-walled carbon nanotubes and fullerenes (C_{60}) in rainbow trout (*Oncorhynchus mykiss*). *Nanotoxicology,* 5**,** 98-108.

Frödin L 1975. Renal transplantation in the rat II. *In Vitro* perfusion of rat kidneys before transplantation. *Scandinavian Journal of Clinical and Laboratory Investigation,* 35**,** 455-462.

Fröhlich E and Roblegg E 2012. Models for oral uptake of nanoparticles in consumer products. *Toxicology,* 291**,** 10-17.

Galloway T, Lewis C, Dolciotti I, Johnston BD, Moger J and Regoli F 2010. Sublethal toxicity of nano-titanium dioxide and carbon nanotubes in a sediment dwelling marine polychaete. *Environmental Pollution,* 158**,** 1748-1755.

Gao J, Youn S, Hovsepyan A, Llaneza VNL, Wang Y, Bitton G and Bonzongo J-CJ 2009. Dispersion and toxicity of selected manufactured nanomaterials in natural river water samples: Effects of water chemical composition. *Environmental Science and Technology,* 43**,** 3322-3328.

Geiser M, Rothen-Rutishauser B, Kapp N, Schürch S, Kreyling W, Schulz H, Semmler M, Hof V, Heyder J and Gehr P 2005. Ultrafine particles cross cellular membranes by nonphagocytic mechanisms in lungs and in cultured cells. *Environmental health perspectives* 113**,** 1555–1560.

Gontier E, Ynsa M-D, Bíró T, Hunyadi J, Kiss B, Gáspár K, Pinheiro T, Silva J-N, Filipe P, Stachura J, Dabros W, Reinert T, Butz T, Moretto P and Surlève-Bazeille J-E 2008. Is there penetration of titania nanoparticles in sunscreens through skin? A comparative electron and ion microscopy study. *Nanotoxicology,* 2**,** 218-231.

Goss GG, Perry SF, Wood CM and Laurent P 1992. Mechanisms of ion and acid-base regulation at the gills of freshwater fish. *Journal of Experimental Zoology,* 263**,** 143-159.

Grasset E, Bernabeu J and Pinto M 1985. Epithelial properties of human colonic carcinoma cell line Caco-2: effect of secretagogues. *American Journal of Physiology - Cell Physiology,* 248**,** C410-C418.

Griffitt RJ, Hyndman K, Denslow ND and arber DS 2009. Comparison of molecular and histological changes in zebrafish gills exposed to metallic nanoparticles. *Toxicological Sciences,* 107**,** 404-415.

Griffitt RJ, Luo J, Gao J, Bonzongo JC and Barber DS 2008. Effects of particle composition and species on toxicity of metallic nanomaterials in aquatic organisms. *Environmental toxicology and chemistry* 27(9)**,** 1972-8.

Grimmer S, Van Deurs B and Sandvig K 2002. Membrane ruffling and macropinocytosis in A431 cells require cholesterol. *Journal of Cell Science,* 115**,** 2953-2962.

Grodzik M and Sawosz E 2006. The influence of silver nanoparticles on chicken embryo development and bursa of Fabricius morphology. *Journal of Animal and Feed Sciences,* 15**,** 111-114.

Grosell M, Wood CM, Wilson RW, Bury NR, Hogstrand C, Rankin C and Jensen FB 2005. Bicarbonate secretion plays a role in chloride and water absorption of the European flounder intestine. *American Journal of Physiology - Regulatory, Integrative and Comparative Physiology,* 288**,** R936-R946.

Gottschalk F, Sonderer T, Scholz RW and Nowack B 2009. Modeled environmental concentrations of engineered nanomaterials (TiO_2, ZnO, Ag, CNT, Fullerenes) for different regions. *Environmental Science and Technology,* 43**,** 9216-9222.

Grosell M, Genz J, Taylor JR, Perry SF and Gilmour KM 2009. The involvement of H+-ATPaseand carbonic anhydrase in intestinal HCO3–secretion in seawater-acclimated rainbow trout. *Journal of Experimental Biology* 212:1940-1948.

Gunshin H, Mackenzie B, Berger UV, Gunshin Y, Romero MF, Boron WF, Nussberger S, Gollan JL and Hediger MA 1997. Cloning and characterization of a mammalian proton-coupled metal-ion transporter. *Nature,* 388**,** 482-488.

Gurr J-R, Wang ASS, Chen C-H and Jan K-Y 2005. Ultrafine titanium dioxide particles in the absence of photoactivation can induce oxidative damage to human bronchial epithelial cells. *Toxicology,* 213**,** 66-73.

Hagens WI, Oomen AG, De Jong WH, Cassee FR and Sips AJaM 2007. What do we (need to) know about the kinetic properties of nanoparticles in the body? *Regulatory Toxicology and Pharmacology,* 49**,** 217-229.

Hamilton R, Wu N, Porter D, Buford M, Wolfarth M and Holian A 2009. Particle length-dependent titanium dioxide nanomaterials toxicity and bioactivity. *Particle and Fibre Toxicology,* 6**,** 35.

Hamrahi-Michak M, Sadeghi SA, Haghighi H, Ghanbari-Kakavandi Y, Razavi-Sheshdeh SA, Noughabi MT and Negahdary M 2012. The toxicity effect of cerium oxide nanoparticles on blood cells of male Rat. *Annals of Biological Research,* 3 (6)**,** 2859-2866.

Han O and Wessling-Resnick M 2002. Copper repletion enhances apical iron uptake and transepithelial iron transport by Caco-2 cells. *American Journal of Physiology - Gastrointestinal and Liver Physiology,* 282**,** G527-G533.

Handy RD and Eddy FB 2004. Transport of solutes across biological membranes in eukaryotes: An environmental perspective. *In*: Van Leeuwen HP, Köster W, (ed s). *Physicochemical kinetics and transport at chemical-biological interphases*. IUPAC series, John Wiley, Chichester. pp. 337-356.

Handy RD, Eddy FB and Baines H 2002a. Sodium-dependent copper uptake across epithelia: a review of rationale with experimental evidence from gill and intestine. *Biochimica et Biophysica Acta (BBA) - Biomembranes,* 1566**,** 104-115.

Handy RD, Eddy FB and Romain G 1989. *In vitro* evidence for the ionoregulatory role of rainbow trout mucus in acid, acid/aluminium and zinc toxicity. *Journal of Fish Biology,* 35:737-747.

Handy RD, Gow IF, Ellis D and Flatman PW 1996. Na-dependent regulation of intracellular free magnesium concentration in isolated rat ventricular myocytes. *Journal of Molecular and Cellular Cardiology,* 28:1641-1651.

Handy RD, Kammer FV, Lead J, Hassellöv M, Owen R and Crane M 2008a. The ecotoxicology and chemistry of manufactured nanoparticles. *Ecotoxicology,* 17**,** 287-314.

Handy RD, Henry TB, Scown TM, Johnston BD and Tyler CR 2008b. Manufactured nanoparticles: their uptake and effects on fish-a mechanistic analysis. *Ecotoxicology,* 17**,** 396-409.

Handy RD, Musonda MM, Phillips C and Falla SJ 2000. Mechanisms of gastrointestinal copper absorption in the African walking catfish: copper dose-effects and a novel anion-dependent pathway in the intestine. *Experimental Biology,* 203**,** 2365-2377.

Handy RD, Runnalls T and Russell PM 2002b. Histopathologic biomarkers in three spined sticklebacks, *Gasterosteus aculeatus*, from several rivers in Southern England that meet the freshwater fisheries directive. *Ecotoxicology,* 11**,** 467-479.

Handy RD and Shaw BJ 2007. Toxic effects of nanoparticles and nanomaterials: Implications for public health, risk assessment and the public perception of nanotechnology. *Health, Risk and Society,* 9**,** 125-144.

Handy RD, van den Brink N, Chappell M, Mühling M, Behra R, Dušinská M, Simpson P,Ahtiainen J, Jha AN, Seiter J, Bednar A, Kennedy A, Fernandes TF and Riediker M 2012. Practical considerations for conducting ecotoxicity test methods with manufactured nanomaterials: What have we learnt so far? *Ecotoxicology,* 21: 933-72.

Hansen S, Michelson E, Kamper A, Borling P, Stuer-Lauridsen F and Baun A 2008. Categorization framework to aid exposure assessment of nanomaterials in consumer products. *Ecotoxicology,* 17**,** 438-447.

Hansen SF, Larsen BH, Olsen SI and Baun A 2007. Categorization framework to aid hazard identification of nanomaterials. *Nanotoxicology,* 1**,** 243-250.

Hao L, Wang Z and Xing B 2009. Effect of sub-acute exposure to TiO_2 nanoparticles on oxidative stress and histopathological changes in Juvenile Carp (*Cyprinus carpio*). *Journal of Environmental Sciences,* 21**,** 1459-1466.

Hartmann NB, Legros S, Von Der Kammer F, Hofmann T and Baun A 2012. The potential of TiO_2 nanoparticles as carriers for cadmium uptake in *Lumbriculus variegatus* and *Daphnia magna*. *Aquatic Toxicology,* 118–119**,** 1-8.

Hauri HP, Sterchi EE, Bienz D, Fransen JA and Marxer A 1985. Expression and intracellular transport of microvillus membrane hydrolases in human intestinal epithelial cells. *The Journal of Cell Biology,* 101**,** 838-851.

Heinrich U, Fuhst R, Rittinghausen S, Creutzenberg O, Bellmann B, Koch W and Levsen K 1995. Chronic inhalation exposure of wistar rats and 2 different strains of mice to diesel-engine exhaust, carbon-black, and titanium-dioxide. *Inhalation Toxicology,* 7**,** 533-556.

Hille S 1982. A literature review of the blood chemistry of rainbow trout. . *Journal of Fish Biology,* 20**,** 535-569.

Hoet P, Bruske-Hohlfeld I and Salata O 2004. Nanoparticles - known and unknown health risks. *Journal of Nanobiotechnology,* 2**,** 12.

Hoyle I and Handy RD 2005. Dose-dependent inorganic mercury absorption by isolated perfused intestine of rainbow trout, *Oncorhynchus mykiss*, involves both amiloride-sensitive and energy-dependent pathways. *Aquatic Toxicology,* 72**,** 147-159.

Hu CW, Li M, Cui YB, Li DS, Chen J and Yang LY 2010. Toxicological effects of TiO_2 and ZnO nanoparticles in soil on earthworm *Eisenia fetida*. *Soil Biology and Biochemistry,* 42**,** 586-591.

Hu R, Gong X, Duan Y, Li N, Che Y, Cui Y, Zhou M, Liu C, Wang H and Hong F 2010. Neurotoxicological effects and the impairment of spatial recognition memory in mice caused by exposure to TiO_2 nanoparticles. *Biomaterials,* 31**,** 8043-8050.

Hund-Rinke K and Simon M 2006. Ecotoxic effect of photocatalytic active nanoparticles (TiO_2) on Algae and Daphnids. *Environmental Science and Pollution Research,* 13**,** 225-232.

Hussain SM, Javorina AK, Schrand AM, Duhart HM, Ali SF and Schlager JJ 2006. The interaction of manganese nanoparticles with PC-12 cells induces dopamine depletion. *Toxicological Sciences,* 92**,** 456-463.

Iavicoli I, Leso L, Fontana L and Bergamaschi A 2011. Toxicological effects of titanium dioxide nanoparticles: a review of *in vitro* mammalian studies. *European review for medical and pharmacological sciences,* 15**,** 481-508.

Iversen T-G, Skotland T and Sandvig K 2011. Endocytosis and intracellular transport of nanoparticles: Present knowledge and need for future studies. *Nano Today,* 6**,** 176-185.

Jahanbakhshi A, Shaluei F and Hedayati A 2012. Detection of silver nanoparticles (Nanosil®) LC_{50} in silver carp (*Hypophthalmichthys molitrix*) and goldfish (*Carassius auratus*). *World Journal of Zoology,* 7**,** 126-130.

Jani P, Halbert GW, Langridge J and Florence AT 1990. Nanoparticle uptake by the rat gastrointestinal mucosa: quantitation and particle size dependency. *Journal of Pharmacy and Pharmacology,* 42**,** 821-826.

Jani PU, McCarthy DE and Florence AT 1994. Titanium dioxide (rutile) particle uptake from the rat GI tract and translocation to systemic organs after oral administration. *International Journal of Pharmaceutics* 105:157-168.

Jemec A, Drobne D, Remškar M, Sepčić K and Tišler T 2008. Effects of ingested nano-sized titanium dioxide on terrestrial isopods (*Porcellio scaber*). *Environmental Toxicology and Chemistry,* 27**,** 1904-1914.

Jesse MJ, Shub C and Fishman AP 1967. Lung and gill ventilation of the African lung fish. *Respiration Physiology,* 3**,** 267-287.

Johannes L and Lamaze C 2002. Clathrin-dependent or not: is it still the question? *Traffic,* 3, 443-51.

Johnston BD, Scown TM, Moger J, Cumberland SA, Baalousha M, Linge K, Van Aerle R, Jarvis K, Lead JR and Tyler CR 2010. Bioavailability of nanoscale metal oxides TiO_2, CeO_2, and ZnO to fish. *Environmental Science and Technology,* 44**,** 1144-1151.

Jortner J and Rao CN 2002. Nanostructured advanced materials.Perspectives and directions. *Pure and Applied Chemistry,* 74**,** 1491-1506.

Kahru A, Dubourguier H-C, Blinova I, Ivask A and Kasemets K 2008. Biotests and biosensors for ecotoxicology of metal oxide nanoparticles: A minireview. *Sensors,* 8**,** 5153-5170.

Kamunde CN, Pyle GG, Mcdonald DG and Wood CM 2003. Influence of dietary sodium on waterborne copper toxicity in rainbow trout, *Oncorhynchus mykiss*. *Environmental Toxicology and Chemistry,* 22**,** 342-350.

Katsikari A, Patronidou C, Kiparissides C and Arsenakis M 2009. Uptake and cytotoxicity of poly(D,L-lactide-*co*-glycolide) nanoparticles in human colon adenocarcinoma cells. *Materials Science and Engineering: B,* 165**,** 160-164.

Khairallah M, Labarthe F, Bouchard B, Danialou G, Petrof BJ and Des Rosiers C 2004. Profiling substrate fluxes in the isolated working mouse heart using ^{13}C-labeled substrates: focusing on the origin and fate of pyruvate and citrate carbons. *American Journal of Physiology - Heart and Circulatory Physiology,* 286**,** H1461-H1470.

Keller AA, Wang H, Zhou D, Lenihan HS, Cherr G, Cardinale BJ, Miller R and Ji Z 2010. Stability and aggregation of metal oxide nanoparticles in natural aqueous matrices. *Environmental Science and Technology,* 44**,** 1962-1967.

Koeneman B, Zhang Y, Westerhoff P, Chen Y, Crittenden J and Capco D 2010. Toxicity and cellular responses of intestinal cells exposed to titanium dioxide. *Cell Biology and Toxicology,* 26**,** 225-238.

Koeneman BA, Zhang Y, Hristovski K, Westerhoff P, Chen Y, Crittenden JC and Capco DG 2009. Experimental approach for an *in vitro* toxicity assay with non-aggregated quantum dots. *Toxicology in Vitro,* 23**,** 955-962.

Komatsu T, Tabata M, Kubo-Irie M, Shimizu T, Suzuki K-I, Nihei Y and Takeda K 2008. The effects of nanoparticles on mouse testis Leydig cells *in vitro*. *Toxicology in Vitro,* 22**,** 1825-1831.

Kreyling WG, Semmler M, Erbe F, Mayer P, Takenaka S and Schulz H 2002. Translocation of ultrafine insoluble iridium particles from lung epithelium to extrapulmonary organs is size dependent but very low. *Journal of Toxicology and Environmental Health Part A,* 65**,** 1513 - 1530.

Krischok S, Höfft O and Kempter V 2002. The chemisorption of H_2O and CO_2 on TiO_2 surfaces: studies with MIES and UPS (HeI/II). *Surface Science,* 507-510**,** 69-73.

Lam C-W, James JT, Mccluskey R, Arepalli S and Hunter RL 2006. A review of carbon nanotube toxicity and assessment of potential occupational and environmental health risks. *Critical Reviews in Toxicology,* 36**,** 189-217.

Lam CW, James JT, Mccluskey R and Hunter RL 2004. Pulmonary toxicity of single-wall carbon nanotubes in mice 7 and 90 days after intratracheal instillation. *Toxicological Sciences,* 77**,** 126-134.

Landsiedel R, Ma-Hock L, Kroll A, Hahn D, Schnekenburger J, Wiench K and Wohlleben W 2010. Testing metal-oxide nanomaterials for human safety. *Advanced Materials,* 22**,** 2601-2627.

Lapied E, Nahmani JY, Moudilou E, Chaurand P, Labille J, Rose J, Exbrayat J-M, Oughton DH and Joner EJ 2011. Ecotoxicological effects of an aged TiO_2 nanocomposite measured as apoptosis in the anecic earthworm Lumbricus terrestris after exposure through water, food and soil. *Environment International,* 37**,** 1105-1110.

Laporte J-M, Andres S and Mason RP 2002. Effect of ligands and other metals on the uptake of mercury and methylmercury across the gills and the intestine of the blue crab (*Callinectes sapidus*). *Comparative Biochemistry and Physiology Part C: Toxicology and Pharmacology,* 131**,** 185-196.

Lead JR and Wilkinson KJ 2006. Aquatic colloids and nanoparticles: Current knowledge and future trends. *Environmental chemistry,* 3**,** 159-171.

Leaner JJ and Mason RP 2002. Methylmercury accumulation and fluxes across the intestine of channel catfish, Ictalurus punctatus. *Comparative Biochemistry and Physiology Part C: Toxicology and Pharmacology,* 132**,** 247-259.

Lee W-M, Kwak JI and An Y-J 2012. Effect of silver nanoparticles in crop plants *Phaseolus radiatus* and *Sorghum bicolor*: Media effect on phytotoxicity. *Chemosphere,* 86**,** 491-499.

Lewis S, Eaton D, Clausen C and Diamond J 1977. Nystatin as a probe for investigating the electrical properties of a tight epithelium. *The Journal of General Physiology,* 70**,** 427-40.

Li LZ, Zhou DM, Peijnenburg WJ, Gestel CA, Jin SY, Wang YJ and Wang P 2011. Toxicity of zinc oxide nanoparticles in the earthworm, *Eisenia fetida* and subcellular fractionation of Zn. *Environmental International,* 37**,** 1098-1104.

Linsebigler AL, Lu G and Yates JT 1995. Photocatalysis on TiO_2 surfaces: Principles, mechanisms, and selected results. *Chemical Reviews,* 95**,** 735-758.

Long TC, Saleh N, Tilton RD, Lowry GV and Veronesi B 2006. Titanium dioxide (P25) produces reactive oxygen species in immortalized brain microglia (BV2): implications for nanoparticle neurotoxicity. *Environmental Science and Technology,* 40**,** 4346-4352.

Lomer MCE, Thompson RPH, Commisso J, Keen CL and Powell JJ. 2000. Determination of titanium dioxide in foods using inductively coupled plasma optical emission spectrometry. *Royal Society of Chemistry*, 125:2339 - 2343.

Lott JA and Nemensanszky E 1987. Lactate dehydrogenase. *In*: Lott JA, Wolf PL, (eds). *Clinical enzymology, a case-oriented approach.* pp. 213–244.

Lovern SB and Klaper R 2006. *Daphnia magna* mortality when exposed to titanium dioxide and fullerene (C-60) nanoparticles. *Environmental Toxicology and Chemistry,* 25**,** 1132-1137.

Lovern SB, Strickler JR and Klaper R 2007. Behavioral and physiological changes in *Daphnia magna* when exposed to nanoparticle suspensions (titanium dioxide, nano-C_{60}, and $C_{60}HxC_{70}Hx$). *Environmental Science and Technology,* 41**,** 4465-4470.

Lövestam G, Rauscher H, Roebben G, Klüttgen BS, Gibson N, Putaud J-P and Stamm H 2010. Considerations on a definition of nanomaterial for regulatory purposes. JRC Reference Report, EUR 24403 EN.

Lyon DY, Fortner JD, Sayes CM, Colvin VL and Hughes JB 2005. Bacterial cell association and antimicrobial activity of a C-60 water suspension. *Environmental Toxicology and Chemistry,* 24**,** 2757-2762.

Macwan D, Dave P and Chaturvedi S 2011. A review on nano-TiO_2 sol–gel type syntheses and its applications. *Journal of Materials Science,* 46**,** 3669-3686.

Mamun SM, Focken U and Becker K 2007. Comparative digestion efficiencies in conventional, genetically improved and genetically male Nile tilapia, *Oreochromis niloticus* (L.). *Aquaculture Research,* 38**,** 381-387.

Masciangioli T and Zhang WX 2003. Environmental technologies at the nanoscale. *Environmental Science and Technology*, 37**,** 102A-108A.

Mcclean S, Prosser E, Meehan E, O'malley D, Clarke N, Ramtoola Z and Brayden D 1998. Binding and uptake of biodegradable poly-dl-lactide micro- and nanoparticles in intestinal epithelia. *European Journal of Pharmaceutical Sciences,* 6**,** 153-163.

Milligan CL and Farrell AP 1991. Lactate utilization by an *in situ* perfused trout heart: effects of workload and blockers of lactate transport. *Journal of Experimental Biology,* 155**,** 357-373.

Miquel-Jeanjean C, Crépel F, Raufast V, Payre B, Datas L, Bessou-Touya S and Duplan H 2012. Penetration study of formulated nanosized titanium dioxide in models of damaged and sun-irradiated skins. *Photochemistry and Photobiology* doi: 10.1111/j.1751-1097.2012.01181.x

Moore MN 2006. Do nanoparticles present ecotoxicological risks for the health of the aquatic environment? *Environment International,* 32**,** 967-976.

Moss DW and Henderson AR 1986. Enzymes. *In*: Burtis CA, Ashwood ER, (eds). *Tietz textbook of clinical chemistry.* 2nd edition. Philadelphia, Saunders Co. pp. 735–896.

Nabi IR and Phuong UL 2003. Caveolae/ raft-dependent endocytosis. *The Journal of Cell Biology*, 161 (4), 4.

Nel A, Xia T, Mädler L and Li N 2006. Toxic potential of materials at the nanolevel. *Science,* 311**,** 622-627.

Nemmar A, Vanbilloen H, Hoylaerts MF, Hoet PHM, Verbruggen A and Nemery B 2001. Passage of intratracheally instilled ultrafine particles from the lung into the systemic circulation in hamster. *American Journal of Respiratory and Critical Care Medicine,* 164**,** 1665-1668.

Oberdörster E 2004. Manufactured nanomaterials (Fullerenes, C-60) induce oxidative stress in the brain of juvenile largemouth bass. *Environmental health perspectives,* 112**,** 1058-1062.

Oberdörster E, Zhu S, Blickley TM, Mcclellan-Green P and Haasch ML 2006. Ecotoxicology of carbon-based engineered nanoparticles: Effects of fullerene (C60) on aquatic organisms. *Carbon,* 44**,** 1112-1120.

Oberdörster G 2000. Toxicology of ultrafine particles: *in vivo* studies. *Philosophical Transactions of the Royal Society A: Mathematical, Physical and Engineering Sciences,* 358**,** 2719-2740.

Oberdörster G, Ferin J, Gelein R, Soderholm SC and Finkelstein J 1992. Role of the alveolar macrophage in lung injury-studies with ultrafine particles. *Environmental health perspectives,* 97**,** 193-199.

Oberdörster G, Maynard A, Donaldson K, Castranova V, Fitzpatrick J, Ausman K, Carter J, Karn B, Kreyling W, Lai D, Olin S, Monteiro-Riviere N, Warheit D and Yang H 2005a. Principles for characterizing the potential human health effects from exposure to nanomaterials: elements of a screening strategy. *Particle and Fibre Toxicology,* 2**,** 8.

Oberdörster G, Oberdörster E and Oberdörster J 2005b. Nanotoxicology: an emerging discipline evolving from studies of ultrafine particles. *Environmental health perspectives,* 113**,** 823 - 839.

Oberdörster G, Oberdörster E and Oberdörster J 2007. Concepts of nanoparticle dose metric and response metric. *Environmental health perspectives,* 115**,** A290-A290.

Ödblom MP and Handy RD 1999. A novel DIDS-sensitive, anion-dependent Mg^{2+} efflux pathway in rat ventricular myocytes. *Biochemical and Biophysical Research Communications,* 264**,** 334-337.

Olmedo DG, Tasat DR, Guglielmotti MB and Cabrini RL 2005. Effect of titanium dioxide on the oxidative metabolism of alveolar macrophages: An experimental study in rats. *Journal of Biomedical Materials Research Part A,* 73A**,** 142-149.

Panariti A, Miserocchi G and Rivolta I 2012. The effect of nanoparticle uptake on cellular behavior: disrupting or enabling functions? *Nanotechnology, Science and Applications,* 5**,** 87-100.

Panessa-Warren BJ, Warren JB, Wong SS and Misewich JA 2006. Biological cellular response to carbon nanoparticle toxicity. *Journal of Physics-Condensed Matter,* 18**,** S2185-S2201.

Park E-J, Yi J, Chung K-H, Ryu D-Y, Choi J and Park K 2008. Oxidative stress and apoptosis induced by titanium dioxide nanoparticles in cultured BEAS-2B cells. *Toxicology Letters,* 180**,** 222-229.

Patel AP, Moody AJ, Sneyd JR and Handy RD 2004. Carbon monoxide exposure in rat heart: evidence for two modes of toxicity. *Biochemical and Biophysical Research Communications,* 321**,** 241-246.

Payan P and Matty AJ 1975. The characteristics of ammonia excretion by a perfused isolated head of trout (*Salmo gairdneri*): Effect of temperature and CO_2-free ringer. *Journal of Comparative Physiology B: Biochemical, Systemic, and Environmental Physiology,* 96**,** 167-184.

Pelletier DA, Suresh AK, Holton GA, Mckeown CK, Wang W, Gu B, Mortensen NP, Allison DP, Joy DC, Allison MR, Brown SD, Phelps TJ and Doktycz MJ 2010. Effects of Engineered Cerium Oxide Nanoparticles on Bacterial Growth and Viability. *Applied and Environmental Microbiology,* 76**,** 7981-7989.

Perry SF, Davie PS, Daxboeck C, Ellis AG and Smith DG 1984. Perfused methods for the study of gill physiology. *Fish Physiology,* 10**,** 325-388.

Perry SF, Payan P and Girard JP 1983. Adrenergic control of branchial chloride transport in the isolated perfused head of the fresh-water trout (Salmo-gairdneri). *Journal of Comparative Physiology,* 154**,** 269-274.

Pineda L, Sawosz E, Hotowy A, Elnif J, Sawosz F, Ali A and Chwalibog A 2012. Effect of nanoparticles of silver and gold on metabolic rate and development of broiler and layer embryos. *Comparative Biochemistry and Physiology - Part A: Molecular and Integrative Physiology,* 161**,** 315-319.

Plummer DT 1971. An introduction to practical biochemistry. *McGraw Hill*, London, pp. 288–289.

Powell JJ, Faria N, Thomas-Mckay E and Pele LC 2010. Origin and fate of dietary nanoparticles and microparticles in the gastrointestinal tract. *Journal of Autoimmunity,* 34**,** J226-J233.

Rae TD, Schmidt PJ, Pufahl RA, Culotta VC and V. O'halloran T 1999. Undetectable intracellular free copper: the requirement of a copper chaperone for superoxide dismutase. *Science,* 284**,** 805-808.

Ragnarsson EGE, Schoultz I, Gullberg E, Carlsson AH, Tafazoli F, Lerm M, Magnusson K-E, Soderholm JD and Artursson P 2008. Yersinia pseudotuberculosis induces transcytosis of nanoparticles across human intestinal villus epithelium via invasin-dependent macropinocytosis. *Laboratory Investigation,* 88**,** 1215-1226.

Rahman Q, Lohani M, Dopp E, Pemsel H, Jonas L, Weiss DG and Schiffmann D 2002. Evidence that ultrafine titanium dioxide induces micronuclei and apoptosis in syrian hamster embryo fibroblasts. *Environmental Health Perspectives,* 110**,** 797–800.

Ramsden C, Smith T, Shaw B and Handy R 2009. Dietary exposure to titanium dioxide nanoparticles in rainbow trout, (*Oncorhynchus mykiss*): no effect on growth, but subtle biochemical disturbances in the brain. *Ecotoxicology,* 18**,** 939-951.

Rao CN 2004. New developments in nanomaterials. *Journal of materials chemistry,* 14**,** E4-E4.

Rehn B, Seiler F, Rehn S, Bruch J and Maier M 2003. Investigations on the inflammatory and genotoxic lung effects of two types of titanium dioxide: untreated and surface treated. *Toxicology and Applied Pharmacology,* 189**,** 84-95.

Reeves PG, Briske-Anderson M and Johnson L 1998. Physiologic concentrations of zinc affect the kinetics of copper uptake and transport in the human intestinal cell model, Caco-2. *The Journal of Nutrition,* 128**,** 1794-1801.

Rice WJ, Young HS, Martin DW, Sachs JR and Stokes DL 2001. Structure of Na^+,K^+-ATPase at 11-Å resolution: comparison with Ca^{2+}-ATPase in E_1 and E_2 states. *Biophysical Journal,* 80**,** 2187-2197.

Ridley AJ 2001. Rho Proteins: Linking Signaling with Membrane Trafficking. *Traffic,* 2**,** 303-310.

Roberts AP, Mount AS, Seda B, Souther J, Qiao R, Lin S, Ke PC, Rao AM and Klaine SJ 2007. *In vivo* biomodification of lipid-coated carbon nanotubes by *Daphnia magna*. *Environmental Science and Technology,* 41**,** 3025-3029.

Robinson RA and Stokes RH 1968. Electrolyte Solutions. *Butterworths***,** p 463.

Roco MC 2003. Nanotechnology: convergence with modern biology and medicine. *Current opinion in biotechnology,* 14**,** 337-346.

Rodal SK, Skretting G, Garred Ø, Vilhardt F, Van Deurs B and Sandvig K 1999. Extraction of cholesterol with methyl-β-cyclodextrin perturbs formation of clathrin-coated endocytic vesicles. *Molecular Biology of the Cell,* 10**,** 961-974.

Romani AMP 2011. Cellular magnesium homeostasis. *Archives of Biochemistry and Biophysics,* 512**,** 1-23.

Roszak J, Stępnik M, Nocuń M, Ferlińska M, Smok-Pieniążek A, Grobelny J, Tomaszewska E, Wąsowicz W and Cieślak M 2013. A strategy for *in vitro* safety testing of nanotitania-modified textile products. *Journal of Hazardous Materials,* 256–257**,** 67-75.

Rothen-Rutishauser BM, Schurch S, Haenni B, Kapp N and Gehr P 2006. Interaction of fine particles and nanoparticles with red blood cells visualized with advanced microscopic techniques. *Environmental Science and Technology,* 40**,** 4353-4359.

Rouse JG, Yang J, Ryman-Rasmussen JP, Barron AR and Monteiro-Riviere NA 2006. Effects of Mechanical Flexion on the Penetration of Fullerene Amino Acid-Derivatized Peptide Nanoparticles through Skin. *Nano Letters,* 7**,** 155-160.

Ryabchikova IE, Mazurkova AN, Shikina VN and Ismagilov RZ 2010. The crystalline forms of titanium dioxide nanoparticles affect their interactions with individual cells. *Journal of medical chemical, biological, and radiological defence,* 8**,** 18.

Salaun C, James DJ and Chamberlain LH 2004. Lipid rafts and the regulation of eocytosis. *Traffic,* 5, 255- 264.

Sanders K, Degn LL, Mundy WR, Zucker RM, Dreher K, Zhao B, Roberts JE and Boyes WK 2012. *In vitro* phototoxicity and hazard identification of nano-scale titanium dioxide. *Toxicology and Applied Pharmacology,* 258**,** 226-236.

Sang Yoo H and Gwan Park T 2004. Biodegradable nanoparticles containing protein-fatty acid complexes for oral delivery of salmon calcitonin. *Journal of Pharmaceutical Sciences,* 93**,** 488-495.

Sato Y, Yokoyama A, Shibata K, Akimoto Y, Ogino S, Nodasaka Y, Kohgo T, Tamura K and Akasaka T 2005. Influence of length on cytotoxicity of multi-walled carbon nanotubes against human acute monocyte leukemia cell line THP-1 *in vitro* and subcutaneous tissue of rats *in vivo*. *Molecular Biosystems,* 1**,** 176-182.

Sawosz E, Binek M, Grodzik M, Zielińska M, Sysa P, Szmidt M, Niemiec T and Chwalibog A 2007. Influence of hydrocolloidal silver nanoparticles on gastrointestinal microflora and morphology of enterocytes of quails. *Archives of Animal Nutrition,* 61**,** 444-451.

Sayes CM, Wahi R, Kurian PA, Liu YP, West JL, Ausman KD, Warheit DB and Colvin VL 2006. Correlating nanoscale titania structure with toxicity: A cytotoxicity and inflammatory response study with human dermal fibroblasts and human lung epithelial cells. *Toxicological Sciences,* 92**,** 174-185.

SCENIHR. 2007. Opinion on the appropriateness of the risk assessment 1333 methodology in accordance with the technical guidance documents for new and existing substances for assessing the risk of nanomaterials. *Scientific Committee*

on Emerging and Newly Identified Health Risks (SCENIHR), European Commission.

Schaeublin NM, Braydich-Stolle LK, Schrand AM, Miller JM, Hutchison J, Schlager JJ and Hussain SM 2011. Surface charge of gold nanoparticles mediates mechanism of toxicity. *Nanoscale,* 3**,** 410-420.

Scherbart AM, Langer J, Bushmelev A, Van Berlo D, Haberzettl P, Van Schooten F-J, Schmidt AM, Rose CR, Schins R and Albrecht C 2011. Contrasting macrophage activation by fine and ultrafine titanium dioxide particles is associated with different uptake mechanisms. *Part Fibre Toxicol,* 8**,** 31.

Schmidt J and Vogelsberger W 2009. Aqueous Long-Term Solubility of Titania Nanoparticles and Titanium(IV) Hydrolysis in a Sodium Chloride System Studied by Adsorptive Stripping Voltammetry. *Journal of Solution Chemistry,* 38**,** 1267-1282.

Scown TM, Santos EM, Johnston BD, Gaiser B, Baalousha M, Mitov S, Lead JR, Stone V, Fernandes TF, Jepson M, Van Aerle R and Tyler CR 2010. Effects of Aqueous Exposure to Silver Nanoparticles of Different Sizes in Rainbow Trout. *Toxicological Sciences,* 115**,** 521-534.

Semis R, Nili SS, Munitz A, Zaslavsky Z, Polacheck I and Segal E 2012. Pharmacokinetics, tissue distribution and immunomodulatory effect of intralipid formulation of nystatin in mice. *Journal of Antimicrobial Chemotherapy,* 67**,** 1716-1721.

Shaw BJ, Al-Bairuty G and Handy RD 2012. Effects of waterborne copper nanoparticles and copper sulphate on rainbow trout, (*Oncorhynchus mykiss*): Physiology and accumulation. *Aquatic Toxicology,* 116–117**,** 90-101.

Shaw BJ and Handy RD 2011. Physiological effects of nanoparticles on fish: A comparison of nanometals versus metal ions. *Environment International,* 37**,** 1083-1097.

Shi J, Chen J, Feng Z, Chen T, Lian Y, Wang X and Li C 2007. Photoluminescence characteristics of TiO_2 and their relationship to the photoassisted reaction of water/methanol mixture. *The Journal of Physical Chemistry C,* 111**,** 693-699.

Shi Y, Wang F, He J, Yadav S and Wang H 2010. Titanium dioxide nanoparticles cause apoptosis in BEAS-2B cells through the caspase 8/t-Bid-independent mitochondrial pathway. *Toxicology Letters,* 196**,** 21-27.

Shukla RK, Sharma V, Pandey AK, Singh S, Sultana S and Dhawan A 2011. ROS-mediated genotoxicity induced by titanium dioxide nanoparticles in human epidermal cells. *Toxicology in Vitro,* 25**,** 231-241.

Shvedova AA, Castranova V, Kisin ER, Schwegler-Berry D, Murray AR, Gandelsman VZ, Maynard A and Baron P 2003. Exposure to carbon nanotube material: Assessment of nanotube cytotoxicity using human keratinocyte cells. *Journal of Toxicology and Environmental Health-Part A,* 66**,** 1909-1926.

Simon M, Barberet P, Delville M-H, Moretto P and Seznec H 2011. Titanium dioxide nanoparticles induced intracellular calcium homeostasis modification in primary human keratinocytes. Towards an *in vitro* explanation of titanium dioxide nanoparticles toxicity. *Nanotoxicology,* 5**,** 125-139.

Smith CJ, Shaw BJ and Handy RD 2007. Toxicity of single walled carbon nanotubes to rainbow trout, (*Oncorhynchus mykiss*): Respiratory toxicity, organ pathologies, and other physiological effects. *Aquatic Toxicology,* 82**,** 94-109.

Song Y, Li X and Du X 2009. Exposure to nanoparticles is related to pleural effusion, pulmonary fibrosis and granuloma. *European Respiratory Journal,* 34**,** 559-567.

Stokes DL and Lacapère JJ 1994. Conformation of Ca^{2+}-ATPase in two crystal forms: effects of Ca^{2+}, thapsigargin, adenosine 5'-(β,γ-methy1ene)triphosphate, and chromium(1II)-ATP on crystallization. *Journal of Biological Chemistry,* 269, 11606 –11613**.**

Stone V, Nowack B, Baun A, Van Den Brink N, Von Der Kammer F, Dusinska M, Handy R, Hankin S, Hassellöv M, Joner E and Fernandes TF 2010. Nanomaterials for environmental studies: Classification, reference material issues, and strategies for physico-chemical characterisation. *Science of The Total Environment,* 408**,** 1745-1754.

Strubelt O 1996. Comparative studies on the toxicity of mercury, cadmium, and copper toward the isolated perfused rat liver. *Journal of Toxicology and Environmental Health,* 47**,** 267-283.

Sun H, Zhang X, Niu Q, Chen Y and Crittenden J 2007. Enhanced accumulation of arsenate in carp in the presence of titanium dioxide nanoparticles. *Water, Air, and Soil Pollution,* 178**,** 245-254.

Sun H, Zhang X, Zhang Z, Chen Y and Crittenden JC 2009. Influence of titanium dioxide nanoparticles on speciation and bioavailability of arsenite. *Environmental Pollution,* 157**,** 1165-1170.

Thevenot P, Cho J, Wavhal D, Timmons RB and Tang L 2008. Surface chemistry influences cancer killing effect of TiO2 nanoparticles. *Nanomedicine: Nanotechnology, Biology and Medicine,* 4**,** 226-236.

Thurn K, Brown E, Wu A, Vogt S, Lai B, Maser J, Paunesku T and Woloschak G 2007. Nanoparticles for Applications in Cellular Imaging. *Nanoscale Research Letters,* 2**,** 430 - 441.

Thurn KT, Arora H, Paunesku T, Wu A, Brown EMB, Doty C, Kremer J and Woloschak G 2011. Endocytosis of titanium dioxide nanoparticles in prostate cancer PC-3M cells. *Nanomedicine: Nanotechnology, Biology and Medicine,* 7**,** 123-130.

Tiede K, Boxall ABA, Tear SP, Lewis J, David H and Hassellöv M 2008. Detection and characterization of engineered nanoparticles in food and the environment. *Food Additives and Contaminants: Part A,* 25**,** 795-821.

Torrubia JOA and Garay R 1989. Evidence for a major route for zinc uptake in human red blood cells: [ZN(HCO3)2CL]−influx through the [CI−/HCO3−] anion exchanger. *Journal of Cellular Physiology,* 138**,** 316-322.

Trouiller B, Reliene R, Westbrook A, Solaimani P and Schiestl RH 2009. Titanium dioxide nanoparticles induce DNA damage and genetic instability *In vivo* in mice. *Cancer Research,* 69**,** 8784-8789.

Uchino T, Tokunaga H, Ando M and Utsumi H 2002. Quantitative determination of OH radical generation and its cytotoxicity induced by TiO_2-UVA treatment. *Toxicology in Vitro,* 16**,** 629-635.

Van Den Berg M, De Jongh J, Poiger H and Olson JR 1994. The toxicokinetics and metabolism of polychlorinated dibenzo-p-dioxins (PCDDs) and dibenzofurans (PCDFs) and their relevance for toxicity. *Critical Reviews in Toxicology,* 24**,** 1-74.

Von Der Kammer F, Ferguson PL, Holden PA, Masion A, Rogers KR, Klaine SJ, Koelmans AA, Horne N and Unrine JM 2012. Analysis of engineered nanomaterials in complex matrices (environment and biota): General considerations and conceptual case studies. *Environmental Toxicology and Chemistry,* 31**,** 32-49.

Van Der Velden JA, Groot JA, Flik G, Polak P and Kolar ZI 1990. Short communication: magnesium transport in fish intestine. *Experimental Biology,* 152**,** 587-592.

Verwey EJW and Overbeek JTG 1948. Theory of the stability of lyophobic colloids: the interaction of sol particles having an electric double layer. New York: Elsevier.

Vevers W and Jha AN 2008. Genotoxic and cytotoxic potential of titanium dioxide (TiO_2) nanoparticles on fish cells *in vitro*. *Ecotoxicology,* 17**,** 410-420.

Wang B, Feng WY, Wang TC, Guang J, Wang M, Shi JW, Zhang F, Zhao YL and Chai ZF 2006. Acute toxicity of nano- and micro-scale zinc powder in healthy adult mice. *Toxicology Letters,* 161**,** 115-123.

Wang H, Kou X, Pei Z, Xiao JQ, Shan X and Xing B 2011. Physiological effects of magnetite (Fe3O4) nanoparticles on perennial ryegrass (Lolium perenne L.) and pumpkin (Cucurbita mixta) plants. *Nanotoxicology,* 5**,** 30-42.

Wang H, Wick RL and Xing B 2009. Toxicity of nanoparticulate and bulk ZnO, Al_2O_3 and TiO_2 to the nematode Caenorhabditis elegans. *Environmental Pollution,* 157**,** 1171-1177.

Wang J, Liu Y, Jiao F, Lao F, Li W, Gu Y, Li Y, Ge C, Zhou G, Li B,Zhao Y, Chai Z and Chen C 2008. Time-dependent translocation and potential impairment on central nervous system by intranasally instilled TiO_2 nanoparticles. *Toxicology,* 254**,** 82-90.

Wang JX, Zhou GQ, Chen CY, Yu HW, Wang TC, Ma YM, Jia G, Gao YX, Li B, Sun J, Li YF, Jiao F, Zhao YL and Chai ZF 2007. Acute toxicity and biodistribution

of different sized titanium dioxide particles in mice after oral administration. *Toxicology Letters,* 168**,** 176-185.

Wapnir RA 1991. Copper-sodium linkage during intestinal absorption: inhibition by amiloride. *Proceedings of the Society for Experimental Biology and Medicine,* 196**,** 410-414.

Wapnir RA and Lee SY 1993. Dietary regulation of copper absorption and storage in rats: effects of sodium, zinc and histidine-zinc. *Journal of the American College of Nutrition,* 12**,** 714-719.

Warheit DB, Hoke RA, Finlay C, Donner EM, Reed KL and Sayes CM 2007a. Development of a base set of toxicity tests using ultrafine TiO_2 particles as a component of nanoparticle risk management. *Toxicology Letters,* 171**,** 99-110.

Warheit DB, Laurence BR, Reed KL, Roach DH, Reynolds GaM and Webb TR 2004. Comparative pulmonary toxicity assessment of single-wall carbon nanotubes in rats. *Toxicological Sciences,* 77**,** 117-125.

Warheit DB, Webb TR, Reed KL, Frerichs S and Sayes CM 2007b. Pulmonary toxicity study in rats with three forms of ultrafine-TiO_2 particles: Differential responses related to surface properties. *Toxicology,* 230**,** 90-104.

Warheit DB, Webb TR, Sayes CM, Colvin VL and Reed KL 2006. Pulmonary instillation studies with nanoscale TiO_2 rods and dots in rats: toxicity is not dependent upon particle size and surface area. *Toxicological Sciences,* 91**,** 227-236.

Weir A, Westerhoff P, Fabricius L, Hristovski K and Von Goetz N 2012. Titanium Dioxide Nanoparticles in Food and Personal Care Products. *Environmental Science and Technology*.

Whihelm M, E. Jaeger D, Schüll-Cablitz H, Hafner D and Idel H 1996. Hepatic clearance and retention of aluminium: studies in the isolated perfused rat liver. *Toxicology Letters,* 89**,** 257-263.

Wu Y, Zhou Q, Li H, Liu W, Wang T and Jiang G 2010. Effects of silver nanoparticles on the development and histopathology biomarkers of Japanese medaka (Oryzias latipes) using the partial-life test. *Aquatic Toxicology,* 100**,** 160-167.

Xie G, Wang C, Sun J and Zhong G 2011. Tissue distribution and excretion of intravenously administered titanium dioxide nanoparticles. *Toxicology Letters,* 205**,** 55-61.

Xu ZP, Niebert M, Porazik K, Walker TL, Cooper HM, Middelberg APJ, Gray PP, Bartlett PF and Lu GQ 2008. Subcellular compartment targeting of layered double hydroxide nanoparticles. *Journal of Controlled Release,* 130**,** 86-94.

Yah CS, Simate GS and Iyuke SE 2012. Nanoparticles toxicity and their routes of exposures. *Pakistan Journal of Pharmaceutical Sciences,* 25**,** 477-491.

Yamamoto H-A 1989. Hyperammonemia, increased brain neutral and aromatic amino acid levels, and encephalopathy induced by cyanide in mice. *Toxicology and Applied Pharmacology,* 99**,** 415-420.

Yang F, Hong FS, You WJ, Liu C, Gao FQ, Wu C and Yang P 2006. Influences of nano-anatase TiO_2 on the nitrogen metabolism of growing spinach. *Biological Trace Element Research,* 110**,** 179-190.

Yang L and Watts DJ 2005. Particle surface characteristics may play an important role in phytotoxicity of alumina nanoparticles. *Toxicology Letters,* 158**,** 122-132.

Yokoyama A, Sato Y, Nodasaka Y, Yamamoto S, Kawasaki T, Shindoh M, Kohgo T, Akasaka T, Uo M, Watari F and Tohji K 2005. Biological behavior of hat-stacked carbon nanofibers in the subcutaneous tissue in rats. *Nano letters,* 5**,** 157-161.

Yue ZG, Wei W, Lv PP, Yue H, Wang LY, Su ZG and Ma GH 2011. Surface Charge Affects Cellular Uptake and Intracellular Trafficking of Chitosan-Based Nanoparticles. *Biomacromolecules,* 12**,** 2440-2446.

Zerounian NR, Redekosky C, Malpe R and Linder MC 2003. Regulation of copper absorption by copper availability in the Caco-2 cell intestinal model. *American Journal of Physiology - Gastrointestinal and Liver Physiology,* 284**,** G739-G747.

Zhang R, Niu Y, Li Y, Zhao C, Song B, Li Y and Zhou Y 2010. Acute toxicity study of the interaction between titanium dioxide nanoparticles and lead acetate in mice. *Environmental Toxicology and Pharmacology,* 30**,** 52-60.

Zhang X, Sun H, Zhang Z, Niu Q, Chen Y and Crittenden J 2007. Enhanced bioaccumulation of cadmium in carp in the presence of titanium dioxide nanoparticles *Chemosphere,* 67**,** 160-166.

Zhang XQ, Yin LH, Tang M and Pu YP 2011. ZnO, TiO_2, SiO_2, and Al_2O_3 Nanoparticles-induced toxic effects on human fetal lung fibroblasts. *Biomedical and Environmental Sciences,* 24**,** 661-669.

Zheng L, Hong F, Lu S and Liu C 2005. Effect of Nano-TiO_2 on Strength of Naturally Aged Seeds and Growth of Spinach. *Biological Trace Element Research,* 104**,** 83-92.

Zhu X, Wang J, Zhang X, Chang Y and Chen Y 2010. Trophic transfer of TiO_2 nanoparticles from daphnia to zebrafish in a simplified freshwater food chain. *Chemosphere,* 79**,** 928-933.

Zhu Y, Zhao QF, Li YG, Cai XQ and Li W 2006. The interaction and toxicity of multi-walled carbon nanotubes with Stylonychia mytilus. *Journal of Nanoscience and Nanotechnology,* 6**,** 1357-1364.

Appendix I

Published Papers

Journal of Fish Biology (2011) **79**, 821–853
doi:10.1111/j.1095-8649.2011.03080.x, available online at wileyonlinelibrary.com

REVIEW PAPER

Effects of manufactured nanomaterials on fishes: a target organ and body systems physiology approach

R. D. Handy*†, G. Al-Bairuty*, A. Al-Jubory*, C. S. Ramsden*, D. Boyle*, B. J. Shaw* and T. B. Henry*‡

**School of Biomedical & Biological Sciences, University of Plymouth, Drake Circus, PL4 8AA Plymouth, U.K. and ‡Department of Forestry Wildlife and Fisheries, Center for Environmental Biotechnology, The University of Tennessee, Knoxville, TN 37996, U.S.A.*

(Received 11 October 2010, Accepted 6 July 2011)

Manufactured nanomaterials (NM) are already used in consumer products and exposure modelling predicts releases of ng to low μg l^{-1} levels of NMs into surface waters. The exposure of aquatic ecosystems, and therefore fishes, to manufactured NMs is inevitable. This review uses a physiological approach to describe the known effects of NMs on the body systems of fishes and to identify the internal target organs, as well as outline aspects of colloid chemistry relevant to fish biology. The acute toxicity data, suggest that the lethal concentration for many NMs is in the mg l^{-1} range, and a number of sublethal effects have been reported at concentrations from *c.* 100 μg to 1 mg l^{-1}. Exposure to NMs in the water column can cause respiratory toxicity involving altered ventilation, mucus secretion and gill pathology. This may not lead, however, to overt haematological disturbances in the short term. The internal target organs include the liver, spleen and haematopoietic system, kidney, gut and brain; with toxic effects involving oxidative stress, ionoregulatory disturbances and organ pathologies. Some pathology appears to be novel for NMs, such as vascular injury in the brain of rainbow trout *Oncorhynchus mykiss* with carbon nanotubes. A lack of analytical methods, however, has prevented the reporting of NM concentrations in fish tissues, and the precise uptake mechanisms across the gill or gut are yet to be elucidated. The few dietary exposure studies conducted show no effects on growth or food intake at 10–100 mg kg^{-1} inclusions of NMs in the diet of *O. mykiss*, but there are biochemical disturbances. Early life stages are sensitive to NMs with reports of lethal toxicity and developmental defects. There are many data gaps, however, including how water quality alters physiological responses, effects on immunity and chronic exposure data at environmentally relevant concentrations. Overall, the data so far suggest that the manufactured NMs are not as toxic as some traditional chemicals (*e.g.* some dissolved metals) and the innovative, responsible, development of nanotechnology should continue, with potential benefits for aquaculture, fisheries and fish health diagnostics.

Key words: behaviour; blood cells; cardiovascular system; gastrointestinal tract; nanoparticles; nervous system.

Nanotoxicology, 2012; Early Online, 1–20

ISSN: 1743-5390 print / 1743-5404 online
DOI: 10.3109/17435390.2012.735268

informa
healthcare

Uptake of titanium from TiO_2 nanoparticle exposure in the isolated perfused intestine of rainbow trout: nystatin, vanadate and novel CO_2-sensitive components

Aliaa R. Al-Jubory & Richard D. Handy

School of Biomedical and Biological Sciences, University of Plymouth, Drake Circus, Plymouth, PL4 8AA, UK

Abstract

Nanoparticle (NP) uptake across the gut is poorly understood. ***In vitro*** gut sac preparations and isolated perfused intestines were used to investigate the absorption mechanism(s). Exposure of whole gut sacs to 1 mg/l TiO_2 NPs for 4 h caused total Ti metal concentrations to increase in the intestine, with 80% or more of the Ti in the mucosa. Perfused intestines showed a saturable time-dependent accumulation of total Ti, which increased when the CO_2 in the gas mixture was lowered to 0.5%. Adding cyanide did not stop Ti uptake, and 100 μmol/l vanadate (ATPase inhibitor) caused a 2.8-fold reduction in the net uptake rate of Ti for TiO_2 NP exposure. Luminal additions of nystatin (endocytosis inhibitor), blocked the uptake of Ti from both bulk and TiO_2 NP treatments. The data demonstrate Ti uptake across the intestine from TiO_2 NP exposures, involving CO_2-dependent and nystatin-sensitive mechanisms.

Keywords: gut epithelium, uptake mechanism, endocytosis, carbon dioxide, dissolution

Appendix II

Poster Presentations

Uptake of TiO_2 Nanoparticles Across the Isolated Perfusate Intestine of Rainbow Trout (*Oncorhynchus mykiss*)

Aliaa R. Al-Jubory and Richard D. Handy
School of Biomedical & Biological Sciences, University of Plymouth, PL4 8AA, UK
Aliaa.al-jubory@plymouth.ac.uk

INTRODUCTION

- The uptake of TiO_2 NP across gills and gut epithelium has been suggested from Ti metal accumulation in tissues (Federici *et al.*, 2007), and the ability of NPs to cross cell membranes. However, the precise rates of uptake of TiO_2 NPs across epithelia is lacking, especially for the intestine.
- The aim of the present study was to measure the uptake rate of TiO_2 NPs across the intestine compared to the bulk powder, and also examining the effects of different gas mixtures on the uptake rate.

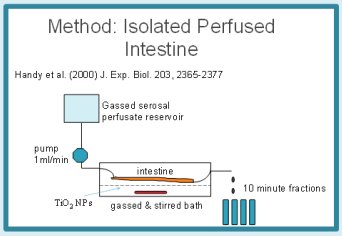

Figure 1. Isolated perfusate intestine method showing the intestine bathed in 500 ml physiological saline and the perfusate collection each 10 minutes over a 4 h perfusion experiment.

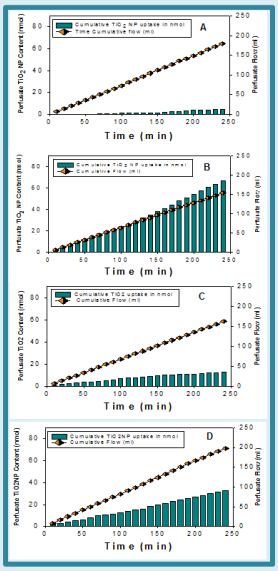

Figure 2. The effect of intestinal exposure to 1 mg l^{-1} of TiO_2 on cumulative TiO_2 content of the serosal perfusate (nmol, bars) and cumulative serosal perfusate flow (ml, diamonds). Graphs are examples of individual perfusions. (A) Control with standard gas mix; (B) TiO_2 NP with standard gas mix; (C) Bulk TiO_2 with standard gas mix; (D) TiO_2 NP with low CO_2.

Results

- A steady appearance of TiO_2 in the eluted perfusate occurred over time in the treated animals compared to controls and also showing differences associated with the type of gas mixture (Figure 2).
- The bulk powder generally showed a lower uptake rate than the nanoscale material (Figure 2).
- The accumulation of the bulk TiO_2 values were higher than the TiO_2 NP in both mid and hind intestine (Figure 3).
- There was at least a 10 fold increase in TiO_2 NPs uptake when the CO_2 was reduced to 0.5 % (Table 1).
- Good viability criteria including low LDH activity (< 1 IU ml^{-1}) in each fraction (Figure 4), and a steady rates appearance of perfusate flow.

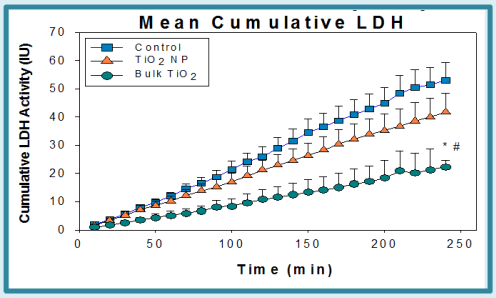

Figure 4. The effect of 1 mg l^{-1} of TiO_2 exposure on the perfusate cumulative LDH activity (IU) for up to 4 h at 18 °C, gassed with standard mix gas. Values are means ± S.E.M (n = 26) *Statistically significant difference (Kruskal-Wallis test, P < 0.05) from the control value at 240 minutes. # Bulk statistically significant difference from TiO_2 NP value.

Materials and Methods

- 1 mg l^{-1} TiO_2 NP was added to the bath at the beginning of the experiment, prepared from a stock solution of 10 g l^{-1} TiO_2 NPs, "Aeroxide" P25 (DeGussa AG), crystal structure was 25 % rutile and 75 % anatase (Federici *et al.*, 2007) and the mean primary particle size was 22.8 ± 0.6 nm (mean ± S.E.M., n = 169).
- Before the experiments all fish were starved for 48 h. Rainbow trout, *Oncorhynchus mykiss*, weighting 239 ± 9 g (mean ± S.E.M., n = 35) were used.
- The intestine was serosally perfused (Figure 1) and gassed with a standard gas mixture (95 % O_2 :5 % CO_2) or low CO_2 (99.5 % O_2 :0.5 % CO_2) for up to 4 h.
- After each experiment all the samples were analysed for the lactate dehydrogenase enzyme (LDH) activity and used as viability criteria for the perfused intestine.

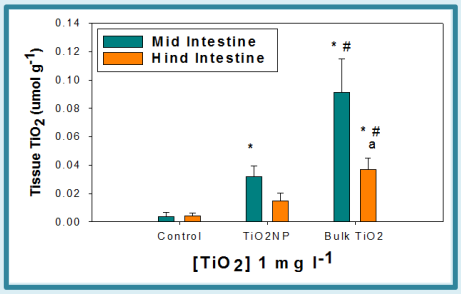

Figure 3. The TiO_2 accumulation in the mid and hind gut after 4 h perfusions with a concentration of 1 mg l^{-1} for TiO_2 NP or bulk TiO_2 gassed with standard gas mix. Data are means ± S.E.M. * Statistically significant difference (Kruskal-Wallis test, P < 0.05) from the control value. # Bulk statistically significant difference from TiO_2 NP value. Letter (a) indicates statistically significant differences between mid and hind intestine.

Conclusions

- This study shows that the isolated perfused intestine preparation works with nanoparticles, and that the viability criteria remain good with these materials.
- This study also demonstrates that NPs have the ability to cross the gut of fish into the serosal side.
- There is a particle-size effect as the nanoform is taken up faster than the bulk powder.
- TiO_2 NP absorption is time-dependent, saturable and the uptake mechanism is affected by the gas mixture used.

Mucosal [TiO_2] (1mg l^{-1})	Net TiO_2 flux, $J_{net,TiO2}$ (nmol g^{-1} h^{-1})		Net water flux, $J_{net,H2O}$ (ml g^{-1} h^{-1})	
	Initial rate	Overall rate	Initial rate	Overall rate
Standard gas mix Control	0.38 ± 0.26	0.43 ± 0.07	-6.22 ± 0.85	-7.50 ± 1.18
Standard gas mix TiO_2 NP	2.58 ± 0.55 *	3.97 ± 1.13 *	-17.56 ± 4.00 *	-18.01 ± 4.16 *
Standard gas mix Bulk TiO_2	1.64 ± 0.78 #	1.42 ± 0.54 #	-26.28 ± 2.52 *#	-28.54 ± 3.19 *#
Low CO_2 Control	0.85 ± 0.24	0.1 ± 0.05	-3.42 ± 1.71	-3.97 ± 0.97
Low CO_2 TiO_2 NP	35.26 ± 31.5	5.45 ± 2.66	-17.13 ± 2.37 *	-22.3 ± 6.41

Table 1. Net flux rates for TiO_2 and water across the perfused trout intestine. Values are means ± S.E.M. (Low CO_2, n = 6. standard gas mix, n = 7. Bulk TiO_2, n = 6) expressed per gram dry mass of intestine. Negative values indicate a net loss from the serosal solution, initial and overall rates data were calculated from cumulative perfusate data at 10 min and 4 h, respectively.* Statistically significant difference (Kruskal-Wallis test and *t*-test, P < 0.05) from the control value. # Bulk statistically significant difference from TiO_2 NP value.

References

- Federici, G., Shaw, B. J. and Handy, R. D. (2007). Toxicity of titanium dioxide nanoparticles to rainbow trout (*Oncorhynchus mykiss*): Gill injury, oxidative stress, and other physiological effects. *Aquatic Toxicology* **84**, 415-430.
- Handy, R. D., Musonda, M. M., Phillips, C. and Falla, S. J. (2000). Mechanisms of gastrointestinal copper absorption in the African walking catfish: copper dose-effects and a novel anion-dependent pathway in the intestine. *Experimental Biology* **203**, 2365-2377.

Mechanisms Uptake of TiO_2 Nanoparticles across the Isolated Perfused Intestine of Rainbow Trout (*Oncorhynchus mykiss*)

Aliaa R. Al-Jubory and Richard D. Handy
School of Biomedical & Biological Sciences, University of Plymouth, PL4 8AA, UK
aliaa.al-jubory@plymouth.ac.uk

Introduction

❖ The mechanisms uptake of nanoparticles (NPs) across the epithelia of fish are unknown. Handy et al. (2008) argues that apical entry of intact NPs into the epithelial cells of fish (gills, gut) is unlikely to occur via the traditional ion transport pathways (e.g., by diffusion through epithelial ion channels), because the NPs are simply far too large, but uptake into the cells by endocytosis remains possible.

❖ The aim of current study was to determine which part of the gut was involved in the uptake of TiO_2 NPs by using isolated whole gut sacs (Hoyle and Handy 1995), and then measure the uptake rate using the isolated perfused intestine (Handy et al., 2000), including pharmacological investigations of the mechanism(s) involved.

Materials and Methods

❖ 1 mg l^{-1} TiO_2 NP was used and prepared from a stock solution of 10 g l^{-1} TiO_2 NPs, "Aeroxide" P25 (DeGussa AG), crystal structure was 25 % rutile and 75 % anatase, the mean primary particle size was 22.8 ± 0.6 nm (mean ± S.E.M., $n = 169$).

❖ For the whole gut sac experiment, the gut was sutured closed at the posterior end, and the lumen filled with 1 mg l^{-1} TiO_2 (NP, Bulk, or no added TiO_2 control as appropriate) in physiological saline.

❖The intestine was serosally perfused and gassed with standerd gas mixture (95 % O_2 :5 % CO_2 or low CO_2 (99.5 % O_2 :0.5 % CO_2) for up to 4 h.

❖ 10 mmol l^{-1} cyanide (KCN) added to both the perfusate and mucosal solutions to determine if the TiO_2 NP uptake had an energy-dependent component.

❖100 µmol l^{-1} sodium orthovanadate (Na_3Vo_4), an ATPase transporter inhibitor, added to the serosal solution of the perfusate.

❖ In separate experiments, 120 IU ml^{-1} nystatin (endocytosis inhibitor), was added to the mucosal solution only.

Results

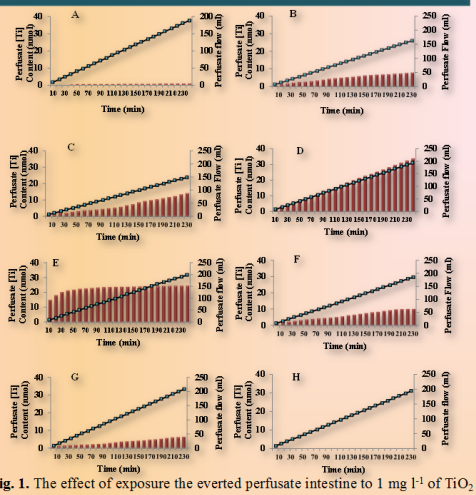

Fig. 1. The effect of exposure the everted perfusate intestine to 1 mg l^{-1} of TiO_2 added in the mucosal solution on cumulative [Ti] content of the serosal perfusate (nmol, bars) and cumulative serosal perfusate flow (ml, diamonds).Graphs are representative examples of individual perfusions from replicated experiments (All groups, n = 6-7). (A) Control; (B) Bulk TiO_2; (C) TiO_2 NP; (D) Bulk TiO_2 gassed with low CO_2; (E) TiO_2 NP gassed with low CO_2 (F) 10 mmol l^{-1} Cyanide exposure with TiO_2 NP; (G) 100 µmol l^{-1} Sodium vanadate exposure with TiO_2 NP; (H) 120 IU ml^{-1} nystatin exposure with TiO_2 NP. Fish weights in the examples are 307, 136.3, 249.9, 648.9, 140.3, 360.7, 137 and 273.9 g, respectively.

References

❖ Handy RD, Musonda MM, Phillips C and Falla SJ. 2000. Mechanisms of gastrointestinal copper absorption in the African walking catfish: copper dose-effects and a novel anion-dependent pathway in the intestine. *Experimental Biology* **203:** 2365-2377.

❖ Hoyle I and Handy RD. 2005. Dose-dependent inorganic mercury absorption by isolated perfused intestine of rainbow trout, *Oncorhynchus mykiss*, involves both amiloride-sensitive and energy-dependent pathways. *Aquatic Toxicology* **72:** 147-159.

❖ Handy RD, Henry TB, Scown TM, Johnston BD and Tyler CR. 2008. Manufactured nanoparticles: their uptake and effects on fish-a mechanistic analysis. *Ecotoxicology* **17:** 396-409.

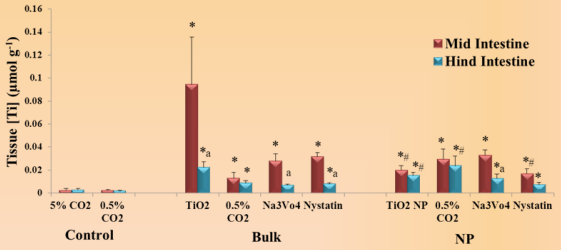

Fig. 2. The Ti metal from TiO_2 accumulation in the mid and hind gut after 4 h perfusions with a concentration of 1 mg l^{-1} for TiO_2 NP or bulk TiO_2 added to the mucosal solution gassed with standard gas mix or low CO_2, showed also the effects of drugs exposure (vanadate and nystatin) on the accumulation of the TiO_2 in the tissue. Data are means ± S.E.M (n = 6-7). * Statistically significant difference from the control (Kruskal-Wallis, $P < 0.05$), # statistically significant difference from the bulk TiO_2 (Kruskal-Wallis, $P < 0.05$). Letter (a) indicates statistically significant difference between mid and hind intestine (t-test, $P < 0.05$).

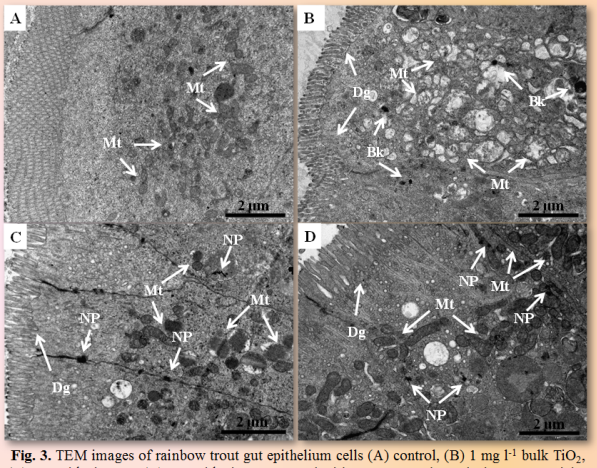

Fig. 3. TEM images of rainbow trout gut epithelium cells (A) control, (B) 1 mg l^{-1} bulk TiO_2, (C) 1 mg l^{-1} TiO_2 NP, (D) 1 mg l^{-1} TiO_2 NP gassed with 0.5 % CO_2 showed TiO_2 nanoparticles uptake (NP) and bulk (Bk), mitochondria (Mt) noticed damaging in the exposure images, degeneration of the villi (Dg). Scale bar = 2 µm.

Table 1. Total [Ti] of gut tissue segments following the exposure to 1 mg l^{-1} TiO_2 in the gut lumen for 4 h.

	[Ti] µmol g^{-1} dry mass				
Treatments	Oesophagus	Stomach	Pyloric caecae	Mid intestine	Hind intestine
Control	<0.003^a	0.003 ± 0.001^a	<0.003^a	0.004 ± 0.001^b	0.006 ± 0.004^a
Bulk TiO_2	0.033 ± 0.009^{b,*}	0.029 ± 0.007^{a,*}	0.016 ± 0.003^{a,*}	0.062 ± 0.018^{b,*}	0.041 ± 0.011^{ab,*}
TiO_2 NP	0.027 ± 0.009^{a,*}	0.017 ± 0.003^a	0.015 ± 0.003^{a,*}	0.027 ± 0.005^{a,*}	0.030 ± 0.006^{a,*}

Values are means ± S.E.M. (n = 6 for each group) expressed as µmol g^{-1} dry mass of intestinal tissue. Whole gut sacs were filled with physiological saline (control), 1 mg l^{-1} TiO_2 NP and 1 mg l^{-1} Bulk TiO_2 at laboratory temperature (18 °C) for 4h.
* Statistically significant difference from the control value within columns (Kruskal-Wallis or ANOVA, $P < 0.05$). Different letters (within rows) indicate a statistically significant difference between regions of the gut (Kruskal-Wallis or ANOVA, $P < 0.05$).

Conclusions

❖ The isolated perfused intestine and the gut sac preparations works with NPs.

❖ TiO_2 NP were mainly absorbed in the mid and hind regions of trout intestine, and mostly concentrated in the mucosa layer.

❖ TiO_2 NP absorption is time-dependent, saturable and the uptake mechanism is affected by the gas mixture used and faster uptake than the bulk powder.

❖ The mechanism was found by testing inhibitors of the main uptake pathways in the gut which indicated a nystatin-sensitive pathway that may involve endocytosis in the intestine.

Acknowledgments

❖ Al-Jubory were financially supported by the Ministry of Higher Education and Scientific Research via the Embassy of the Republic of Iraq.

❖ Many thanks for Peter Bond for his technical help in electron microscopy studies.

Uptake and Retention of TiO_2 Nanoparticles in Caco-2 Cells; Implications for Human Health

Constantinos Gitrowski, Aliaa R. Al-Jubory and Richard D. Handy
School of Biomedical & Biological Sciences, University of Plymouth, PL4 8AA
Email: constantinos.gitrowski@plymouth.ac.uk

Introduction

- Titanium dioxide powder is used extensively in a wide variety of commercial products. Estimates indicate that people in the western world ingest around 5 - 50 mg / day. *in vivo* researchs has suggested that uptake of nano TiO_2 occurs, although little is known about the rates and mechanisms of this process.
- The aims of this study were to measure the uptake rates of TiO_2 bulk powder and nanopowder of differing crystal types, assess the toxicity, and, elucidate the uptake mechanisms in Caco-2 cells.

Materials and Methods

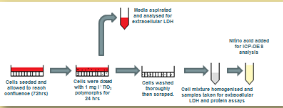

Fig. 1 General experimental methodology

- 1 mg l^{-1} TiO_2 NP containing media was prepared for each of the TiO_2 crystal types (Anatase, Rutile, and a mixture of both "P25") at the beginning of the experiment. These were prepared from a stock solution of 500 mg l^{-1}.The primary particle size measurement of 103.2 ± 16 nm, 22.8 ± 0.6 nm, 16.4 ± 2.4 nm, and 30.8 ± 2.5 for bulk, P25, anatase and rutile, respectively. A bulk particle control of 1mg l^{-1} was used for comparative results.
- Further experiments investigated the effect of a range of inhibitors on particle uptake mechanism (vanadate, nystatin, chloropromazine and genistein).
- Cell health and morphology was visually inspected throughout the experiments. Membrane integrity was assessed using LDH leakage (low leakage indicates an uncompromised membrane).
- Cells were elementally analyzed using ICP-OES in order to assess the effect of TiO_2 exposure on intracellular electrolytes. Some cells were analysed using SEM, TEM, X-ray microanalysis, and block face analysis techniques in order to confirm that ICP detected TiO_2 was intracellular in nature.

Results

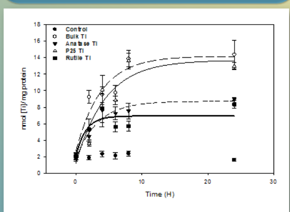

Fig. 2 Titanium uptake in Caco-2 cells incubated with 1 mg l^{-1} titanium dioxide polymorphs for 24 hrs. The plots are means from the triplicate data (plus SEM) and are expressed as nmol [Ti] mg^{-1} protein. Uptake of all titanium polymorphs is significantly different to the controls (ANOVA $P<0.05$). Furthermore the uptake of Bulk and P25 titanium polymorphs at 24 hrs is significantly greater than the anatase and rutile polymorphs (ANOVA $P<0.05$). Uptake was characterized by the equation $f = y0+a*(1-exp(-b*x))$. R^2 values for the fitted lines were 0.9008, 0.875, 0.952, 0.731, for Bulk, P25, anatase and rutile respectively.

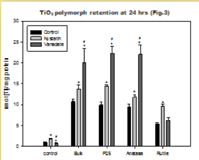

Fig. 3 Drug effects on Ti retention in Caco-2 cells incubated with 1mg l^{-1} titanium polymorphs at 24 hrs. The plots are means ± SEM (n = 6) from the replicate data and are expressed as 'nmol [Ti] mg^{-1} protein'. !20 IU Nystatin increases Ti retention for all polymorphs of titanium significantly compared to the control (ANOVA $p < 0.05$ (*)). 100 umol Vanadate significantly increases Ti retention for cells exposed to bulk,P25 and Anatase TiO_2 polymorphs (ANOVA $p <0.05$).

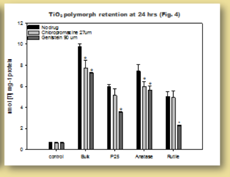

Fig. 4 Drug effects on Ti retention in Caco-2 cells incubated with 1mg l^{-1} titanium polymorphs for 24 hrs. The plots are means ± SEM (n = 3) from the replicate data and are expressed as 'nmol [Ti] mg^{-1} protein'. Chloropromazine significantly decreased Ti retention in cells dosed with Bulk and anatase TiO_2 (ANOVA $p < 0.05$) relative to the no drug trials except in the case of rutile exposure Genistein significantly decreased retention of TiO_2 for all polymorphs relative to the no drug trials (ANOVA $p < 0.05$).

Table 1. Total intracellular K^+, Ca^{2+}, Mg^{2+} and Na^{2+} in nmol [Metal] mg^{-1} protein following exposure to 1mg l^{-1} TiO_2 polymorphs and drugs for 24 hrs.

TiO_2 1 mg l^{-1}	Electrolytes (nmol mg^{-1} protein)											
	K^+			Ca^{2+}			Mg^{2+}			Na^{2+}		
	No drug	Nystatin	Vanadate	No drug	Nystatin	Vanadate	No drug	Nystatin	Vanadate	No drug	Nystatin	Vanadate
control	718.8 ± 14.2	927.9 ± 50.8#	466.8 ± 43.8~	10.6 ± 1.2	25.7 ± 9.4#	20.9 ± 3.6~	42.6 ± 1.1	56.2 ± 2.9#	30.9 ± 3.4~	4518 ± 160	6303 ± 468	3632 ± 427
Bulk	663.9 ± 28.3*	828.8 ± 62.3#	479.6 ± 36.9~	14.3 ± 7.0	19.8 ± 2.2*	25.2 ± 4.6~	47.8 ± 2.2*	55.3 ± 2.8#	38.9 ± 3.1*~	4666 ± 576	5253 ± 445	4246 ± 406
P25	643.8 ±19.6*	815.7 ± 30*#	469.3 ± 26.9†~	28.0 ± 12.4*	27.8 ± 5.7	18.0 ± 7.2~	53.4 ± 2.7*	55.0 ± 1.8	39.4 ± 2.7*~	4793 ± 231	5144 ± 308	3982 ± 311
Anatase	637.9 ± 27.6*	822.7 ± 57.9*#	513.3 ± 16.9*~	20.8 ± 5.4*	14.4 ± 4.6*	18.7 ± 4.1	49.8 ± 1.4*	56.2 ± 4.4#	43.8 ± 2.3†*~	5109 ± 624	5748 ± 455	4457 ± 216
Rutile	611.1 ± 11.4*	807.1 ± 41.2*#	490.7 ± 37.1~	19.1 ± 8.2*	17.7 ± 3.1*	29.1 ± 2.4*~	50.7 ± 1.5*	55.0 ± 3.1#	40.9 ± 2.8†*~	4319 ± 350	5202 ± 417	4534 ± 568

Data are expressed as means ± S.E.M (n = 6 for each group). * statistically significant difference from the control values within columns. (ANOVA $p < 0.05$). # statistically significant difference of nystatin values relative to the no drug trials within rows and electrolytes (ANOVA $p < 0.05$). ~ statistically significant difference of vanadate values relative to the no drug trials within rows and electrolytes (ANOVA $p < 0.05$). Intracellular Potassium levels decreased in Caco-2 cells exposed to TiO_2 polymorphs in the absence of drugs but increased in magnesium level relative to the (no drug, no TiO_2) control. Incubating cells with nystatin resulted in an increase in intracellular potassium and magnesium levels relative to the no drug trials. Vanadate had the opposite effect on intracellular electrolytes, magnesium and potassium levels dropped significantly compared to the no drug trial.

Table 2. Total intracellular K^+, Ca^{2+}, Mg^{2+} and Na^{2+} in nmol [Metal] mg^{-1} protein after exposed to drugs with 1mg l^{-1} TiO_2 polymorphs for 24 hrs.

TiO_2 1 mg l^{-1}	Electrolytes (nmol mg^{-1} protein)															
	K+				Ca 2+				Mg 2+				Na 2+			
	No drug	Chloropromazine	Genistein	Amiloride HCL	No drug	Chloropromazine	Genistein	Amiloride HCL	No drug	Chloropromazine	Genistein	Amiloride HCL	No drug	Chloropromazine	Genistein	Amiloride HCL
Control	684.2 ± 16.8	565.2 ± 16.2 #	642.5 ± 31.3	1039.8 ± 273†	15.5± 1.6	12.5± 1.3#	48.3 ± 8.1~	104.1± 17.5†	40.2 ± 1.1	37.3 ± 1	38.4 ± 1.6	84.0 ± 5.0†	6007 ± 359	1364± 160#	3858± 396~	4118± 457†
Bulk	650.2 ± 31.8	553.3 ± 40.3#	634.6 ± 35.8	977.1 ± 154†	28.5± 5.1	12.8± 1.6#	37 ± 2.9~	173.9± 69.8†	40.7 ± 0.6	38.8 ± 29	40.6 ± 1.7	70.4 ± 7.5†	5671 ± 474	1266± 136#	4038± 257~	3708± 902†
P25	655.4 ± 19.7	534.4 ± 22.2#	686.5 ± 36.5	771.7 ± 120†	32.1± 7.3	11.7± 1.5#	38.2 ± 7.7~	86.4 ± 41.1†	41.5 ± 2	36.2 ± 17	43.7 ± 2.7	68.4 ± 3.7†	5654 ± 365	1100± 73#	4080± 342~	3318± 802†
Anatase	638.5 ± 25	561.3 ± 33.2#	653.7 ± 33.6	795 ± 199†	26.9± 4.9	12.2± 0.8#	40.5 ± 2.4~	70.1 ± 16.2†	39.5 ± 0.9	38.6 ± 24	42.4 ± 0.8	71.4 ± 12.2†	5528 ± 477	1070± 50#	4176± 208~	3358± 1175†
Rutile	600.8 ± 34.3	550.9 ± 18.5#	663.4 ± 19.3	827.1 ± 121†	17.9± 1.4	10.1± 1.2#	36.1 ± 7.1~	68.6 ± 11.1†	37.7 ± 2.1	38.3 ± 13	43.9 ± 0.2	79.9 ± 8.3†	4251 ± 337	1041± 45#	4874± 843	3067± 521†

Data are expressed as means ± S.E.M (n = 3 for each group). * statistically significant difference from the control values within columns and electrolytes (ANOVA $p < 0.05$). # statistically significant difference of Chloropromazine values relative to the no drug trials within rows (ANOVA $p < 0.05$). ~ statistically significant difference of Genistein values relative to the no drug trials within rows (ANOVA $p < 0.05$). † statistically significant difference of Amiloride HCL values relative to the no drug control trials within rows (ANOVA $p < 0.05$). Intracellular Potassium levels decreased in Caco-2 cells exposed to TiO_2 polymorphs in the absence of drugs but increased in magnesium level relative to the (no drug, no TiO_2) control. Incubating cells with Chloropromazine resulted in a decrease in intracellular potassium, magnesium, calcium and sodium levels relative to the no drug trials. Genistein had no effect on magnesium and potassium levels but caused an increase in calcium and a decrease in sodium in comparison to the no drug trials. Amiloride HCL caused an increase in magnesium, potassium and calcium whilst decreasing sodium levels relative to the no drug controls.

Microscopy

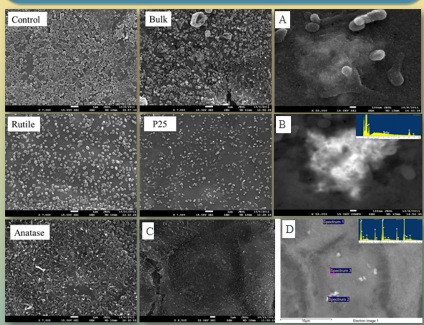

Fig. 5 Labelled images: Scanning electron microscopy of Caco-2 cells 96hrs after seeding having been exposed to 1mg l^{-1} TiO_2 polymorphs for 24 hrs. Rutile and P25 nano TiO_2 exposures seems to affect microvilli density negatively in comparison to the control, bulk and anatase. The scale bar represents 1 um. Images (A-D): SEM images of Caco-2 cells 96 hrs after seeding having been exposed to 1mg l^{-1} TiO_2 polymorphs. A) SEI image of cell surface exposed to P25 TiO_2. The cell membrane appears to have covered the TiO_2 (projections are microvilli, scale bar represents 100 nm); B) Backscatter image (BSI) of 'A' showing subsurface Ti with associated spectra; C) Secondary electron image(SEI) of the cell surface (scale bar represents 1 um) exposed to anatase TiO_2; D) BSI of 'C' showing subsurface Ti with xrma spectra.

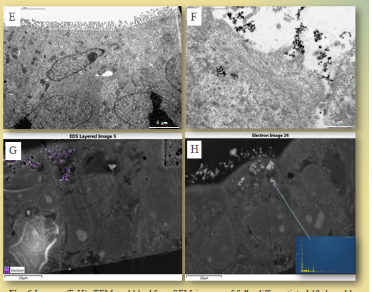

Fig. 6 Images (E-H): TEM and blockface SEM images of fully differentiated 18 day old cells exposed to 10 mg l^{-1} TiO_2 P25 for 25 hrs; E) TEM image of control cells (no exposure) (scale bar is 5 μm); F) TEM image of exposed cells (note the endocytic vesicle invagination with NPs inside of it) (Scale bar is 1 μm); G) Block face BSI layered with Ti spectra (purple). Note the Ti is within the cells (Scale bar 10 μm); H) Block face BSI with Xray spectra showing intracellular Ti (scale bar 10 μm).

Results

- TiO_2 polymorph uptake occurred in a time dependent saturable manner. Rates of uptake seem to be influenced by crystal type. Bulk and P25 NPs exhibited the most prolonged uptake and subsequent retention reaching saturation at 8 hrs (Fig. 2).
- Cells incubated with either nystatin (cholesterol binding agent) or vanadate (P-type ATPase inhibitor) caused an increase in retention relative to the no drug controls.
- Incubating with genistein (tyrosine kinase inhibitor) and chloropromazine (Clathrin mediated endocytosis inhibitor) caused a decrease in TiO_2 retention.
- TiO_2 polymorph exposure caused changes in total intracellular metal concentrations relative to non dosed cells. All Ti polymorphs caused an increase in intracellular magnesium and calcium and a decrease in intracellular potassium relative to the control.

Conclusions

- This study demonstrates that TiO_2 NPs are taken up in a time dependent saturable process.
- Uptake rates are affected by particle size and crystal structure.
- NPs have the ability to cross the apical membrane of Caco-2 cells and this is mediated by energy dependent mechanisms.
- Drug incubation studies indicate predominant method of TiO_2 uptake is mediated by tyrosine kinase / phosphatase regulation implicating calveolae mediated mechanisms as a major uptake pathway[2].
- TEM images show intracellular vesicles occupied by nanoparticle aggregates supporting the idea that an endocytic mechanism[1] is responsible for uptake (Image E)
- 1 mg l^{-1} doses of TiO_2 NPs are sub lethal however electrolyte levels are altered which may contribute to pathologies.

References

- Handy RD, Henry TB, Scown TM, Johnston BD and Tyler CR 2008. Manufactured nanoparticles: their uptake and effects on fish-a mechanistic analysis. *Ecotoxicology* **17:** 396-409.
- Parton RG and Richards AA 2003. Lipid rafts and caveolae as portals for endocytosis: New insights and common mechanisms. Traffic 4: 724-738.

Acknowledgment

- Constantinos Gitrowski and Aliaa R. Al- Jubory are equal contributors to this study.
- Al-Jubory were financially supported by the Ministry of Higher Education and Scientific Research via the Embassy of the Republic of Iraq.